Zeolite Encapsulated Complexes of Fe, Co, Ni, Cu and Pd: Synthesis, Characterization and Catalysis

Jyothi Mariam John

Department of Applied Chemistry
Cochin University of Science and Technology
Kochi, KERALA, 682 022

March 2003

Certificate

This is to certify that the thesis entitled ***"Zeolite encapsulated complexes of Fe, Co, Ni, Cu, and Pd: synthesis, characterization, and catalysis,"*** submitted for the award of the degree of Doctor of Philosophy of Cochin University of Science and Technology, is a record of *bona fide* research work carried out by Ms. Jyothi Mariam John under my supervision in the Department of Applied Chemistry.

Prof. K.K. Mohammed Yusuff
Department of Applied Chemistry
Cochin University of Science and Technology
Kochi-22

21 April 2003

Preface

The growing demand for the design and development of environmentally benign products and processes has led to the emergence of 'green chemistry.' One of the basic thrusts of 'green chemistry' is on minimizing the production of waste in chemical processes. In line with this need we undertook the studies on zeolite Y encapsulated transition metal complexes and their application as catalysts for some selective oxidation reactions of vital importance.

Encapsulation inside the zeolite cages makes the catalysts more stable. Further, the framework prevents the complexes from dimerising. The topology of the void influences the complex's geometry, and brings about changes in its electronic and magnetic properties. The steric constraints in zeolite may distort the encapsulated complex molecule to induce different stability and reactivity for them. The ligands modify and fine-tune the electronic and steric environment of the reaction site. Thus the zeolite encapsulated complexes become reaction centers, which bind small molecules used for catalysis. The present thesis deals with the synthesis, characterization, and catalytic activity studies of some zeolite encapsulated complexes. The thesis is divided into nine chapters.

Chapter 1 is a general introduction on zeolite encapsulated complexes and their application as catalysts in certain oxidation reactions, and Chapter 2 describes the materials and methods used in the present study. Chapter 3 is divided into two sections. Section A deals with the synthesis and characterization of Schiff bases of Fe(III), Co(II), Ni(II), and Cu(II) complexes of the *N,N'*-bis(3-pyridylidene)-1,2-phenylenediamine and *N,N'*-bis(3-pyridylidene)-1,4-phenylenediamine. Section B deals with Co(II), Ni(II), and Cu(II) complexes of salicylaldehyde semicarbazone encapsulated in the zeolite Y cage. Chapter 4 is a comparative study on the neat and encapsulated complexes of

2-styrylbenzimidazole complexes of Cu(II). Chapter 5 is about the zeolite encapsulated dithiocarbamate complexes, and has two sections. Section A presents the studies on Fe(III) dithiocarbamates, and Section B is on Co(III), Ni(II), and Cu(II) morpholinedithiocarbamates. Chapter 6 of the thesis deals with the study of the zeolite encapsulated palladium complexes of DMG, SALSC, and MDTC. Chapters 7, 8, and 9 focus on catalytic activity studies using the synthesized encapsulated complexes. The general conclusions drawn from the investigation are given at the end of the thesis.

Contents

Chapter 1	**General Introduction**	1
1.	Introduction	2
1.1.	Catalytic oxidation reactions	3
1.2.	Zeolite encapsulated metal complexes	8
1.2.1.	Zeolites	9
1.2.2.	Classification of zeolites	11
1.2.3.	Structural aspects of zeolites	11
1.2.4.	Synthesis of encapsulated complexes	14
1.2.4.1.	Flexible ligand method	14
1.2.4.2.	Ship-in-a-bottle synthesis	15
1.2.4.3.	Zeolite synthesis method	17
1.2.5.	Characterization techniques	17
1.2.6.	Zeolites as micro reactors	18
1.2.7.	Guest host interactions between complex and support	19
1.2.8.	Zeozymes: encapsulated complexes that mimic enzymes	21
1.3.	Scope of the present study	23
	References	26
Chapter 2	**Materials and methods**	32
2.1.	Introduction	33
2.2.	Reagents	33
2.3.	Synthesis of ligands	34
2.3.1.	Preparation of dimethylglyoxime (DMG)	34
2.3.2.	Synthesis of styrylbenzimidazole (SB)	34
2.3.3.	Synthesis of carbodithioate and dithiocarbamates	35
2.3.4.	Synthesis of *N,N'*-bis(3-pyridylidene)-1,2-phenelenediamine (SPO)	35
2.3.5.	Synthesis of *N,N'*-bis(3-pyridylidene)-1,4-phenylenediamine (SPP)	35
2.3.6.	Synthesis of salicylaldehyde semicarbazone (SALSC)	36
2.4.	Synthesis of zeolite Y encapsulated metal complexes	36
2.4.1.	Preparation of sodium exchanged zeolite (NaY)	36
2.4.2.	Preparation of transition metal ion exchanged zeolite (MY)	36
2.4.3.	Encapsulation of metal complexes in zeolite	37
2.4.3.1.	Encapsulation by heating in a sealed ampule	37
2.4.3.2.	Encapsulation by refluxing the metal exchanged zeolite with the ligand	38
2.5.	Synthesis of neat complex	38
2.6.	Catalysis procedures	38
2.6.1.	Decomposition of hydrogen peroxide	38

2.6.2.	Hydroxylation of phenol to hydroquinone	39
2.6.3.	Partial oxidation of benzyl alcohol to benzaldehyde	39
2.7.	Characterization methods	39
2.7.1.	Chemical analysis	40
2.7.1.1.	Analysis of Si, Al, Na, and transition metal ion in the zeolite sample	40
2.7.1.2.	Determination of metal in neat complex	41
2.7.1.3.	Determination of chlorine	41
2.7.2.	CHN analysis	42
2.7.3.	Surface area and pore volume analysis	42
2.7.4.	X-ray diffraction studies	43
2.7.5.	Spectroscopic analysis	44
2.7.5.1.	Electronic spectra	44
2.7.5.2.	Infrared spectra	45
2.7.5.3.	EPR spectra	45
2.7.6.	Magnetic measurement studies	46
2.7.7.	Scanning electron microscopy	46
2.7.8.	Thermo gravimetric analysis	47
2.7.9.	Conductance measurement	47
2.8.	Catalytic studies	47
2.8.1.	Gas chromatography	47
2.8.2.	Thin layer chromatography	48
	References	49
Chapter 3	**Zeolite-Y encapsulated complexes of the Schiff bases *N,N'*-bis(3-pyridylidene)-1,2-phenylenediamine, *N,N'*-bis(3-pyridylidene)-1,4-phenylenediamine, and salicylaldehyde semicarbazone**	50
3.	Introduction	51
Section A	**Zeolite encapsulated Fe(III), Co(II), Ni(II) and Cu(II) *N,N'*-bis(3-pyridylidene)-1,2-phenylenediamine and *N,N'*-bis(3-pyridylidene)-1,4-phenylenediamine complexes**	52
3A.1.	Introduction	52
3A.2.	Experimental	53
3A.2.1.	Synthesis of ion exchanged zeolites	53
3A.2.2.	Synthesis of zeolite encapsulated Fe(III), Co(II), Ni(II) and Cu(II) complexes of *N,N'*-bis(3-pyridylidene)-1,2-phenylenediamine, and *N,N'*-bis(3-pyridylidene)-1,4-phenylenediamine	53
3A.3.	Characterization techniques	54
3A.4.	Results and discussion	54
3A.4.1.	Ion exchanged zeolite	54
3A.4.1.1.	Chemical analysis	54
3A.4.1.2.	X - ray diffraction patterns	56

3A.4.1.3.	Surface area and pore volume	58
3A.4.1.4.	FTIR spectrum	58
3A.4.1.5.	Diffuse reflectance spectra	60
3A.4.1.6.	EPR spectrum	60
3A.4.2.	Zeolite encapsulated complexes	62
3A.4.2.1.	Chemical analysis	62
3A.4.2.2.	Scanning electron micrographs	63
3A.4.2.3.	X-ray diffraction patterns	63
3A.4.2.4.	Surface area and pore volume	67
3A.4.2.5.	Magnetic moment	68
3A.4.2.6.	Diffuse reflectance spectra	70
3A.4.2.7.	FTIR spectra	75
3A.4.2.8.	EPR spectra	80
3A.4.2.9.	TG analysis	84
Section B	**Zeolite encapsulated Co(II), Ni(II) and Cu(II) complexes of salicylaldehyde semicarbazone**	88
3B.1.	Introduction	88
3B.2.	Experimental	89
3B.2.1.	Synthesis of zeolite encapsulated Co, Ni and Cu complexes of salicylaldehyde semicarbazone	89
3B.3.	Characterization techniques	89
3B.4.	Results and discussion	89
3B.4.1.	Chemical analysis	89
3B.4.2.	X-ray diffraction studies	90
3B.4.3	Surface area and pore volume	91
3B.4.4.	Magnetic moment	92
3B.4.5.	Diffuse reflectance spectra	93
3B.4.6.	FTIR spectra	96
3B.4.7.	EPR spectra	98
3B.4.8.	TG analysis	99
	References	102
Chapter 4	**A comparison of neat and encapsulated complexes of copper 2-styrylbenzimidazole**	104
4.1.	Introduction	105
4.2.	Experimental	105
4.2.1.	Synthesis of neat $Cu(SB)_2Cl_2$	106
4.2.2.	Synthesis of zeolite encapsulated 2-styrylbenzimidazole complex	106
4.3.	Characterization techniques	106
4.4.	Results and discussion	106
4.4.1.	Chemical analysis	107
4.4.2.	X-ray diffraction patterns	108
4.4.3.	Scanning electron microscopy	108

4.4.4.	Surface area and pore volume	108
4.4.5.	Magnetic moment	111
4.4.6.	Diffuse reflectance spectra	111
4.4.7.	FTIR spectra	113
4.4.8.	EPR spectra	113
4.4.9.	TG analysis	118
	References	121
Chapter 5	**Zeolite-Y encapsulated dithiocarbamates of Fe, Co, Ni and Cu**	123
5.	Introduction	124
Section A	**Zeolite Y encapsulated Fe(III) dithiocarbamate and carbodithioate complexes**	125
5A.1.	Introduction	125
5A.2.	Experimental	126
5A.2.1.	Synthesis of zeolite encapsulated iron carbodithioate and dithiocarbamates	126
5A.3.	Characterization techniques	126
5A.4.	Results and discussion	127
5A.4.1.	Chemical analysis	127
5A.4.2.	X-ray diffraction patterns	127
5A.4.3.	Scanning electron micrographs	128
5A.4.4.	Surface area and pore volume	130
5A.4.5.	Magnetic moment	130
5A.4.6.	Diffuse reflectance spectra	131
5A.4.7.	FTIR spectra	133
5A.4.8.	TG analysis	138
Section B	**Zeolite encapsulated Co(III), Ni(II) and Cu(II) morpholine-*N*-carbodithioate complexes**	139
5B.1.	Introduction	139
5B.2.	Experimental	139
5B.2.1.	Synthesis of zeolite encapsulated Co(III), Ni(II) and Cu(II) morpholine-*N*-carbodithioate complexes	139
5B.3.	Characterization techniques	140
5B.4.	Results and discussion	140
5B.4.1.	Chemical analysis	140
5B.4.2.	X-ray diffraction patterns	141
5B.4.3.	Scanning electron micrographs	141
5B.4.4.	Surface area and pore volume data	144
5B.4.5.	Magnetic moment	144
5B.4.6.	Diffuse reflectance spectra	145
5B.4.7.	FTIR spectra	147

5B.4.8.	EPR spectrum	150
5B.4.9.	TG analysis	151
	References	153
Chapter 6	**Zeolite encapsulated palladium complexes**	154
6.1.	Introduction	155
6.2.	Experimental	157
6.2.1.	Synthesis of zeolite encapsulated palladium complexes	157
6.3.	Characterization techniques	157
6.4.	Results and discussion	158
6.4.1.	Chemical analysis	158
6.4.2.	X-ray diffraction patterns	158
6.4.3.	Scanning electron microscopy	160
6.4.4.	Surface area and pore volume	161
6.4.5.	Magnetic moment	161
6.4.6.	Diffuse reflectance spectra	162
6.4.7.	FTIR spectra	164
6.4.8.	TG analysis	169
	References	171
Chapter 7	**Catalytic activity of zeolite encapsulated complexes in the decomposition of hydrogen peroxide**	172
7.1.	Introduction	173
7.2.	Experimental	173
7.2.1.	Materials	173
7.2.2.	Procedure for the decomposition of hydrogen peroxide	174
7.3.	Results	174
7.3.1.	Screening studies	174
7.3.2.	Blank run	177
7.3.3.	Factors influencing the decomposition of hydrogen peroxide	179
7.3.3.1.	Influence of the volume of hydrogen peroxide	179
7.3.3.2.	Influence of the amount of catalyst	180
7.3.3.3.	Influence of solvent polarity of the reaction solution	182
7.3.4.	Addition of pyridine	184
7.3.5.	Recycled catalysts	185
7.4.	Discussion	188
	References	193
Chapter 8	**Hydroxylation of phenol to hydroquinone using zeolite encapsulated complexes**	194
8.1.	Introduction	195
8. 2.	Experimental	195
8.2.1.	Materials	195
8.2.2.	Procedure for the hydroxylation of phenol	196

8.3.	Results	196
8.3.1.	Screening studies	196
8.3.2.	Blank run	198
8.3.3.	Factors influencing the hydroxylation of phenol to form hydroquinone	198
8.3.3.1.	Influence of reaction time	198
8.3.3.2.	Influence of the amount of catalyst	200
8.3.3.3.	Influence of H_2O_2 : phenol (oxidant/substrate) ratio	202
8.3.3.4.	Influence of solvents	203
8.3.3.5.	Influence of reaction temperature	204
8.3.4.	Addition of poison	205
8.3.5.	Recycled catalyst	205
8.4.	Discussion	206
	References	213
Chapter 9	**Catalytic activity of zeolite encapsulated complexes in the partial oxidation of benzyl alcohol to benzaldehyde**	214
9.1.	Introduction	215
9.2.	Experimental	215
9.2.1.	Materials	215
9.2.2.	Procedure for the partial oxidation of benzyl alcohol to benzaldehyde	216
9.3.	Results	216
9.3.1.	Screening studies	216
9.3.2.	Blank run	218
9.3.3.	Factors influencing the partial oxidation of benzyl alcohol to benzaldehyde	218
9.3.3.1.	Effect of reaction time	218
9.3.3.2.	Effect of the amount of catalyst	220
9.3.3.3.	Effect of oxidant: substrate ratio	221
9.3.3.4.	Effect of solvents	222
9.3.3.5.	Effect of reaction temperature	223
9.3.4.	Addition of poison	224
9.3.5.	Recycled catalyst	225
9.4.	Discussion	226
	References	230
	Summary and conclusion	231

Chapter 1

General Introduction

1. Introduction

Modern man relies heavily on chemicals and has constantly been on the lookout for new chemicals and easy means to obtain them. Catalysis, the method of enhancing chemical processes by the use of appropriate material, has therefore been an area of vital interest. Nearly 90 % of the products manufactured today require processes which involve at least one catalytic step. As chemical processes always hold a potential threat to the environment, the nature of the catalyst used assumes special importance in relation to environmental protection. In the words of R.A. Sheldon, " The chemical industry is under increasing pressure to minimize or preferably eliminate waste production in chemical manufacture" [1]. The goal now is to synthesize catalysts that do not get deactivated and can be recovered with 100% efficiency.

The search for efficient catalytic processes having high activity and selectivity is of perennial importance. The recent urge for environmental protection has added a new dimension to the search for new catalysts. The need to use regenerable and safe solid catalysts is being increasingly felt. Transition metal complexes are accessible in a series of oxidation states and are good catalysts for many reactions including oxidation. However, they have certain disadvantages because of their homogeneous nature. Furthermore, many of the transition metal complexes are expensive to purchase and prepare. One method to overcome these limitations is to encapsulate them in zeolite pores. Such immobilisation of the complexes on to a support facilitates simple extraction as well as recycling, ensuring commercial advantages besides ease of manipulation. Efforts are being made by investigators worldwide to design and develop zeolite catalysts for active and selective organic transformations, especially for refining organic chemicals derived from the oxidation of hydrocarbons [2,3], and most of them use catalytic oxidations.

Chemical processes involving catalysis are often preferred over their non-catalytic alternatives as they take place more efficiently under milder conditions, producing higher yields with lower energy consumption, and minimizing environmental pollution. Further introduction of new and safe processes leads to high quality products. Active research is being carried out in the following aspects to develop new catalytic systems:

- spectroscopy of catalysts and catalyst models
- kinetics of catalytic reactions
- quantum chemical calculations for reactants, intermediates and products from measured spectra and quantum chemical calculations
- microkinetic modeling.

The transformation of functional groups by selective oxidation using metal complexes as catalysts is a basic reaction in organic chemistry. Oxidation reactions are the preferred processes in chemical synthesis, because of the ease with which the primary oxo product can be converted into secondary products like acids, diols, amines or esters [4]. By selecting the appropriate catalyst and reaction conditions, it is possible to direct the reaction along one selected pathway (lower energy pathway) to obtain the desired product.

1.1. Catalytic oxidation reactions

The ability of transition metals to exist in different oxidation states makes them excellent catalysts for many reactions. Several transition metal complexes act as catalysts for oxidation reactions. Molecular oxygen and air are attractive oxidants as they are inexpensive and yield no environmentally harmful side products. But since catalytic processes with these oxidants require elevated temperatures and pressures, oxidation is generally carried out using active oxygen reagents such as peroxides. Among the peroxides, hydrogen peroxide is one of the most readily available peroxide [5,6].

Even though there are many types of useful oxidation reactions, the present work is limited to the study of three oxidation reactions, namely, the decomposition of hydrogen peroxide, hydroxylation of phenol, and oxidation of benzyl alcohol. Therefore a brief review on these oxidation reactions is presented in this chapter.

Hydrogen peroxide is industrially and chemically important because of its use in a variety of processes [7]. The decomposition of hydrogen peroxide is considered as a standard reaction for the determination of the catalytic activity of metal complexes [8,9]. The reaction can be catalyzed by several transition metal ions and transition metal complexes, provided the coordination sphere is accessible to H_2O_2 or HOO^- ion [10,11]. The disproportionation of hydrogen peroxide catalyzed by metal complex has received much attention because this reaction is catalyzed by the naturally occurring heme enzyme catalase [12]. This enzyme is used by some bacteria to catalyze the conversion of hydrogen peroxide to oxygen and water. As hydrogen peroxide is an unwanted byproduct in many redox reactions involving oxygen in living systems, this reaction, an effective method for removing hydrogen peroxide, continues to receive the attention of bioinorganic chemists.

Sharma and Schubert have made a detailed study on the kinetics and decomposition of hydrogen peroxide by copper complexes and chelates [13,14]. They have observed the effect of the chelate ring size on hydrogen peroxide decomposition [15]. Efforts have been made to prepare coordination compounds containing dioxygen groups and subsequently to use these complexes for catalytic oxidation reactions. Examples of such systems can be found in nature. SALEN *N,N'*-ethylenebis(salicylideneamine)] complexes and SALSC (salicylaldehyde semicarbazone) complexes of transition metals have been reported to be mimics of catalase [16] and superoxidedismutase [17] which are known to catalyze the decomposition of hydrogen peroxide and superoxide ions. One of the major

disadvantages of metal SALENS in homogeneous solution is the formation of μ-oxo dimer and other polymeric species leading to catalytic deactivation.

All the above-mentioned oxidation reactions are catalyzed by homogeneous catalysts. Homogeneous systems have several drawbacks; these catalysts show a tendency for self-degradation, and there is difficulty in reusing them. Thus homogeneous catalysts are found to have limited commercial application in large-scale preparations, as the homogeneous systems lack continuous processing technology and recycling ability. The expense for catalyst recovery is also high. When the products are not readily separated from the catalyst, homogeneous catalysts can cause product contamination and catalyst loss. For these reasons many homogeneous processes are not used on an industrial scale in spite of their advantages.

The other oxidation reaction selected for study is phenol hydroxylation. Phenol, a by-product in many industries, is used as a precursor of many organic petrochemical compounds. It is readily biodegraded in the neutral environment if its concentration is low, but artificial methods have to be used for its degradation if the concentration is high. The accumulation of waste containing phenol leads to serious environmental problems. Researchers are now trying to develop efficient and inexpensive processes for the disposal of this type of waste. Highly specific first step oxidation products are obtained with mild oxidizing agents and suitable catalysts, while quinones and other degradation products are obtained in the presence of strong oxidants.

One method for the disposal of phenol is its conversion to industrially useful diphenols (catechol and hydroquinone). But vigorous reaction conditions like high temperatures and pressure are required for the processes and make such processes uneconomical for phenol oxidation [18]. Further industrial applications of diphenols and their derivatives motivated the discovery of new methods for their production from phenol. Catechol and hydroquinone belong to the class of

low volume but high value fine chemicals. The principal large-scale application of hydroquinone is in photography, as a photographic film developer [19].

Phenol hydroxylation has been carried out using different oxidants and a variety of processes. The processes using hydrogen peroxide as the oxidant have disadvantages owing to its decomposition during reaction and the threat of explosion, and it is not economically favorable in many oxidation processes. But it is still preferred because of the environmental advantage. The most efficient contemporary processes involve the oxidation of phenol with H_2O_2 to produce a mixture of catechol and hydroquinone. Leading producers following this route are Rhône – Poulenc, Brichima,and Enichem.

The Rhône–Poulenc process [20] is based on phenol hydroxylation by hydrogen peroxide catalyzed by strong mineral acid. In the industrial process, perchloric acid is used in its azeotropic mixture with water. The reaction is performed at 90 °C using phenol, H_2O_2 and $HClO_4$ in the molar ratio 20:1:0.1. The disadvantage of the process is the formation of a high amount of tar. Hydroxylation of phenol using hydrogen peroxide and iron based Fentons reagent was the procedure adopted by Brichima in Italy [21-25]. During the reaction ferrous salts are consumed, breaking off the redox reaction [26]. Ferrocene also has good catalytic properties for this reaction [27]. The formation of high amounts of tar is the major disadvantage of this method also.

Hydroxylation of phenol is also catalyzed by simple metal ions and their complexes [28,29]. In spite of the high activity of these catalysts, they have the inherent disadvantages of homogeneous catalysts. A notable disadvantage of homogeneous catalysis is the high ortho : para ratio which is close to 2.

The conventional methods of phenol hydroxylation using heterogeneous catalysts result in a mixture of ortho and para hydroxy phenols. Many of the acid

catalyzed reactions which require very corrosive acids in homogeneous catalysis can be carried out using zeolites and related acid catalysts [30,31].

Zeolite-based catalysts are now used for the production of hydroquinone as they offer advantages over existing processes. The shape selective nature of zeolites favours the production of hydroquinone [32,33]. The hydroxylation of phenol with hydrogen peroxide has been carried out in the presence of zeolite modified with rare earth catalyst [34]. Hydroquinone formation takes place only in the intra crystalline space of the zeolite catalyst whereas catechol and tarry products can be formed either on the outer surface of the catalyst or on the inner surface when sufficient space is available [35,36]. The first industrial application of a zeolite catalyst for phenol hydroxylation was in the Enichem process [37,38].

Partial oxidation of benzyl alcohol involving the metal complexes was also studied as a part of the work embodied in the present thesis. This reaction is of great importance in the preparation of fine chemicals, as it makes the production of intermediate compounds easy. Side chain oxidation reactions resulting in an intermediate product with high selectivity is not very common with neat complexes. There are reports of studies on benzyl alcohol oxidation to benzaldehyde taking place using atmospheric oxygen and hydrogen peroxide. On adding hydrogen peroxide to metal complexes the corresponding per-oxo compounds are generated. The per-oxo compounds formed provide an attractive route for the preparation of synthetic intermediates and other oxygen containing organic substrates. Metal complexes have thus attracted attention as dioxygen activating catalysts [39-41]. Benzyl alcohol to benzaldehyde oxidation has been carried out using hydrogen peroxide as oxidant and Co(II) acetate as catalyst at 70 °C [42]. Sumathi has reported benzyl alcohol oxidation using perovskite catalysts [43]. A convenient and efficient method for the synthesis of benzaldehyde from benzyl alcohol using ruthenium oxo-complexes has been reported by Seok [44].

1.2. Zeolite encapsulated metal complexes

In catalysis the primary goal is to promote reactions that have high selectivity with high yields. Site isolation of the active centres by bonding to the support is a convenient method to achieve high selectivity. This procedure stabilizes the complex species and makes them act as heterogeneous solid catalysts for liquid phase oxidation [45].

There are several methods of supporting homogeneous catalysts, and such supported catalysts can be classified into the following categories:

i. supported liquid phase catalysts
ii. catalysts anchored on functionalised solids
iii. polymerized complexes
iv. tethered or grafted complexes
v. intercalated catalysts, and
vi. encapsulated catalysts.

Of these, the present study employs the method of encapsulation. Many desired effects in catalysis that can be realized neither by homogeneous systems nor by conventional heterogeneous systems can be achieved by encapsulating complexes in zeolite pores. Heterogenised homogeneous catalysis has emerged as a method having the advantages of both homogeneous catalysis (specificity and activity) and heterogeneous catalysis (easy removal of catalyst) [46]. Such catalysts are regarded as *third generation catalysts*.

Metal complexes immobilized in zeolite super cages are found to have almost the same activity or more as compared to free complexes in solution. Because of size restriction, the complex stays in the zeolite and cannot diffuse out. This provides a route for dispersing the complexes in the solid structure. The main objective is to improve the stability of the complex by reducing dimerisation or aggregation of the complex. Zeolite encapsulated complexes are now commonly used as active catalysts in a wide range of chemical reactions [47-77].

1.2.1. Zeolites

Discovered by the Swedish mineralogists Cronstedt in 1756 [78] zeolite crystals contain water, which was found to be lost when heated. This led Cronstedt to call the mineral 'zeolite,' which in Greek means 'boiling stone.' There is another story, which is contrary to the popular belief that he named them after the Greek words meaning boiling stone. According to this story Zeolite was named after Cronstedt's dog that dug up the rocks when it went out for a walk. Zeolite is a Swedish word meaning 'dog.' The story goes on to say that the first zeolite identified was called 'stilbite,' because his dog was still biting it when he got home. Later it was noted that zeolites showed the properties of reversible water loss [79]. Chabazite was found to have the ability to ion exchange and differentially absorb molecules. Several workers in the 1800's noted the ability of zeolite to remove odour from air [80]. During the period 1930 – 32 Mc Bain in his studies on zeolites observed their capacity to absorb small molecules from large ones, just like a sieve. Hence the name 'molecular sieves' was given to zeolites. This sieving activity is possible because zeolites are micro porous, highly crystalline substances. These zeolites have an internal structure that can be easily tailored to absorb any number of species.

The industrial use of zeolites as catalysts and molecular sieves started after Barrer's pioneering work in the early 1940's. This prompted chemists to seek synthetic methods for the preparation of pure zeolites. Ever since, many synthetic species have been reported, and most of them are without any natural counterparts. More than 150 framework structures have been reported so far. These micro porous solids are found to occupy a prominent place in the landscape of solid state and material science, heterogeneous catalysis and clean technology. The first reported synthetic zeolite was Linde A. This was synthesized in 1949 by Milton, working at Union Carbide. This was found to have the formula

$$M_{x/m}\,[Al_xSi_{(1-x)}O_2].\,nH_2O$$

where M is a cation of valency m.

In the 1950's it was observed that zeolite based catalysts, especially those containing rare earth ions and protons, possessed activity much greater than that of conventional silica - alumina catalysts for cracking hydrocarbons. The economic success of synthetic zeolites, particularly as catalysts, prompted scientists to seek alternative sources of their natural counterparts. The shape selectivity of the materials further enhanced their chemical usefulness. Great efforts were made to find new molecular sieves, with tunable properties, altered / tailored structures, or chemical composition. Crystalline faujasites were synthesized in the 1960's. The synthesis of the pentasil family of zeolites, ZSM-5, and ZSM-11 was also reported. These zeolites function in a shape selective manner in certain alkylation, isomerization, and dehydrative syntheses as well as in a variety of delicate molecular separations [81].

In the early 1980's there emerged a new, large, family of micro porous aluminophosphates (ALPO's) [82]. There are many ALPO's or MAPO's (frame work substituted metal alumino phosphates where M could be Mg, Mn, Co, Fe, etc.) that exhibit framework structures that are the same as those of either natural or synthetic zeolites. In the early 1980's Italian workers discovered that Ti (IV) ions isomorphously substituted for Si (IV) in open framework, yielded T S-1 and T S-2 zeolites [81]. They show high activity and selectivity in oxidation reactions. Another novel open structure titanosilicate ETS-10 was synthesized later [83]. Isomorphous substitution of Si^{4+} by Al^{3+} or Ga^{3+} is an important way to modify zeolite properties and is of much interest in zeolite chemistry [84].

The recent productions of mesoporous siliceous solids have opened up a new era to pure and applied scientists. MCM-41, a large-pore mesoporous structure was reported by Kresge et al. [85] and Beck et al. [86]. When these are modified by replacing Si with Al or B they act as ideal shape selective catalysts for bulky molecules. With the high surface area and thermal stability of mesoporous

supports, opportunities exist not only for heterogenising homogeneous catalysts but also for assembling biomimetic catalysts.

1.2.2. Classification of zeolites

Zeolites are classified in different ways. They are sometimes classified on the basis of Si/Al ratio. Typical examples of low Si/Al ratio zeolites are A and X, which have Si/Al ratio between 1 and 1.5. Intermediate zeolites Y, L, and erionite have Si/Al ratio between 2 and 5. High Si/Al ratio is seen in ZSM-5, ZSM-11, EU-2, mordenite, ferrierite etc.

Barrer has classified zeolites into three groups based on the difference in their effective pore diameter [87,88]. They are small pore zeolites (eg. Linde A, Chabazite), intermediate pore zeolites (eg. ZSM-5, ZSM-11, EU-2, ferrierite etc.) and large pore zeolites (eg. Linde-L, Zeolite X and Y). Mortier's classification of zeolites is based on secondary building unit (SBU) [89].

1.2.3. Structural aspects of zeolites

Zeolites are members of the tectosilicate family of minerals [84,90-92]. They are highly crystalline, perfect micro porous materials. Structurally the zeolite framework consists of SiO_4 and AlO_4 tetrahedra (TO_4 tetrahedra, where T = Si/Al) joined by shared oxygen bridges forming three-dimensional network. The corner linkages are accomplished through T-O-T bridges. The tetrahedra can arrange themselves in many ways to form different porous crystal structures. Each oxygen is shared between two neighbouring tetrahedra. The tetrahedra (primary building unit) form rings of various sizes, which are linked to form complex units (secondary building units) [93]. Twenty-four tetrahedra (silica and alumina) form a sodalite unit, which is a cubo-octahedron with 24 vertices and consisting of six four member rings (or four faces) and eight six member rings (or six faces). The

sodalite units formed in this way are the basic building units of X and Y. The sodalite unit encloses a cavity known as sodalite cavity or β cage.

Zeolite X and Y are formed by joining of the hexagonal 6 - membered faces of sodalite unit (through D6R). The sodalite units are arranged like the carbon in diamond and generate a large cavity or super cage with 12 -, six and four - faces. Access to the super cage (α - cage) is restricted by a 12 - face or window [94]. The α cage has a diameter of 13 Å and cage mouth opening of about 7 - 8 Å, while the β cages have a diameter of 6.6 Å and an aperture of 2.2 Å. In the case of zeolite Y, 4 small windows open into the 13 Å super cage. The Si/Al ratio of zeolite X is ~ 1.25 while that of zeolite Y is ~ 2.5. The unit cell formula and other characteristics of X and Y zeolites are given in Table 1.1.

Silicon can take four oxygen atoms around it in a tetrahedral combination maintaining electrical neutrality. When a trivalent aluminium atom is similarly bound to 4 oxygen atoms, the resultant aluminium tetrahedron will have a negative valency. The net negative charge on the lattice is counterbalanced by exchangeable cation at the following well-defined sites [95]: centre of D6R (Site I), inside of β - cage adjacent to D6R (Site I'), near the single - ring, but outside the sodalite in the large cavity (Site II), inside the sodalite cage at the centre of single-6–ring (Site II'), and the wall of the large cavity (12 - ring aperture) (Site III). The presence of aluminium in the zeolite framework has several effects like introduction of an electrical field (this makes the zeolite more hydrophilic), introduction of catalytic centers, introduction of ion–exchange properties and lowering the thermal stability of the zeolite.

Crystalline aluminosilicates are thermally and hydrothermally stable because of the structure resulting from the interconnection of Si and Al tetrahedra through the oxygen bridges. The stability increases as Si/Al ratio in the structure increases. The zeolite structure remains stable at temperatures as high as 700 °C [96].

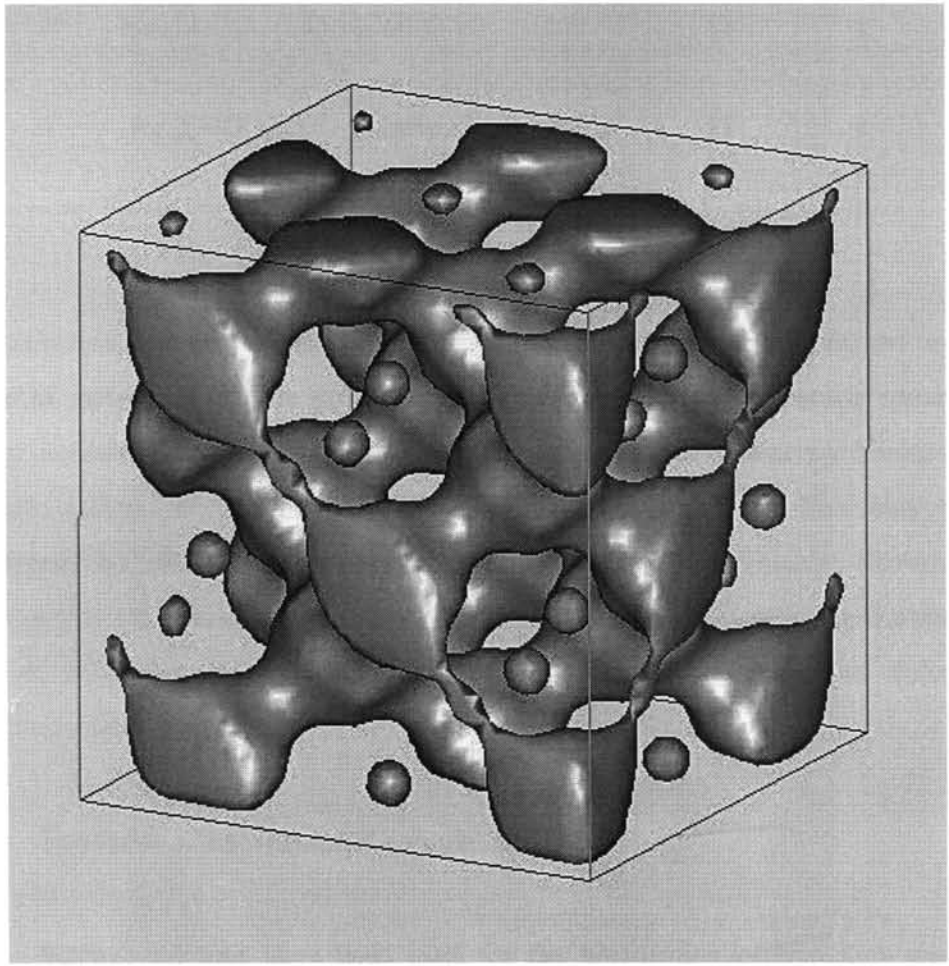

Figure 1 The cavity and channel structure of zeolite Y

Table 1.1 Properties of zeolites X and Y

Zeolite	Unit cell formula	Mole ratio SiO_2/Al_2O_3	α cage Diameter (Å)	β cage Aperture (Å)
X	$Na_{86}(AlO_2)_{86}(SiO_2)_{106}\ nH_2O$	25:1	13	8
Y	$Na_{56}(AlO_2)_{56}(SiO_2)_{136}\ nH_2O$	5:1	13	8

This structural diversity of the zeolites discussed above is responsible for the wide range of interesting zeolite properties such as ion exchange capacity, specific absorption behaviour, catalytic activity due to acidity, shape selectivity caused by the size and polarity of molecules, thermal stability, and wide flexibility for adjustment by isomorphous substitution of framework constituents. However, these porous materials present some specific limitations in catalytic applications, such as pore plugging, poisoning, migration, leaching, and structural defects involving guests in general.

1.2.4. Synthesis of encapsulated complexes

Several methods have been used for the preparation of transition metal complexes in the zeolite matrix.

1.2.4.1. Flexible ligand method

This idea was first introduced by Herron to prepare Co-SALEN complexes in the supercages of faujasite [97]. This method takes advantage of the flexibility of the ligand which enables it to enter the cavities of the zeolite host material through the restricting windows. The SALEN is able to enter the pores of zeolite

due to possible free rotation around the carbon-carbon sigma bond which connects two salicylidene moieties of the ligand. The ligand gets access to larger cages where they react with the transition metal ions previously introduced into the lattice. Once the ligand has entered the zeolite cage and complexed with previously exchanged transition metal ions, the complex adopts a square planar configuration, which is unable to escape from the zeolite void. Later on SALEN complexes with Mn(II) [98], Fe(III) [99], Rh(II) [100], and Pd(II) [101] were synthesized within zeolite cages.

Research in this field continued with variations in transition metal ion as well as the structure of the Schiff base ligands [98,102]. The resulting compounds have been shown to act as oxygen carriers mimicking hemoglobin and also as selective oxidation catalysts [97,103]. This same synthetic method was used for the preparation of complexes of transition metal ions with bipyridine. By adjusting the ligand to metal ion ratio and the temperature of synthesis highly selective bis- or tris- coordination complexes were synthesized [104,105]. These encapsulated complexes were found to exhibit good catalytic activity [106]. Cr(III), Fe(III), Bi(III), Ni(II), and Zn(II), complexes of *N,N'*-bis(salicylidene)propane-1,3-diamine encapsulated in zeolite Y were also prepared by the flexible ligand method. The encapsulated materials were found to be active catalysts for the decomposition of H_2O_2 [69].

1.2.4.2. Ship-in–a-bottle synthesis

The ship-in-a-bottle method was first suggested by Romanovsky and coworkers to encapsulate transition metal phthalocyanines in zeolites [107-109]. The first stage in the synthesis is the introduction of metal via ion exchange pre-adsorption of a labile metal complex (such as a carbonyl or a metallocene) followed by reaction with 1,2-dicyanobenzene. This procedure was adopted for the synthesis of phthalocyanine complexes of cobalt, nickel, copper, iron, and manganese [110-116].

This complex was also prepared by heating ion exchanged zeolite with 1,2-dicyanobenzene (DCB) in vacuum at temperature between 250 °C and 350 °C [110]. Complexation takes place according to the stoichiometry given by the following equation

$$M^{2+}Y + 4DCB + H_2O \rightarrow MPcY + \tfrac{1}{2} O_2 + 2H^+$$

The optimum temperature varies with the type of transition metal ion and the structure of the zeolite. The optimum complexation temperature can be determined by differential scanning calorimetry [111,113]. The ion exchanged zeolite used for this was not strongly dehydrated as water acts as an electron source for this process [110].

Another method of ship-in- a- bottle synthesis involves the introduction of the transition metal in zeolite by the absorption of the corresponding carbonyl complex in the zeolite, followed by the synthesis of the phthalocyanine ligand around the transition metal. This can happen in two ways. The carbonyl is first decomposed thermally or photochemically whereby small metal clusters are formed, or a direct ligand exchange of CO by 1,2-dicyanobenzene occurs at low temperatures. The carbonyl route for the reaction is represented by the equation

$$M(CO)_n + Y + 4DCB \rightarrow MPcY + nCO$$

This indicates that no acid sites (no protons) are produced during complex formation. The reaction can be carried out using metallocenes which act as transition metal supplying agents. Here again small amount of water is required for phthalocyanine synthesis.

$$M(Cp)_2 + Y + 4DCB + H_2O \rightarrow MPcY + 2Cpen + \tfrac{1}{2} O_2$$

An advantage of this method is that the zeolite is free from uncomplexed metal species.

Zeolite encapsulated substituted phthalocyanines were also synthesized. The syntheses of intrazeolite tetra-*t*-butyl-substituted iron-phthalocyanines, and perfluorophthalocyanines of iron, cobalt, copper and manganese have been reported [117-120].

The method was used for the preparation of porphyrin type ligands in the supercages of zeolite Y. Nakamura et al. have reported the encapsulation of iron- and manganese- tetramethylporphyrins in zeolite Y [121]. Encapsulation was carried out by refluxing transition metal exchanged zeolite with pyrrole and acetaldehyde in methanol solution. This method was also used for the synthesis of tetraphenylporphyrins from pyrrole and benzaldehyde [122]. The same method has been used for the synthesis of zeolite encapsulated complexes of rhodium. [123,124].

1.2.4.3. Zeolite synthesis method

Zeolite synthesis method is one of the recent methods for synthesizing zeolite encapsulated complexes. In this method, a zeolite structure is synthesized around the pre-formed complex [125]. The transition metal complex has to satisfy the following conditions for this type of synthesis:

- the complex should be stable at the temperature and in the hydrothermal and pH conditions under which zeolite synthesis takes place
- it should be sufficiently soluble in the synthesis medium to enable random distribution of the complex in the synthesis mixture.

The zeolite synthesis method is advantageous in that it requires only mild preparation conditions and it yields well-defined encapsulated metal complexes.

1.2.5. Characterization techniques

A variety of experimental techniques have been developed for the characterization of the catalysts and for tracing the course of catalytic reactions. Characterization of zeolite samples is carried out to get a better understanding of the acid sites, distribution of complex in the host, the degree of complexation, the

influence of host guest interaction on the structure of the complex, the stability of the encapsulated complex compared to that of the neat complex in the solid or in the neat dissolved state, the ability to exhibit free coordination sites for catalysis, absence of surface species, and preservation of zeolite framework even after encapsulation. The techniques used for the characterization of zeolite encapsulated complexes are: chemical analysis, thermal analysis (TG, DTG, DTA), acidity measurements by temperature programmed desorption, x-ray diffraction methods, XPS, ESCA, SEM, TEM, ESR, infrared and Raman spectroscopy, NMR and magic angle spinning nuclear magnetic resonance, Mossbauer spectroscopy, diffuse reflectance spectra, magnetic susceptibility measurement, surface area and pore volume analysis, electrochemical methods (cyclic voltammetry), molecular modelling and simulation. The characterization studies of zeolite encapsulated complexes have been reviewed by Ekloff and Ernst [126].

1.2.6 Zeolites as micro reactors

An elementary molecular catalytic reactor refers to organized and constrained media which provide cavities or/and surfaces to accommodate the substrate molecules and allow chemical reactions to occur [127]. It may contain components which generate a field of molecular interactions, securing the molecular recognition, deciding the specificity of the reaction, and be sufficiently mobile to adapt itself to conditions for a proper mutual orientation of reactants determining the regio- and stereo- selectivity [128].

Like a molecular catalytic reactor the zeolite encapsulated complexes contain active centers composed of one or more transition metal atoms surrounded by appropriate ligands with one or more vacant coordination sites. The intrinsic properties of the active center depend on the number and type of metal atoms, their orbital structure and occupancy, number of vacant coordination sites, and the properties of the ligand. Its extrinsic properties are functions of the type of the support, its type of bonds, its electronic structure as well as structure of the

surface. The net negative charge of the zeolite framework and the distribution of the positive charges of the cations can produce an electric field, which might modify the properties of the molecule in the cage as in a molecular catalytic reactor.

1.2.7. Guest host interactions between complex and support

The influence of zeolite moiety on the structure and reactivity of the encapsulated complex has to be understood to facilitate its use as catalysts in chemical reactions. According to Mochida et al. an isolated metal ion attached to a molecular sieve would be expected to behave quite differently from a metal ion in an ordinary metal oxide [129]. Zeolites with low Si/Al ratios have a great number of compensating cations which will produce high electrostatic fields and field gradients in channels and cavities. The electric field produced could reach up to 6-7 V at distances of a few angstroms from the cation site. Fields of this magnitude in the internal voids of the pores stabilize positive species in a similar way as highly polar, non-nucleophilic solvents do [130]. This is the reason why a variety of organic cations can be easily generated and stabilized inside zeolite [131,132].

The presence of ligands attached to the metal ion can influence the selectivity of metal exchanged zeolites. The topology of the void has an influence on the complex's geometry and can bring about changes in its electronic and magnetic properties. The steric constraints in zeolite may distort the encapsulated complex molecule to induce different stability and reactivity for them. Spectral and electrochemical studies were carried out study the host guest interaction in zeolite encapsulated complexes. These interactions would enhance the catalysis of molecules that are in zeolite pores [133,134].

Dimeric copper acetate and copper chloro acetate encapsulated in zeolite Y catalyse the *o*-hydroxylation of phenol to catechol. The turn-over frequency for phenol conversion increases upon encapsulation. Due to enhanced Cu-Cu binding

upon encapsulation, the strength and lability of Cu-phenolate and Cu-dioxygen bonds are modified by a trans axial ligand effect, which accounts for the enhanced reactivity of the encapsulated complex [135].

Zeolite encapsulated Co(II) , Ni(II), and Cu(II) complexes of 3-formylsalicylic acid were synthesized and used for the catalytic oxidation of benzyl alcohol . Of the three, the Cu(II) complex has remarkable efficiency and is stable enough to be recycled without much deterioration [136].

Comparative study of neat cobalt SALEN complex and the encapsulated cobalt SALEN complex was carried out and marked difference in behaviour was noted. Cobalt SALEN complex within the α cage identified by the reflectance spectrum is almost identical with that in solution. The pyridine adduct of the encapsulated complex shows an affinity for oxygen [97]. The EPR spectrum of this corresponds to the Co(SALEN)(py)(O_2) complex. The formation of peroxodimer in neat complex deactivates it. This is prevented in the zeolite matrix and the oxygen adduct can be dissociated by simple evacuation [137].

Chandra and Ratnasamy have reported the decomposition of hydrogen peroxide using substituted copper SALENS encapsulated in zeolite. The rate of decomposition on using substituted SALENS has been found to come close to that of enzyme catalase [16]. There are further reports by Ratnasamy et al. that encapsulated SALEN compounds act like catalase [138]. Cu-SALEN was used for the decomposition of hydrogen peroxide as well as for the oxidation of phenol and *p*-xylene [139]. Another recent report is by Maurya et al. [69].

Cyclic voltammetric experiments with encapsulated complexes provide information concerning the redox couple near the surface of the zeolite. This highlights the importance of combining electrochemical methods with conventional spectroscopic techniques (IR, UV-VIS and EPR) to assess the differing nature and distribution of the entrapped transition metal complexes [140].

Herron et al. have reported the changes in the properties of nickel carbonyl on encapsulation [141]. Encapsulated species has the formula $Ni(CO)_3$ whereas no such reactive species can exist in solution phase since it is highly reactive. These examples indicate the influence of the zeolite matrix on the stability of the complex.

1.2.8. Zeozymes: encapsulated complexes that mimic enzymes

Enzymes are powerful catalysts in life processes, and are responsible for many complicated chemical reactions in living systems, which would not take place in their absence. An enzyme is composed of a metal complex which acts as the active site embedded in a large protein structure. The shape assumed by the protein knots is determined by the sequence of amino acids making up the protein. The protein part protects active sites from self- destruction and helps to induce selectivity for a particular product. It exhibits high chemo-, regio-, and stereo-selectivities for the specific transformation to take place. There exists a complementary relationship between the active site of the enzyme and the substrate. Zeolite encapsulated complexes exhibit this characteristic feature of enzymes, and so they are called zeozymes. Thus, zeozymes are 'mimics' of enzymes in zeolites [53]. Metal complexes encapsulated inside zeolite cage exhibit enzyme-like activity, the zeolite part protecting the complex and ensuring proper steric environment for the complex and the reaction pathway. The channels and cages in the zeolite framework are similar to those created by the protein structure of natural enzymes [142-144].

Enzyme mimicking involves the building of active centre of enzyme into the matrix which allows a larger operational temperature domain and broader spectrum of solvents. This is because the operational domain of enzyme is narrow as far as temperature and solvents are concerned. This permits the immobilized active part to be used like heterogeneous catalysts in reactors in which the liquid or

gaseous substrate is passed over a solid material. Non-natural metallo-enzymes are studied because of the non-natural activity that may be expected from them. The advantage of such techniques lies in the ease with which the catalyst can be separated from the reactants.

Zeolite encapsulated porphyrin type complexes mimicking enzyme cytochromeP-450 have received the attention of researchers [121,122,145]. Zeolite encapsulated tetraphenyl porphyrins have been synthesized from pyrrole and benzaldehyde. This complex mimics cytochromeP-450, which enhances the selective oxidation of saturated hydrocarbons using hydrogen peroxide as oxidant [136,137]. Several mimics of cytochromeP-450 have been reported [142,146,147]. According to these reports encapsulation prevents the metal complexes from dimerising. Further, the internal channels impose selectivity in the same way as do the channels created by the protein structure of an enzyme.

Another efficient mimic of cytochromeP-450 is iron-phthalocyanine complex encapsulated in zeolite Y which in turn is embedded in polydimethylsiloxane (PDMS) membrane [53]. This is the first zeozyme to be incorporated in PDMS [148,149]. When this catalyst was brought in a membrane set up for the oxidation of cyclohexane with TBHP, a remarkable six fold increase in activity was observed as compared with the best possible experimental set up for nonembedded FePcY. The reason for this effect was the influence of PDMS on the relative amounts of reagents that were sorbed in the zeolite pore. This system is environmentally friendly. When Zn-phthalocyanine zeolite Y incorporated in PDMS was used in the photosensitized oxidation of 1-methyl-1-cyclohexene in ethanol, very high activity was observed [150]. Another zeozyme $[Mn(bpy)_2]^{2+}Y$ was incorporated in PDMS for the epoxidation of olefines. Good catalytic activity was obtained for reagents that diffused easily through the polymer and sorbed well in the zeolite [151]. Zeolite encapsulated Co SALEN is also suggested as synthetic mimic for studying the oxygen binding properties of haemoglobin [97,143]. These adducts show excellent resistance to auto oxidation even at elevated temperatures.

In contrast to haemoglobin, these complexes exhibit negative co-operativity between the cobalt binding sites.

The oxygenase mimicking activity of copper acetate dimers in the regioselective ortho-hydroxylation of L-tyrosine to L-dopa is enhanced on encapsulation in zeolite Y [152]. The spectra of this zeozyme reveals that the Cu-Cu separation in the dimer shortens to 2.4 Å in the encapsulated state from 2.64 Å in the neat complex, providing greater overlap of metal orbitals in the encapsulated stage [137]. The complex catalyzes the *o*-hydroxylation of phenol to catechol. Due to enhanced Cu-Cu binding upon encapsulation, the strength and lability of the Cu-phenolate and Cu-dioxygen bonds are modified by a trans-axial ligand effect. This explains the enhanced reactivity of the encapsulated complex.

Among the different support materials, zeolites are the obvious choice for anchoring metal complexes. Their pore diameter and pore geometry introduce size and shape selectivity in reaction. The advantage of enzyme catalysis is that it facilitates reactions in mild conditions. They work well in dilute aqueous solutions and at moderate temperature, pressure and pH, and provide energy-efficient routes for carrying out a particular reaction. The reactions catalyzed are by and large environmentally friendly in that by-products and waste materials are a minimum. The catalysts and the materials they synthesize are generally biodegradable. The desire to exploit the enzyme-like property of zeozymes has prompted researchers to synthesize complex molecules embedded in inorganic molecules so that they can be employed in synthetically useful reactions.

1.3. Scope of the present study

Selective oxidation reactions are of prime importance in the synthesis of fine chemicals and a variety of other processes in chemical industry. Transition metal complexes often serve as effective catalysts in selective oxidation reactions. But neat transition metal complexes have drawbacks, as they show loss in activity

and difficulty of separation, and necessitate expensive regeneration processes. It is possible to enhance the activity, selectivity, stability, and ease of separation of a transition metal complex and reduce the regeneration cost by encapsulating it in a zeolite support. The zeolite supports are known to play an important role in dispersing the active metal complex and influencing its electronic and adsorption properties, thereby changing the catalytic properties.

The present study was undertaken with a view to

- synthesizing and characterizing new zeolite encapsulated complexes which might work as good eco-friendly catalysts;
- examining the effect of the zeolite framework on the structure and geometry of the complex;
- making a comparative study of the neat complexes and zeolite encapsulated complexes as catalysts;
- assessing the catalytic activity of the synthesized complexes in
    - (i) the decomposition of hydrogen peroxide
    - (ii) the selective hydroxylation of phenol to hydroquinone, and
    - (iii) the partial oxidation of benzyl alcohol to benzaldehyde;
- substituting aqueous hydrogen peroxide as oxidant in place of organic oxidants / concentrated hydrogen peroxide, thus making use of a clean, safe, and enviro-economic system;
- examining the correlation between the activity and the structure of the complex;
- assessing the shape-selective effect of the catalysts;
- studying the reaction by varying the different parameters; and
- verifying the poison resistance and recyclability of the catalysts.

With these objectives, some new zeolite encapsulated complexes of iron(III), cobalt(II), cobalt(III), nickel(II), copper(II) and palladium(II) were

synthesized and characterized. The ligands used for the preparation of the complexes were:

1) 2-styrylbenzimidazole (SB)

2) morpholine-*N*-carbodithioate (MDTC)

3) *N*-ethyl-*N*-phenyl dithiocarbamate (EPDTC)

4) *di*-iso-propyl dithiocarbamate (IPDTC)

5) dimethylglyoxime (DMG)

6) salicylaldehyde semicarbazone (SALSC)

7) *N,N'*-bis(3-pyridylidene)-1,2-phenylenediamine (SPO)

8) *N,N'*-bis(3-pyridylidene)-1,4-phenylenediamine (SPP)

Some of the encapsulated complexes of copper and palladium are found to be active catalysts for the decomposition of hydrogen peroxide, hydroxylation of phenol to hydroquinone, and the partial oxidation of benzyl alcohol to benzaldehyde. Further advantages of these catalysts are the easy separation of the catalyst, possibility of recycling and amenability to continuous processing.

References

1. P. Baumeister, M.Studer, and F. Roessler in *Handbook of Heterogeneous Catalysis*, Vol. 5, G. Ertl, H. Knözinger, and J. Weitkamp (Eds.), Wiley-VCH, New York, 1997, 2252.
2. R.A. Sheldon, *Catal. Today* 1, 5 (1987) 351.
3. P.A. Sermon, Y. Sun, and K.M. Keryon, *Catal. Today 17* (1993) 391.
4. C.D. Wood and P.E. Garrou, *Organometallics* 3 (1984) 170.
5. T.D. Manly, *Chem. Ind.* London (1962) 12.
6. J.P. Schirmann and S.Y. Delavarenne, *Hydrogen Peroxide in Organic Chemistry*, Information Chimie, Paris, 1979.
7. J.H. Baxendale, *Adv. Catal.* 4 (1952) 31.
8. E. Tsuchida and H. Nishide, *Adv. Polym. Sci.* 24 (1977) 1.
9. R. Sreekala and K.K Mohammed Yusuff, *Ind. J. Chem.*, 34A (1995) 994.
10. H. Sigel, *Angew. Chem.* 81 (1969) 161.
11. H. Sigel, *Angew. Chem., Int. Ed. Engl.* 8 (1969) 167.
12. P. Jones and I. Wilson, *Met. Ions Biol. Syst.* 7 (1978) 185.
13. J. Schubert, V.S. Sharma, E.R. White, and L.S. Bergelson, *J. Am. Chem. Soc.* 90 (1968) 4476.
14. J. Schubert and V.S. Sharma, *Proc. Int. Conf. Coord. Chem., 11th* (1968) 19.
15. V.S. Sharma and J. Schubert, *Inorg. Chem.*, 10, 2 (1971) 251.
16. Chandra R. Jacob, Saji P. Varkey, and Paul Ratnaswamy, *Appl. Catal. A* 168, 2 (1998) 353.
17. Jayendra Patole, Sabari Dutta, Subhash Padhye, and Ekkehard Sinn, *Inorg. Chim. Acta* 318 (2001) 207.
18. M. Krajnem and J. Lever, *Appl. Catal. B.* 3, 2–3 (1994) 101.
19. C.E.K. Mees, *The Theory of the Photographic Processes*, Vol. 33, Macmillan, New York, 1942.
20. F. Bourdin, M. Costantini, M. Jouffret, and G. Latignan, Ger. Patent 2 064 497, 1971.
21. G.A. Hamilton, J. P. Friedman, and P.M. Campbell, *J. Am. Chem. Soc.* 88 (1966) 5266.
22. K. Hotta, S. Tamagaki, Y. Suzuki, and W. Tagaki, *Chem. Lett.* (1981) 789.
23. S. Tamagaki, M. Sasaki, and W. Tagaki, *Bull. Chem. Soc. Jpn.* 62 (1989) 153.
24. I. Yu Litivinsev, Yu V. Mitnik, A. I. Mikhailyuk, S. V. Timofeev, and N. V. Sapunov, *Kinet. Katal. (I)* 34 (1993) 56.
25. P. Maggioni, US Patent 391 432, 1975.
26. P. Maggioni and F. Minisci, *Chim. Ind.* 59 (1977) 239.
27. P. Maggioni, US Patent 3 929 913, 1975.
28. D.R.C. Huybrechts, I. Vansen, H.X. Li, and P.A. Jacobs, *Catal. Lett.* 8 (1991) 237.

29. S. Lin, Y. Zhen, S.M. Wang, and Y.M. Dai, *J. Mol. Catal.* 156 (2000) 113.
30. U. Romano, A. Esposito, F. Maspero, C. Neri, and M.G. Clerici, *Stud. Surf. Sci. Catal.* 55 (1990) 33.
31. C.D. Chang and S.D. Hellring, US Patent 4 578 521, 1986.
32. Felipe Alagarra, M Alexandra Esteves, Vincente Fornes, Herminegildo Garcia, and Jalme Primo, *New J. Chem.* (1998) 333.
33. Rolfe Fricke, Hendrik Kesslick, Günter Lischke, and Manfred Richter, *Chem. Rev.* 100 (2000) 2303.
34. H.S. Bloch, US Patent 3 580 956, 1971.
35. A. Tuel, S.M. Khouzami, Y.B. Taarit, and C. Naccache, *J. Mol. Catal.* 68 (1991) 45.
36. J.A. Martens, P.H. Buskens, P.A. Jacobs, A. van der Pol, J.H.C. van Hooff, C. Ferrini, H.W. Kouwenhoven, P.J. Kooyman, and H. van Bekkum, *Appl. Catal. A* 99 (1993) 71.
37. A. Esposito, M.Taramasso, and C. Neri, US Patent 4 396 783, 1983.
38. A. Esposito, M.Taramasso, C. Neri, and F. Buonomo, British Patent 2 116974, 1985.
39. J.E. Bäckvall, A.K. Aswathi, and Z.D. Renko, *J. Am. Chem. Soc.* 109 (1987) 4750.
40. J.E. Bäckvall, *Stud. Surf. Sci. Catal.* 41 (1988) 105.
41. J.E. Bäckvall, R.B. Hopkins, H. Grennberg, M. Mader, and A.K. Aswathi, *J. Am. Chem. Soc.* 112 (1990) 5160.
42. A.Puzari, L. Nath, and Jubaraj B. Baruah, *Ind. J. Chem.* 37 A (1998) 723.
43. R. Sumathi, K. Johnson, B. Viswanathan, and T.K. Varadarajan, *Ind. J. Chem.* 38 A (1999) 40.
44. Won K. Seok, *Bull. Korean Chem. Soc.* 20, 4 (1999) 395.
45. A. Corma and H. Garcia, *Chem Rev.* 102 (2000) 3837.
46. J.C. Bailar, Jr., *Cat. Rev. Sci. Eng.* 10 (1974) 17.
47. T. Joseph, D.P. Sawant, C.S. Gopinath, and S.B. Halligudi, *J. Mol. Catal.*184, 1-2 (2002) 289.
48. A. Kozlov, A. Kozlova, K. Asakura, and Y. Iwasawa,. *J. Mol. Catal.* 137, 1-3 (1999) 223.
49. J.M. Sabater, A. Corma, A. Domenech, V. Fornes, and H. Garcia, *Chem. Commun.* 14 (1997) 1285.
50. B. Fan, R. Li, W. Fan, J. Cao, and Z. Bing, *J. Natural Gas Chemistry* 9, 2 (2000) 157.
51. S.A. Chavan, D. Srinivas, and P. Ratnasamy, *Chem. Commun.* (Cambridge, United Kingdom) 12 (2001) 1124.
52. S.N. Rao, K.N. Munshi, and N.N. Rao, *J. Mol. Catal.* 145, 1-2 (1999) 203.
53. R.F. Parton, Ivo F.J. Vankelecom, M.J.A. Casselman, C.P. Bezoukhanova, J.B. Uytterhoeven, and P.A. Jacobs, *Nature* 370 (1994) 541.
54. Agnes Zsigmond, Ferenc Notheisz, and J.E. Bäckvall , *Catal. Lett.* 65, 1-3 (2000) 135.
55. T. Kimura, A. Fukuoka, and M. Ichikawa, *Catal. Lett.* 4, 4-6 (1990) 279.
56. S. Seelan, D. Srinivas, M.S. Agashe, N.E. Jacob, and S. Sivasankar, *Stud. Surf. Sci. Catal.* 135 (2001) 2224.

57. R. Raja and P. Ratnasamy, *Stud. Surf. Sci. Catal.* 105 (1997) 1037.
58. M. Ichikawa, T. Kimura, and A. Fukuoka, *Stud. Surf. Sci. Catal.* 60 (1991) 335.
59. N. Herron, *J. Coord. Chem.* 19 (1988) 25.
60. R. Raja and P. Ratnasamy, *Stud. Surf. Sci. Catal.* 101 (1996) 181.
61. R. Raja, Chandra R. Jacob, and Paul Ratnasamy, *Catal. Today* 49, 1-3 ((1999)171.
62. Chris Bowers and Prabir K. Dutta, *J. Catal.* 122, 2 (1990) 271.
63. Saji P. Varkey, Chandra Ratnasamy, and Paul Ratnasamy, *J. Mol. Catal.* 135, 3 (1998) 295.
64. Saji P. Varkey and Chandra R. Jacob, *Ind. J. Chem.* 37A, 5 (1998) 407.
65. I.W.C.E. Arends, Pellizon M. Birelli, and R.A. Sheldon, *Stud. Surf. Sci. Catal.* 110 (1997) 1031.
66. R. Raja and P. Ratnasamy, *Catal. Lett.* 48 (1997) 1.
67. K.J. Balkus, Jr., A.K. Khanmamedova, M.K. Dixon, and F. Bedioui, *Appl. Catal.A* 143, 1 (1996) 159.
68. Trissa Joseph, C.S. Sajanikumari, S. Deshpande, and S. Gopinathan, *Ind. J. Chem.* 38A, 8 (1999) 792.
69. M.R. Maurya, S.J.J. Titinchi, S. Chand, and I.M. Mishra, *J. Mol. Catal.*180, 1-2 (2002) 201.
70. Saji P. Varkey and Chandra R. Jacob, *Ind. J. Chem.* 38A, 4 (1999) 320.
71. P.P. Knops-Gerrits, D.E De Vos, F. Thibault-Starzyk, and P.A. Jacobs, *Nature* 369 (9194) 543.
72. P.P. Knops-Gerrits, F. Thibault-Starzyk and P.A. Jacobs, *Stud. Surf. Sci. Catal.* 84 (1994) 1411.
73. A.W. vande Made, J.W.H. Smeets, R.J.M. Nolte, and W. Drenth, *J. Chem. Soc., Chem. Commun.* (1983) 1204.
74. R. Grommen, P.Manikandan, Y. Gao, T. Shane, J.J. Shane, R.A. Schoonheydt, B.M. Weckhuysen, and D. Goldfarb, *J. Am. Chem. Soc.* 122 (2000) 11488.
75. T. Tatsumi, M. Nakamura, and H. Tominaga, *Catal. Today* 6 (1989) 163.
76. S.B. Ogunwumi and T. Bein, *Chem. Commun.* (1997) 901.
77. T. Joseph, S.B. Halligudi, C. Satyanarayanan, D.P. Sawant, and S. Gopinathan, *J. Mol. Catal.* 168, 1-2 (2001) 87.
78. A.F. Cronstedt, *Akad. Handl.* 17 (1756) 120.
79. M.A. Damour, *Ann. Chimie.* 3, 53 (1858) 438.
80. I.G. Kovzun, Y.I. Tarasevich, Y.V. Maslyakevich, and A.I. Zhukova, *Ukr. Khim. Zh.* 43 (1977) 247.
81. John Meurig Thomas, Osamu Terasaki, L. Pratibha Gai, Wuzong Zhou, and Jose Gonzalez – Calbet, *Acc. Chem. Res.* 34 (2001) 583.
82. S.T. Wilson, B.M. Lok, C.A. Messina, I.R. Cannan, and E.M. Flanigen, *J. Am. Chem. Soc.* 104 (1982) 1145.
83. M.W. Anderson, O. Terasaki, T. Ohsuna, I. Philippou, S.P. Mackay, J. Rocha, and S. Lidin, *Nature* 367 (1994) 347.
84. J. Dwyer and K. Karim, *J. Chem. Soc., Chem. Commun.* (1991) 905.
85. C.T. Kresge, M.E. Leonowicz, W.J. Roth, J.C. Vartuli, and J.S. Beck,

Nature 359 (1992) 710.
86. J.S. Beck, J.C. Vartuli, W.J. Roth, M.E. Leonowicz, C.T. Kresge, K.D. Schmidt, C.T.W. Chu, D.H. Olson, E.W. Sheppard, S.B. Mc Cullen, J.B. Higgins, and J.L. Schlenker, *J. Am. Chem. Soc.* 114 (1992) 10834.
87. R.M. Barrer, *Hydrothermal Chemistry of Zeolites*, Academic Press, New York, 1982.
88. R.M. Barrer, *Hydrothermal Chemistry of Zeolites,* Academic Press, London, 1983.
89. W.J. Mortier, *Compilation of Extra Framework Sites in Zeolites*, Butterworths, London, 1982.
90. R.M. Barrer, *Zeolites and Clay Minerals as Sorbents and Molecular Sieves*, Academic Press, London, 1978.
91. J.V. Smith, *Adv. Chem. Ser.* 101 (1971) 171.
92. J.V. Smith, *Chem. Rev.* 88 (1988) 149.
93. J.A. Rabo, *Zeolite Chemistry and Catalysis, ACS Monograph 171*, American Chemical Society, Washington DC, 1976.
94. Young Hoon Yeom, Yang Kim, Seung Hwan Song, and Karl Seff, *J. Phys. Chem.* 101 (1997) 2140.
95. P.G. Menon , in *Lectures on Catalysis,* 41st Annual Meeting, Ind. Acad. Sci., S. Ramasheshan (Ed.) 43, 1975.
96. A. Corma and Augstin Martinez, *Adv. Mater.* 7, 2 (1995) 137.
97. N. Herron , *Inorg. Chem.* 25 (1986) 4714.
98. C. Bowers and P.K. Dutta, *J. Catal.* 112 (1990) 271.
99. L. Gaillion, N. Sajot, F. Bedioui, J. Devynck, and K.J. Balkus, Jr., *J. Electroanal. Chem.* 345 (1993) 157.
100. K.J. Balkus, Jr., A.A. Welch, and B.E. Gnade, *Zeolites* 19 (1990) 722.
101. S. Kowalak, R.C. Weiss, and K.J. Balkus, Jr., *J. Chem. Soc., Chem. Commun.* (1991) 57.
102. F. Bedioui, L. Roue, J. Devynck, and K.J. Balkus, Jr., *Stud. Surf. Sci. Catal.* 84 (1994) 917.
103. D.E. De Vos, F. Thibault-Starzyk, and P.A. Jacobs, *Angew. Chem. Int. Ed. Engl.* 33 (1994) 432.
104. W.H. Quale, G. Peeters, G.L. De Roy, E.F. Vansant, and J.H. Lunsford, *Inorg. Chem.* 21 (1982) 2226.
105. W. De Wilde, G. Peeters, and H. Lunsford, *J. Phys. Chem.* 84 (1980) 2306.
106. P.P. Knops-Gerrits, D.E. De Vos, F. Thibault-Starzyk, and P.A. Jacobs, *Nature* 369 (1994) 543.
107. B.V. Romanovsky, in *Proc. 8th Int. Congr. Catal.,* Vol. 4, Verlag Chemie, Weinheim 1984, 657.
108. V.Y.Zakharov and B.V. Romanovsky, *Vest. Mosk.Univ., Ser. 2 Khim.*, 18 (1977) 142.
109. B.V. Romanovsky and A.G. Gabrielov, *J. Mol. Catal.* 74 (1992) 293.
110. G. Meyer, D. Wöhrle, M. Mohl, and G. Schulz-Ekloff, *Zeolites* 4 (1984) 30.
111. K.J. Balkus, Jr., and J.P. Ferraris, *J. Phys. Chem.* 94 (1990) 8019.
112. E. Páez-Mozo, N. Gabriunas, F. Lucaccioni, D.D. Acosta, P. Patrono, A. La

Ginestra, P. Ruiz, and B. Delmon, *J. Phys. Chem.* 97 (1993) 12819.
113. J.P. Ferraris, K.J. Balkus, Jr., and A. Schade, *J. Incl. Phenom.* 14 (1992) 163.
114. N. Herron, G.D. Stucky, and C.A. Tolman, *J. Chem. Soc., Chem. Commun.* (1986) 1521.
115. T. Kimura, A. Fukuoka, and M. Ichikawa, *Catal. Lett.* 4 (1990) 279.
116. Ziqi Jiang and Zuwei Xi, *Fenzi Cuihua* 6, 6 (1992) 467.
117. M. Ichikawa, T. Kimura, and A. Fukuoka, *Stud. Surf. Sci. Catal.* 60 (1991) 335.
118. A.G. Gabrielov, K.J. Balkus, Jr., S.L. Bell, F. Bedioui, and J. Devynck, *Microporous Materials* 2 (1994) 119.
119. F. Bedioui, L. Roué, L. Gaillion, J. Devynck, S.L. Bell, and K.J. Balkus, Jr., *Preprints Div. of Petroleum Chemistry,* ACS 38, 3 (1993) 529.
120. K.J. Balkus, Jr., A.G. Gabrielov, S.L. Bell, F. Bedioui, L. Roué, and J. Devynck, *Inorg. Chem.* 33 (1994) 67.
121. M. Nakamura, T. Tatsumi, and H. Tominaga, *Bull. Chem. Soc. Jpn.* 63 (1990) 3334.
122. Y.W. Chan and R.B. Wilson, *Preprints Div. of Petroleum Chemistry*, ACS 33, 3 (1988) 453.
123. J. Wöltinger, J.E. Bäckvall, and A. Zsigmond, *Eur. Chem. J.* 5 (1999) 2084.
124. Ágnes Zsigmond, Krisztián Bogár, and Ferenc Notheisz, *J. Catal.* 213 (2003) 103.
125. L.A. Rankel and E.W. Valyocsik, US Patent, 4 500 503, 1985.
126. G. Schulz-Ekloff and S. Ernst in *Handbook of Heterogeneous Catalysis* Vol. 1, G. Ertl, H. Knözinger, and J. Weitkamp (Eds.), Wiley-VCH, New York, 1997, 374.
127. Chen-Ho Tung, Li-Zhu Wu, Li-Ping Zhang, and Bin Chen, *Acc. Chem. Res.* 36 (2003) 39.
128. J. Haber, *Pure and Appl. Chem.* 66, 8 (1994) 1597.
129. Isao Mochida, Akio Kato, and Tetsuro Seiyama , *Bull. Chem. Soc. Jpn.* 45 (1972) 2230.
130. A. Maldotti, A. Molinari, and R. Amadelli, *Chem. Rev.* 102 (2002) 3811.
131. X.Z. Qin and A.D. Trifunac, *J. Phys. Chem.* 94 (1990) 4751.
132. K.B. Yoon, *Chem. Rev.* 93 (1993) 321.
133. B.V. Romanovsky, V.Y. Zakharov, and T.G. Borisava, *Moscow Univ. Publ.* (1982) 170.
134. J.H. Lunsford, *Catal. Rev. -Sci. Eng.* 12 (1975) 137.
135. S. Chavan, D. Srinivas, and P. Ratnasamy, *J. Catal.* 192, 2 (2000) 286.
136. K.O. Xavier, J. Chacko, and K.K. Mohammed Yusuff, *J. Mol. Catal.* 178, (2002) 275.
137. G.A. Ozin and Caroline Gil, *Chem. Rev.* 89 (1989) 1749.
138. Chandra R. Jacob, Saji P. Varkey, and Paul Ratnasamy, *Appl. Catal. A* 168 (1998) 353.
139. S. Deshpande, D. Srinivas, and P. Ratnasamy, *J. Catal.* 188, 2 (1999) 261.
140. A. Domenech, P. Formentin, H. Garcia, and M.J. Sabater, *European J. Inorg. Chem.* 6 (2000) 1339.

141. N. Herron, G.D. Stucky, and C.A. Tolman, *Inorg. Chim. Acta.* 100 (1985) 135.
142. N. Herron, *New J. Chem.* 13 (1989) 761.
143. N. Herron, *Chem. Tech.* Sept. (1995) 542.
144. D.E. De Vos, F. Thibault-Starzyk, P.P. Knops-Gerrits, R.F. Parton, and P.A. Jacobs, *Macromol. Symp.* 80 (1994) 157.
145. J.T. Groves and T.E. Nemo, *J. Am. Chem. Soc.* 105 (1983) 5786.
146. N. Herron and C.A. Tolman, *J. Am. Chem. Soc.* 109 (1987) 2837.
147. R.F. Parton, L. Uytterhoeven, and P.A. Jacobs, *Stud. Surf. Sci. Catal.* 59 (1991) 395.
148. Ivo F.J. Vankelecom, R.F. Parton, J.A.C. Mark, J.B. Uytterhoeven, and P.A. Jacobs, *J. Catal.* 163 (1996) 457.
149. Ivo F.J. Vankelecom, *Chem. Rev.* 102 (2002) 3779.
150. F.M.P.R. van Laar, F. Holsteyns, I.F.J. Vankelecom, S. Smeets, W. Dehaen, and P.A. Jacobs, *J. Photochem. Photobiol. A. Chem.* 144 (2001) 141.
151. R.F. Parton, I.F.J. Vankelecom, D. Tas, K. Janssen, P.P. Knops-Gerrits, and P.A. Jacobs, *J. Mol. Catal.* 113, 1-2 (1996) 283.
152. S. Chavan, D. Srinivas, and Paul Ratnasamy, *Topics in Catalysis* 11/12, 1-4 (2000) 359.

Chapter 2

Materials and methods

2.1. Introduction

This chapter presents details of reagents and other materials used in the present study. It describes the methods used for the synthesis of ligands, simple complex, metal exchanged zeolite Y, and zeolite Y encapsulated complexes. The various physico-chemical methods employed for the characterisation of the zeolite Y encapsulated complexes are discussed. Details of the different instruments and methods used for the study of the catalytic activity of the compounds prepared are also given.

2.2. Reagents

The following metal salts were used: $Fe(NO_3)_3$ $9H_2O$ (S.D. Fine. Chem. Ltd. GR); $CoCl_2$ $6H_2O$ (E. Merck, GR); $NiCl_2$ $6H_2O$ (E. Merck, GR); $CuCl_2$ $2H_2O$ (E. Merck, GR); $PdCl_2$ (SRL GR); NaCl (E. Merck , GR).

Zeolite Y with a Si/Al ratio 2.4 and particle density 2.5 x 10^3 kg/m^3, obtained from Sud-Chemie India Ltd., Binanipuram, Kochi, was used as support. Dimethylglyoxime (E. Merck); salicylaldehyde (E. Merck); ethylene glycol (Aldrich); semicarbazide hydrochloride (Loba Chemie Pvt. Ltd.); pyridine-3-carboxaldehyde (E. Merck); *o*-phenylenediamine (BDH); *p*-phenylenediamine (CDH); cinnamic acid (Aldrich); carbon disulphide (CDH); *N*-ethylaniline (E. Merck); morpholine (SRL) ; *di*-iso-propylamine (Riedel-De Haen AG Seelz-Hannover) were used for the syntheses of ligands.

Hydrogen peroxide (30% w/v, E. Merck), benzyl alcohol (SRL) and phenol (Nice Chemicals Pvt. Ltd.) were used for catalytic studies on simple and supported complexes. Unless otherwise specified, all reagents used were of analytical reagent grade. The solvents used were either of 99% or purified by known laboratory procedures.

Liquid nitrogen (Sterling gases, Kochi) was used for surface area measurements. Air, nitrogen, and hydrogen gas cylinders (Sterling gases, Kochi) were used for catalytic studies.

2.3. Synthesis of ligands

2.3.1. Preparation of dimethylglyoxime (DMG)

Dimethylglyoxime was purified by recrystallising it from methanol. The pure crystals were dried over anhydrous calcium chloride.

2.3.2. Synthesis of 2-styrylbenzimidazole (SB)

Styrylbenzimidazole was prepared following the procedure suggested by Dubey and Ramesh [1]. The synthesis was carried out in two stages. Details of the preparation are given below.

a) Preparation of *o*-phenylenediamine dihydrochloride

A solution containing concentrated hydrochloric acid (60 ml), water (40 ml) and $SnCl_2$ (2 g) was prepared, and *o*-phenelenediamine was added to it. To this solution decolourising carbon was added and it was heated to boiling. The solution was filtered, and concentrated hydrochloric acid was added to it. Finally it was cooled in freezing mixture. The crystals that separated were filtered, washed with hydrochloric acid, and dried in a vacuum desicator over sodium hydroxide [2].

b) Synthesis of styrylbenzimidazole

A mixture of *o*-phenylenediamine dihydrochloride (1.81g, 10mmoles) and cinnamic acid (1.48 g, 10 mmoles) in ethylene glycol (10ml) was refluxed for 5

hours. The reaction mixture was cooled to room temperature and poured into water (100ml). The solid separated was filtered, washed with water, dried, recrystallised using methanol, and finally dried over anhydrous $CaCl_2$ [1].

2.3.3. Synthesis of carbodithioate and dithiocarbamates

Morpholine-*N*-carbodithioate (MDTC), *N*-ethyl-*N*-phenyldithiocarbamate (EPDTC) and *di*-iso-propyldithiocarbamate (IPDTC) were synthesized using the following procedure [3]. Sodium hydroxide (20g, 0.5moles) and the amine (morpholine, *di*-iso-propylamine, or *N*-ethylaniline) (0.5mole) were mixed together in a 500ml two-necked flask. This was cooled in a freezing mixture of ice and salt. Carbon disulphide (31ml, 0.5moles) was added drop-wise from a separating funnel, stirring the mixture using an electric stirrer. The addition was carried out very slowly, in nearly two hours. The solid that separated was washed several times with hexane and recrystallised from water and dried over anhydrous calcium chloride.

2.3.4. Synthesis of *N,N'*-bis(3-pyridylidene)-1,2-phenelenediamine (SPO)

The Schiff base *N,N'*-bis(3-pyridylidene)-1,2-phenelenediamine was prepared by refluxing pyridine-3-carboxaldehyde (2.14g, 0.02mole) and *o*-phenylenediamine (1.08g, 0.01mole) for five hours. The yellow product was filtered and washed with benzene several times. It was recrystallised from absolute alcohol and dried over anhydrous calcium chloride [4].

2.3.5. Synthesis of *N,N'*-bis(3-pyridylidene)-1,4-phenylenediamine (SPP)

The ligand was prepared in the same way as *N,N'*-bis(3-pyridylidene)-1,2-phenelenediamine, using *p*-phenylenediamine in the place of *o*-phenylenediamine, the quantities of reagents being the same. The product was filtered, washed with

benzene, and recrystallised from alcohol. It was dried over anhydrous calcium chloride.

2.3.6. Synthesis of salicylaldehyde semicarbazone (SALSC)

This ligand was prepared using the procedure suggested by Jayendra Patole et al. To an aqueous solution of semicarbazide hydrochloride (1g, 0.008mole) and sodium acetate (1.5g, 0.01mole), salicylaldehyde (0.5g, 0.004mole) was added with stirring. The mixture was refluxed on a water bath for 2 hours. The semicarbazone separated was filtered, washed with ethanol, and recrystallised from 1-propanol [5].

2.4. Synthesis of zeolite Y encapsulated metal complexes

2.4.1. Preparation of sodium exchanged zeolite (NaY)

The standard ion exchange procedure was used for the preparation of NaY. Zeolite Y (HY, 5g) was mixed with NaCl solution (0.1, 500ml) and stirred for 24 hours at room temperature. This was done to remove extra framework iron and ion exchangeable impurities. The solution was filtered and washed with deionised water till the filtrate was free of chloride ions. The NaY formed was dried at 100 °C for 2 hours. The procedure was based on the one reported by Edward et al. [6] with slight modification.

2.4.2. Preparation of transition metal ion exchanged zeolite (MY)

(M = Fe, Co, Ni, Cu, Pd)

Sodium exchanged zeolite (5.0g) was stirred with metal salt solutions of ferric nitrate and chlorides of cobalt, nickel, copper, and palladium (500 ml; 0.01M / 0.001M) at 90 °C for 12 hours. Low concentration of metal salt solutions of pH 4.0-4.5 was used as dealumination occurs at higher concentrations [7]. The slurry

was filtered and washed with deionised water to make it free from anions. It was dried at 100 °C for 2 hours and finally dehydrated at 450 °C for 4 hours [8].

2.4.3. Encapsulation of metal complexes in zeolite

The flexible ligand method was used for encapsulating metal complexes in the cages of the zeolite [9]. Many of the free ligand molecules are flexible enough to pass through the restricting windows giving access to the super cages. These ligands can react with the metal ions already present in the super cages, and encapsulated complexes can be formed. Two general procedures are followed for this kind of encapsulation.

2.4.3.1. Encapsulation by heating in a sealed ampule

Metal exchanged zeolite MY (3.0g) was mixed thoroughly with excess of ligand (ligand to metal mole ratio ~2 - 4). It was placed in a glass vial and the open end of the tube was sealed so as to form an ampule. It was then heated in a furnace at an optimum temperature and for a definite period. This allows the sorbate molecules to disperse uniformly throughout the sample so that complexation occurs effectively. Complex formation involves physical entrapment of metal complexes in the cages of the zeolite rather than covalent or ionic attachment to the walls. Because of size restriction the complex stays in the zeolite and cannot diffuse out, provided the complex is stable. The product obtained was soxhlet extracted using a suitable solvent to remove excess ligand and surface species in cases where the complex and the ligand are soluble in that particular solvent. When the solubilities of the complex and ligand are different, they have to be soxhlet extracted with the suitable solvents. The soxhlet extraction was continued until the extract becomes colourless indicating complete removal of the species to be eliminated. The uncomplexed metal remaining in the zeolite was removed by back exchange of the

zeolite with NaCl solution (0.01M, 250ml) for 24 hours. It was then filtered, washed free of chloride ions, and finally dried at 100°C for 2 hours [10].

2.4.3.2. Encapsulation by refluxing the metal exchanged zeolite with the ligand

Metal exchanged zeolite MY (3.0g) was added to a solution of the ligand (excess ligand should be present) in a suitable solvent (ligand to metal mole ratio~2-4). The mixture was refluxed for 10 hours over a water bath. The ligand penetrates through the channels of zeolite and complexes are formed. Soxhlet extraction, back ion exchange, and removal of chloride are to be done in this case also for the removal of excess ligands and surface complexes.

2.5. Synthesis of neat complex

Cupric chloride was mixed with styrylbenzimidazole in methanol. It was refluxed for 3 hours. The crystals that separated were filtered, and dried using anhydrous calcium chloride.

2.6. Catalysis procedures

2.6.1. Decomposition of hydrogen peroxide

The catalytic activity of the synthesized samples was evaluated by monitoring the volume of oxygen evolved from the liquid phase using a gas burette attached to the reaction flask. The rate of oxygen gas evolution was monitored at room temperature and atmospheric pressure using gas burette. The volume of the evolved gas was monitored at intervals of 5 minutes in all the cases. The procedure is given in detail in Chapter 7.

2.6.2. Hydroxylation of phenol to hydroquinone

The hydroxylation of phenol was carried out by stirring a mixture of phenol, catalyst, water and hydrogen peroxide. The reaction mixture was filtered to remove the catalyst, and the product obtained was analysed using gas chromatograph. The quantities of the reactants used and detailed procedure for each reaction are given in Chapter 8.

2.6.3. Partial oxidation of benzyl alcohol to benzaldehyde

A mixture of benzyl alcohol, hydrogen peroxide, the activated catalyst, and solvent (water) was stirred in a reaction flask of 50ml capacity for a definite period of time using a magnetic paddle. The aqueous and organic layers were separated. The organic layer was analysed using thin layer chromatography (TLC) to detect the formation of benzaldehyde. It was finally analysed using gas chromatography to quantify the amount of substrate and product. The detailed procedure and the quantities of the reactants used for each reaction are given in Chapter 9.

2.7. Characterization methods

A variety of techniques have been developed for the characterisation of the catalysts and to trace the course of catalytic reactions. Characterization of the zeolite sample is carried out to get a better understanding of encapsulation, the physico-chemical properties of the complex, distribution of the complex in the host, the influence of the guest host interaction on the structure of the complex, the stability of the encapsulated complex compared to that of the neat complex, retaining of the zeolite framework even after encapsulation, and so on. The following techniques are generally used for the characterization of neat and zeolite encapsulated samples. The various techniques are:

i) chemical analysis

ii) surface area and pore volume analysis

iii) x-ray diffraction studies

iv) spectroscopic methods

v) magnetic susceptibility measurements

vi) scanning electron microscopy

vii) thermal analysis

viii) conductometric measurement

2.7.1. Chemical analysis

2.7.1.1. Analysis of Si, Al, Na, and transition metal ion in the zeolite sample

Analyses of Si, Al, Na and the transition metal ions are done by destroying the zeolite lattice-using con. H_2SO_4. A known weight (w_1) of the sample was taken in a beaker, and treated with concentrated sulphuric acid (95%, 40 ml) and was heated until SO_3 fumes were evolved. It was then cooled, diluted with water and filtered using ash-less filter paper. The filtrate was collected in a standard flask. The residue was heated in a platinum crucible and was weighed again (w_2). To the calcinated material 40% HF was added in drops, warmed and strongly heated to dryness. The procedure was repeated five to six times. During this process Si is converted into H_2SiF_6. It was again incinerated to 800 °C for 1 hour, cooled and weighed (w_3). From the loss in weight the amount of silica present in the sample can be estimated using the equation:

$$\% SiO_2 = (w_3-w_2) \times 100 / w_1$$

The residue was then fused with potassium persulphate (2-3 g) to form a clear molten mass. The mass when cooled was dissolved in water, and this was added to the filtrate collected in the standard flask. This solution was analysed for Al, Na and metal contents using Perkin Elmer Model 3110 Atomic Absorption

Spectrophotometer. Knowing Si, Al, Na, and transition metal mole ratio it is possible to get the unit cell formula of ion exchanged zeolite.

2.7.1.2. Determination of metal in neat complex

A known weight (0.20-0.30g) of the complex was treated with concentrated sulphuric acid (5ml) followed by concentrated nitric acid (20ml). After the reaction subsided perchloric acid (60%; 5ml) was added. This solution was maintained at boiling temperature for 3 hours on a sand bath. The clear solution thus obtained was evaporated to dryness, cooled, treated with concentrated nitric acid (5ml) and was again evaporated to dryness on a water bath. The residue was dissolved in water and was used for the estimation of metals. Iodometric method was employed for the estimation of copper in the complex [11].

2.7.1.3. Determination of chlorine

Chloride estimation was carried out as follows [11]. In a nickel crucible a layer of Na_2CO_3 was taken, and a layer of Na_2O_2 was set above the layer of Na_2CO_3. A definite quantity of the sample, accurately weighed out, was placed over this. This was then covered with another layer of Na_2O_2 and then with a layer of Na_2CO_3.The mixture was heated to get a fused mass. The nickel crucible with substance was immersed in water taken in a beaker and heated over a water bath until the substance dissolved completely, and then the crucible was taken out. The solution was neutralised with 1:1 HNO_3, adding the acid till effervescence ceased and then in slight excess. Any residue that was present was filtered off and the chloride in the solution was estimated using Volhard method [11].

2.7.2. CHN analysis

Microanalyses of carbon, hydrogen and nitrogen were done at the Sophisticated Instrumentation Centre for Applied Research and Testing, Anand, Gujarat. The CHN analyses were done on a Carto Erba Analyser Model 1108. The results were related to the amounts of metal obtained from AAS for the encapsulated complexes. This helped to find the amount of uncomplexed metal ions if any, which remain in lattice.

2.7.3. Surface area and pore volume analysis

It is necessary to know the surface area of a solid for catalytic application. This fundamental property of the solid is called surface area and is generally given as m^2/g of solid. The surface areas of the zeolite samples were determined by the BET method [12] of nitrogen adsorption at liquid nitrogen temperature using 'Micromeritics Gemini 2360'. The weighed amount of sample is taken in a dry, clean sample tube. The volume of gas adsorbed by the sample was monitored at different relative pressures in the range 0.1-0.9. The zeolite sample was heated to 473 K and maintained at this temperature for 3 hours in a stream of dry nitrogen atmosphere (50 ml/h) to remove any volatile components from the surface of the solid. After this pre-treatment the sample was cooled to room temperature. The sample tube together with substance was weighed and was fixed to the instrument with the help of sample holders. It was then brought to 77 K using liquid nitrogen as coolant and mixture of nitrogen and hydrogen was passed over the catalyst. Only nitrogen was physically adsorbed on the surface of the solid at this liquid nitrogen temperature. This decreases the pressure in the chamber until the adsorbed gas is in equilibrium with the free gas phase.

Surface area is calculated using the following BET equation

$$1/V_{ads}\,(P_o-P) = 1/V_mC + [(C-1)/V_mC]\,P/P_o \quad \text{where}$$

V_{ads} = volume of gas adsorbed at relative pressure P/P_o

P_o = saturated vapour pressure

V_m = volume of gas adsorbed for monolayer coverage

C = BET constant

By plotting the left side of the BET equation against P/P_o (up to 0.3), a straight line is obtained with a slope of $(C-1)/V_mC$ and an intercept $1/V_mC$. From these values, V_m and hence X_m, the number of moles of N_2 adsorbed, can be calculated.
BET surface area is calculated using the equation

$S_{BET} = X_m N A_m 10^{-20}$ where

N = Avogadro's number

A_m = cross-sectional area of the adsorbate molecule in $Å^2$

The total pore volume of the sample at P/Po ~ 0.9 is computed by converting the volume of N_2 adsorbed at P/Po ~ 0.9 to the volume of liquid equivalent to it using the following equation:

$V_{tot} = V_{ads} D$ where

V_{tot} = total pore volume at P/Po ~ 0.9

V_{ads} = volume of gas adsorbed at relative pressure ~0.9

D = density conversion factor

2.7.4. X-ray diffraction studies

X-ray diffraction can be used to determine the zeolite's internal structure. The method serves as a basic finger printing technique, as two substances cannot have absolutely identical diffraction patterns. The patterns of the sample in the present study were obtained on a 'Philips P W 1710 / Rigaka D-Max C' X-ray diffractometer. The measurements were carried out with X-ray source, Ni filtered CuK_α radiation with $\lambda = 1.5404$ and a movable detector which scans the intensity of the diffracted beam as a function of the angle 2θ between the incident and the

diffracted beams. The range of 2θ used was between 5 and 70°. The XRD patterns of the ion exchanged zeolite and zeolite encapsulated complex are compared with that of parent zeolite (NaY) to know whether there is any loss in crystallinity.

2.7.5. Spectroscopic analysis

Spectroscopic methods are employed as a reliable means for the characterization of complexes and the study of catalysis. They provide information regarding the nature and structure of the complex, and the reactivity of the surface. Further the methods can be easily adopted for insitu studies to gain vital information on reaction mechanism.

2.7.5.1. Electronic spectra

The characterisation technique is based on the electronic transition in the UV-VIS-NIR region of the electronic spectrum. Usually diffuse reflectance spectroscopy is made use of for the analysis of zeolite samples. It gives information regarding d-d transitions, intra ligand bands, charge transfer spectra, structure of complexes, kinetics of reactions etc.

The diffuse reflectance spectra were recorded at room temperature in the range 200-2000nm on a Cary Win spectrophotometer at Regional Sophisticated Instrumentation Centre, Indian Institute of Technology, Chennai and between 200nm-800nm on a Perkin Elmer 320 spectrometer. NaY was used as blank for zeolite samples and finely ground $BaSO_4$ / MgO was used as reference in the case of neat complexes. The spectra were computer processed and plotted as percentage reflectance versus wavelength using the principle of Kubelka-Munk analysis [13,14,15] or as percentage absorbance versus wavelength

2.7.5.2. Infrared spectra

Infrared spectroscopy was used for the identification of functional groups, and for detecting the coordinaton of ligands to transition metals. Infrared spectra of the ligand, simple complex, metal exchanged zeolite and supported complexes in the region $4000cm^{-1}$- $400cm^{-1}$ were recorded using Schimadzu 8000 Fourier Transform Infrared Spectrophotometer / Brukker IFS 66v FTIR Spectrometer. The characteristic bands due to the coordination sites of ligands exhibit well-defined shift upon complexation / chelation. But many of these bands may be masked by strong bands of zeolite in zeolite encapsulated complexes. The framework vibrations of zeolites are observed in the spectral range between $1250cm^{-1}$ and $400cm^{-1}$. The samples were mixed with KBr, made into pellets and analysed.

2.7.5.3. EPR spectra

EPR spectroscopy has been used as a powerful tool for investigating various physico-chemical problems such as identification of paramagnetic species, its geometry, electronic structure, identification of catalytically active species in a reaction and to investigate the influence of the host on the geometry of the complex. The X-band EPR spectra of powdered samples of zeolite encapsulated Cu(II) complexes and glass spectra of simple complexes were recorded at room temperature and at liquid nitrogen temperature using a Varian E-109 X/Q band spectrophotometer. The g values were estimated relative to tetracyanoethylene (TCNE, g = 2.0027). The magnetic moment was determined from the EPR data using the following equation [16]

$$\mu^2_{eff} = g_{II}^2/4 + g_{\perp}^2/4 + 3kT/\lambda o\ (\ g - 2)$$

where λo is the spin orbit coupling constant for the free metal ion.

The density of unpaired electrons at the central metal atom was computed using the equation

$$\alpha^2_{Cu} = (A_{II}/P) + (g_{II}-2) + 3/7(g_{\perp}-2) + 0.04$$

where, α^2 gives information about the nature of the bonding. Complete ionic bonding is indicated by α^2 value of 1, and α^2 value of 0.5 suggests complete covalent bonding. Covalency associated with the bonding of metal ion to the ligand is measured as $1-\alpha^2$.

2.7.6. Magnetic measurement studies

Magnetic susceptibility studies were carried out at room temperature on a simple Gouy balance. The studies were made using $Hg[Co(NCS)_4]$ as standard, as suggested by Figgis and Nyholm [18,19], and diamagnetic corrections were applied [20]. The effective magnetic moment was calculated using the equation

$\mu_{eff} = 2.84 (X'_m T)^{1/2}$ BM where

T = absolute temperature

X'_m = molar susceptibility corrected for diamagnetism of all atoms present in the complex using Pascal's constant and that of the zeolite frame work per unit metal.

2.7.7. Scanning electron microscopy

The morphology of the sample is examined using scanning electron microscopy. Electron microscopy involves the kinetic energy analysis of electrons ejected out of a specimen when it is subjected to a beam of electrons. The analysis is carried out by passing a narrow beam of electrons from a tungsten filament over the surface of the sample and determining the yield of secondary or back-scattered radiation as a function of the primary beam. Scanning electron microscopy analysis of a representative zeolite complex before and after soxhlet extraction was performed on a Leica Steroscan-440 microscope.

2.7.8. Thermo gravimetric analysis

Thermal analysis incorporates those techniques in which some physical parameters of a given system are determined as a function of temperature. Thermo gravimetric analysis is carried out to study the thermal stabilities of neat and zeolite encapsulated complexes. Thermo gravimetry is a technique in which a substance in a desired environment is heated or cooled at a controlled rate and the weight or mass of the substance is recorded as a function of temperature. The analysis provides a quantitative measurement of weight change associated with the thermal decomposition reaction. Using TG it is possible to explain the thermodynamics and kinetics of various reactions. Thermo gravimetric analysis was performed on a Shimadzu TGA-50 / TGAV5.1A du Pont / NETZSCH Simultaneous Thermal Analysis System at a heating rate of 10°C/minute in air/an inert atmosphere in the temperature range 30-800 °C. About 10mg sample was taken for each analysis in a platinum crucible hung from one arm of the balance in the instrument. The TG data were computer processed and plotted, with the % weight against temperature.

2.7.9. Conductance measurement

The molar conductance of the simple complex was determined at room temperature in methanol (10^{-3} M) using an 'Elico PR 9500' conductivity bridge with a dip type cell and a platinised platinum electrode.

2.8. Catalytic studies

2.8.1. Gas chromatography

Gas chromatographs are essential instruments in catalysis research as they are used for the separation of molecules. Gas Chromatograph Chemito 8510 was used for analysing the reactants and products of the catalytic reactions over zeolite

complexes. An SE-30 column was used for separating various components in the reaction mixture.

The sample is injected into a heating block where it is immediately vaporised and swept by the carrier gas stream into the column. The solutes are adsorbed at the head of the column by the stationary phase and then desorbed by the carrier gas. The adsorption- desorption process occurs repeatedly as the sample moves towards the column outlet. Each solute travels at its characteristic rate through the column. The bands separate to a degree that is determined by the individual partition rates. The solute then enters the detector attached to the column exit. The peaks that appear on the recorder are characteristic of the different components. The peak area is proportional to the concentration of the component in the mixture.

2.8.2. Thin layer chromatography

Glass plates coated with dried and activated silica gel (adsorbent) were used for thin layer chromatography. The substance to be separated was spotted near one end of the adsorbed layer and was placed vertically in a jar containing a suitable solvent or a mixture of solvents. The solvent passes through the adsorbed layer as per the principle of capillary action. The plate was taken out from the jar and kept in air. Visualisation was achieved by exposure to iodine vapours.

References

1. P.K. Dubey and Ramesh Kumar, *Ind. J. Chem.* 38 B (1999) 1211.
2 A.I. Vogel, *A Text Book of Practical Organic Chemistry*, Longman, London, 1972.
3 K.K.M. Yusuff, Ph.D. Thesis, University of Kerala, Trivandrum, August 1976.
4 M. Kumar and S. Arabinda Kumar, *Asian J. Chem.* 6, 4 (1994) 782.
5 Jayendra Patole, Sabari Dutta, Subhash Padhye, and Ekkehard Sinn, *Inorganica Chimica Acta* 318 (2001) 207.
6 Edward H. Yonemoto, Yeong Il Kim, Russel H. Schmehl, Jim O. Wallin, Ben A. Shoulders, Benny R. Richardson, James F. Haw, and Thomas E. Mallouk, *J. Am. Chem. Soc.* 116 (1994) 10537.
7 P.G. Menon, *Lectures on Catalysis, 41st Ann. Meeting, Ind. Acad. Sci.*, S. Ramasheshan (Ed.) 1975.
8 Robert J. Taylor, Russel S. Drago, and James E. George, *J. Am. Chem. Soc.* 111 (1989) 6610.
9 N. Herron, *Inorg. Chem.* 25 (1986) 4714.
10 N. Ulagappan and V. Krishnasamy, *Ind. J. Chem.* 35A (1996) 787.
11 A.I. Vogel, *A Text Book of Quantitative Inorganic Analysis*, (4th edn.), Longman-Green, London, 1978. Rpt. 1986.
12 S. Brunauer, P.H. Emmett, and E.J. Teller, *Am. Chem. Soc.* 60 (1938) 309.
13 H.G. Hecht, *Modern Aspects of Reflectance Spectroscopy*, W.W. Wendlandt, (Ed.) Plenum Press, New York, 1968.
14 S.K. Tiwary and S. Vasudevan, *Inorg. Chem.* 37 (1998) 5239.
15 R.W. Frei and J.D. Mc Neil, *Diffuse Reflectance Spectroscopy in Environmental Problem Solving,* CRC Press, Cleveland (1973).
16 B.V. Agarwala, *Inorg. Chim. Acta.* 36 (1979) 209.
17 D. Kivelson and R. Neiman, *J. Phys. Chem.* 35 (1961) 149.
18 B.N. Figgis and R.S. Nyholm, *J. Chem. Soc.* (1958) 4190.
19 B.N. Figgis and J. Lewis in *Modern Coordination Chemistry*, J. Lewis and R.C. Wilkins (Eds.) Interscience, New York 1960.
20 R.L. Dutta and A. Syamal, *Elements of Magnetochemistry*, S. Chand and Co., New Delhi, 1982.

Chapter 3

Zeolite-Y encapsulated complexes of the Schiff bases *N,N'*-bis(3-pyridylidene)-1,2-phenylenediamine, *N,N'*-bis(3-pyridylidene)-1,4-phenylenediamine, and salicylaldehyde semicarbazone

Abstract

This chapter, dealing with the synthesis and characterization of zeolite encapsulated Schiff base complexes, is divided into two sections. The first section gives a comparative study of the complexes of Fe(III), Co(II), Ni(II) and Cu(II) with *N,N'*-bis(3-pyridylidene)-1,2-phenylenediamine and *N,N'*-bis(3-pyridylidene)-1,4-phenylenediamine.The second section deals with study of Co(II), Ni(II), and Cu(II) with salicylaldehyde semicarbazone. Elemental analysis and CHN analysis were done to understand the stoichiometry of the complex. Si/Al ratio and XRD patterns suggest that there is no change in the crystalline nature of the zeolite even after encapsulation. Magnetic susceptibility measurements diffuse reflectance and EPR spectra gave information regarding the geometry of the complex. The formation of complex inside the zeolite pore was confirmed by IR spectra. The TG/DTG patterns gave qualitative idea regarding the thermal stability of the complex and the probable composition of the expelled group.

3. Introduction

Schiff bases contain azomethine groups, and the stability of the Schiff base depends on the strength of the C=N bond, basicity of the imino group and steric factors. Recent advancements in the coordination chemistry of Schiff base are essentially concerned with the properties and structures of metal chelates. The presence of electron releasing or electron withdrawing groups or an aromatic ring can tune the electronic and magnetic properties of metal complexes of Schiff bases. The presence of a second functional group with a replaceable hydrogen atom, preferably a functional group close to the imino group, allows the ligand to form a fairly stable four, five, six, membered ring on chelation to the metal atom. The relative stability of such ligands allows distortion in the structure of the complexes. The extent of distortion depends on the nature of the metal and the apical and axial ligands.

The complexes of Schiff bases are found to have antibacterial, antifungal, anti-inflammatory, antileukaemic and such other properties [1-3]. These complexes have wide applications, as homogeneous catalysts for oxidation, carboxylation and decarboxylation [4,5]. Schiff base complexes also find applications as heterogeneous catalysts for these reactions. One of the methods for modifying the homogeneous catalysts into heterogeneous catalysts is the encapsulation of the complexes inside zeolite cages. It was considered worthwhile to synthesize the complexes inside zeolite cages and understand the nature of the complexes inside the cages.

In this chapter, our studies on the zeolite encapsulated Fe(III), Co(II), Ni(II) and Cu(II) with *N,N'*-bis(3-pyridylidene)-1,2-phenylenediamine, *N,N'*-bis(3-pyridylidene)-1,4-phenylenediamine and Co(II), Ni(II), and Cu(II) with salicylaldehyde semicarbazone are presented. For convenience the chapter is divided into two sections, Section A and Section B. Section A deals with the

studies on the Fe(III), Co(II), Ni(II) and Cu(II) complexes of with *N,N'*-bis(3-pyridylidene)-1,2-phenylenediamine, and *N,N'*-bis(3-pyridylidene)-1,4-phenylenediamine and Section B, deals with the studies on Co(II), Ni(II), and Cu(II) complexes with salicylaldehyde semicarbazone.

Section A

Zeolite encapsulated Fe(III), Co(II), Ni(II) and Cu(II) *N,N'*-bis(3-pyridylidene)-1,2-phenylenediamine and *N,N'*-bis(3-pyridylidene)-1,4-phenylenediamine complexes

3A.1. Introduction

Schiff bases may form monomeric or dimeric neat complexes with metal ions. *N,N'*-Bis(3-pyridylidene)-1,2-phenylenediamine forms both monomeric and dimeric complexes with Fe, Co, Ni and Cu [6,7]. Complexes of Fe, Co, Ni and Cu with *N,N'*-bis(3-pyridylidene)-1,2-phenylenediamine (SPO) were encapsulated in zeolite and it was found that the encapsulated complexes formed only monomeric species. The experiment was repeated with *N,N'*-bis(3-pyridylidene)-1,4-phenylenediamine (SPP) encapsulated in zeolite. These encapsulated complexes were also found to form only monomeric complexes.

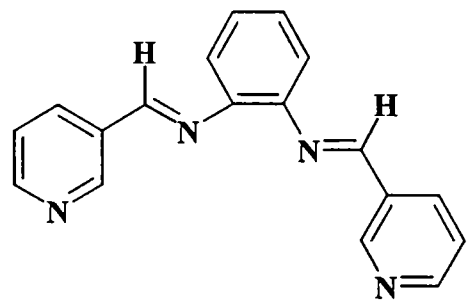

Figure 3A.1 Structure of *N,N'*-bis(3-pyridylidene)-1,2-phenylenediamine (SPO)

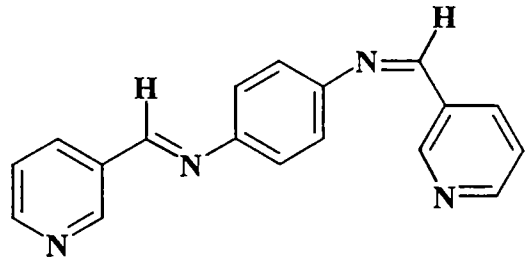

Figure 3A.2 Structure of *N,N'*-bis(3-pyridylidene)-1,4-phenylenediamine (SPP)

3A.2. Experimental

3A.2.1. Synthesis of ion exchanged zeolites

Details regarding the synthesis of ion exchanged zeolites are given in Chapter 2. The metal ions have preference for certain sites in the zeolites. After metal exchange the metal ions in the zeolite may exist in the form of hexa aqua complexes, which are localized in the supercage. On dehydration the coordinated water molecules are removed and the vacant sites are occupied by lattice oxygen. The metal can migrate to other sites also. Rehydration shifts the cation back to the supercage. Thus the metal ion can be considered to be in dynamic state, where the metal migrates to the most favourable position to get the best coordination.

3A.2.2. Synthesis of zeolite encapsulated Fe(III), Co(II), Ni(II) and Cu(II) complexes of *N,N'*-bis(3-pyridylidene)-1,2-phenylenediamine, and *N,N'*-bis(3-pyridylidene)-1,4-phenylenediamine

Metal exchanged zeolite (3.0g) was added to a solution of the ligand in ethanol, keeping the ligand to metal mole ratio ~ 2 (slightly higher than 2). The mixture was refluxed for six hours to ensure complexation. The ligand penetrates

through the pores of the zeolite and complexes with the metal ions already present within the zeolite. The complexed product becomes too large to pass through the aperture of the supercage and will be retained inside the cages. The resultant mass was soxhlet extracted with methanol until the extracting solvent became colourless, ensuring the complete removal of surface species (ligand and complexes adhering to the surface). The uncomplexed metal ions in the zeolite and ionisable protons of the ligand were removed by ion exchange with NaCl solution (0.1M, 250ml) for 24 hours. It was filtered, washed free of chloride ions and finally dried at 100 °C for 2 hours and stored in vacuum over anhydrous calcium chloride.

3A.3. Characterization techniques

Details regarding the characterization techniques are given in Chapter 2.

3A.4. Results and Discussion

3A.4.1. Ion exchanged zeolite

3A.4.1.1. Chemical analysis

The analytical data of NaY and metal exchanged zeolites are presented in Table 3A.1. The Si/Al ratio for NaY is found to be 2.4 which corresponds to a unit cell formula of $Na_{56}(AlO_2)_{56}(SiO_2)_{136}$ [8]. The unit cell formula represents the composition of a unit cell in the metal exchanged zeolite. The Si/Al ratio remains the same in all the metal exchanged zeolites, indicating that no destruction of zeolite framework has occurred during ion exchange by dealumination. Preservation of the zeolite framework on exchanging with dilute metal salt solutions has been noted by earlier workers also [9]. The process of ion exchange can be represented as

$$Na_{56}Y + x\,M^{2+} \rightarrow M_xNa_{56-2x}Y + 2x\,Na^+$$

Table 3A.1 Analytical data of metal exchanged zeolites

Sample	% Si	% Al	% Na	% M
NaY	21.76	8.60	7.5	-----
FeY	21.62	8.56	6.2	0.53
CoY	21.71	8.50	5.9	0.25
NiY	21.59	8.55	6.1	0.50
CuY	21.48	8.48	6.6	1.12
PdY	21.50	8.51	6.9	0.164

Table 3A.2 Composition of metal exchanged zeolites

Ion exchanged zeolite	Degree of ion exchange (%)	Unit cell formula
NaY	—	$Na_{56}(AlO_2)_{56}(SiO_2)_{136}nH_2O$
FeY	8.97	$Na_{50.97}Fe_{1.676}(AlO_2)_{56}(SiO_2)_{136}\ nH_2O$
CoY	2.67	$Na_{54.5}Co_{0.749}(AlO_2)_{56}(SiO_2)_{136}\ nH_2O$
NiY	5.30	$Na_{53.0}\,Ni_{1.500}(AlO_2)_{56}(SiO_2)_{136}\ nH_2O$
CuY	10.90	$Na_{49.88}Cu_{3.060}(AlO_2)_{56}(SiO_2)_{136}\ nH_2O$
PdY	0 .97	$Na_{55.45}Pd_{0.270}(AlO_2)_{56}(SiO_2)_{136}\ nH_2O$

where x represents the atom fraction of M^{2+} ions introduced into the zeolite [10]. Strong interaction between the support and the metal leads to high loadings of metal ions inside the zeolite. The loadings in the metal exchanged zeolites were in the range 0.5% to 1.12%. The degree of ion exchange was found to increase in the order Pd < Co < Ni < Fe < Cu.

The degree of ion exchange is represented as the percentage of Na^+ ions replaced by metal ions from the total amount of sodium which is equivalent to the aluminium content of the zeolite. The value of degree of ion exchange in various metal exchanged zeolites used in the present study is comparable to that reported in the literature [11].

3A.4.1.2. X - ray diffraction patterns

The X-ray diffraction patterns of the zeolite samples NaY, and CoY are given in Figure 3A.3. The XRD patterns of metal exchanged zeolites are very similar to those of the parent HY zeolite as well as to those reported in literature [12]. This indicates that the crystalline structure of the zeolites is preserved even after the ion exchange. The crystalline structure of zeolite is known to be affected by dealumination on metal exchange using metal salt solution of concentration > 0.02 M and pH < 4.0 [9]. Therefore in the present study very low concentration of the metal ion is used. Further, crystalline phases of metal ions were not detected in any of the patterns. This implies that the metal ions are finely dispersed at the cation phases of the zeolite rendering them undetectable by XRD.

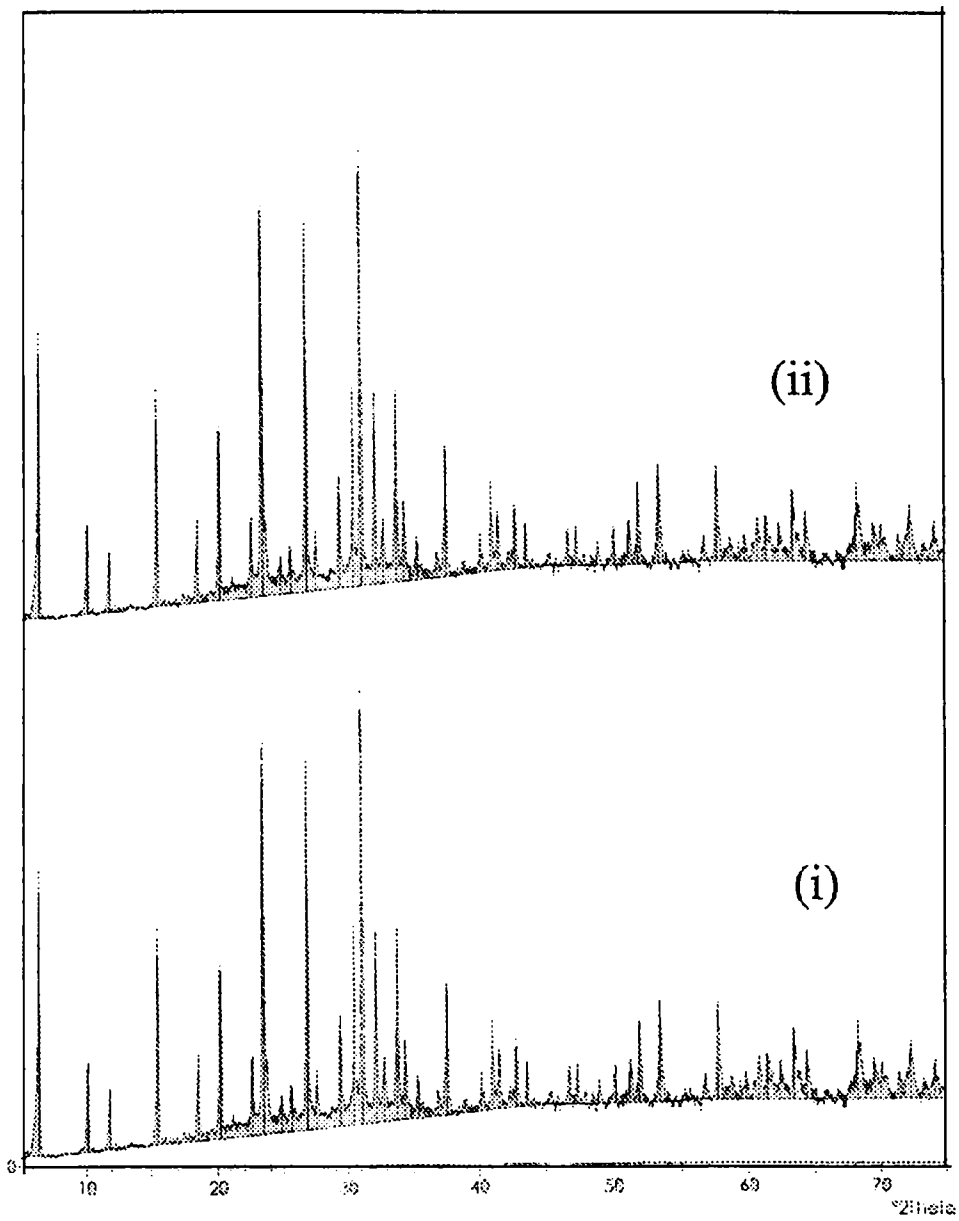

Figure 3A.3 XRD patterns of (1) NaY, (2) CuY

3A.4.1.3. Surface area and pore volume

The surface area and pore volume of HY and metal exchanged zeolites are determined by nitrogen adsorption at low temperature and at relative pressures P/P_o in the range 0.1 to 0.9. The surface area and pore volume data are given in Table 3A.3. The values indicate that the introduction of metal ions into the zeolite lattice by ion exchange causes only marginal reduction in the surface area. This helps to rule out the possibility of the destruction of the zeolite matrix on ion exchange. The surface area obtained for the metal exchanged zeolites agrees with the values reported earlier [13].

Table 3A.3 Surface area and pore volume data of HY and ion exchanged zeolite

Sample	Surface area m^2/g	Pore volume ml/g
HY	546	0.3045
NaY	540	0.3021
FeY	529	0.2982
CoY	532	0.2986
NiY	528	0.2974
CuY	530	0.2983
PdY	500	0.2870

3A.4.1.4. FTIR spectrum

The FTIR spectrum of NaY is shown in Figure 3A.4. The IR absorptions in both the hydroxyl region (wave number beyond 3000 cm^{-1}) and the framework region (wave number below 1500 cm^{-1}) are listed in Table 3A.4. Framework vibrations are observed in the spectral range between 1250 cm^{-1} and 400cm^{-1}. Symmetric stretching modes, antisymmetric stretching modes, bending modes of

TO_4 [$(Si/Al)O_4$] tetrahedra, and structure sensitive vibration band (called double ring vibration band) [14,15] can be seen in Figure 3A.4. The broad absorption at ~ 1000cm^{-1} is attributed to external asymmetric stretching vibration of TO_4. The symmetric stretching T-O-T vibration gives rise to bands seen at 630-870cm^{-1}. The stretching and bending vibrations of water molecules present in the zeolite lattice can be seen at ~ 3500 cm^{-1} and ~ 1640 cm^{-1} respectively [16].

Table 3A.4 IR spectral data of metal exchanged zeolites

Range of wave numbers cm^{-1}	Assignment
1250-980	asymmetric T-O-T stretching
870-630	symmetric T-O-T stretching
550-620	structure sensitive double five ring vibration
ca. 450	T-O-T bending mode

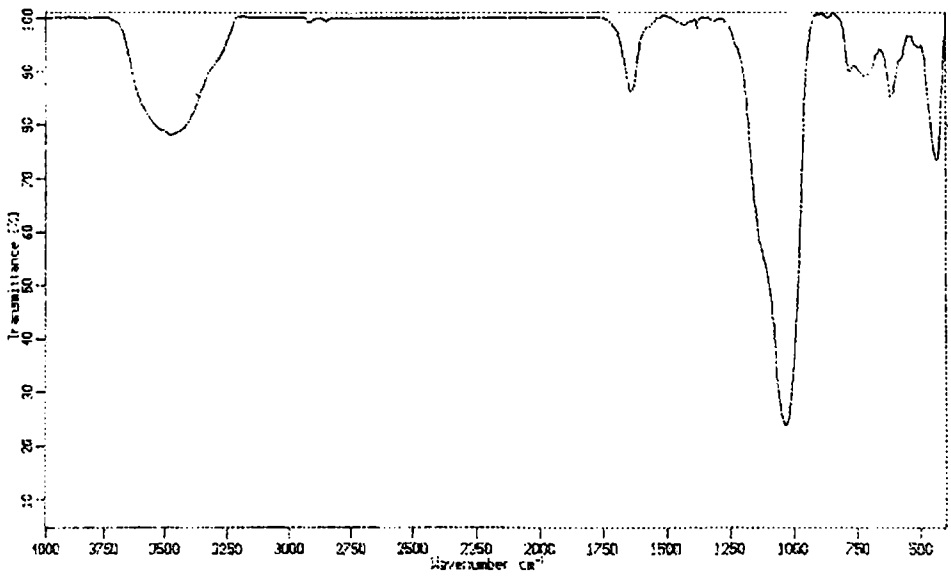

Figure 3A.4. FTIR spectrum of NaY

The IR bands of metal exchanged zeolite appear almost at the same position as those of the parent zeolite Y. Further, these values are almost the same as the values reported in earlier studies [14,15,17]. Therefore the zeolite framework remains unaffected on ion exchange using the metal ion solution of low concentration used in the present study.

3A.4.1.5. Diffuse reflectance spectra

The electronic spectra of metal exchanged zeolites are given in Figure 3A.5. The transition metal ions get coordinated to the oxide ions in the lattice and to the water molecules present in zeolite. These being weak ligands, the complexes are expected to be in high spin state. The data indicate octahedral structure for the species inside the zeolite cages [18].

3A.4.1.6. EPR spectrum

The EPR parameters of copper exchanged zeolites are given in Table 3A.5. The g_{II} value is higher than the usually reported value, but such high value has been observed by Sakaguchi and Addison [19] for copper exchanged zeolites. The high value can be attributed to the tetrahedral distortion of a square planar chromophore, decreased covalency of metal ligand bond, or due to the increasing positive charge on the donor atom.

Table 3A.5 EPR parameters of copper exchanged zeolites

Ion exchanged zeolite	g_{II}	$g_{\perp}$	A_{II} (cm^{-1})	$A_{\perp}$ (cm^{-1})
CuY	2.37	2.08	136.66	66.66

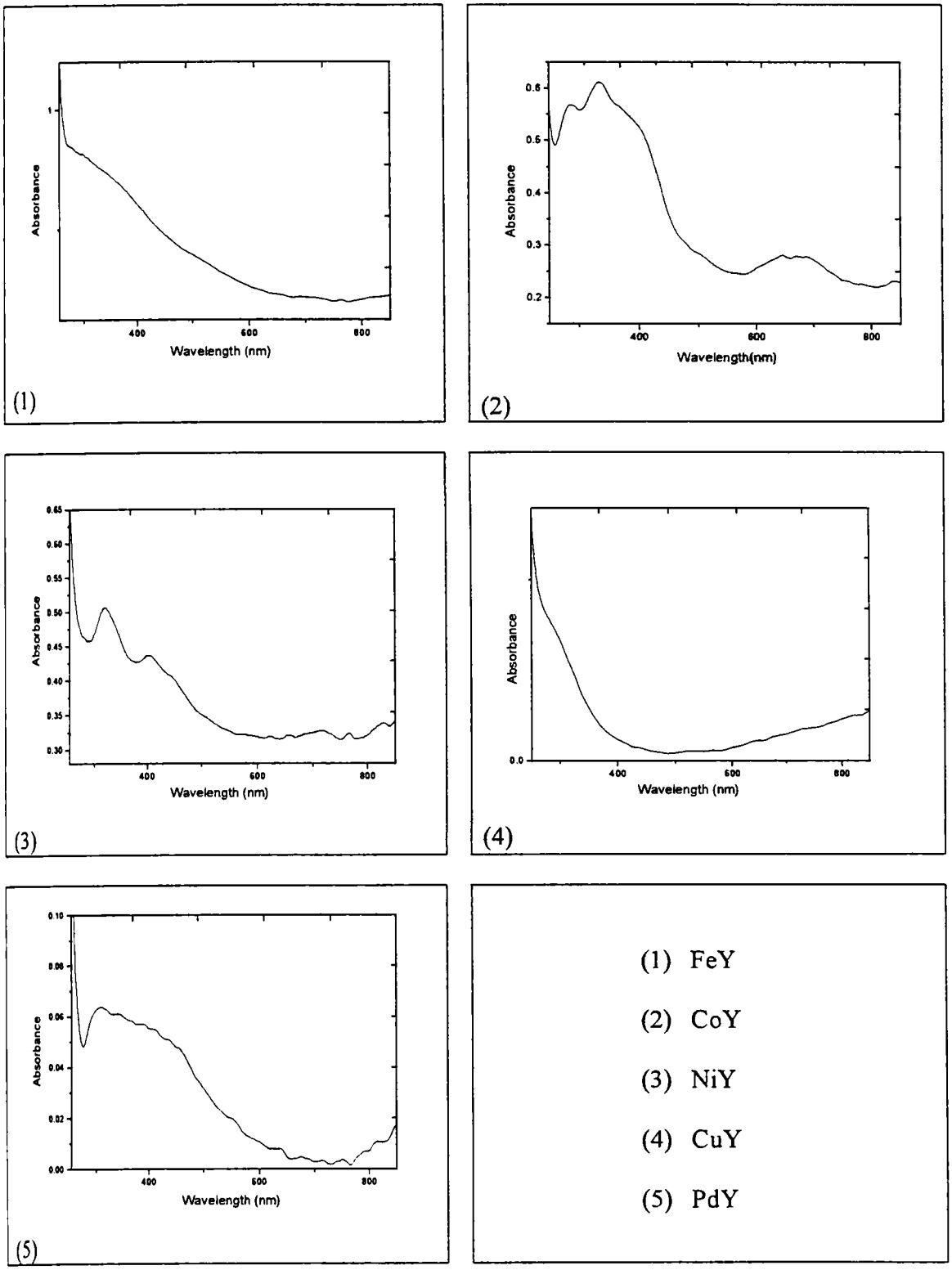

Figure 3A.5 Electronic spectra of ion exchanged zeolites

3A.4.2. Zeolite encapsulated complexes

3A.4.2.1. Chemical analysis

The process of complex formation inside the cage for divalent metal ions can be represented as:

$$M_xNa_{56-2x}Y + L \rightarrow [(ML_n)]_xNa_{56-2x}Y$$

where L represents the ligand coordinated to the metal center [10].

The analytical data of the zeolite encapsulated complexes are given in Table 3A.6. Analytical data show that the Si/Al ratio of the zeolite complex is 2.4 as in the case of metal exchanged zeolites. This again is an indication of the zeolite framework remaining unaffected on encapsulation. Similar observation with regard to the Si/Al ratio has been made by earlier workers [20,21]. The ligands, SPO and SPP, form complexes in the super cages probably by breaking the metal-lattice oxygen bonds [22].

Table 3A.6 Analytical data

Sample	% Si	% Al	% Na	%C	% M
FeYSPO	18.64	7.60	5.40	3.60	0.50
CoYSPO	18.46	7.48	5.36	1.35	0.23
NiYSPO	18.54	7.63	5.38	3.00	0.47
CuYSPO	18.71	7.67	5.41	5.60	0.93
FeYSPP	18.79	7.83	5.60	3.53	0.51
CoYSPP	18.79	7.74	5.90	1.22	0.22
NiYSPP	18.90	7.91	6.00	1.81	0.30
CuYSPP	18.93	7.82	5.85	5.45	0.89

The positive charge of the encapsulated complex will be compensated through the interaction of negatively charged oxide ions of zeolite matrix. The loadings of the metal in the ion exchanged zeolite and the zeolite encapsulated complexes are quite close in value to each other which suggests that almost all the metal ions present in the zeolite lattice get complexed and the uncomplexed metal ions are removed during back exchange. The ligand to metal mole ratio is 2 in neat monomeric complexes of Co(II), Ni(II) and Cu(II) with SPO ligands [6,7]. Though the same value is expected in zeolite encapsulated complexes, the actual value is observed to be slightly lower than 2. This could be because some metal ions get trapped in the cavities of the zeolite and the metal complexes that surround them prevent ion exchange with sodium ions.

3A.4.2.2. Scanning electron micrographs

Scanning electron micrographs of zeolite encapsulated species before and after soxhlet extraction are shown in Figure 3A.6. In the SEM taken before soxhlet extraction, the surface is crowded with particles. In the SEM taken after soxhlet extraction, the surface is clean, indicating the removal of the surface species during soxhlet extraction. The complexes formed inside the zeolite cages remain trapped and are not able to come out. Similar reports of clear zeolite surface in the case of phthalocyanine and salen are seen in the literature [23,24].

3A.4.2.3. X-ray diffraction patterns

X-ray diffraction patterns of both the SPO and SPP complexes are given in Figure 3A.7 and Figure3A.8. The XRD patterns of the complexes were compared with those of NaY and ion exchanged zeolite. The XRD patterns are found to be similar to those of the corresponding metal exchanged zeolite and the parent zeolite.

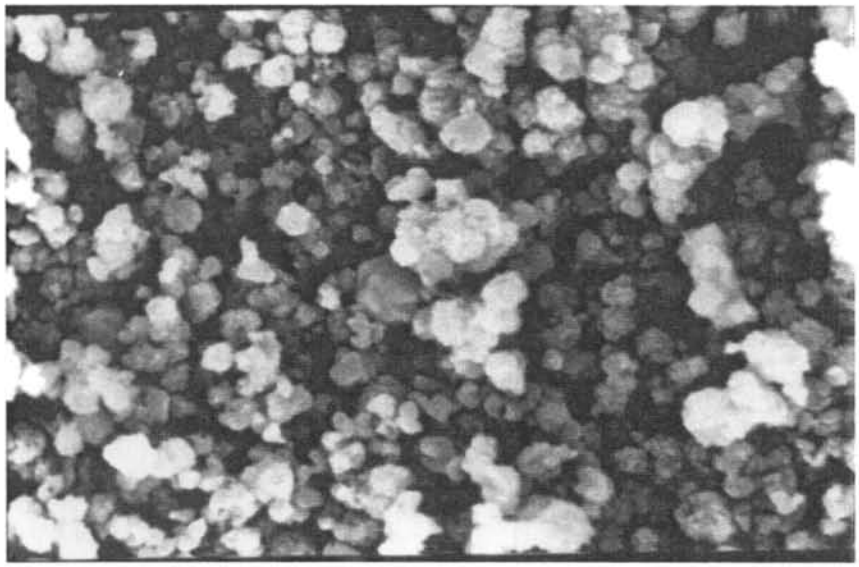

(i)

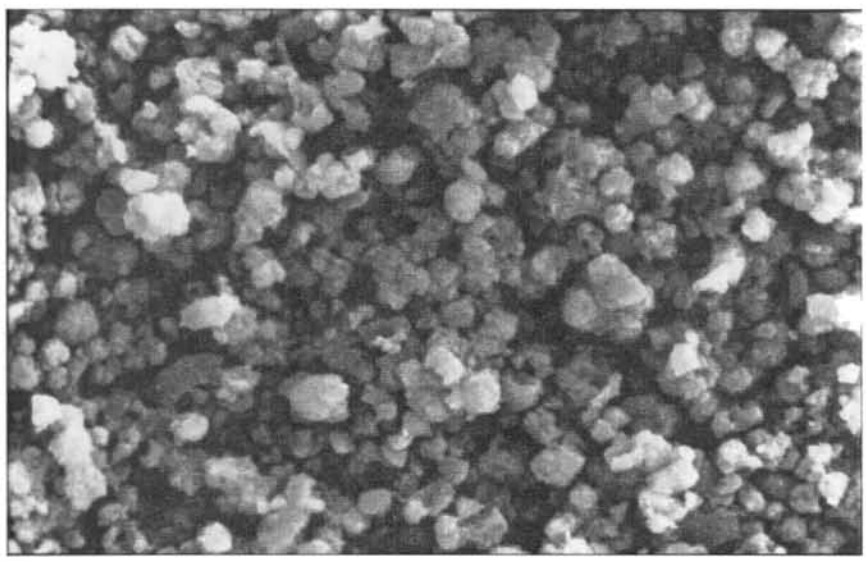

(ii)

Figure 3A.6 SEM

i) Before soxhlet extraction
ii) After soxhlet extraction

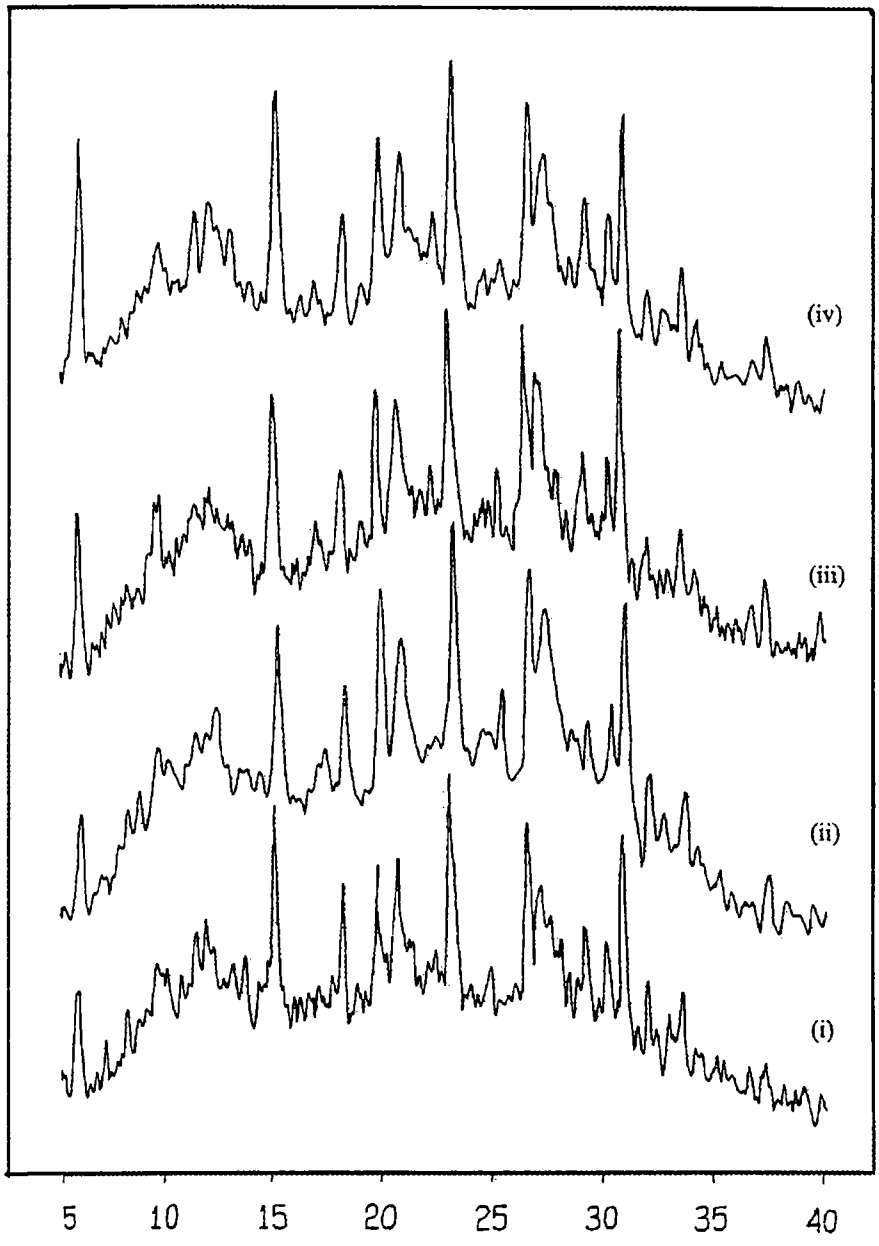

Figure 3A. 7 XRD patterns of SPO complexes

i) FeYSPO, ii) CoYSPO, iii) NiYSPO, iv) CuYSPO

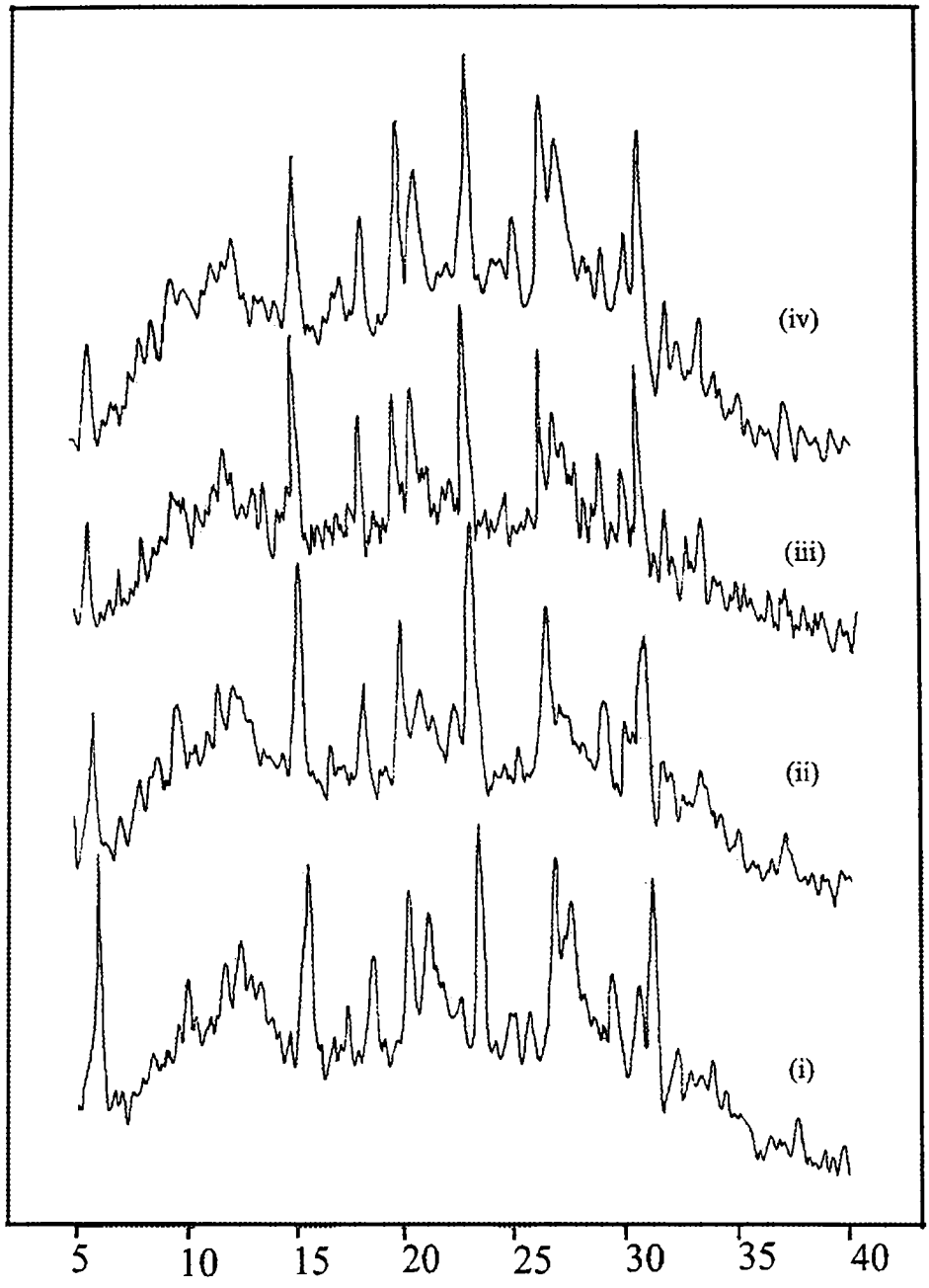

Figure 3A. 8 XRD patterns of SPP complexes

i) FeYSPP, ii) CoYSPP, iii) NiYSPP, iv) CuYSPP

This indicates that the zeolite structure has not been damaged even after the synthesis of metal complexes in the cavities. It has been reported that the presence of the large encapsulated phthalocyanine complex does not make the zeolite network more fragile [25].

3A.4.2.4. Surface area and pore volume

The surface area and pore volume of encapsulated SPO and SPP complexes of Fe, Co, Ni and Cu were measured by nitrogen adsorption. The surface area of zeolite is mainly internal surface area, and so it should decrease when there is blocking of the pores. The data (Table 3A.7 and Table 3A.8) reveal that the surface area values are lower in the case of zeolite encapsulated complexes than those of the corresponding metal exchanged zeolites. The lowering of surface area and pore volume can be attributed to the filling of the zeolite pores with metal complexes. Such lowering of surface area and pore volume on encapsulation has been reported by earlier workers [11,26,27]. The loss in surface area varies between 68.3% and 73.3% for the encapsulated SPO and SPP complexes and the loss in pore volume varies between 74.6% and 76.6% for the encapsulated SPO and SPP complexes. This provides strong evidence of the encapsulation of the complex within the zeolite pore.

Table 3A.7 Surface area and pore volume data of complexes of SPO Ligand

	Surface area (m^2/g)			Pore volume (ml/g)		
Sample	MY	MYSPP	% loss	MY	MYSPP	% loss
FeY	529	170	68.3	0.2982	0.0758	74.6
CoY	532	155	70.9	0.2966	0.0706	76.2
NiY	528	152	71.2	0.2974	0.0701	76.2
CuY	530	147	71.7	0.2983	0.0691	76.4

Table 3A.8 Surface area and pore volume data of complexes of SPP ligand

Sample	Surface area (m^2/g)			Pore volume (ml/g)		
	MY	MYSPP	% loss	MY	MYSPP	% loss
FeY	529	162	69.8	0.2982	0.0710	76.2
CoY	532	150	71.8	0.2966	0.0700	76.4
NiY	528	145	72.5	0.2944	0.0690	76.6
CuY	530	139	73.3	0.2930	0.0685	76.6

3A.4.2.5. Magnetic moment

The magnetic moments were measured at room temperature using Gouy method. This method gives only qualitative idea regarding magnetic moment due to high diamagnetic contribution from zeolite framework, paramagnetic contribution from the trace iron present in the zeolite lattice as impurity, and also because of the very low concentration of the complex within the zeolite.

Table 3A.9 Magnetic moments of SPO and SPP complexes

Sample	Magnetic moment (BM)	
	Gouy method	EPR
FeYSPO	5.94	-
CoYSPO	5.10	-
NiYSPO	3.00	-
CuYSPO	1.84	1.87
FeYSPP	5.90	-
CoYSPP	5.15	-
NiYSPP	3.10	-
CuYSPP	1.86	1.87

However the susceptibility of NaY was measured and its contribution to the magnetic moment of the encapsulated complex per mole of metal ion was calculated. The diamagnetic contribution of the ligand molecule was also taken into account.

The room temperature magnetic moments of the SPO and SPP complexes are given in Table 3A.9. The values indicate that all the complexes are paramagnetic. The magnetic moment of FeYSPO and FeYSPP are 5.94 and 5.90 BM. These values are closer to those of high spin Fe(III) complexes [28], suggesting a high spin octahedral geometry for the Fe(III) encapsulated complex. The magnetic moment is not of much use in identifying the geometry in the case of neat Fe(III) complexes, but is useful in assigning geometry to neat Co(II) complexes [29]. Octahedral Co(II) complexes normally have magnetic moments in the range 4.80 to 5.20 BM which is higher than spin only values of 3.89 BM. This difference from the spin only value is due to the considerable orbital contribution [29,30]. The magnetic moments of 5.10 and 5.15 BM for CoYSPO and CoYSPP indicate an octahedral structure. The simple Co(II) SPO monomeric complex is reported to have square planar geometry [6]. In the case of zeolite encapsulated complexes, the oxide ions of the zeolite lattice or water molecules can also participate in the coordination to the metal ion resulting in an octahedral geometry.

The magnetic moment of NiYSPO is 3.00 BM and that of NiYSPP is 3.10 BM. The value suggests an octahedral geometry for the complex as Ni(II) octahedral complexes usually have magnetic moments in the range 2.90-3.30 BM. The neat complex of SPO with Ni(II) is reported to have square planar geometry [6]. The change in geometry can be attributed, as in the case of zeolite encapsulated cobalt(II) complex to the interaction of the zeolite framework on the Ni(II) complex. The magnetic moment values are higher than the spin only values of 2.83 BM, suggesting some orbital contribution to magnetic moments which

may arise due to mixing of the ground state with the first excited triplet state $^3T_{2g}$ having electronic configuration $t_{2g}^5eg^3$.

The magnetic moments of Cu(II) complexes are generally in the range of 1.7-2.2 BM [30]. CuYSPO and CuYSPP have magnetic moments 1.84 and 1.86 BM respectively. Cu(II) square planar complexes show magnetic moments near the lower limits. The low value in the present case suggests square planar structure for the two Cu(II) complexes.

3A.4.2.6. Diffuse reflectance spectra

Electronic spectra in the diffuse reflectance mode are preferred over the absorbance mode for zeolite compounds since the radiations scattered by zeolites interfere with absorption due to electronic transition. The electronic spectral data of encapsulated complexes and their tentative assignments are given in Table 3A.10 and Table 3A.11, and the spectra are given in Figure3A.9 and Figure3A.10. The electronic spectra of Fe(III) complexes of SPO and SPP show a broad band with a maximum around 22000cm^{-1}. This corresponds to a combination of $^4T_{1g} \leftarrow {}^6A_{1g}$, $^4T_{2g} \leftarrow {}^6A_{1g}$, $^4E_g \leftarrow {}^6A_{1g}$ spin forbidden transitions in octahedral symmetry [31]. The band at 18180cm^{-1} seen in the case of FeYSPP may be due to spin forbidden d-d transition in high spin Fe(III). The bands at 29400cm^{-1} and 33300 cm^{-1} in the spectra of FeYSPO and FeYSPP (respectively) can be due to charge transfer transition [32].

Co(II) (d^7 system) complexes are expected to show three spin allowed transitions in octahedral geometry corresponding to transition $^4T_{2g}$ (P) $\leftarrow {}^4T_{1g}$(F), $^4A_{2g}$(F) $\leftarrow {}^4T_{1g}$(F), and $^4T_{1g}$(P) $\leftarrow {}^4T_{1g}$(F). The band ν_2 is a two electron transfer from t_{2g}^5 to $t_{2g}^3e_g^4$ and therefore would be of very low intensity [30]. In the case of CoYSPO and CoYSPP the bands at 16390cm^{-1}and 15150cm^{-1} correspond to $^4A_{2g}$(F) $\leftarrow {}^4T_{1g}$(F) transition and the bands at 19600cm^{-1} and 21600cm^{-1} can be assigned to $^4T_{1g}$(P) $\leftarrow {}^4T_{1g}$(F) transition in octahedral geometry [6].

Ni(II) complexes are reported to exhibit three spin allowed transitions in the regions 8000cm^{-1}-29000cm^{-1} in cubic field. In the case of NiYSPO all the three expected transitions are seen. One is observed at 12500cm^{-1} corresponding to $^3T_{2g}(F) \leftarrow {}^3A_{2g}(F)$, another at 18000cm^{-1} due to $^3T_{1g}(F) \leftarrow {}^3A_{2g}(F)$, and the third one is observed at 28000cm^{-1}, due to $^3T_{1g}(P) \leftarrow {}^3A_{2g}(F)$ transitions. In the case of NiYSPP, of the three expected transitions, only two are seen, one at 14000cm^{-1} corresponding to $^3T_{1g}(F) \leftarrow {}^3A_{2g}(F)$ transition and the other at 25000cm^{-1} due to $^3T_{1g}(P) \leftarrow {}^3A_{2g}(F)$ transitions [30].

Copper(II) complexes are susceptible to Jahn-Teller distortion and hence they do not form regular octahedral complexes. Tetragonally distorted octahedral complexes, which finally end up with square planar structures are usually formed.

Table 3A.10 Electronic spectral data of SPO complexes

Sample	Abs. max. (cm^{-1})	Assignment
FeYSPO	22000	$^4T_{1g} \leftarrow {}^6A_{1g}$
		$^4T_{2g} \leftarrow {}^6A_{1g}$
		$^4E_g \leftarrow {}^6A_{1g}$
	29400	Charge transfer transition
CoYSPO	16390	$^4A_{2g}(F) \leftarrow {}^4T_{1g}(F)$
	19600	$^4T_{1g}(P) \leftarrow {}^4T_{1g}(F)$
	29940	Charge transfer transition
NiYSPO	12500	$^3T_{2g}(F) \leftarrow {}^3A_{2g}(F)$
	18000	$^3T_{1g}(F) \leftarrow {}^3A_{2g}(F)$
	28000	$^3T_{1g}(P) \leftarrow {}^3A_{2g}(F)$
	30150	Charge transfer transition
CuYSPO	13160	d-d transition
	29000	Charge transfer transition

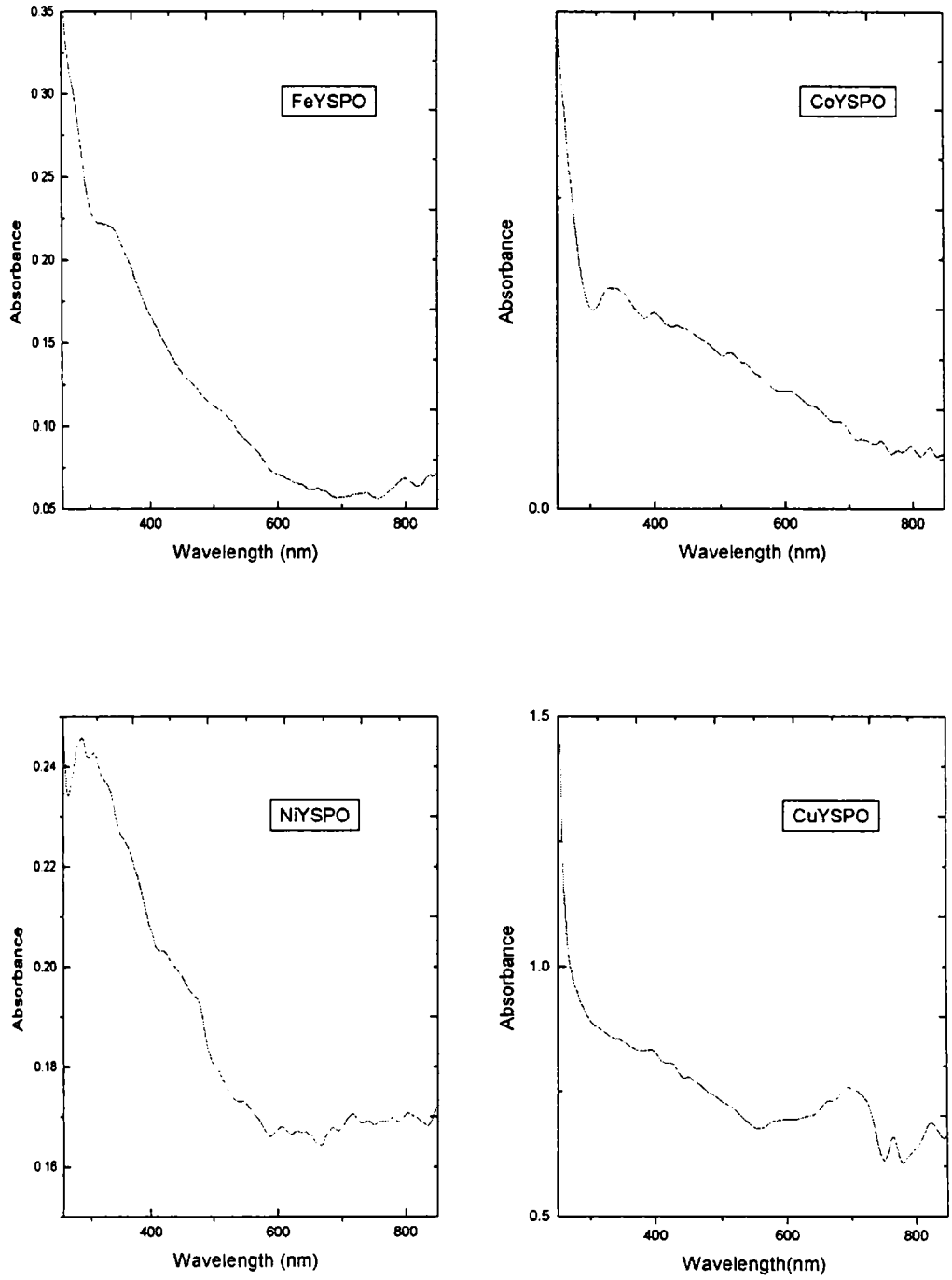

Figure 3A.9 **Electronic spectra of SPO complexes**

Table 3A.11 Electronic spectral data of SPP complexes

Sample	Abs. max. (cm^{-1})	Assignment
FeYSPP	18180	d-d transition
	22000	$^4T_{1g} \leftarrow {}^6A_{1g}$
		$^4T_{2g} \leftarrow {}^6A_{1g}$
		$^4E_g \leftarrow {}^6A_{1g}$
	33300	Charge transfer transition
CoYSPP	15150	$^4A_{2g}(F) \leftarrow {}^4T_{1g}(F)$
	21600	$^4T_{1g}(P) \leftarrow {}^4T_{1g}(F)$
	29500	Charge transfer transition
NiYSPP	14000	$^3T_{1g}(F) \leftarrow {}^3A_{2g}(F)$
	25000	$^3T_{1g}(P) \leftarrow {}^3A_{2g}(F)$
	29850	Charge transfer transition
CuYSPP	12500	d-d transition
	29325	Charge transfer transition

Many Cu(II) complexes give a broad band in the region 11000-16000cm^{-1} resulting in the blue or green colour. The bands at 13160cm^{-1} and 12500cm^{-1} in the spectra of the complexes CuYSPO and CuYSPP correspond to d-d transitions. Magnetic susceptibility data suggest square planar geometry for the encapsulated complex. The structures of neat Cu(II) complexes of SPO and SPP also exhibit bands in the region 13000-14000cm^{-1}. The bands at 29000cm^{-1} and 29325cm^{-1} in the electronic spectra of the encapsulated complexes are due to charge transfer transitions.

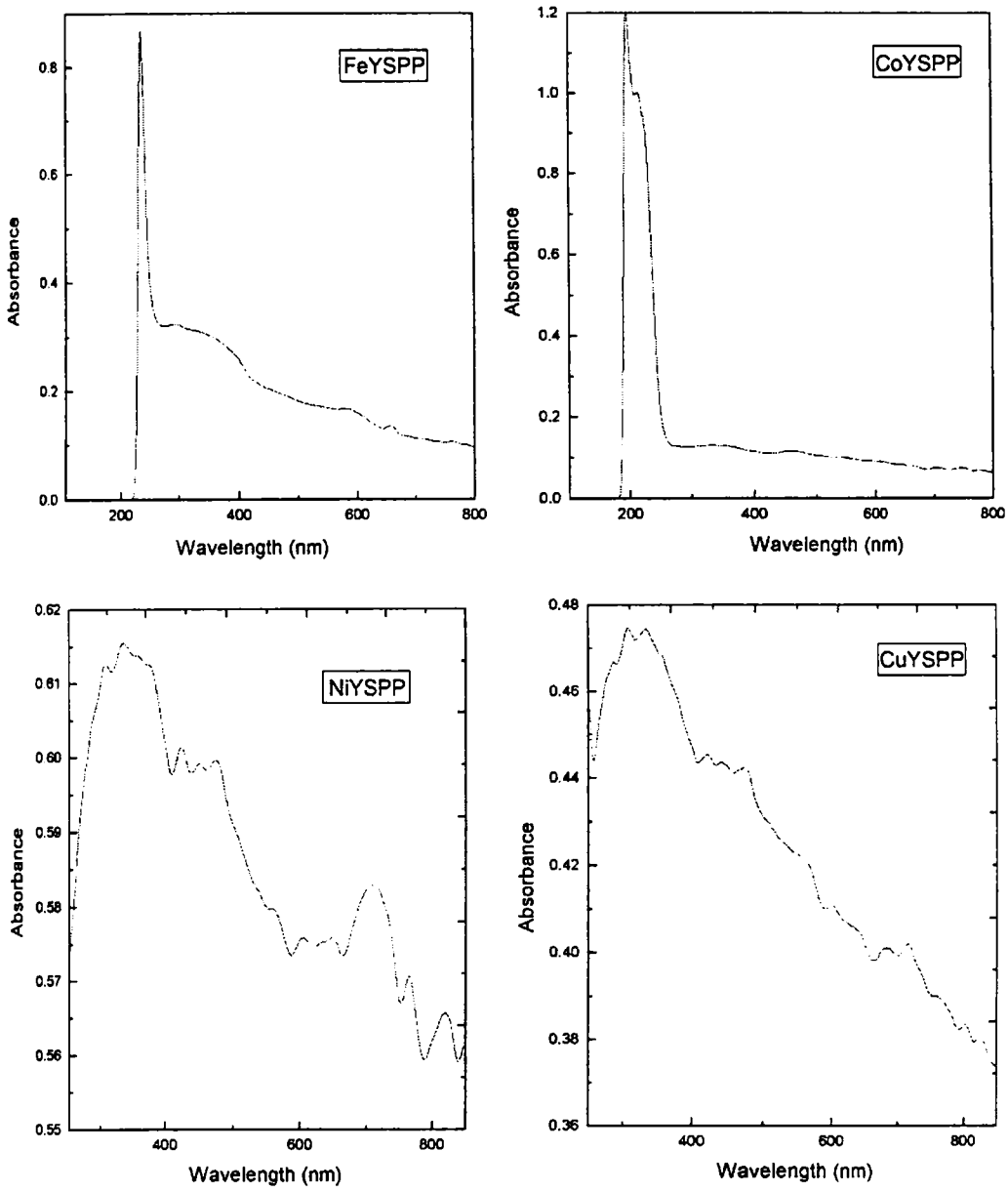

Figure 3A.10 Electronic spectra of SPP complexes

3A.4.2.7. FTIR spectra

The IR spectra of ligand SPO and zeolite encapsulated SPO complexes are given in Figure 3A.11, and those of ligand SPP and zeolite encapsulated SPP complexes are given in Figure 3A.12. The IR absorption frequencies of SPO ligand and encapsulated SPO complexes are presented in Table 3A.12, and those of SPP and its complexes are presented in Table 3A.13. The strong band at 1581cm^{-1} in the spectrum of the ligand SPO is shifted to the lower energy region 1560-1545cm^{-1} in the spectrum of the complexes, indicating coordination of azo-methine nitrogen. Some of the bands of the ligand are masked by strong absorption of the zeolite support. Some new bands seen in the spectrum of the encapsulated complex are those of the zeolite support. The OH stretching and bending vibration of water is seen as a broad band at 3450-3470cm^{-1} and 1630-1640cm^{-1} in the spectra of all the encapsulated complexes. Bands around 1030cm^{-1} and 700cm^{-1} may be attributed to the rocking and wagging modes of water.

The band at 1610cm^{-1} corresponds to υC=N stretching vibration of the ligand SPP. This band is seen between 1540 and 1560cm^{-1} in all the complexes indicating coordination through nitrogen. As in the case of SPO complexes, the OH stretching vibration of water is seen as a broad band in the range 3440-3470cm^{-1} and bending vibration between 1635 and 1640cm^{-1} in the spectra of all the encapsulated complexes. The rocking and wagging modes of water are also seen in the spectra of the complexes.

Table 3A.12 Infrared spectral data of SPO complexes

SPO cm^{-1}	FeYSPO cm^{-1}	CoYSPO cm^{-1}	NiYSPO cm^{-1}	CuYSPO cm^{-1}
470			469	464
536				567
623	630	640	635	640
703	700	700	720	730
747				
817				
957				
	1023	1025	1040	1050
1114				
1126				
1317				
1432				
1538				
1581	1560	1545	1550	1550
	1640	1640	1641	1640
1925				
	2375	2375	2368	2368
2789				
3103				
3439	3470	3480	3474	3480

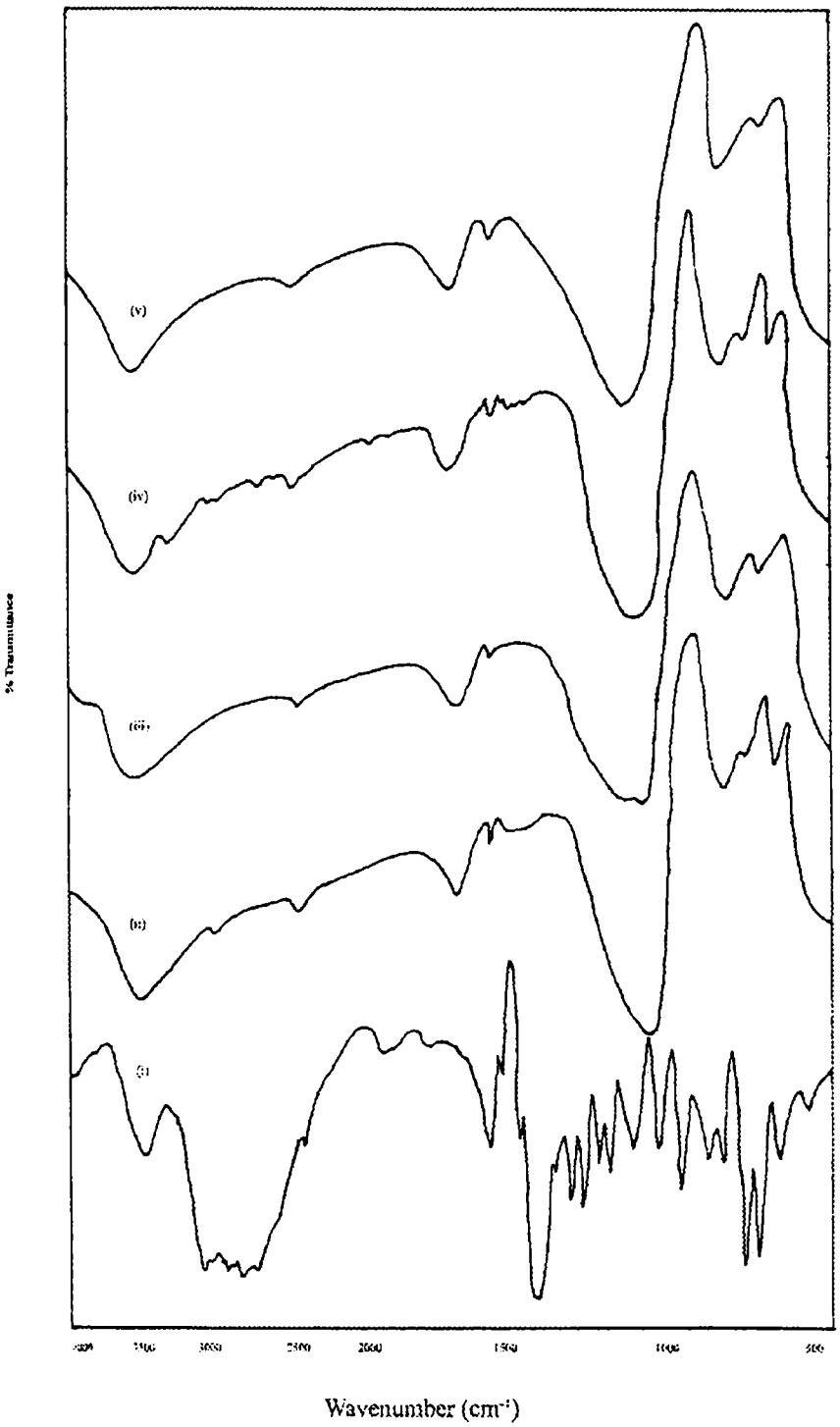

Figure 3A.11 IR spectra of SPO complexes
i) SPO ii) FeYSPO, iii) CoYSPO, iv) NiYSPO, v) CuYSPO

Table 3A.13 Infrared spectral data of SPP complexes

SPP cm^{-1}	FeYSPP cm^{-1}	CoYSPP cm^{-1}	NiYSPP cm^{-1}	CuYSPP cm^{-1}
442				
578				
625	615	620	607	610
700	723	730	723	726
752				
900				
1027	1040	1045	1043	1044
	1111		1100	1105
1176				
1294				
1401				
1514				
1610	1540	1540	1560	1545
	1635	1640	1640	1640
2339		2368	2375	2375
2371				
3202				
3390				
	3460	3461	3460	3467

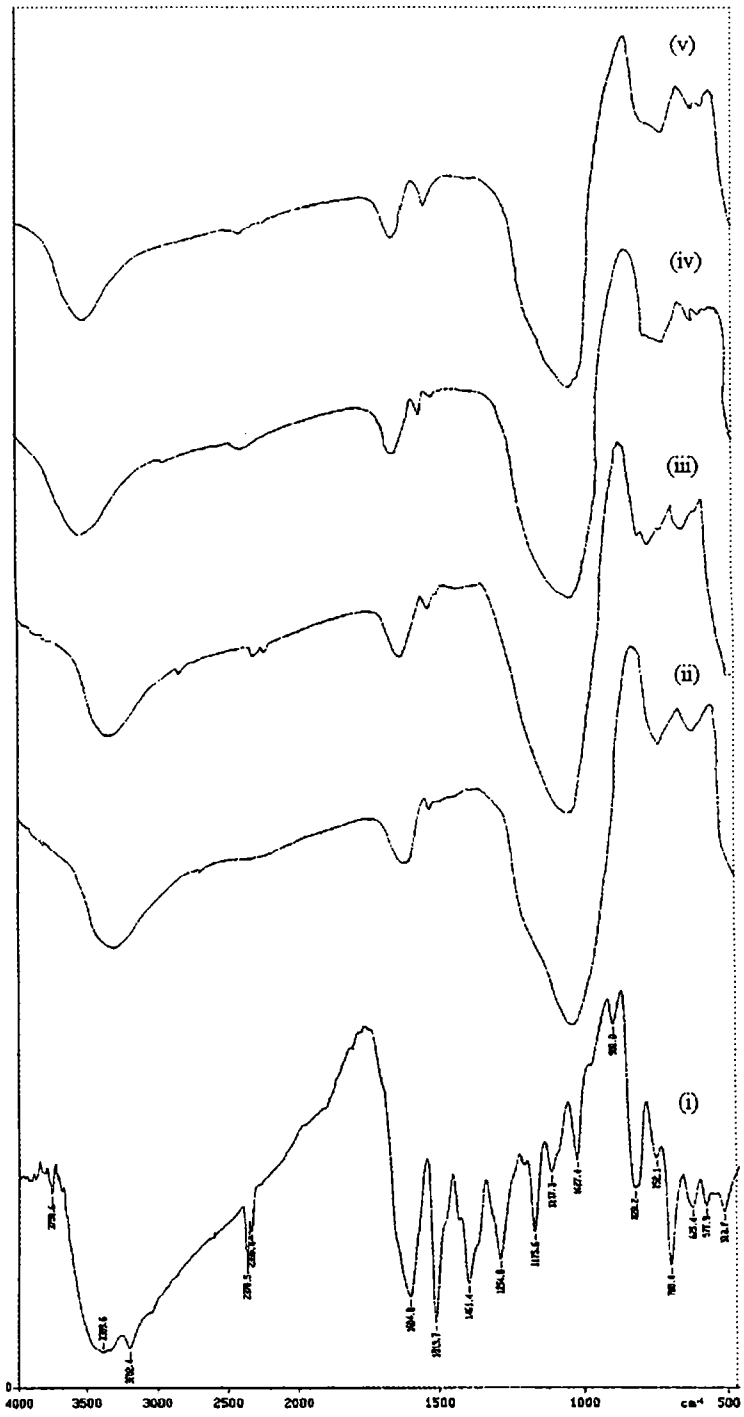

Figure 3A.12 IR spectra of SPP complexes
i) SPP, ii) FeYSPP, iii) CoYSPP, iii) NiYSPP, iv) CuYSPP

3A.4.2.8. EPR spectra

The powder spectra of the zeolite encapsulated Cu(II) complexes of SPO and SPP were recorded at room temperature and at liquid nitrogen temperature. Glass spectra of neat Cu(II) complexes of SPO and SPP were also recorded at liquid nitrogen temperature. EPR parameters were determined without computer simulation in the present study. However these parameters provide a qualitative idea about the nature of coordination in the encapsulated complexes. EPR spectra of neat and encapsulated SPO and SPP complexes are shown in Figure3A.13 and Figure3A.14. The EPR parameters, unpaired electron density and magnetic moment were calculated from EPR spectral data, and the results are given in Table 3A.14 and Table 3A.15. The well defined hyperfine features similar to that in dilute solution in the case of encapsulated complexes indicate the encapsulation of monomeric complexes in the zeolite lattice. The g_{II} values of CuYSPO and CuYSPP are 2.35 and 2.36 respectively. These are higher than the expected values. The reasons for such high g_{II} values have been discussed by Sakaguchi and Addison [19]. The high g value obtained in the present case may be due to the distortion of structure caused by the zeolite ligand and the zeolite oxygen atom on coordination. The trend $g_{II} > g_{\perp} > 2.0023$ observed for this complex shows that the unpaired electron is delocalized in the $dx^2\text{-}y^2$ orbital [33]. This is typical of tetragonal distortion of Cu(II) environment which finally leads to a square planar structure.

The ratio g_{II}/A_{II} is 133cm and 125cm respectively for the encapsulated SPO and SPP complexes. These values come within the range 105-135cm reported for square planar complexes and suggest square planar structure for the encapsulated CuYSPO and CuYSPP complexes. Hyperfine splitting was clearly seen in the spectrum of neat copper SPO complex while it was not observed in the spectrum of neat copper SPP complex even at liquid nitrogen temperature. The broad EPR spectrum in the case of neat copper SPP complex can be due to the nearest

neighbour's spin-spin interaction. The spectra of the copper complexes at room temperature showed no splitting at all.

Table 3A.14 EPR parameters of SPO complexes of copper

EPR parameters	CuSPO	CuYSPO
g_{II}	g_{II}	2.35
A_{II}	225 x 10^{-4} cm^{-1}	179 x 10^{-4} cm^{-1}
g_{II} /A_{II}	107	133cm
$g_{\perp}$	2.09	2.06
$A_{\perp}$	30.88 x 10^{-4} cm^{-1}	59.36 x 10^{-4} cm^{-1}
α^2	0.9105	0.9132
μ_{eff}	1.9	1.87
P	-0.727	-0.6846

Table 3A.15 EPR parameters of SPP complexes of copper

EPR parameters	CuSPP	CuYSPP
g_{II}	2.4	2.36
A_{II}	150 x 10^{-4} cm^{-1}	188 x 10^{-4} cm^{-1}
g_{II} /A_{II}	130cm	125cm
$g_{\perp}$	2.04	2.04
$sA_{\perp}$	20 x 10^{-4} cm^{-1}	29.1 x 10^{-4} cm^{-1}
α^2	0.874	0.874
μ_{eff}	1.87	1.87
P	-0.5463	-0.5463

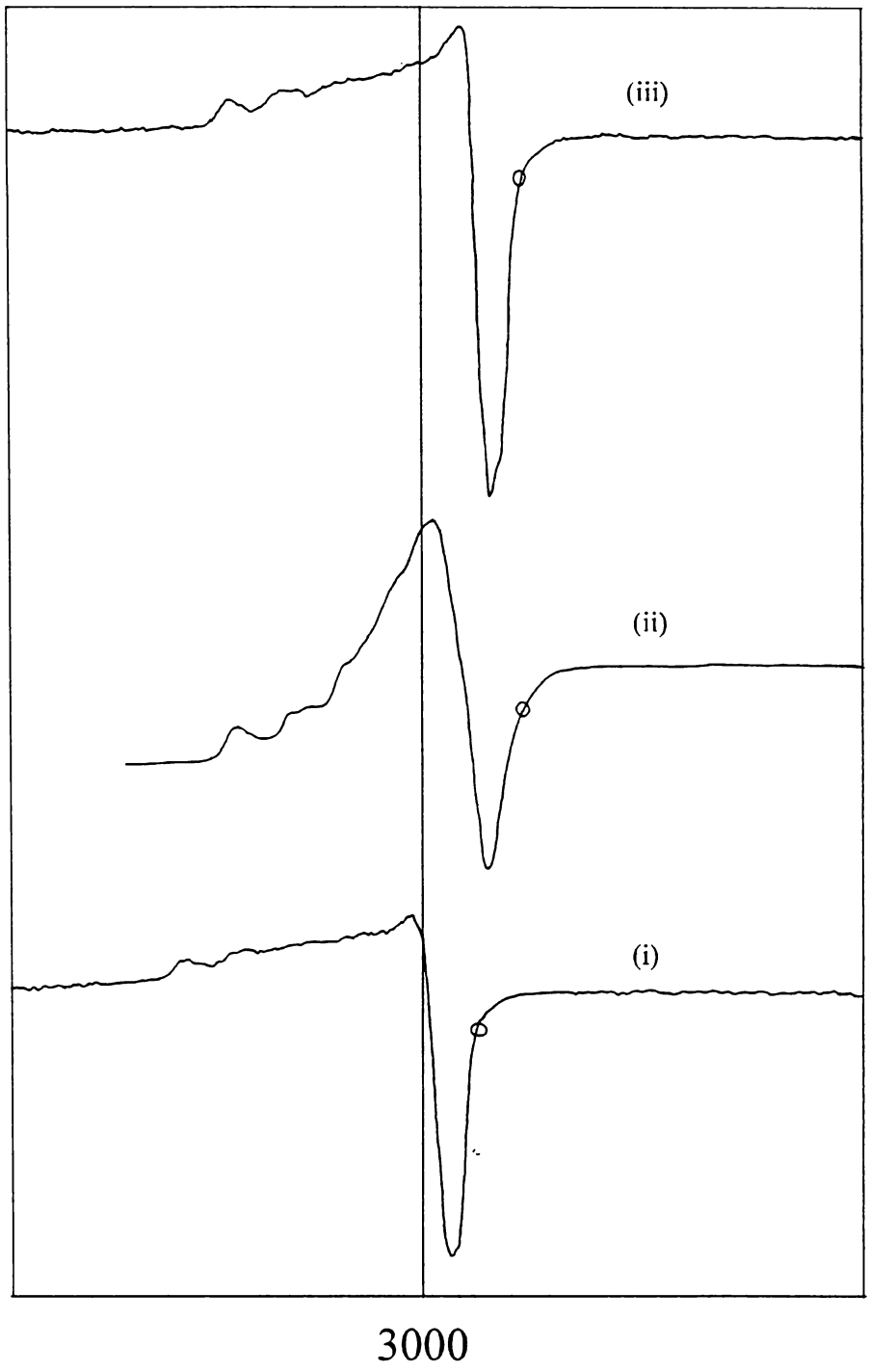

Figure 3A.13 EPR spectra of SPO complexes
i) CuYSPO at RT, ii) CuSPO at LNT, iii) CuYSPO at LNT

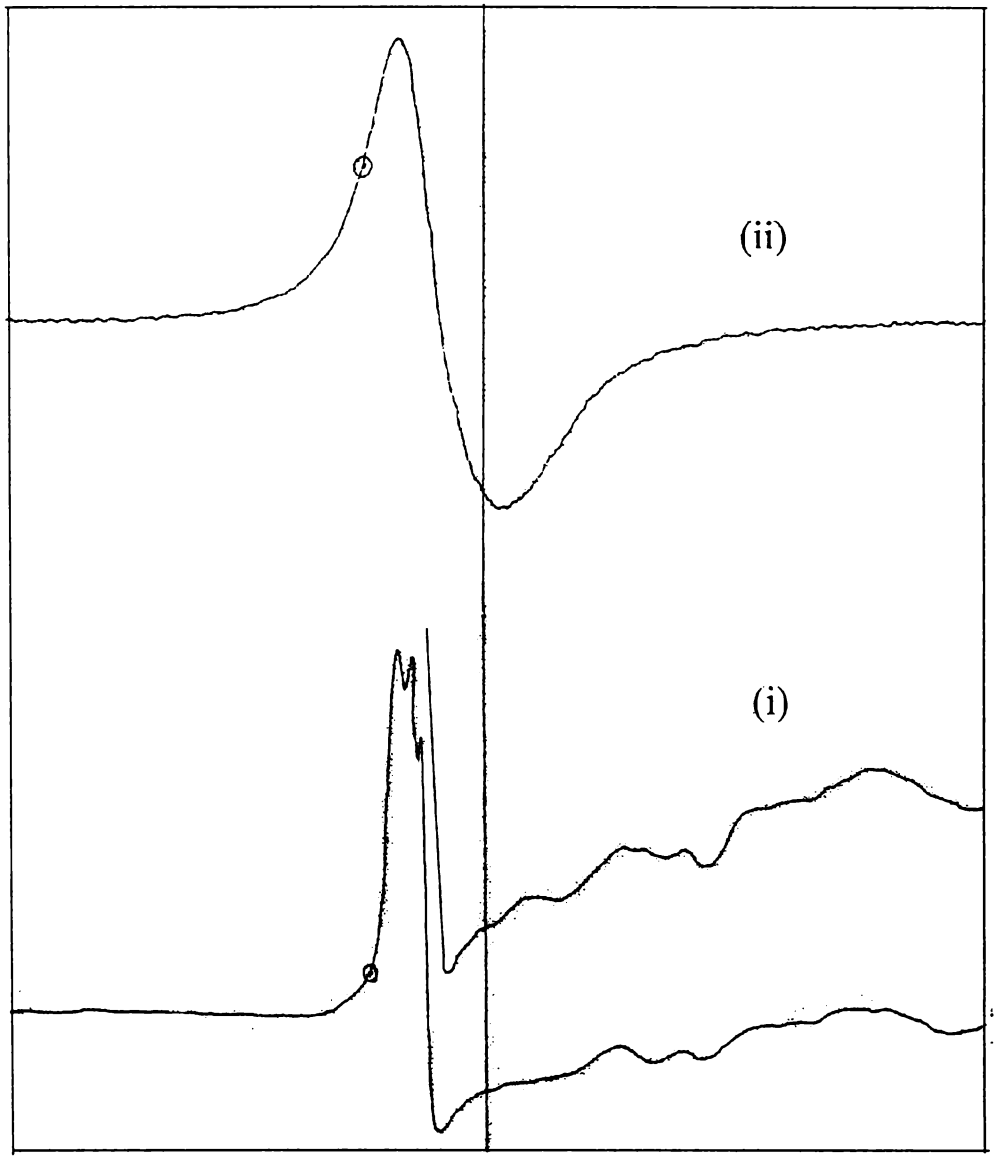

Figure 3A.14 EPR spectra of SPP complexes
i) CuYSPP at LNT, ii) CuSPP at LNT

The density of unpaired electrons at the metal atom and the magnetic moments of the neat and encapsulated copper complexes of SPO and SPP were calculated from EPR parameters. The in plane covalence parameter, α^2 values of 0.9105, 0.9132, 0.874, and 0.874 for the neat copper SPO, CuYSPO, neat copper SPP, and CuYSPP respectively indicate an ionic environment for Cu^{2+} ions. The magnetic moments (1.87 BM for the CuYSPO and CuYSPP complexes) are in agreement with the values obtained from magnetic susceptibility measurements at room temperature. All these are suggestive of square planar structure for the copper encapsulated complexes.

3A.4.2.9. TG analysis

Thermo gravimetric analysis provides a quantitative measurement of any weight change associated with a transition. The thermal behavior of SPO and SPP complexes have been studied, and the thermal analytical data for the complexes are presented in Table 3A.16. The TG curves of SPO complexes are given in Figure 3A.15 and those of SPP complexes in Figure 3A.16. Generally, well-defined TG patterns are seen in the case of neat complexes during the removal of ligand moieties. Such well-defined patterns are not seen in the case of zeolite encapsulated complexes. Because of the low concentration of metal complexes in the zeolite cage, a correlation of mass loss with expelled ligand moieties was not attempted in the present study. However, the TG curves help to get an idea about the approximate temperature of decomposition. The mass loss around 30-110 °C in the TG of both the SPO and the SPP series corresponds to the expulsion of intrazeolite free water molecules. The mass loss in the temperature range 110-500 °C corresponds to the removal of coordinated water and the partial decomposition of the complex and the mass loss corresponding to the temperature range 500-800 °C can be due to the decomposition of the complex and partial decomposition of the zeolite. The IR spectra of the residue after analysis indicate that the encapsulated complex has completely decomposed. According to reports obtained

from literature, the stability of the complexes is believed to be enhanced on heterogenising them, especially on encapsulating them in zeolite pores [34].

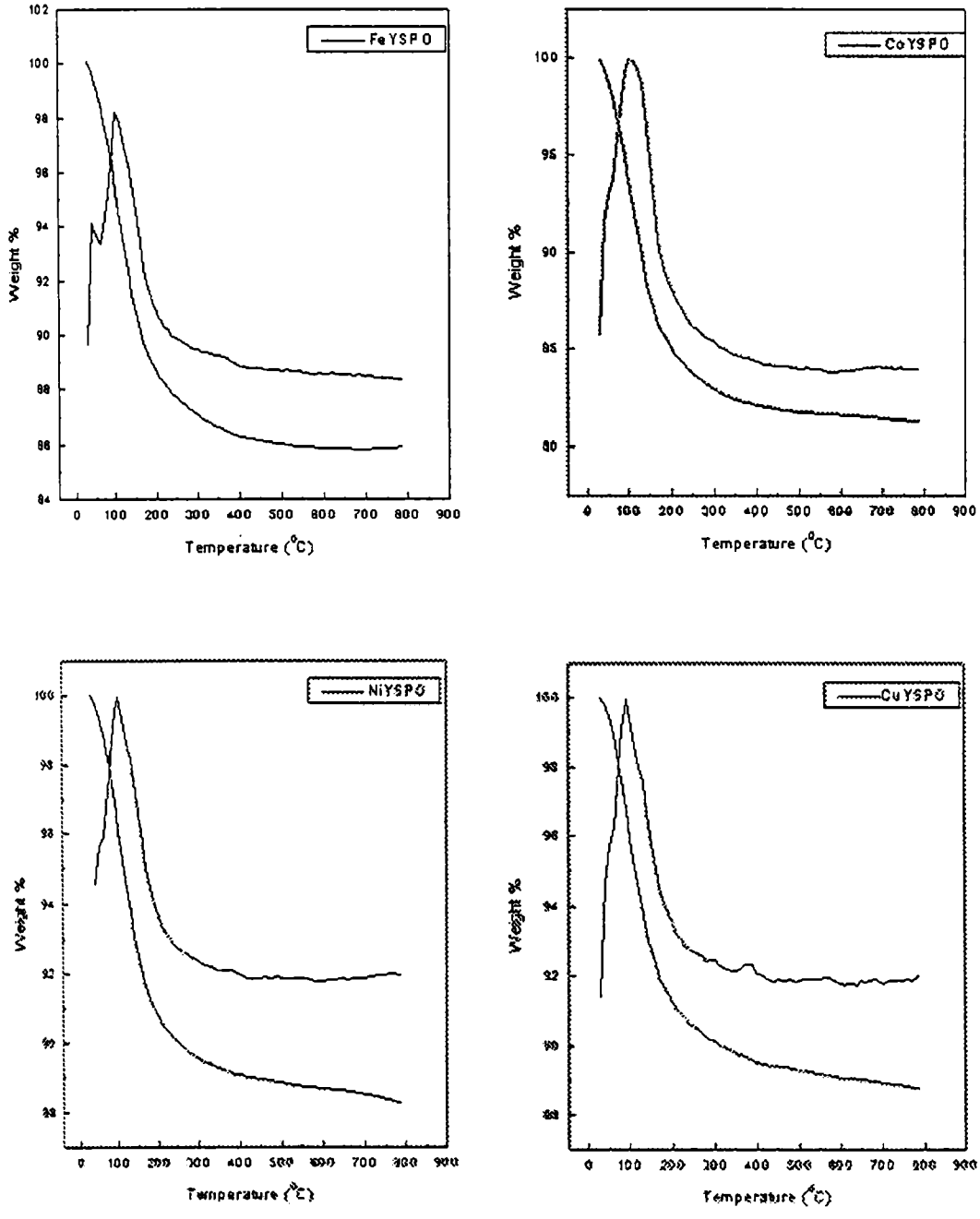

Figure 3A. 15 TG/ DTG curves of SPO complexes.

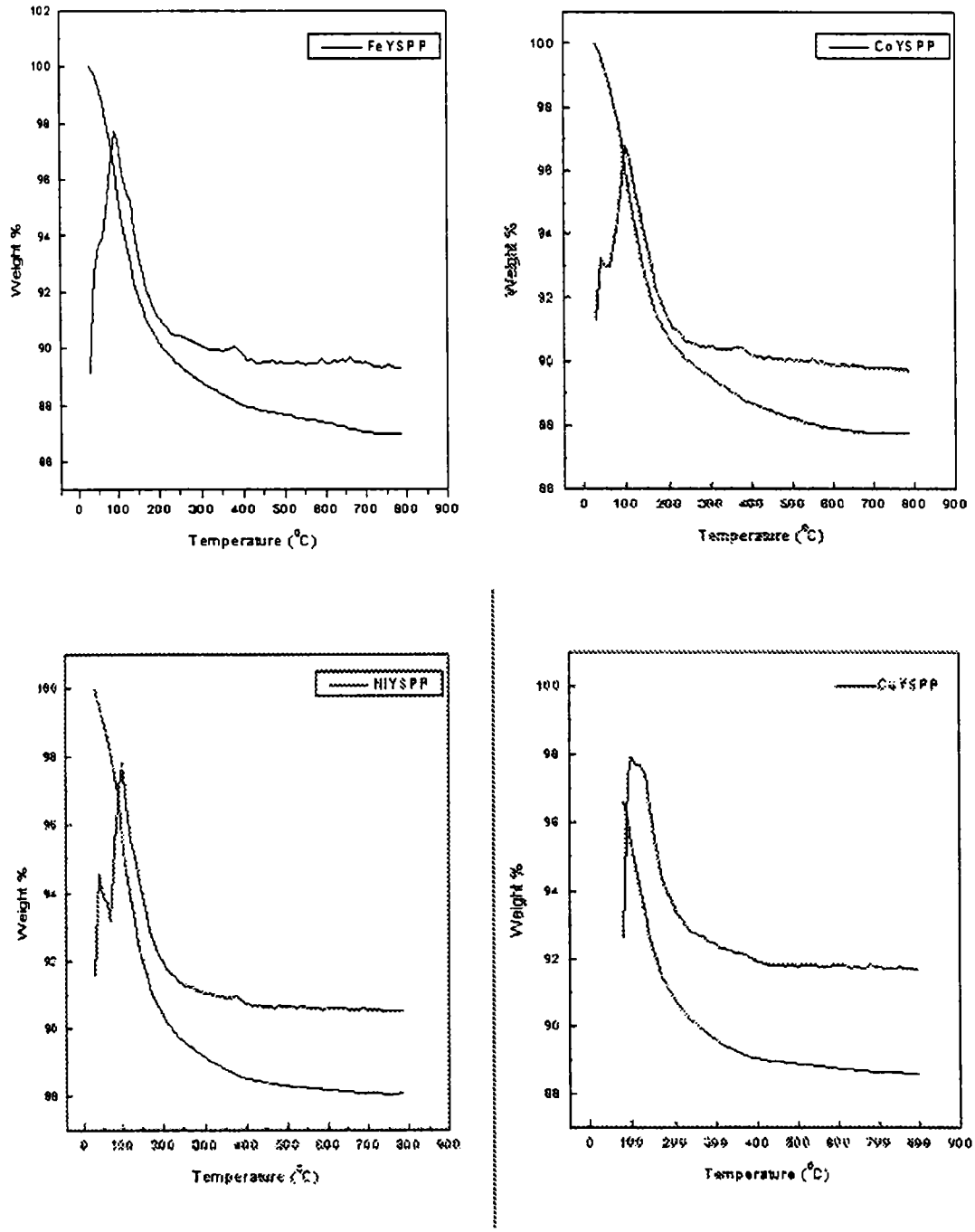

Figure 3A. 16 TG/DTG curves of SPP complexes.

Table 3A.16 Thermal decomposition data of SPO and SPP complexes

Sample	Temp. Range TG (°C)	% Mass loss from TG
FeYSPO	30-110	5.75
	110-500	8.23
	500-800	0.11
CoYSPO	30-110	7.61
	110-500	10.5
	500-800	1.53
NiYSPO	30-110	4.52
	110-500	6.38
	500-800	0.59
CuYSPO	30-110	4.87
	110-500	5.85
	500-800	0.54
FeYSPP	30-110	5.52
	110-500	6.83
	500-800	0.70
CoYSPP	30-110	4.86
	110-500	6.90
	500-800	0.48
NiYSPP	30-110	5.37
	110-500	6.32
	500-800	0.23
CuYSPP	30-110	5.33
	110-500	5.79
	500-800	0.29

Section B

Zeolite encapsulated Co(II), Ni(II) and Cu(II) complexes of salicylaldehyde semicarbazone

3B.1. Introduction

Schiff base complexes with oxygen coordination have both structural and biological significance. These include Schiff bases derived from semicarbazides, aminophenols, amino acids etc. Semicarbazones act as monodentate/ bidentate ligands depending on the pH of the reacting medium, or as a tridentate ligand depending on the aldehyde residue attached to semicarbazide moiety. Their chemistry is interesting as only β-nitrogen coordinates to the metal atom, while the α nitrogen remains uncoordinated. The oxygen atom shows a tendency to form strong covalent bonds with the metal atom.

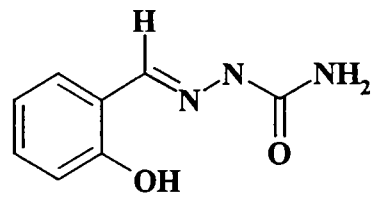

Figure 3B.1. Structure of SALSC ligand

Neat complexes with salicylaldehyde semicarbazone have been reported [35]. Neat copper SALSC complexes have been reported to show superoxide dismutase (SOD) activity, and it can be increased by the addition of heterocyclic bases. Studies on the encapsulated Co, Ni, and Cu complexes with salicylaldehyde semicarbazone were undertaken to know whether any structural and other changes occur during encapsulation. The results of the studies are presented in this section.

3B.2. Experimental

3B.2.1. Synthesis of zeolite encapsulated Co, Ni and Cu complexes of salicylaldehyde semicarbazone

Metal exchanged zeolite (3.0 g) was mixed with the ligand salicylaldehyde semicarbazone in such a way that the ligand to metal mole ratio is 1. However a slight excess of the ligand was used. This was ground well, and heated in a fused tube (ampule) for 6 hours at 200 °C and cooled to room temperature. The super cage entrance is large enough to access the cobalt, nickel and copper sites. The product was soxhlet extracted first with methanol to remove unreacted ligand, and then with chloroform to remove any surface species. The uncomplexed metal ions were removed by sodium exchange, made free of chloride ions, dried at 100 °C for 2 hours and stored in vacuum desicator over anhydrous calcium chloride.

3B.3. Characterization techniques

Details of the analytical methods of encapsulated SALSC complexes and other characterization techniques are given in Chapter 2.

3B.4. Results and Discussion

3B.4.1. Chemical analysis

The metal percentage was determined using AAS, and the analytical data are presented in Table 3B.1. The Si/Al ratio of NaY is retained in the encapsulated complexes, indicating the absence of dealumination and the preservation of crystal structure. The metal to ligand ratio is found to be 1:1 in neat complexes [35]. The same ratio is expected in the case of encapsulated complexes also. But the percentage of metal is slightly higher than that required for 1:1 complexes. This shows that all the metal ions are not removed by the back exchange of Na^+ ions.

The small percentage of metal that remains uncomplexed may be metal ions trapped in the cage by the complex formed around it. These traces of uncomplexed metal ions are unlikely to cause any serious interference in the behaviour of the encapsulated complexes. Similar observations have been made in the case of other zeolite encapsulated complexes by earlier workers also [23].

Table 3B.1 Analytical data

Sample	% Si	% Al	% Na	% M	%C
CoYSALSC	18.75	7.64	5.41	0.25	0.30
NiYSALSC	18.69	7.59	5.85	0.49	0.69
CuYSALSC	18.80	7.76	5.79	0.95	1.21

3B.4.2. X-ray diffraction studies

X-ray diffraction patterns of Co, Ni and Cu encapsulated SALSC complexes and NaY are presented in Figure 3B.2. The diffraction patterns of the encapsulated complex were more or less similar to those of NaY which suggests that there is no loss in crystallinity on encapsulation. This again confirms that the complexes are formed inside the large cavities, and the formation of the complex does not affect the zeolite lattice.

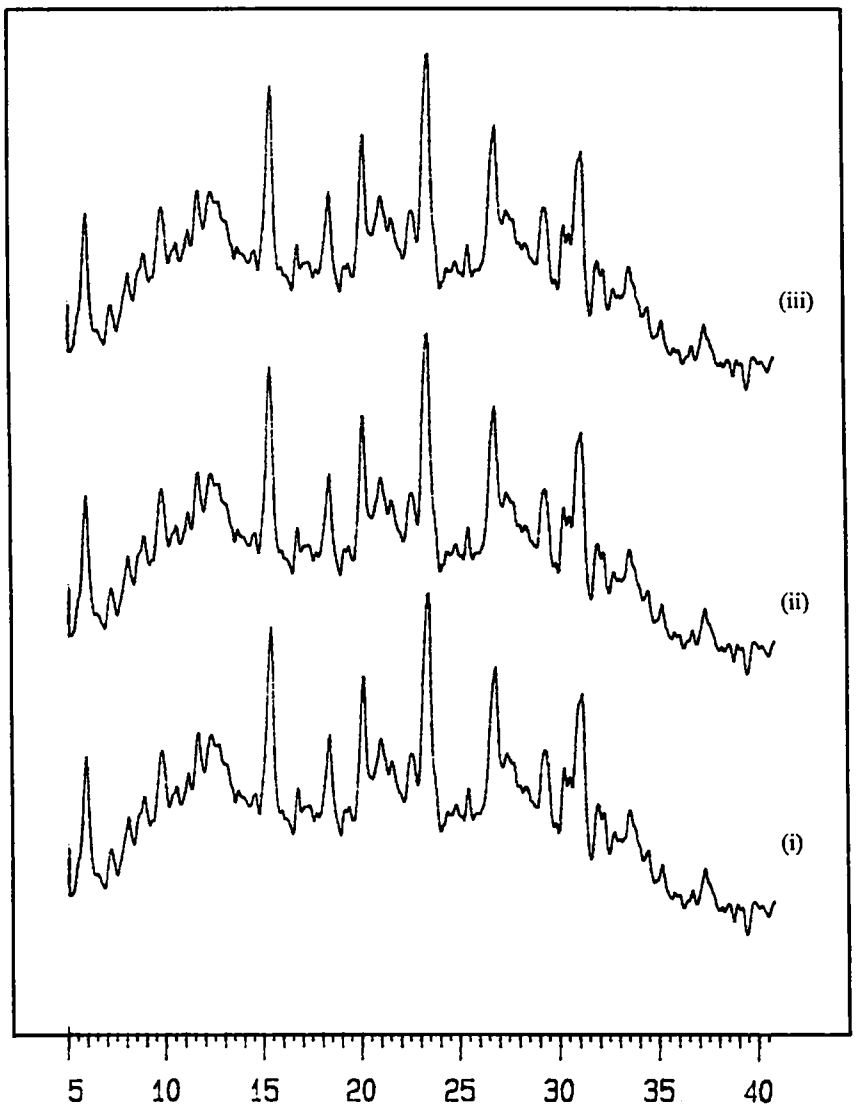

Figure 3B.2 XRD patterns of SALSC complexes
i) CoYSALSC, ii) NiYSALSC, iii) CuYSALSC

3B.4.3. Surface area and pore volume

Surface area and pore volume values of the SALSC complexes are presented in Table 3B.2. The surface area analyses provide good evidence for encapsulation, as in the case of SPO and SPP complexes. This decrease in surface area has been found to be a strong indication of encapsulation [26].

Table 3B.2 Surface area and pore volume

Sample	Surface area (m^2/g)			Pore volume (ml/g)		
	MY	MYSALSC	% loss	MY	MYSALSC	% loss
CoY	532	231	56.4	0.2986	0.1313	56.03
NiY	528	235	55.5	0.2974	0.1324	55.48
CuY	530	240	54.7	0.2983	0.1331	55.38

3B.4.4. Magnetic moment

Magnetic moments of Co, Ni and Cu complexes were calculated, as in the case of the encapsulated complexes of SPO and SPP. The magnetic moments are presented in Table 3B.3. The magnetic moments of CoYSALSC and NiYSALSC complexes nearly agree with the reported values of neat Co(II) and Ni(II) complexes of SALSC (4.93 BM and 3.35 BM respectively), which are suggested to have an octahedral geometry [36]. It may therefore be inferred that that the encapsulated complexes also have an octahedral geometry.

Table 3B.3 Magnetic moment

Sample	Magnetic moment (BM)	
	Gouy method	EPR
CoYSALSC	4.85	-
NiYSALSC	3.16	-
CuYSALSC	1.78	1.85

Neat Cu(II) complex is reported to have a value of 1.75 BM [37]. The encapsulated Cu(II) has a value of 1.78 BM by Gouy method and a value of 1.85 BM from EPR measurements. The low value suggests a square planar structure for the Cu(II) complex. Thus the magnetic moments of the neat and the encapsulated complexes agree with each other.

3B.4.5. Diffuse reflectance spectra

The electronic spectra of encapsulated SALSC complexes of Co(II), Ni(II) and Cu(II) were recorded in the diffuse reflectance mode . The electronic spectra of SALSC complexes are presented in Figure 3B.3 and the electronic spectral data are presented in Table 3B.4. All the three SALSC complexes show strong ligand to metal charge transfer bands in the region 33000-33560cm^{-1} [31].

The electronic spectra of CoYSALSC shows two bands at 15600cm^{-1} and 18200cm^{-1} attributable to $^4A_{2g}(F) \leftarrow {}^4T_{1g}(F)$ (υ_2), and $^4T_{1g}(P) \leftarrow {}^4T_{1g}(F)$ (υ_3) in octahedral field [29,31]. All the three transitions corresponding to υ_1, υ_2 and υ_3 in octahedral geometry for Co(II) complex have been reported by Maurya et al. while a tetrahedral structure has been reported by Ray for the same neat complex [37].

The analysis of the spectrum of NiYSALSC reveals an octahedral geometry for the metal ion. Of the three spin allowed transitions in cubic field, only two are observed. The reflectance spectrum exhibits bands at 18000cm^{-1} and 25640cm^{-1} attributable to $^3T_{1g}(F) \leftarrow {}^3A_{2g}(F)$ and $^3T_{1g}(P) \leftarrow {}^3A_{2g}(F)$ transitions [31]. These bands correspond to the υ_2 and υ_3 transitions in octahedral geometry. In the case of neat complex of SALSC all the three spin allowed transitions are observed in the regions 8500cm^{-1}, 14500cm^{-1} and 25000cm^{-1} respectively. These transitions were assigned to $^3T_{2g}(F) \leftarrow {}^3A_{2g}(F)$, $^3T_{1g}(F) \leftarrow {}^3A_{2g}(F)$ and $^3T_{1g}(P) \leftarrow {}^3A_{2g}(F)$ transitions respectively, characteristic of octahedral geometry [36].

Table 3B.4 Electronic spectral data of salicylaldehyde semicarbazone complexes

Sample	Abs. max. (cm^{-1})	Assignment
CoYSALSC	15600	$^4A_{2g}(F) \leftarrow {}^4T_{1g}(F)$
	18200	$^4T_{1g}(P) \leftarrow {}^4T_{1g}(F)$
	33330	Charge transfer transition
NiYSALSC	18000	$^3T_{1g}(F) \leftarrow {}^3A_{2g}(F)$
	25640	$^3T_{1g}(P) \leftarrow {}^3A_{2g}(F)$
	33560	Charge transfer transition
CuYSALSC	12000	d-d transition
	26525	Charge transfer transition
	33000	Charge transfer transition

CuYSALSC complex exhibits a broad band at 12000cm^{-1} assignable to d-d transition. The magnetic moment of 1.78 BM supports a square planar structure for CuYSALSC. The geometry of neat Cu(II) complex of SALSC has been reported as octahedral but, Jayendra Patole's crystal structure studies reveal a distorted square planar geometry for the copper (II) complex [35].

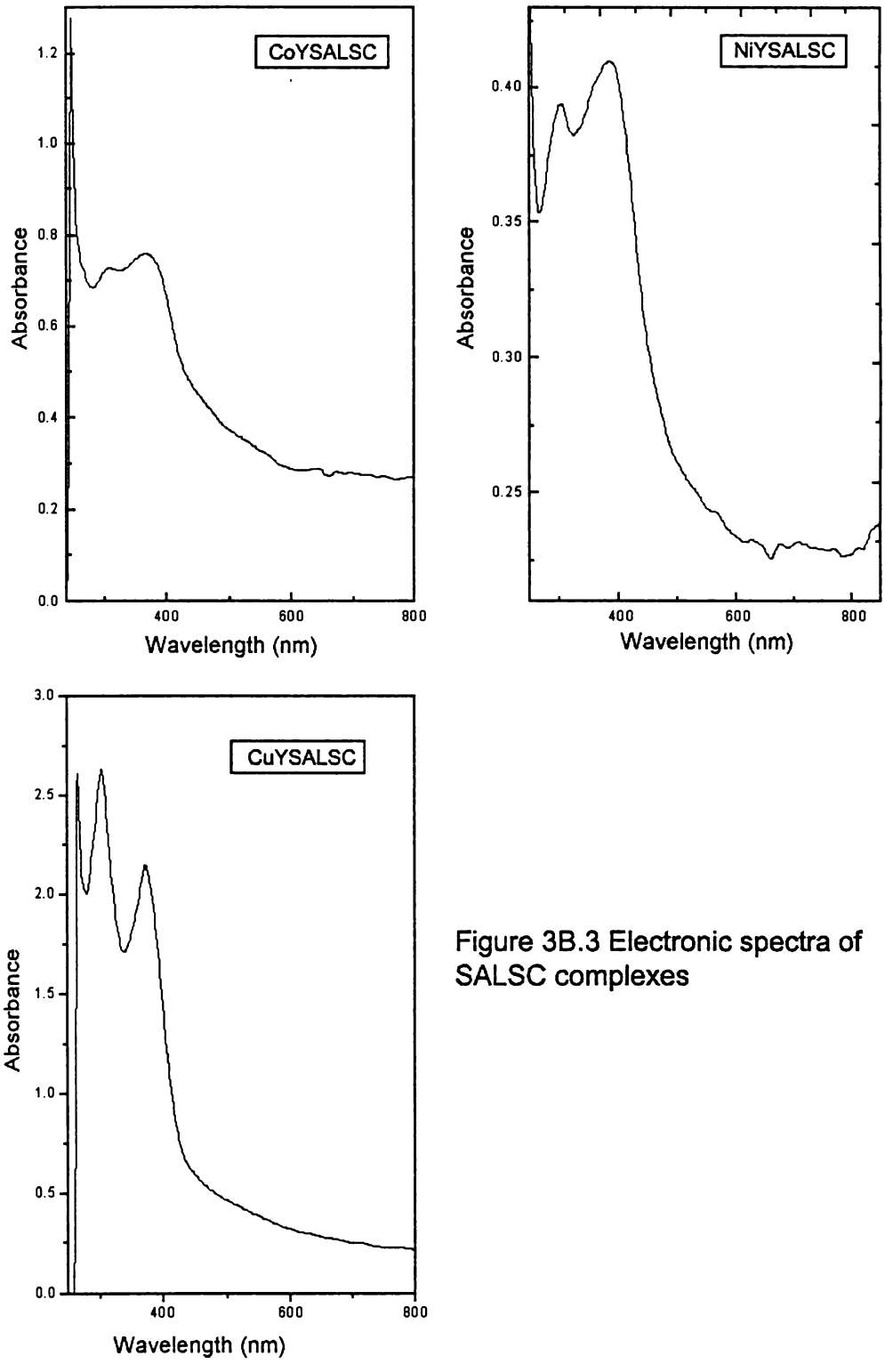

Figure 3B.3 Electronic spectra of SALSC complexes

3B.4.6. FTIR spectra

The ligand SALSC contains three donor atoms, namely, the oxygen of the phenolic hydroxyl, the nitrogen of the azo-methine group, and the oxygen of the carbonyl group. The IR spectra of the ligand SALSC and the encapsulated complexes are given in Figure 3B.4, and Table 3B.5 presents the spectral data.

Table 3B.5 IR spectral data of SALSC complexes

SALSC cm^{-1}	CoYSALSC cm^{-1}	NiYSALSC cm^{-1}	CuYSALSC cm^{-1}
459			
561	570	570	570
	611	616	609
679			
750	771	774	724
894			
980			
1030	1030	1032	1030
1110			
1151			
1201			
1273			
1353			
1384	1382	1382	1384
1486			
1620	1550	1545	1545
	1640	1640	1645
1740			
2830	2833	2832	
3417	3476	3460	3468
3777		3776	

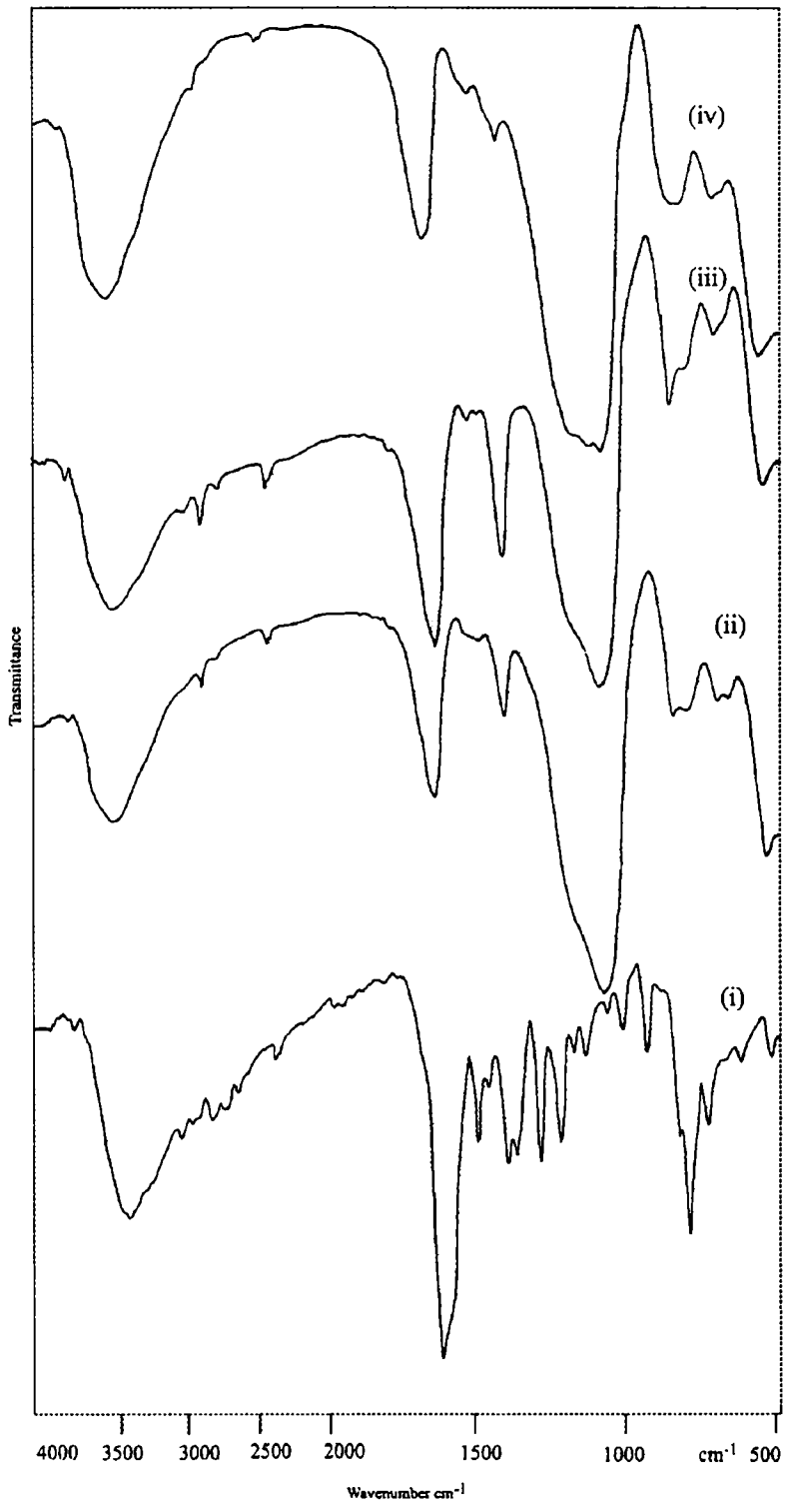

Figure 3B.4 Infrared spectra of SALSC complexes

A comparative study of the IR bands of the ligand and the complexes was carried out. Some of the ligand absorptions are masked by the absorptions of the zeolite. The ligand absorption at 1620cm^{-1} due to υC=O is shifted to a lower region (1550-1545cm^{-1}) in the complexes. Azo-methine υC=N of the Schiff base, seen in the region 1485cm^{-1} [38] might have shifted to lower regions in the complexes, though this is not clearly visible in the case of all the complexes, possibly because it gets merged with other peaks. The band appearing at 1273cm^{-1} is assigned to the vibration of the phenolic C=O group [39]. The shift of this band is not seen in the spectrum of the complexes as it is masked by the broad band of the zeolite. The broad band seen around 3250 - 3500cm^{-1} in the ligand can be due to the merging of υO-H and υN-H frequencies. The υO-H and υN-H absorptions observed in the spectra of the encapsulated SALSC complexes indicate the presence of the water molecules of zeolite, and the uncoordinated NH_2 group [40].

3B.4.7. EPR spectra

The EPR spectrum of CuYSALSC is shown in Figure 3B.5 and the EPR parameters are given in Table 3B.6.

Table 3B.6 EPR parameters of CuYSALSC

EPR parameters	Values
$g_{\|\|}$	2.34
$A_{\|\|}$	179 x 10^{-4} cm^{-1}
$g_{\|\|}/A_{\|\|}$	130cm
$g_{\perp}$	2.04
$A_{\perp}$	54.98 x 10^{-4} cm^{-1}
α^2	0.8940
μ_{eff}	1.85 BM
P	0.5589

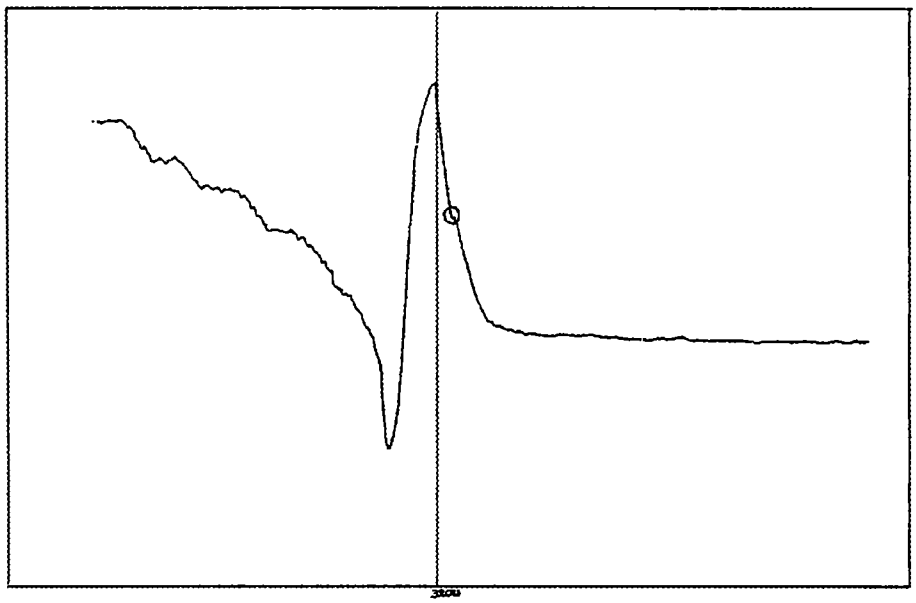

Figure 3B.5 EPR spectrum of CuYSALSC

The $g_{||}$ of CuYSALSC is 2.34 which is slightly higher than that expected for square planar complexes. The $g_{||}/A_{||}$ ratio is in the range reported for square planar complexes. The EPR of neat CuClSALSC is reported to be of typical distorted square planar geometry [35]. This indicates that there is a slight change in the structure on encapsulation, which can be due to restriction imposed by the zeolite cavity. The α^2 value of 0.894 suggests an ionic environment for Cu(II) ions. The magnetic moment of 1.8 BM agrees with that obtained from magnetic susceptibility measurements.

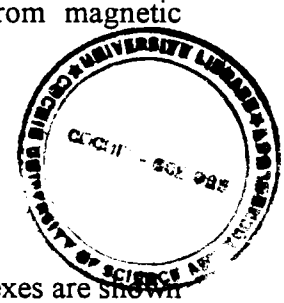

3B.4.8. TG analysis

The TG curves recorded for the encapsulated SALSC complexes are shown in Figure 3B.6 and the data are presented in Table 3B.7. Thermal studies of neat SALSC complexes have been made by Petrovic et al. [41]. Well-defined TG curves are obtained for neat complexes. Such types of curves are not obtained in

Table 3B.7 Thermal decomposition data

CoYSALSC		NiYSALSC		CuYSALSC	
Temp Range (°C)	% Mass loss	Temp Range (°C)	% Mass loss	Temp Range (°C)	% Mass loss
30-100	5.24	40 -192	7.50	32-149	9.40
100-250	5.93	192 - 250	1.30	149-216	2.40
250-500	2.30	250 – 505	3.00	216-325	0.87
500-690	0.33	505-700	0.45	325-700	1.13

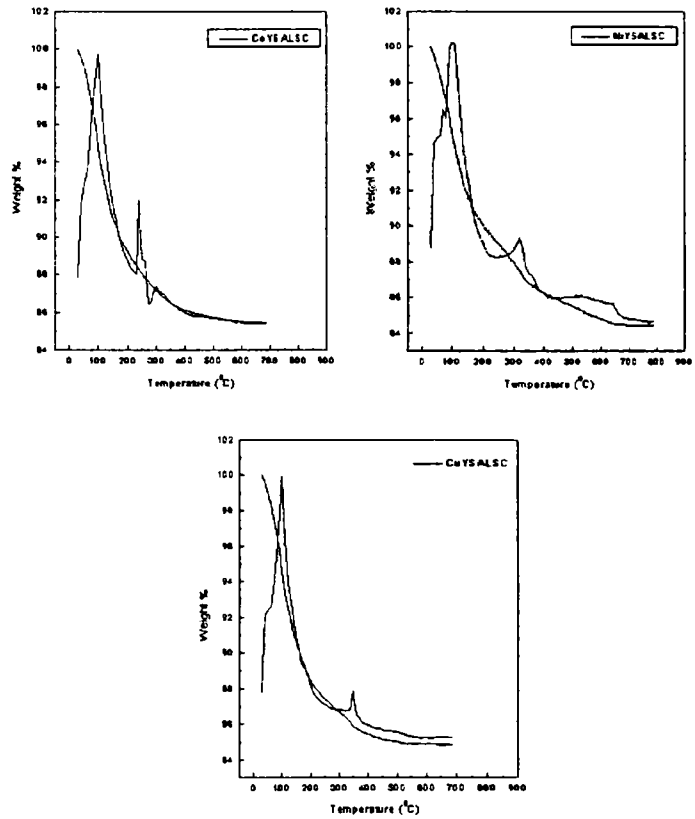

Figure 3B.6 TG curves of SALSC complexes

the case of encapsulated complexes. The stages are continuous rather than distinct. This can be due to the very low concentration of the complex in the zeolite support.

The weight loss due to the decomposition of ligand does not occur at a distinct stage. This may be due to the very low concentration of the complex inside the zeolite pore. However the mass loss in the temperature range 30-100 °C in all the complexes can be due to loss of free water; that between 100 and 500 °C can be due to the removal of coordinated water and the decomposition of the complex. The mass loss between 500 and 670 °C can be due to the partial decomposition of the complex and also due to the partial decomposition of zeolite.

References

1. M.A. Ali and S.E. Livingston, *Coord. Chem. Rev.* 13 (1974) 101.
2. D.H. Jones, R. Slack, S. Squires, and K.R.H. Wooldridge, *J. Med. Chem.* 8 (1965) 676.
3. R.W. Brockman, J.R. Thomson, M.J. Bell, and H.E. Skipper, *Cancer Res.* 16 (1956) 167.
4. Suhas A. Chavan, D. Srinivas, and Paul Ratnasamy, *Chem. Commun.* (2001) 1124.
5. Carmen Schuster, Eugen Mőllmann, Andras Tompos, and Wolfgang F. Hőlderich, *Catal. Lett.* 74, 1-2 (2001) 69.
6. M. Kumar and S. Arabinda Kumar, *Asian J. Chem.* 6, 4 (1994) 782.
7. M. Kumar, *Asian J. Chem.* 6, 3 (1994) 576.
8. C. Tollman and H. Herron, *Symposium on Hydroc. Oxidation, 194th National Meeting of American Chemical Society*, New Orleans, LA, Aug. 30 - Sep. 4, 1987.
9. P.G. Menon, in *Lectures in Catalysis, 41st Ann. Meeting, Ind. Acad. Sci.*, S. Ramasheshan (Ed.) 1975.
10. Carol A. Bessel and Debra R. Rolison, *J. Phys. Chem. B* 101 (1997) 1148.
11. E. Paez-Mozo, N. Gabriunas, F. Luccaccioni, D. D. Acosta, P. Patrono, A. La Ginestra, P. Ruiz, and B. Delmon, *J. Phys. Chem.* 97 (1993) 12819.
12. H. Van Koningsveld, J.C. Jansen, and H. Van Bekkum, *Zeolites* 10 (1990) 235.
13. N. Herron, *J. Coord. Chem.* 19 (1988) 25.
14. E.M. Flanigen, in *Zeolite Chemistry and Catalysis*, J.A. Rabo (Ed.) ACS Monograph, American Chemical Society, Washington D.C., 1976.
15. P.A. Jacobs, H.K. Beyer, and J. Valyon, *Zeolites* 1 (1981) 161.
16. K. Nakamoto, *Infrared and Raman Spectra of Inorganic and Coordination Compounds* (5th edn.), John Wiley and Sons Inc., New York, 1997.
17. Bindu Jacob, Ph.D. Thesis, Cochin University of Science and Technology, 1998.
18. K. Klier, *J. Am. Chem. Soc.* 91 (1969) 5392.
19. U. Sakaguchi and A.W. Addison, *J. Chem. Soc. Dalton Trans.* (1979) 600.
20. J. Strutz, H. Diegruber, N.I. Jaeger, and R. Mosler, *Zeolites* 3 (1983) 102.
21. K. Mizuno and J.H. Lunsford, *Inorg. Chem.* 22 (1983) 3483.
22. T.A. Egerton, A. Hagan, F.S. Stone, and J.C. Vickerman, *J. Chem. Soc. Faraday Trans.* 168 (1972) 723.
23. J.M. Thomas and C.R.A. Catlow, *Progr. Inorg. Chem.* 35 (1988) 1.
24. R. Raja and P. Ratnasamy, *J. Catal.* 170 (1997) 244.
25. Fethi Bedioui, Lionel Roué, Emmanuel Briot, Kenneth J. Balkus, Jr., and J. Felipe Diaz, *New J. Chem.* 20 (1996) 1235.

26. K.J. Balkus, Jr., and A.G. Gabrielov, *J. Inclusion Phenom. Mol. Recogn. Chem.* 21 (1995) 159.
27. S.P. Varkey and C.R. Jacob, *Ind. J. Chem.* 37A (1998) 407.
28. F.A. Cotton and G. Wilkinson, *Advanced Inorganic Chemistry*, Wiley - Interscience, New York, 1980.
29. A. Earnshaw, *Introduction to Magnetic Chemistry*, Academic Press, London, 1968.
30. N.N. Greenwood and A. Earnshaw, *Chemistry of Elements* (1st edn.), Pergamon Press, Oxford 1984. Rpt.1989.
31. A.B.P. Lever, *Inorganic Electronic Spectroscopy*, Elsevier, Amsterdam,1968.
32. A.B.P. Lever, G. London, and P.J. McCarthy, *Can. J. Chem.* 55 (1977) 3172.
33. B.Singh, B.P. Yadava, and R.C. Agarwal, *Ind. J. Chem.* 23A (1984) 441.
34. H. Diegruber, P.J. Plath, G. Schulz-Ekloff, and M. Mohl, *J. Mol. Catal.* 24 (1984) 115.
35. J. Patole, S. Dutta, S. Padhye, and E. Sinn, *Inorg. Chim. Acta* 318 (2001) 207.
36. P.L. Maurya, B.V. Agarwala, and A.K. Dey, *Ind. J. Chem.*19A (1980) 807.
37. R.N. Ray and B.K. Mohapatra, *Ind. J. Chem.*19A (1980) 590.
38. R.M. Silverstein and G.C. Bassler, *Spectrometric Identification of Organic Compounds* (4th edn.), John Wiley, New York, 1968.
39. V.M. Leovac, L. Bjelica, and L. Jovanovic, *Polyhedron* 4, 2 (1985) 233.
40. P.K. Singh, J.K. Koacher, and J.P. Tandon, *J. Inorg. Nucl. Chem.* 43 (1981) 1755.
41. A.F. Petrovic, D.M. Petrovic, V.M. Leovac, and M. Budimir, *J. Thermal Studies and Calorimetry* 58 (1999) 589.

Chapter 4

A comparison of neat and encapsulated complexes of copper 2-styrylbenzimidazole

Abstract

Neat and zeolite Y encapsulated copper 2-styrylbenzimidazole complexes were synthesized and a comparative study of the two complexes was undertaken. Surface area, pore volume, and XRD studies provide evidence for the encapsulation of the complexes without the destruction of the zeolite crystallinity. The TG-DTG curves gave information regarding the thermal stability of the complex and the probable composition of the expelled group. The formation of the complex was confirmed by IR spectroscopy. Magnetic moment suggests square planar geometry for both the neat and encapsulated complexes. Electronic spectra suggest the possibility of d-d transitions in both the complexes. Square planar structure is confirmed by the g_{II}/A_{II} ratio from EPR.

4.1. Introduction

Benzimidazole forms a significant part of the structure and function of a number of biologically important molecules [1-4]. Derivatives of benzimidazole with antifungal [5], anthelmintic [6], anti-HIV [7], antihistaminic [8-9], cardio tonic [10], antihypertensive [11,12], neuroleptic [13] and such other pharmacological effects are in clinical use. Several reports reveal that substitution at the 1, 2, and 5 positions of the benzimidazole ring. may influence their pharmacological effect [14,15].

2-Substituted phenylbenzimidazole with antibacterial [16], antiviral [17], antitumoral [18,19], anti-inflammatory [20] and other types of biological activities have been reported. 2-Subsituted styrylbenzimidazole complexes of Cu(II) were prepared, in order to study the influence of steric effects on catalysis reaction. The complexes may also be interesting with regard to their biological activities, even though no attempt was made to study their biological properties.

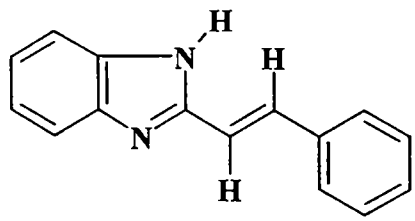

Figure 4.1 Structure of 2-styrylbenzimidazole

4.2. Experimental

Details regarding the synthesis and purification of the ligand styrylbenzimidazole and the preparation of Cu(II) exchanged zeolite Y are given in Chapter 2.

4.2.1. Synthesis of neat $Cu(SB)_2Cl_2$

Cu(II) chloride dihydrate (10 mmol) was dissolved in methanol (25 ml) and added to a solution of styrylbenzimidazole (20 mmol, 25ml) in methanol. This mixture was refluxed for 3-4 hours. It was kept in the refrigerator overnight. Crystals of styrylbenzimidazole complex that separated out were filtered, dried in vacuo, and finally recrystallised from methanol to obtain pure styrylbenzimidazole complex.

4.2.2. Synthesis of zeolite encapsulated 2-styrylbenzimidazole complex

The general procedure for encapsulating the complex in zeolite Y is described in Chapter 2. Copper(II) exchanged zeolite, CuY (3g), was mixed with excess of ligand (ligand to metal mole ratio > 2) and introduced into a glass ampule, sealed, and heated at 150 °C for four hours. The resulting material was purified by soxhlet extraction using methanol for 24 hours. Uncomplexed metal ions present in the zeolite was removed by back exchanging with NaCl solution (0.01M in 250cc). This was made chloride free by washing with distilled water. The zeolite encapsulated complex was stored in vacuum over anhydrous calcium chloride after drying at 110 °C for 2 hours.

4.3. Characterization techniques

The various physico-chemical techniques to characterize the prepared complexes are given in Chapter 2.

4.4. Results and Discussion

Zeolite Y encapsulated copper styrylbenzimidazole complex and neat copper styrylbenzimidazole were synthesized. The neat complex is crystalline, non-hygroscopic, green in colour, and is stable to aerial oxidation. The complex is

soluble in methanol, ethanol, acetone, and DMSO, and is insoluble in solvents like chloroform, benzene, hexane, and dichloromethane. The molar conductance of the complex measured in 10^{-3} M methanol solution is in the range of 1.1 ohm^{-1} cm^2mol^{-1} indicating its non-electrolytic nature [21].

4.4.1. Chemical analysis

The results of chemical analysis of styrylbenzimidazole complexes are given in Table 4.1. The data obtained in CHN analysis, metal analysis, and chlorine analysis are in good agreement with the calculated value of carbon, hydrogen, nitrogen, copper, and chlorine for the empirical formula, $CuCl_2(SB)_2$. Chemical analysis of CuYSB shows that the Si/Al ratio is 2.4, which is the same as the Si/ Al ratio of NaY and CuY, indicating retention of the zeolite framework. The metal content in CuY is 1.12% and that in CuYSB is 0.45%. About 40% of the metal initially present in the metal exchanged zeolite was found to remain in the zeolite after complexation and the rest was removed during the final ion exchange with NaCl solution.

Table 4.1 Analytical data of styrylbenzimidazole complexes

Sample	% Si	% Al	% Na	% C	% H	% N	% Cl	% Cu
NaY	20.60	8.50	7.50	-	-	-	-	-
CuY	20.48	8.48	6.60	-	-	-	-	1.12
CuYSB	20.48	8.40	6.20	0.30	2.40	0.04	-	0.45
$Cu(SB)_2Cl_2$*	-	-	-	61.96	4.18	9.33	11.80	10.50
$Cu(SB)_2Cl_2$**	-	-	-	62.56	4.20	9.70	12.30	11.03

$Cu(SB)_2Cl_2$* : Found $Cu(SB)_2Cl_2$**: Calculated

The charge neutralization of the complex in the zeolite cage is probably achieved by co-ordination of the metal sites to the oxide ions of the lattice. The ligand to metal mole ratio in the neat complex is 2:1. But the mole ratio is less than 2 in the case of the encapsulated complex. The lower mole ratio of the zeolite complex may be because of the presence of un-exchanged metal ions in the lattice, which have not been removed, in the final ion exchange with sodium chloride. The encapsulated complexes might have kept these metal ions trapped, thus preventing ion exchanging with Na^+ ions.

4.4.2. X-ray diffraction patterns

Figure 4.2 shows the XRD patterns of CuY and CuYSB. The XRD patterns of the encapsulated complex exactly match those of the copper exchanged zeolite. This shows that the crystalline structure is retained even after encapsulating the complex within the lattice.

4.4.3. Scanning electron microscopy

The scanning electron micrographs (Figure 4.3) before soxhlet extraction and after soxhlet extraction indicate the removal of surface particles.

4.4.4. Surface area and pore volume

Surface area and pore volume data are given in Table 4.2. The surface area and pore volume of metal exchanged zeolite is higher compared to those of the encapsulated complex. The lowering of the surface area and pore volume of the encapsulated complex can be due to the filling of the zeolite pore with metal complex. This is again strong evidence for the encapsulation of the complex in zeolite pore [22].

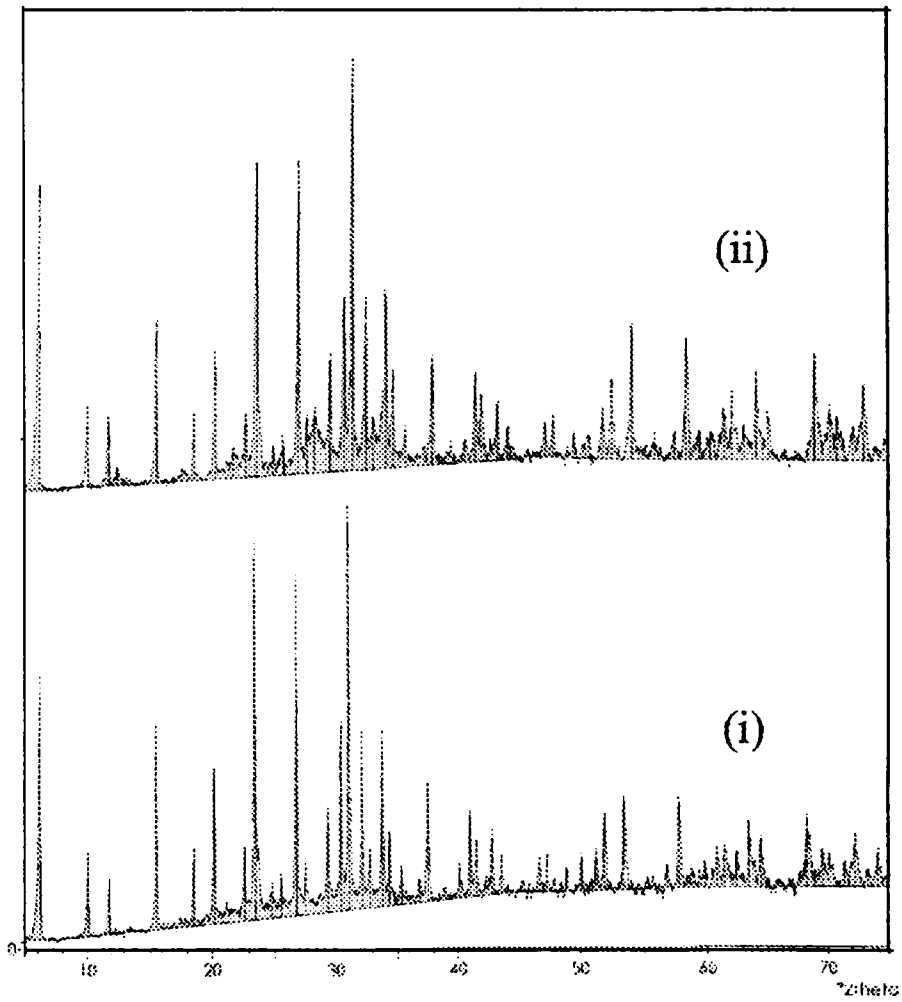

Figure 4.2 XRD patterns

i) CuYSB and ii) CuY

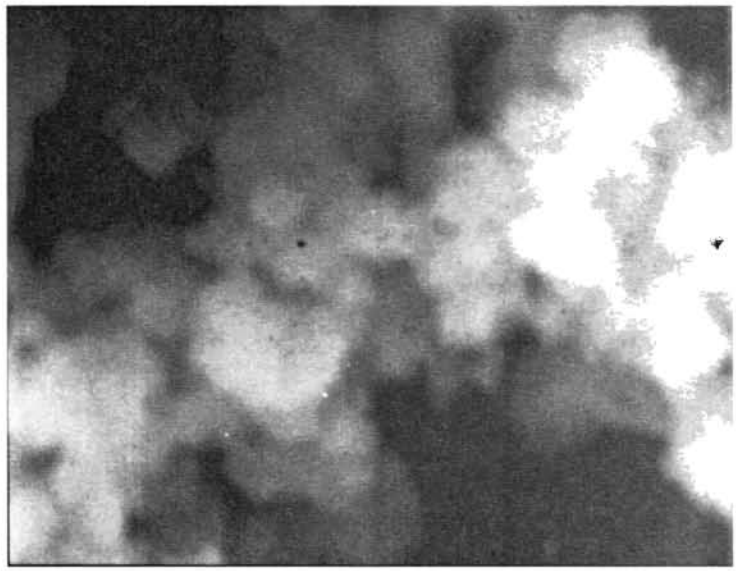

(i)

(ii)

Figure 4.3 SEM of CuYSB

i) Before soxhlet extraction
ii) After soxhlet extraction

Table 4.2 Surface area and pore volume data

Surface area (m^2/g)			Pore volume (ml/g)		
CuY	CuYSB	% loss	CuY	CuYSB	% loss
520	150	71.2	0.293	0.069	76.3

4.4.5. Magnetic moment

The magnetic moment for $CuCl_2(SB)_2$ and CuYSB at room temperature are 1.80 and 1.81 BM. respectively. This indicates that the complexes are monomeric in nature and may have square planar or distorted square planar structure [23]. Further the values suggest absence of any metal-metal interaction in the complexes [24].

Table 4.3 Magnetic moment

Sample	Magnetic moment (BM)
$CuCl_2(SB)_2$	1.80
CuYSB	1.81

4.4.6. Diffuse reflectance spectra

The electronic spectral data and the tentative assignment are given in Table 4. 4, and the spectra are given in Figure 4.4. The electronic spectra of the neat and encapsulated complexes show a band in the region 12500cm^{-1} which could be

assigned to d-d transitions. The band around 29400cm^{-1} in the spectra of the neat and encapsulated complexes can be attributed to a charge – transfer transition [25,26].

Table 4.4 Electronic spectral data of copper complexes of styrylbenzimidazole

Sample	Abs. max. (cm^{-1})	Assignment
CuYSB	12500	d-d transition
	29400	Charge transfer transition
$Cu(SB)_2Cl_2$	12500	d-d transition
	29400	Charge transfer transition

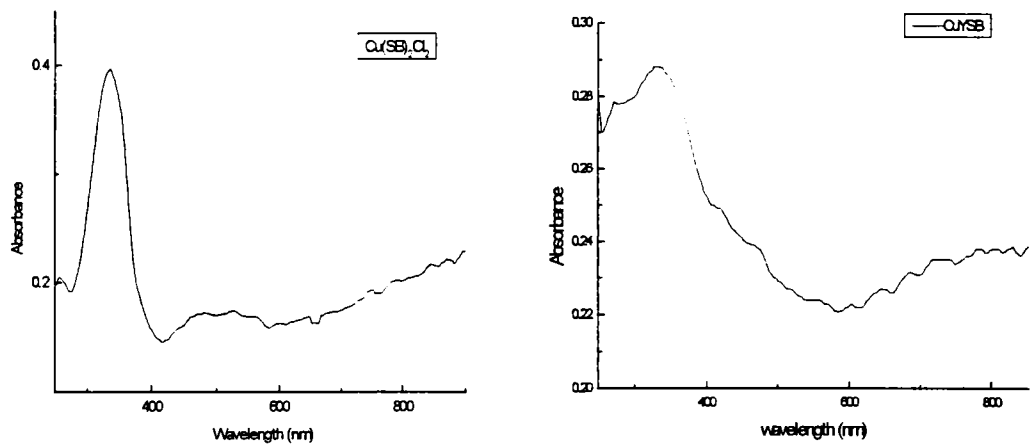

Figure 4.4 Electronic spectra of SB complexes

Square planar geometry can be assigned to both neat and encapsulated complexes. In the case of the neat complex, two of the four ligands are chloride ions, whereas in the case of the zeolite encapsulated complex they can be oxide ions of the zeolite framework or molecules of water.

4.4.7. FTIR spectra

Figure 4.5 shows the IR spectra of the styrylbenzimidazole ligand, and its neat and encapsulated complexes. The spectral data of the styrylbenzimidazole ligand, the neat complex, and of the encapsulated complex are presented in Table 4.5. From the table, the ligand bands in the encapsulated complexes which are not masked by zeolite bands can be readily identified. The band of medium intensity at 1516cm^{-1} in the spectrum of the free ligand SB may be attributed to the C-N stretching vibration. In the case of the neat and encapsulated complexes this band shifts to 1500 cm^{-1}. The shifting of this band to lower frequency is due to the coordination of nitrogen of the SB to the metal atom. The broad band at ~ 3500cm^{-1} can be attributed to the stretching vibration of water.

4.4.8. EPR spectra

EPR spectra of the neat copper styrylbenzimidazole (glass spectra) and the encapsulated complex recorded at liquid nitrogen temperature are shown in Figure 4.6. Table 4.6 gives the EPR parameters, unpaired electron density, and magnetic moment, calculated from EPR data. The EPR of $CuCl_2(SB)_2$ in DMSO shows a set of four copper hyperfine lines on the $g_{\parallel}$ position in the low field range, while such hyperfine lines are not so conspicuous in the $g_{\perp}$ position in the high field region. No super-hyperfine splitting from the ligand is observed either. The $g_{\parallel}$ and $g_{\perp}$ values of $CuCl_2(SB)_2$ are 2.32 and 2.05, and those of the zeolite encapsulated complexes are found to be 2.34 and 2.05 respectively.

Table 4.5 IR spectra of the styrylbenzimidazole ligand and its complexes

SB cm^{-1}	$Cu(SB)_2Cl_2$ cm^{-1}	CuYSB cm^{-1}
433	430	450
495	480	
699	700	
750	760	780
845	820	
903		890
965	960	
1020	1040	
1151	1140	
1182	1200	
1227	1250	
	1340	
1381		
1423	1440	
1485		
1516	1500	1500
1558	1550	
1588		
1645	1640	1640
1946	1900	
2608	2600	
2731	2720	
2808		
2849	2880	
2971		
3054	3040	
	3180	
		3400

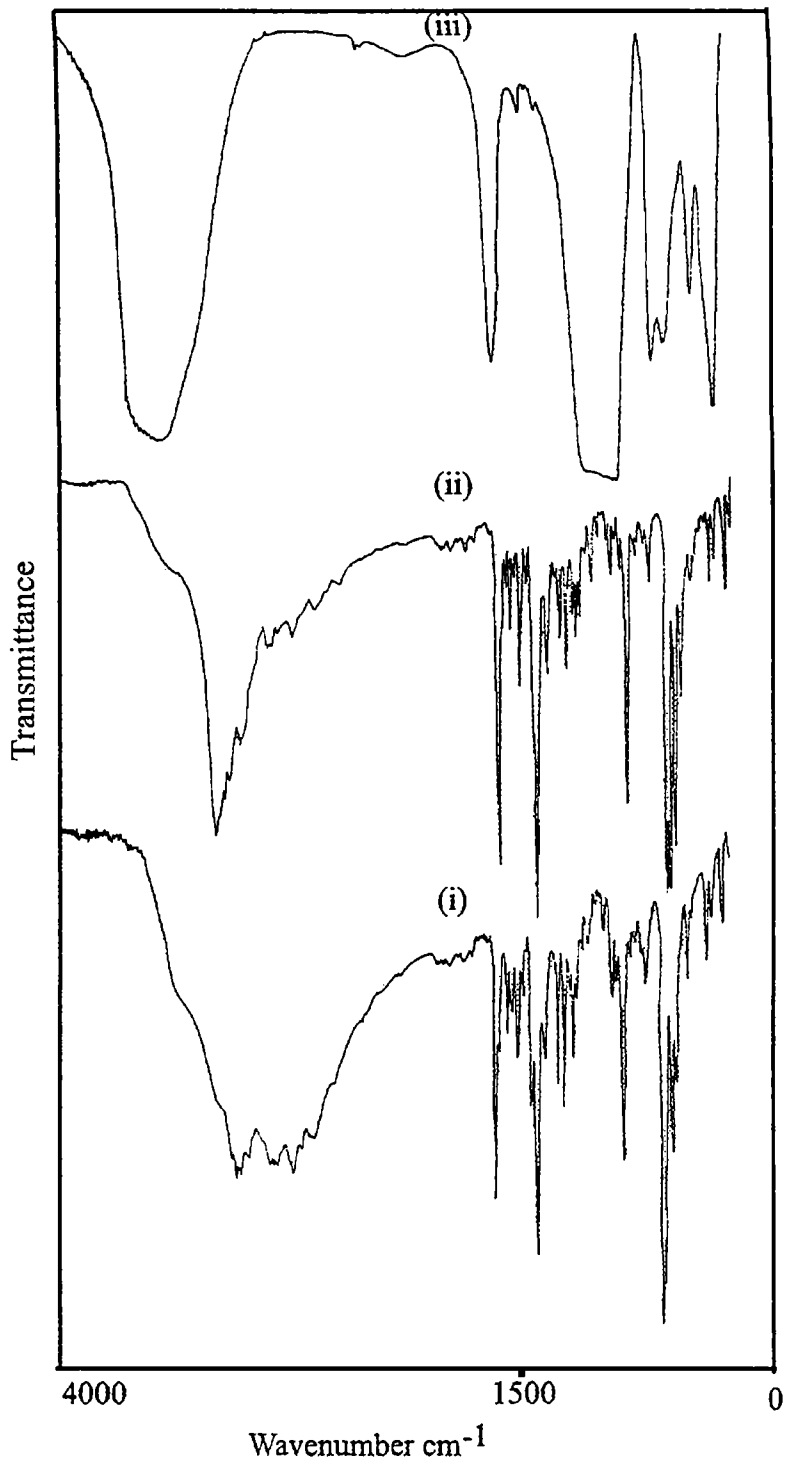

Figure 4.5 IR spectra of the styrylbenzimidazole ligand and its complexes (i) styrylbenzimidazole, (ii) $Cu(SB)_2Cl_2$, (iii) CuYSB

The g_{II}/A_{II} value of $CuCl_2(SB)_2$ is 119.6 cm while that of CuYSB is 122.5 cm, suggesting a square planar geometry for the neat and the encapsulated complexes. The α^2 values of 0.72 and 0.8 for the neat and encapsulated complexes suggest that the metal ligand bond is intermediate between ionic and covalent. The trend $g_{II} > g_{\perp} > 2.0023$ observed for these complexes indicate square planar structure for these complexes. The magnetic moment, μ_{eff} for $CuCl_2(SB)_2$ and CuYSB are1.84 and 1.86 BM, which is in agreement with the value obtained from room temperature magnetic susceptibility measurement by Gouy method [27]. The well resolved hyperfine splitting similar to that for the neat complex in dilute solution indicates that the complex species in the zeolite cavity are monomeric in nature.

Table 4.6 EPR parameters

EPR parameters	$Cu(SB)_2Cl_2$	CuYSB
g_{II}	2.32	2.34
A_{II}	194×10^{-4} cm^{-1}	191×10^{-4} cm^{-1}
g_{II}/A_{II}	119.6cm	122.5cm
$g_{\perp}$	2.05	2.05
$A_{\perp}$	36×10^{-4} cm^{-1}	34×10^{-4} cm^{-1}
α^2	0.72	0.8
μ_{eff}	1.84	1.86

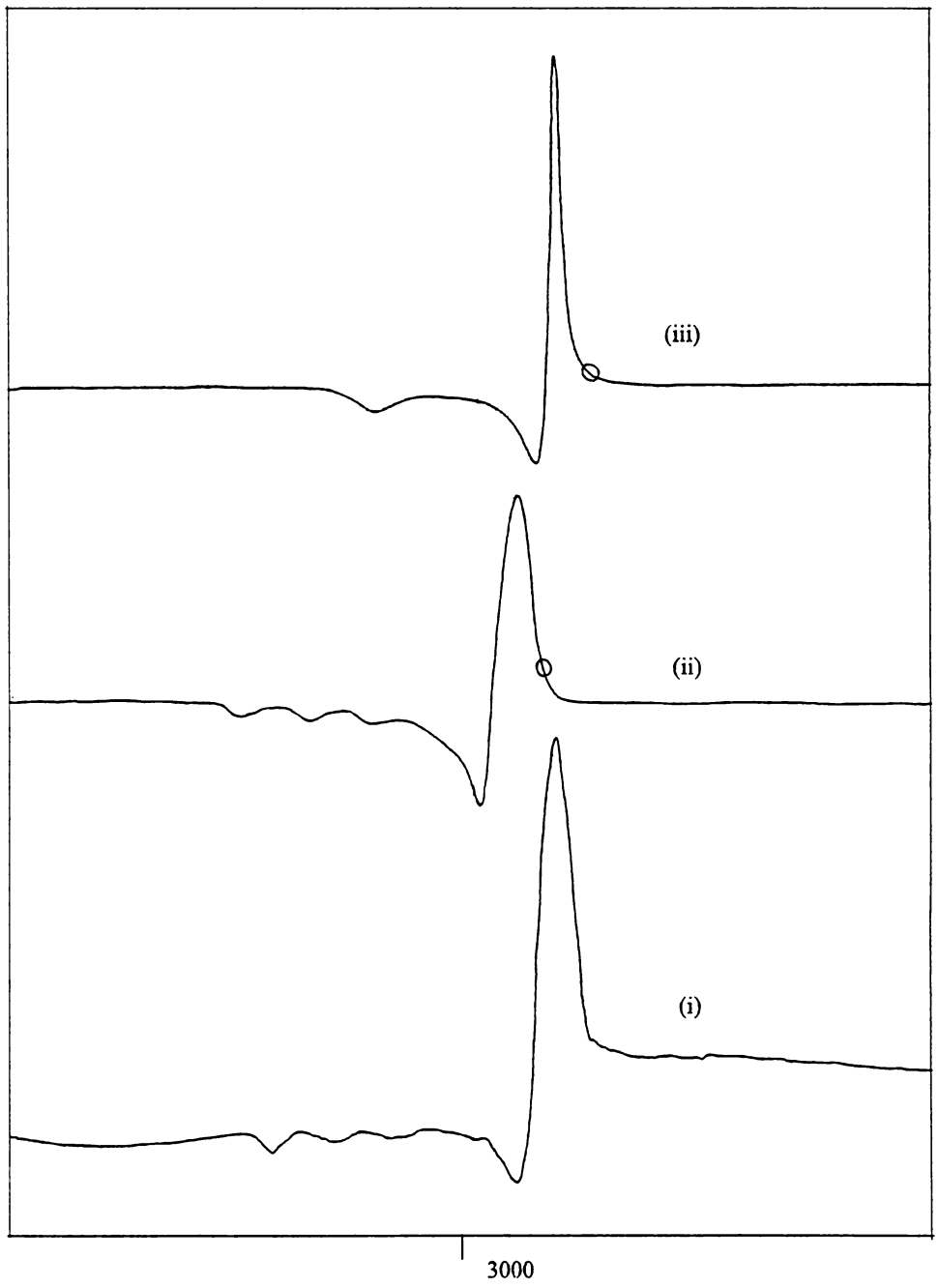

Figure 4. 6 EPR parameters of SB complexes of copper
i) CuYSB at LNT ii) $Cu(SB)_2Cl_2$ at LNT iii) CuYSB at RT

4.4.9. TG analysis

The TG/DTG curves of $Cu(SB)_2Cl_2$ were recorded in an atmosphere of nitrogen from room temperature to 1200 °C at a heating rate of 10 °/min and the TG curve of the encapsulated complex was recorded in air from room temperature to 800 °C at a heating rate of 10 °C/min. Figure 4.6 (i) shows the TG/DTG curves of $Cu(SB)_2Cl_2$ and Figure 4.6 (ii) shows the TG curve of CuYSB. Thermo analytical data for the complexes are presented in Table 4.7. The percentage mass loss and the probable composition of the expelled groups are also given in this table.

Table 4.7 Thermal decomposition data

Sample	Peak temp. DTG (°C)	Temp. range TG (°C)	Stage	% Mass loss from TG Found (Calc.)	Probable composition of expelled group
$Cu(SB)_2Cl_2$	396	202-551	I	40.26 (38.42)	SB
	737.4	551-975	II	48.26 (50.73)	SB + 2Cl
CuYSB	-----	30 - 100	-	5.36	Water
		100 - 534	-	12.87	Water and ligand
		534 - 799	-	0.5391	Ligand and zeolite

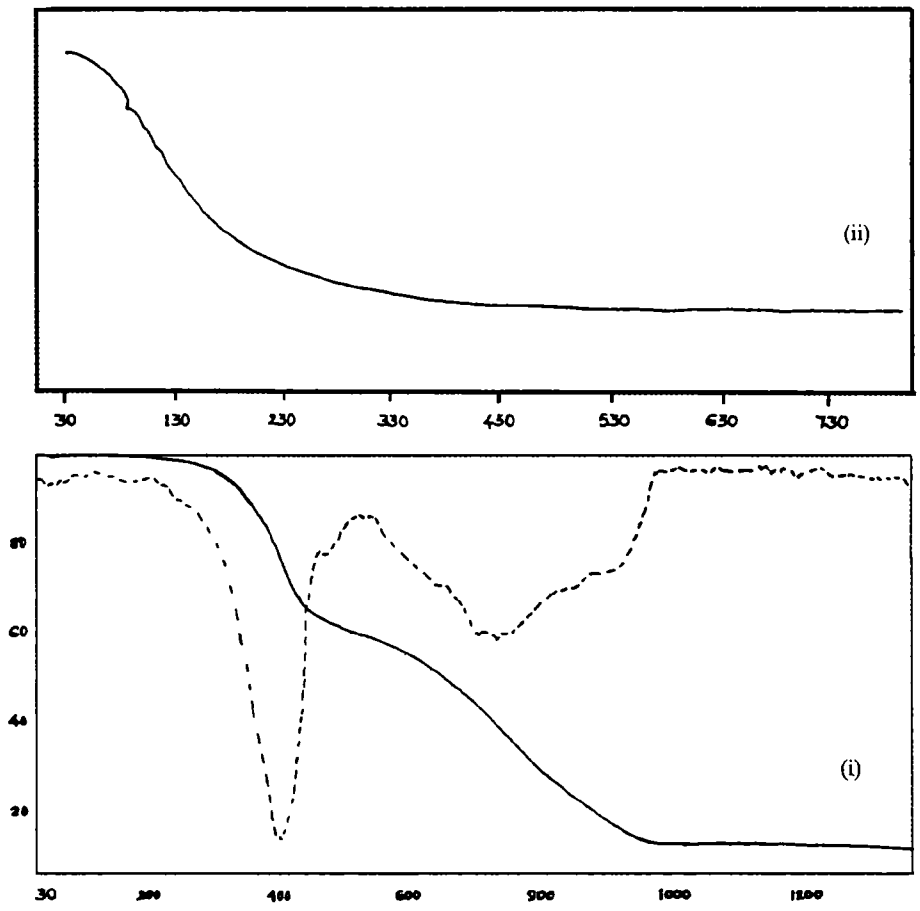

Figure 4.7 (i) TG/DTG curves of $Cu(SB)_2Cl_2$ and (ii) TG curve of CuYSB.

In the case of $Cu(SB)_2Cl_2$ the mass loss in the first stage corresponds to the expulsion of one styrylbenzimidazole. The IR spectrum of the residue after this stage showed the presence of styrylbenzimidazole indicating that only one styrylbenzimidazole is removed. The elemental analysis after the first stage indicated the approximate composition of the intermediate complex to be $Cu(SB)Cl_2$. The second stage of decomposition corresponds to the removal of one

styrylbenzimidazole and two chlorine atoms. The residue after the final stage of decomposition was found to be Cu_2O (ultimately oxidized to CuO).

From the TG curve of the encapsulated complex we get only a qualitative idea. The curve shows that most of the intrazeolite free water molecules are released in the temperature range 30-100 °C. The mass loss due to the expulsion of the ligand is not clearly visible as in the case of the neat complex. The mass loss in the temperature range 100-534 °C can be due to the removal of ligands and coordinated water if any. The absence of well-defined patterns as in the case of neat complexes can be due to the very low concentration of the metal complexes inside the zeolite pore. The mass loss corresponding to the temperature range between 534 °C and 800 °C can be due to the loss of ligand and the decomposition of the zeolite itself. The IR spectrum of the residue at the end of this stage indicates that the encapsulated complexes have decomposed completely.

References

1. M.N. Hughes, *The Inorganic Chemistry of Biological Processes* (2nd edn.), Wiley, London, 1981.
2. R.W. Hay, *Bio-inorganic Chemistry*, Ellis Horwood Limited, England,1984.
3. H.C. Freeman, in *Inorganic Biochemistry*, G.L. Eichhorn (Ed.), Elsevier, Armsterdam, 1973.
4. Cannon KUS, *Turk. J. Chem.* 26 (2002) 559.
5. D. Berg, K.H. Buchel, M. Plempel, and A. Zywietz, *Mykosen* 29 (1986) 221.
6. A.G. Salmot, A.C. Cremleux, J.M. Hay, A. Meulemans, M.D Glovanangeli, B. Delaitre, and F.P. Coulaud, *Lancet* 17 (1983) 652.
7. A. Chimirri, S. Grasso, A. M. Monforte, P. Monforte, and M. Zappala, *Il Farmaco* 46 (1991) 925.
8. C.J.E. Niemegeers, F. Awouters, and P.A.J. Jannsen, *Agents and Actions* 18 (1986) 141.
9. R. Iemura, M. Hori, and H. Ohtaka, *Chem. Pharm. Bull.* 37 (1989) 962.
10. K. Ishihara, T. Ichikawa, Y. Komuro, S. Ohara, and K. Hotta, *Arzneim.-Forsch./Drug Res.* 44 (1994) 827.
11. D.Y. Graham, A. Mccullough, M. Sklar, J. Sontag, W.M. Roufail, R. Stone, R.H. Bishop, N. Gitlin, A.J. Cagliola, R.S. Berman, and T. Humphries, *Digetive Diseases and Sciences* 35 (1990) 66.
12. G. Piazzesi, L. Morano, and J. C. Rűegg, *Arzneim.-Forsch./Drug Res. 37 (1987) 1141.*
13. I. Wiedemann, H. Peil, H. Justus, S. Adamus, V. Brantl, and H. Lohmann, *Arzneim.-Forsch./Drug Res. 35 (1985) 964.*
14. H. Gőker and C. Kuş, *Arch. Pharm. (Weinheim)* 328 (1995) 425.
15. L. Garuti, M. Roberti, and G. Gentilomi, *Il Farmaco* 55 (2000) 35.
16. R.A. Coburn, M.T. Clark, R.T. Evans, and R.J. Genco, *J. Med. Chem.*30 (1987) 205.
17. T. Roth, M.L. Morningstar, P.L. Boyer, S.H. Hughes, R.W. Buckheit, and C.J. Michejda, *J. Med. Chem.* 40 (1997) 4199 .
18. A.Y. Chen, C. Yu, A. Bodley, L.F. Peng, and L.F. Liu, *Cancer Research* 53 (1993) 1332.
19. W.A. Denny, C.W. Rewcastle, and B.C. Baguley, *J. Med. Chem.* 33 (1990) 814.
20. D. Evans, T.A. Hicks, W.R.N. Williamsom, W.Dawson, S.C.R. Meacock, and E.A. Kitchen, *Eur. J. Med. Chem.* 31 (1996) 635.
21. W.J. Geary, *Coord. Chem. Rev.* 7 (1971) 81.
22. E. Paez-Mozo, N. Gabriunas, F. Lucaccioni, D.D. Acosta, P. Patrono, A.L.Ginestra, P. Ruiz, and B. Delmon, *J. Phys. Chem.* 97 (1993) 12819.

23. B.V. Romanovsky and A.G. Gabrielov, *J. Mol. Catal.* 74 (1992) 293.
24. Y.M. Issa and W.H. Hegazy, *Synth. React. Inorg. Met.– Org. Chem.* 30, 9 (2000) 1731.
25. K. Krishnankutty and J. Michael, *J. Indian Chem. Soc.* 72 (1995) 461.
26. P.G. Edward, J.S. Fleming, and S.S. Liyanage, *J. Chem. Soc. Dalton Trans.* 2 (1997) 193.
27. N.N. Greenwood and A. Earnshaw, *Chemistry of Elements* (1st edn.) Pergamon Press, Oxford, 1984. Rpt.1989.

Chapter 5

Zeolite encapsulated dithiocarbamates of Fe, Co, Ni and Cu

Abstract

Fe(III) dithiocarbamates of MDTC, IPDTC, and EPDTC and Co(III), Ni(II) and Cu(II) carbodithioates of MDTC were encapsulated in the super cages of zeolite Y. Si/Al ratio, XRD patterns, surface area, and pore volume data suggest the encapsulation of the complex without affecting the crystalline structure of the zeolite. SEM shows a clean surface. Magnetic moment and electronic spectra indicate octahedral structure for the Fe(III) complexes and Ni(II) and Co(II) complexes. The Cu(II) complex has square planar geometry. This is further confirmed by the g_{II}/A_{II} ratio. Different stages are not distinct in the TG curves and they are continuous.

5. Introduction

The coordination chemistry of dithiocarbamates has been a subject of great research interest for a number of years. Dithiocarbamates form a wide range of complexes with transition metals. The most investigated group of dithiocarbamates is that derived from secondary amines because of their stability and redox properties. Another significant fact is that dithiocarbamates can act as both monodentate and bidentate ligands.

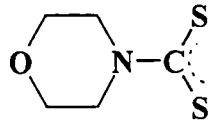

(i)

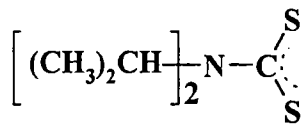

(ii)

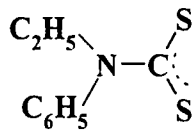

(iii)

Figure 5.1 Structure of the dithiocarbamate ligands

i) morphine-*N*-carbodithioate (MDTC), ii) *di*-iso-propyldithiocarbamate (IPDTC), and iii) *N*-ethyl-*N*-phenyldithiocarbamate (EPDTC)

The dithiocarbamate anion has a 4-electron-three-centre π system. The bonding of the ligand to transition metals is through the two S atoms, and both the M-S distances are equal. In a planar MS_2CN system, an extensive π-delocalization exists with a high contribution to the resonance structures, and with relatively high electron density on the metal [1]. The peculiar properties of dithiocarbamates are a consequence of their high covalency and special type of electronic ground state delocalization. Schrauzer attributes this delocalization to the interaction of the lowest occupied π-MOs of *the* ligands, with the metal *p*-orbitals of appropriate symmetry, producing a low-lying molecular orbital delocalized over the whole molecule or complex [2]. Researchers have explored the role of dithio ligands in the design of several electrically conducting molecular solids. The current interest is due to their structure [3], electrochemical properties [4], and photo-redox property [5]. Further, metal dithiocarbamato complexes find application as accelerators in the vulcanization of rubber. It was therefore considered worthwhile to encapsulate the metal complexes of Fe(III), Co(III), Ni(II) and Cu(II) dithiocarbamates inside zeolite Y by the flexible ligand method to study the effect of encapsulation on the geometries, and on the magnetic, spectral, and catalytic properties. This chapter is divided into 2 sections. Section A deals with the synthesis and characterization of Fe(III) dithiocarbamates; and Section B deals with the synthesis and characterization of Co(III), Ni(II), and Cu(II) morpholinecarbodithioates.

Section A

Zeolite-Y encapsulated Fe(III) dithiocarbamate and carbodithioate complexes

5A.1. Introduction

Iron dithiocarbamates and carbodithioate complexes in the oxidation states II, III, and IV have been studied extensively. It has been reported that $Fe(R_2DTC)_2$

is unstable and quickly gets oxidized in air to $Fe(R_2DTC)_3$. The redox properties of *tris* chelated Fe(III) have been investigated in detail [8-11]. Iron dithiocarbamates have widespread use as spin trap agents for nitric oxide detection. However these complexes have not been encapsulated in zeolite Y cages and studied. Encapsulation is found to impart improved properties to many systems, which have been explored for various applications. The results of the studies on zeolite Y encapsulated Fe(III) dithiocarbamates are presented in this section.

5A.2. Experimental

The details regarding the synthesis and characterization of the ligands morpholine-*N*-carbodithioate (MDTC), *N*-ethyl-*N*-phenyldithiocarbamate (EPDTC) and *di*-iso-propyldithiocarbamate (IPDTC) are presented in Chapter 2.

5A.2.1. Synthesis of zeolite encapsulated iron carbodithioate and dithiocarbamates

Iron(III) exchanged zeolites (3 g) is mixed with excess dithiocarbamate ligands in 50 ml of water (the concentration was adjusted to have a ligand to metal ratio greater than 3) and it was refluxed for 5 hours. Similar procedure has been reported for the synthesis of Fe(II) complex in HEU zeolite with *N,N*,-diethyldithiocarbamate [13]. The complex was washed several times with water to remove any uncomplexed ligand, and soxhlet extracted using methanol for 24 hours to remove surface species. These were finally sodium exchanged using NaCl solution (0.01M. 250 ml), washed free of chloride, dried at 110 °C, and stored in vacuum over anhydrous $CaCl_2$.

5A.3. Characterization techniques

Details of the various physicochemical techniques for the characterization of the complexes are given in Chapter 2.

5A.4. Results and Discussion

5A.4.1. Chemical analysis

The analytical data of encapsulated Fe(III) complexes are given in Table 5A.1. The Si/Al ratio of these complexes was found to be 2.4 as in the case of the metal exchanged zeolites.

Table 5A.1 Analytical data of the encapsulated Fe(III) carbodithioate and dithiocarbamates

Sample	% Si	% Al	% Na	% M	%C
FeYMDTC	18.48	7.83	5.40	0.53	1.56
FeYEPDTC	18.40	7.78	5.55	0.51	2.90
FeYIPDTC	18.70	7.91	5.80	0.50	2.25

The metal to ligand ratio in neat iron dithiocarbamates is 1:3 [14,15]. The analytical data for the complexes suggest that the percentage of metal is in the range as that required for 1:3 complex (with slight excess of metals).

5A.4.2. X-ray diffraction patterns

XRD provides information on crystallinity [16,17] as well as change in unit cell parameters that might result from encapsulation. XRD patterns of FeYMDTC, FeYEPDTC, and FeYIPDTC are given in Figure 5A.1.

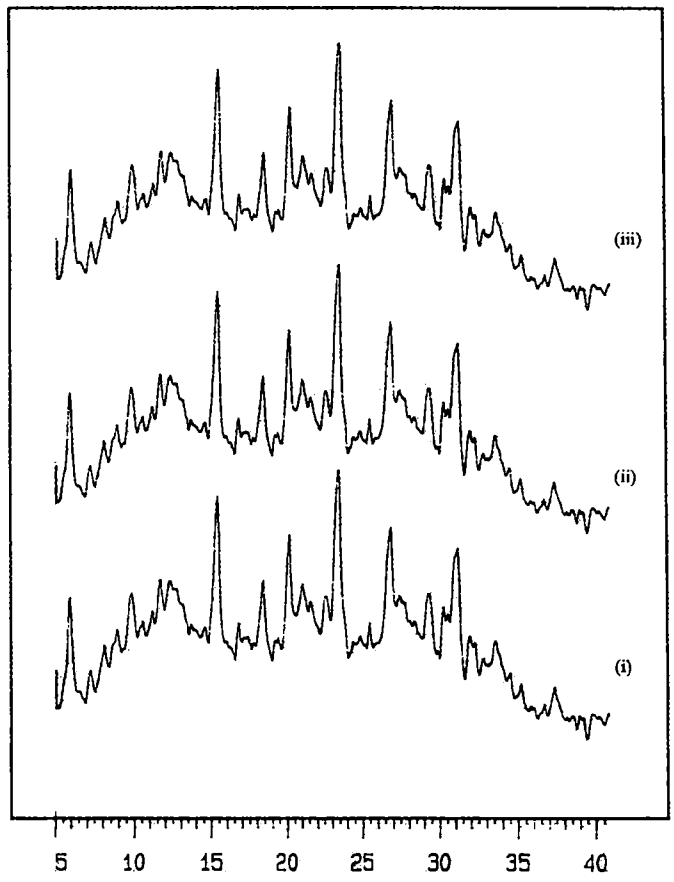

Figure 5A.1 XRD patterns of encapsulated iron dithiocarbamate complexes i) FeYMDTC, ii) FeYIPDTC, iii) FeYEPDTC

The XRD pattern obtained for the ion exchanged and encapsulated complexes were similar in nature. This indicates that there is no change in the overall crystallinity of zeolite Y lattice on encapsulation.

5A.4.3. Scanning electron micrographs

The scanning electron micrographs of FeYMDTC before soxhlet extraction and after soxhlet extraction are presented in Figure 5A.2. The picture shows a clean surface compared to that before soxhlet extraction.

(i)

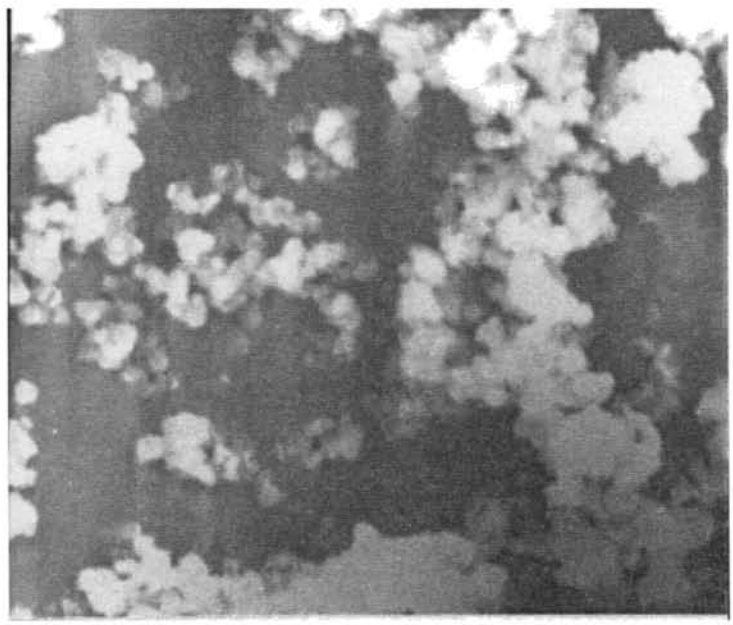

(ii)

Figure 5A.2 SEM

i) Before soxhlet extraction
ii) After soxhlet extraction

5A.4.4. Surface area and pore volume

Surface area and pore volume data are given in Table 5A.2. The surface area and pore volume of metal exchanged zeolites were found to be lowered on encapsulation. The lowering of surface area and pore volume confirms the encapsulation of the complex in the zeolite pores.

Table 5A.2 Surface area and pore volume data

Sample	Surface area (m^2/g)			Pore volume (ml/g)		
	FeY	FeYL	% loss	FeY	FeYL	% loss
FeYMDTC	530	257	51.50	0.2982	0.1390	53.39
FeYIPDTC	530	236	55.45	0.2982	0.1359	54.43
FeYEPDTC	530	230	56.67	0.2982	0.1300	56.41

5A.4.5. Magnetic moment

The magnetic moments of Fe(III) dithiocarbamates at room temperature are close to those observed for high spin Fe(III) octahedral complexes. The results obtained from magnetic moment measurements are presented in Table 5A.3.

Table 5A.3 Magnetic moment

Sample	Magnetic moment (BM)
FeYMDTC	5.87
FeYEPDTC	5.81
FeYIPDTC	5.79

5A.4.6. Diffuse reflectance spectra

The reflectance spectral data and tentative assignments are given in Table 5A.4, and the reflectance spectra in Figure 5A.3. Similar spectra are seen in the case of all the encapsulated Fe(III) complexes. The band around 14080-14100 cm^{-1} seen in all the complexes can be the result of the following three transitions, $^4T_{1g} \leftarrow {}^6A_{1g}$, $^4T_{2g} \leftarrow {}^6A_{1g}$,, $^4E_g \leftarrow {}^6A_{1g}$ [18,19] in octahedral symmetry. The bands at 20830 and 21000cm^{-1} for all the complexes could be considered d-d bands [18]. Charge transfer transitions are seen in the high-energy region around 32790-33330cm^{-1}. The room temperature magnetic susceptibility measurements are fully consistent with the high spin octahedral structure of Fe(III) complexes. The results indicate that the structure of the neat complexes is retained in the zeolite cages. Neat Fe(III) dithiocarbamates are reported to exist in octahedral geometry [14].

Table 5A.4 Electronic spectral data

Sample	Abs. max. (cm^{-1})	Assignment
FeYMDTC	14100	$^4T_{1g} \leftarrow {}^6A_{1g}$ $^4T_{2g} \leftarrow {}^6A_{1g}$ $^4E_g \leftarrow {}^6A_{1g}$
	20900	d-d transition
	32800	Charge transfer transition
FeYEPDTC	14080	$^4T_{1g} \leftarrow {}^6A_{1g}$ $^4T_{2g} \leftarrow {}^6A_{1g}$ $^4E_g \leftarrow {}^6A_{1g}$
	20830	d-d transition
	33330	Charge transfer transition
FeYIPDTC	14080	$^4T_{1g} \leftarrow {}^6A_{1g}$ $^4T_{2g} \leftarrow {}^6A_{1g}$ $^4E_g \leftarrow {}^6A_{1g}$
	21000	d-d transition
	33330	Charge transfer transition

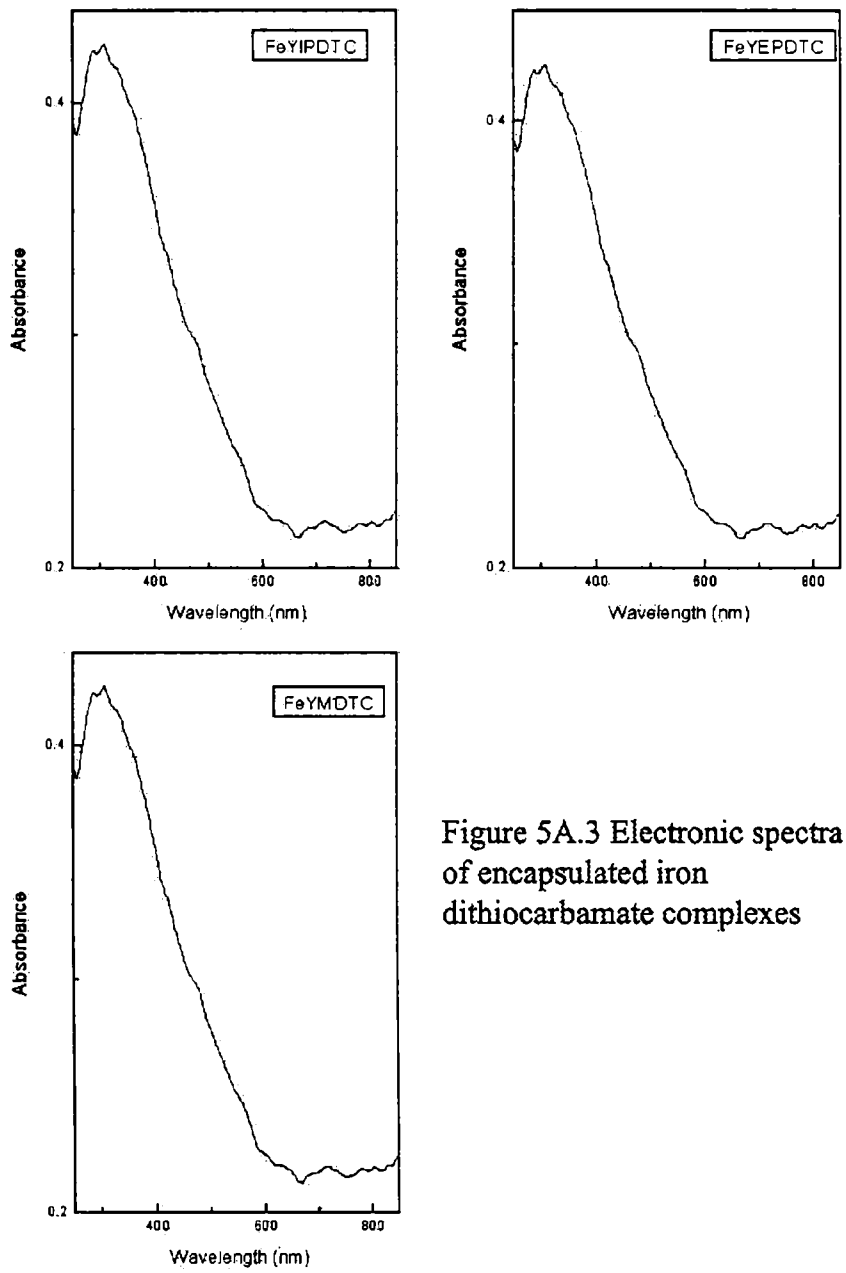

Figure 5A.3 Electronic spectra of encapsulated iron dithiocarbamate complexes

5A.4.7. FTIR spectra

Infrared spectra of morpholinecarbodithioate, *N*-ethyl-*N*-phenyldithiocarbamate, *di*-iso-propyldithiocarbamate and the encapsulated complexes are shown in Figures 5A.4, 5A.5, 5A.6. IR spectral data of MDTC, EPDTC, IPDTC, and the Fe(III) encapsulated complexes are presented in Table 5A.5. $\nu N{=}CS_2$ absorption occurs at 1440cm^{-1} in the spectrum of IPDTC, 1450cm^{-1} in the spectrum of EPDTC, and 1460cm^{-1} in the spectrum of MDTC. Similar observations have been made by earlier workers [19]. This is shifted to higher frequency regions on complexation. The bands are seen at 1480cm^{-1} in the case of FeYIPDTC, 1490cm^{-1} in the case of FeYEPDTC, and 1485cm^{-1} in the case of FeYMDTC. The positive shift in $\nu N{=}CS_2$ vibration may be indicative of the interaction of the sulphur atoms with metal on coordination [20]. The absorption in the region 941-1140cm^{-1} in the spectra of the ligands may be attributed to symmetric and asymmetric C-S stretching vibrations [21]. These absorptions shift to lower frequency on complexation. Similar lowering is expected in the case of the encapsulated complexes also. But the new bands are not observed in the spectra of zeolite complexes as they might have been masked by the broad zeolite absorption at around 1000cm^{-1}. Absorption bands due to the O-H stretching vibrations of the zeolites lie in the range of 3440-3470cm^{-1} and are seen in all the complexes [19]. Most of the absorptions of the ligands are masked by the zeolite peaks.

Table 5A.5 IR spectral data of iron complexes

MDTC cm^{-1}	FeYMDTC cm^{-1}	IPDTC cm^{-1}	FeYIPDTC cm^{-1}	EPDTC cm^{-1}	FeYEPDTC cm^{-1}
481					
540				558	
639	618	610	618	620	618
				692	
	724		719		726
		780		757	
888		846		816	
				903	
983		941		992	
	1033	1035	1035	1058	1033
1110		1143		1122	
1213		1193		1235	
1260		1301	1321	1270	
		1301			
1363	1352	1364	1352	1392	1352
1416					
1460	1485	1440	1480	1450	1490
1615		1609		1598	
	1635		1630		1642
2115		2070		2067	
				2373	
2851					
2908		2968		2969	
3379		3420		3378	
	3453		3443		3468

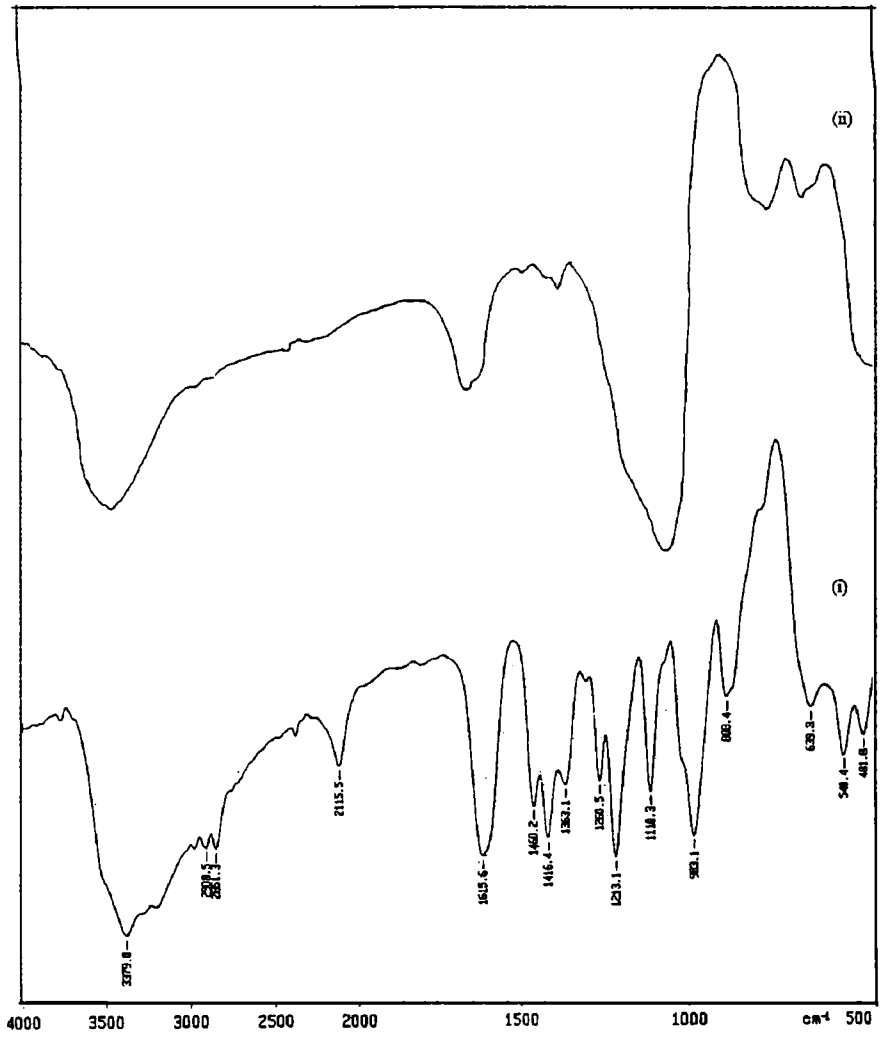

Figures 5A.4 IR spectra

i) MDTC and ii) FeYMDTC

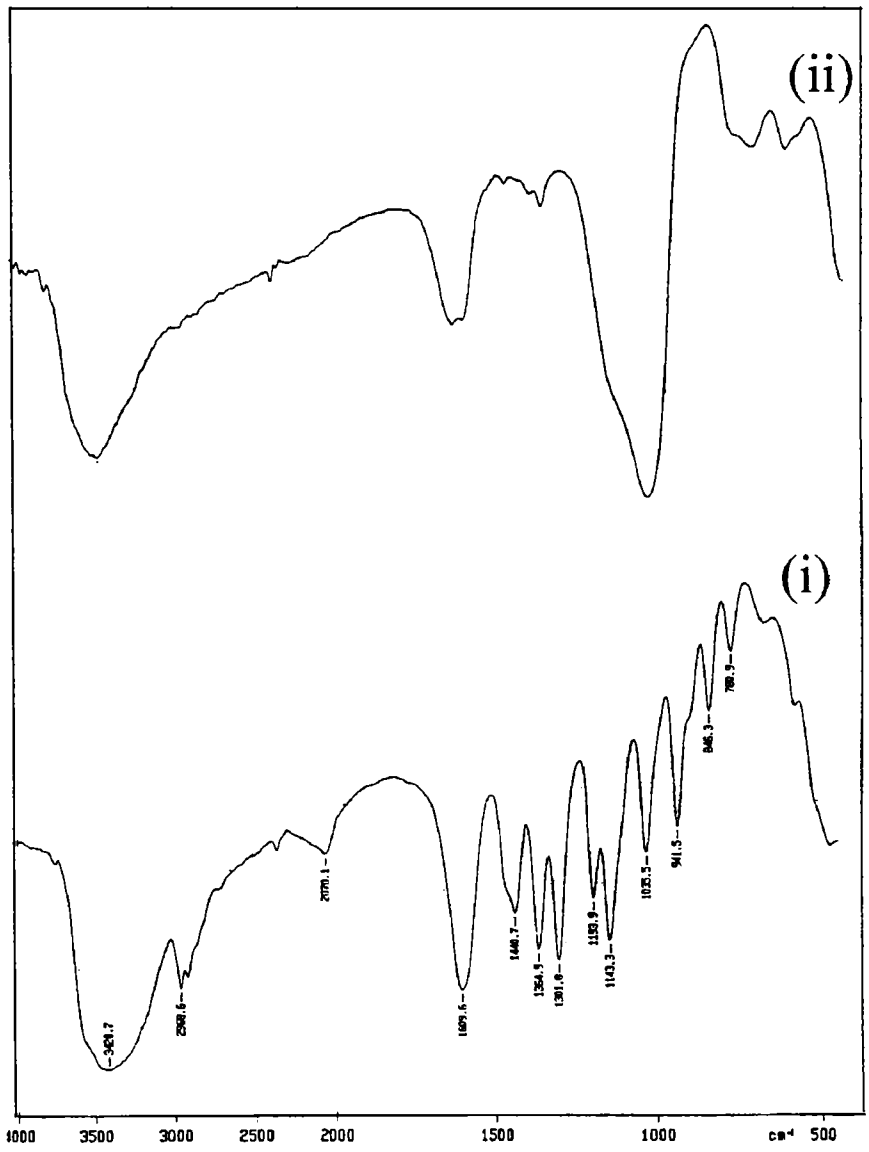

Figures 5A.5 IR spectra

i) IPDTC and ii) FeYIPDTC

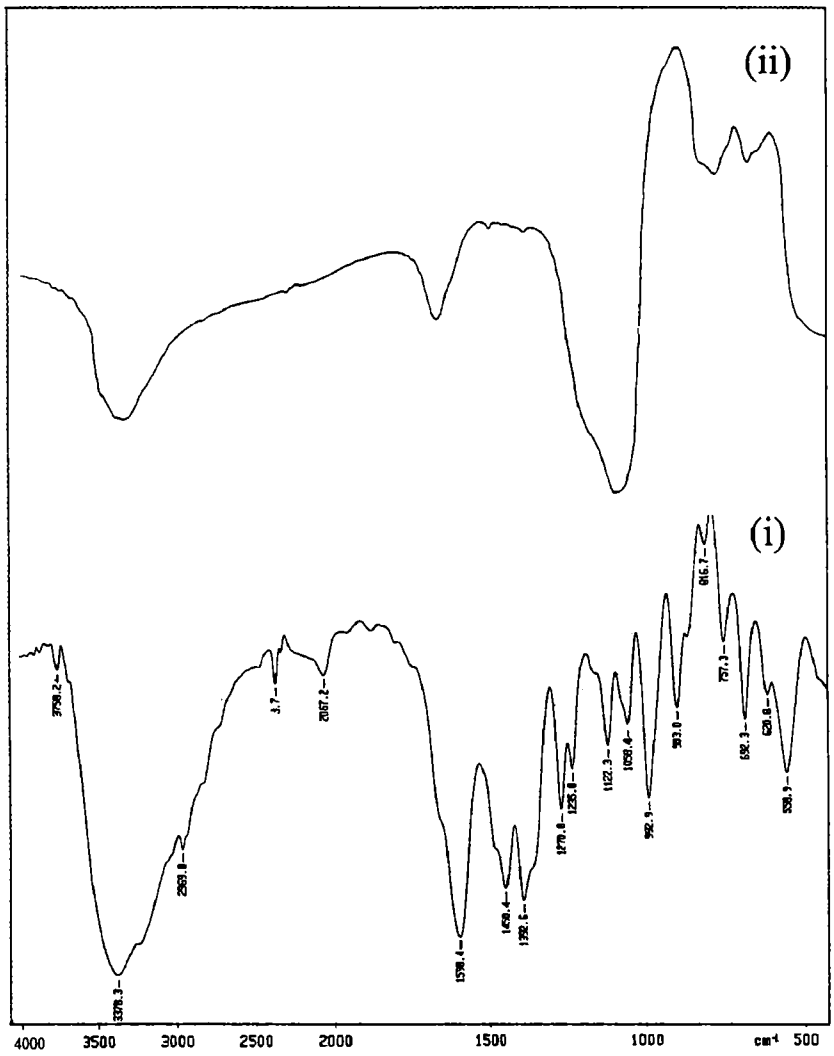

Figures 5A.6 IR spectra

i) EPDTC and ii) FeYEPDTC

5A.4.8. TG analysis

The TG curve of FeYIPDTC is shown in Figure 5A.7. The different stages in the decomposition of the complex and the zeolite cannot be clearly distinguished here.

Table 5A.6 Thermal decomposition data

FeYIPDTC	
Temp range (°C)	% Mass loss
30 -101	4.90
101 - 401	9.81
401 - 799	0.43

Free water associated with the zeolite is lost in the temperature range between 30 °C and 100 °C. The mass loss in the temperature range 101 – 401 °C can be due to the loss of coordinated water and partial decomposition of the ligand. A mass loss of 0.43% occurs in the range 401 – 799 °C, which represents the partial decomposition of the complex as well as the zeolite matrix. The complete decomposition of the complex at 800 °C was confirmed by analyzing the residue obtained, using infrared spectroscopy.

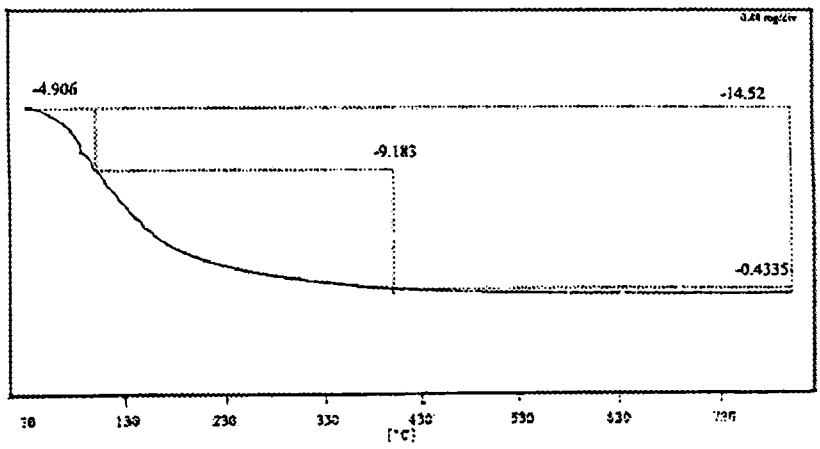

Figure 5A.7 TG curve of FeYIPDTC

Section B

Zeolite encapsulated Co(III), Ni(II),and Cu(II) morpholine-*N*-carbodithioate complexes

5B.1 Introduction

Co(III), Ni(II) and Cu(II) morpholine-*N*-carbodithioate complexes have been studied. However, the effects of encapsulating these complexes inside zeolite Y cages have not yet been studied. In this section our studies on the synthesis and characterization of the encapsulated morpholinecarbodithioate complexes are presented.

5B.2. Experimental

The details regarding the synthesis and characterization of the ligand morpholine-*N*-carbodithioate (MDTC), and the ion-exchanged zeolite are presented in Chapter 2.

5B.2.1. Synthesis of zeolite encapsulated Co(III), Ni(II) and Cu(II) morpholine-*N*-carbodithioate complexes

The general method for synthesizing zeolite encapsulated complexes is given in Chapter 2. A mixture of metal exchanged zeolite and morpholine-*N*-carbodithioate in the ligand to metal mole ratio greater than 3 was refluxed over a water bath for 5 hours. The resulting complex was washed with water and soxhlet extracted using methanol. This procedure was adopted for the synthesis of the encapsulated Co(II), Ni(II), and Cu(II) complexes. But the encapsulated cobalt complex, which was green in colour, leached out during soxhlet extraction

(became colorless after soxhlet extraction). So a different procedure was used for the encapsulation of CoYMDTC. Encapsulated Co (II) complex was oxidized to Co(III) by passing air through an aerator while heating the solution over a water bath at 90 °C. The process was continued until the colour of the zeolite complex changed completely to blue. Co(III)YMDTC forms *tris* complexes with MDTC and will have size large enough to be trapped in the super cage. This was washed with water and soxhlet extracted using chloroform.

The uncomplexed metal remaining in the zeolite in each of the three cases was removed by back-exchange of the zeolite with 0.01M NaCl solution for 24 hours. It was then washed with water to remove chloride ions, dried at 100 °C for 2 hours, and stored in vacuum over anhydrous calcium chloride.

5B.3. Characterization techniques

The various analytical techniques used for the characterization of the prepared complex are given in Chapter 2.

5B.4. Results and Discussion

5B.4.1. Chemical analysis

Zeolite Y encapsulated MDTC complexes of Co(III), Ni(II) and Cu(II) were synthesized. The analytical data of encapsulated MDTC are presented in Table 5B.1. The cobalt (II) complexes could not be encapsulated in the zeolite cages. The complexes were found to leach out of the cage, which might be due to smaller size of the *bis* complex and also might be due to the labile nature of the complex. The data reveal that the Si/Al ratio of the metal exchanged zeolites (2.4) remains unchanged in zeolite complexes indicating the capability of the zeolite structure to withstand encapsulation conditions. Analytical data suggest that almost all the metal ions get complexed.

Table 5B.1 Analytical data

Sample	% Si	% Al	% Na	% M	%C
CoYMDTC	18.46	7.80	5.32	0.25	0.76
NiYMDTC	18.52	7.70	5.60	0.50	1.50
CuYMDTC	18.48	7.56	5.75	1.01	1.90

5B.4.2. X-ray diffraction patterns

The XRD patterns of CoYMDTC, NiYMDTC, and CuYMDTC are given in Figure5B.1. The encapsulated materials exhibited well-resolved XRD patterns identical to that of metal exchanged zeolites. The incorporation of the complex did not alter the XRD patterns, indicating that no structural change or decrease in crystallinity has taken place.

5B.4.3 Scanning electron micrographs

The scanning electron micrographs of FeYMDTC before soxhlet extraction and after soxhlet extraction were taken. The micrograph taken after soxhlet extraction showed that most of the particles were removed by this process. This is shown in Figure 5B.2.

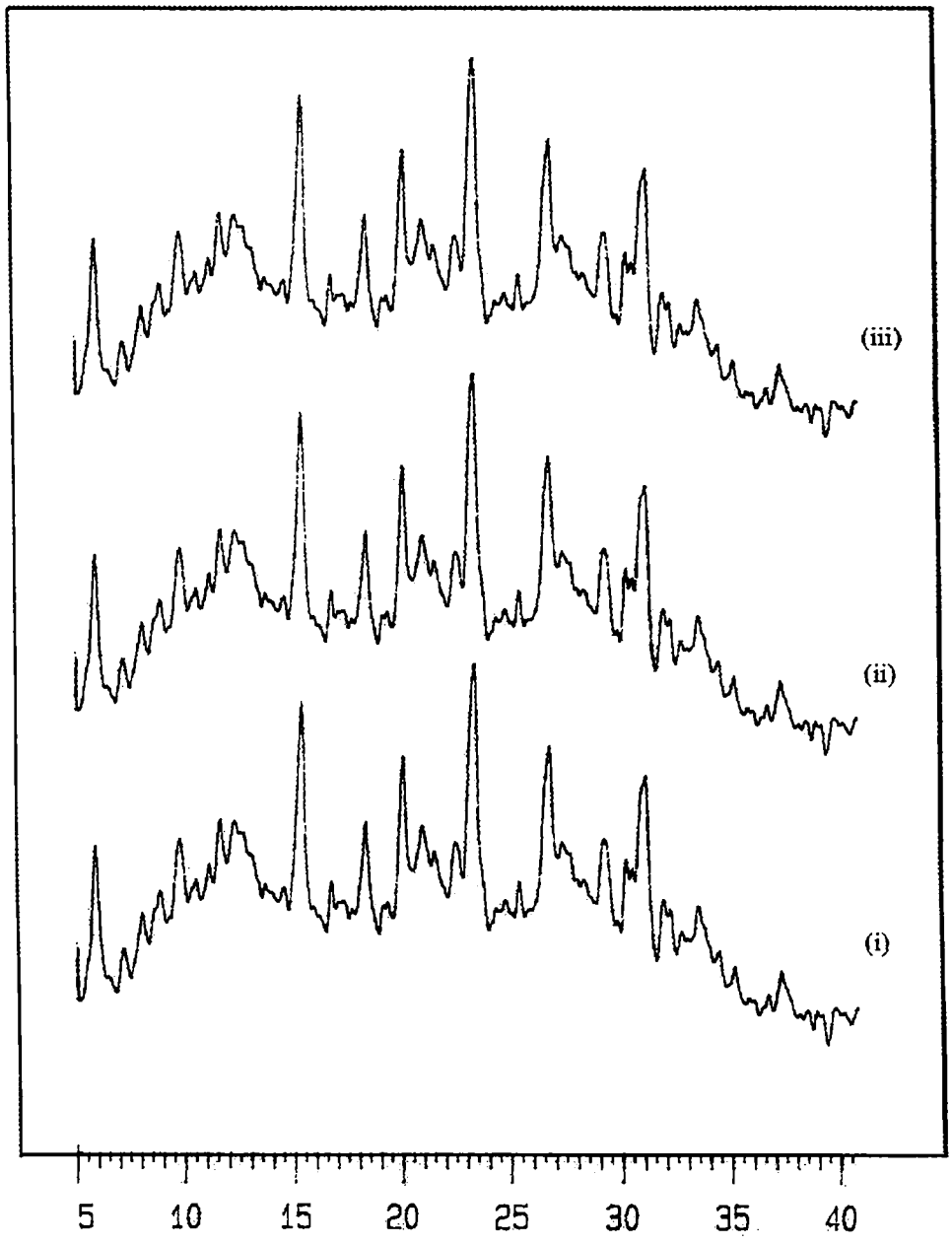

Figure 5B.1 XRD pattern of i) CoYMDTC, ii) NiYMDTC and iii) CuYMDTC

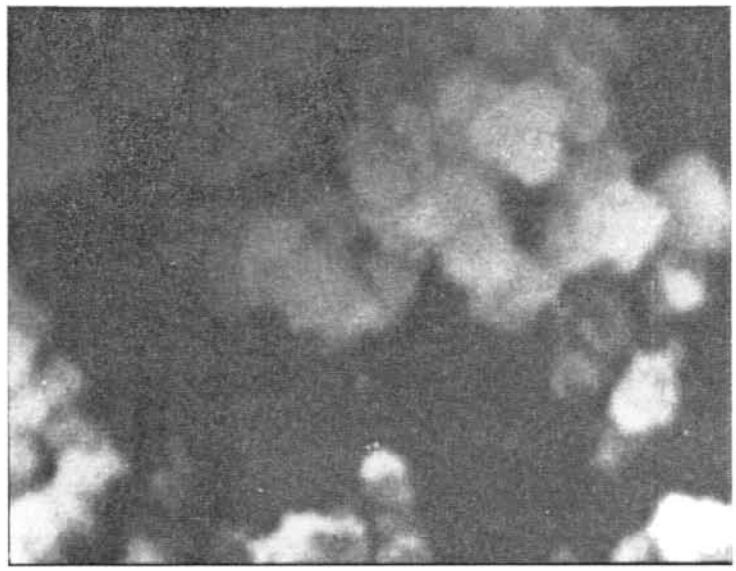

(i)

(ii)

Figure 5B.2 SEM

i) Before soxhlet extraction
ii) After soxhlet extraction

5B.4.4. Surface area and pore volume data

Surface area and pore volume data are given in Table 5B.2. The lowering of surface area and pore volume on encapsulation is indicated in the table. Surface area and pore volume analyses provide strong evidence for encapsulation.

Table 5B.2 Surface area and pore volume data

Sample	Surface area (m^2/g)			Pore volume (ml/g)		
	MY	MYMDTC	% loss	MY	MYMDTC	% loss
CoY	532	250	53.0	0.2986	0.1385	53.6
NiY	528	261	50.6	0.2974	0.1384	53.3
CuY	530	244	53.9	0.2983	0.1342	52.3

5B.4.5. Magnetic moment

The magnetic moment calculated from magnetic susceptibility data are summarized in Table 5B.3. Co(III)YMDTC is found to be diamagnetic. The magnetic moment 3.20 BM observed for NiYMDTC indicates an octahedral geometry for the Ni(II) ion, even though a neat complex of nickel dithiocarbamate has a square planar geometry [22]. CuYMDTC exhibits a magnetic moment of 1.82 BM, which suggests a square planar geometry for the complex.

Table 5B.3 Magnetic moment

Sample	Magnetic moment (BM)
CoYMDTC	–
NiYMDTC	3.20
CuYMDTC	1.82

5B.4.6. Diffuse reflectance spectra

The electronic spectral data of encapsulated MDTC complexes are given in Table 5B.4 and the spectra are given in Figure 5B.3. The spectrum of CoYMDTC shows bands at 16000cm^{-1} and 24390cm^{-1}. These absorptions agree with those reported for octahedral complexes of Co(III) [18]. These bands could be attributed to $^1T_g \leftarrow {}^1A_g$ and $^1T_{2g} \leftarrow {}^1A_g$ transitions in octahedral Co(III) complexes. The transition at 30120cm^{-1} is a charge transfer transition.

Table 5B.4 Electronic spectral data

Sample	Abs. max. (cm^{-1})	Assignment
CoYMDTC	16000	$^1T_{1g} \leftarrow {}^1A_{1g}$
	24390	$^1T_{2g} \leftarrow {}^1A_{1g}$
	30120	Charge transfer transition
NiYMDTC	15000	$^3T_{1g}(F) \leftarrow {}^3A_{2g}(F)$
	25000	$^3T_{1g}(P) \leftarrow {}^3A_{2g}(F)$
	31060	Charge transfer transition
CuYMDTC	14900	$B_{2}g \leftarrow B_{1}g$
	17000	$A_{1}g \leftarrow B_{1}g$
	28570	Charge transfer transition

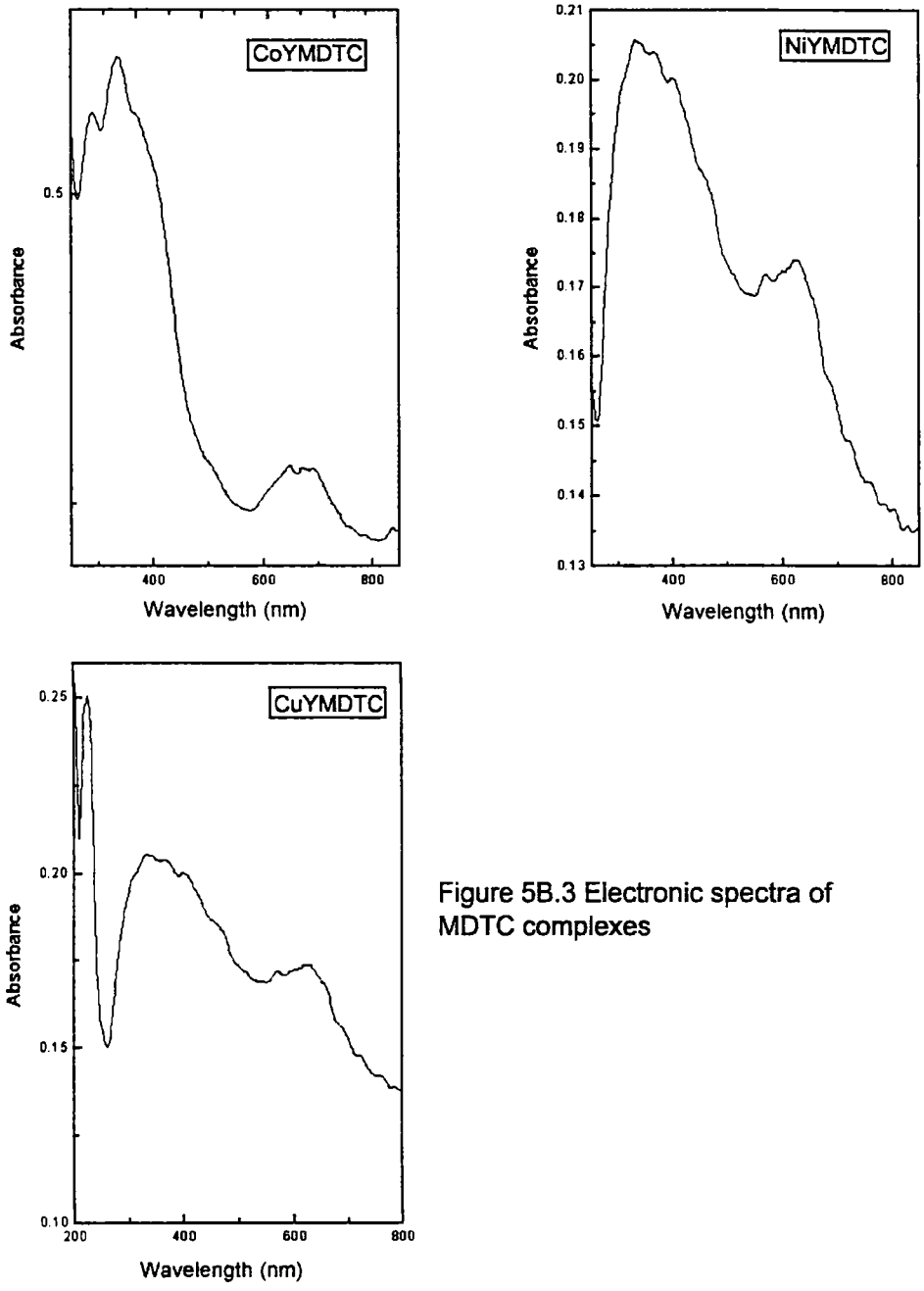

Figure 5B.3 Electronic spectra of MDTC complexes

NiYMDTC also exhibits transitions characteristic of octahedral complexes. In the case of NiYMDTC the bands seen at at 15000cm^{-1} and 25000cm^{-1} could be attributed to $^3T_{1g}(F) \leftarrow {}^3A_{2g}(F)$ and $^3T_{1g}(P) \leftarrow {}^3A_{2g}(F)$ transitions [18]. The charge transfer transition is seen at 31060cm^{-1}. The magnetic moment of 3.20 BM observed for encapsulated Ni(II) complex also suggests an octahedral geometry. Neat nickel dithiocarbamate complexes are reported to have square planar geometry. The water molecules in the zeolite lattice or the oxide ions of the framework are likely to involve in the octahedral geometry for Ni(II) ion.

CuYMDTC exhibits transitions at 14900cm^{-1} and 17000cm^{-1} in accordance with $B_{2g} \leftarrow B_{1g}$ and $A_{1g} \leftarrow B_{1g}$ transitions [18, 23] indicating square planar geometry around the Cu(II) ion. The high-energy band at 28570cm^{-1} can be attributed to charge transfer transition. The magnetic moment of 1.82 BM of CuYMDTC agrees with the square planar structure.

5B.4.7. FTIR spectra

The important infrared spectral data of MDTC complexes are presented in Table 5B.5 and the spectra are shown in Figure 5B.4. The absorption at 1461cm^{-1} in the spectrum of the ligand MDTC arises due to $\nu N{=}CS_2$ vibration. This $\nu N{=}CS_2$ is seen in the Co(III), Ni(II), and Cu(II) complexes in the region 1485cm^{-1} to 1500cm^{-1}. The positive shift of this absorption may be an indication of the interaction of the chelated sulphur atoms with the metal. [20]. The νC-S stretching vibration seen in the spectrum of the ligand in the region 980-1060cm^{-1} might have shifted to lower frequency on complexation. But these bands are not observed in the spectra of Co and Ni zeolite encapsulated complexes as these have been masked by the broad zeolite absorption around 1000cm^{-1}. This is seen at 950cm^{-1} in the spectrum of the Cu complex.

Table 5B.5 Infrared spectral data

MDTC cm^{-1}	CoYMDTC cm^{-1}	NiYMDTC cm^{-1}	CuYMDTC cm^{-1}
416			409
483	469	460	488
540			503
580	570	570	570
637	621		
	713	700	711
980			950
1023	1030	1020	1020
1112			
1215		1234	
1261		1267	1264
1322			
1346		1354	
1385	1385		
1418			
1461	1485	1500	1500
1625			
	1640	1635	1630
2112			
2335	2336	2335	2336
2361	2361	2361	2361
2756			
2852			
2967		2970	
3196			
3279			
3364	3475	3475	3472

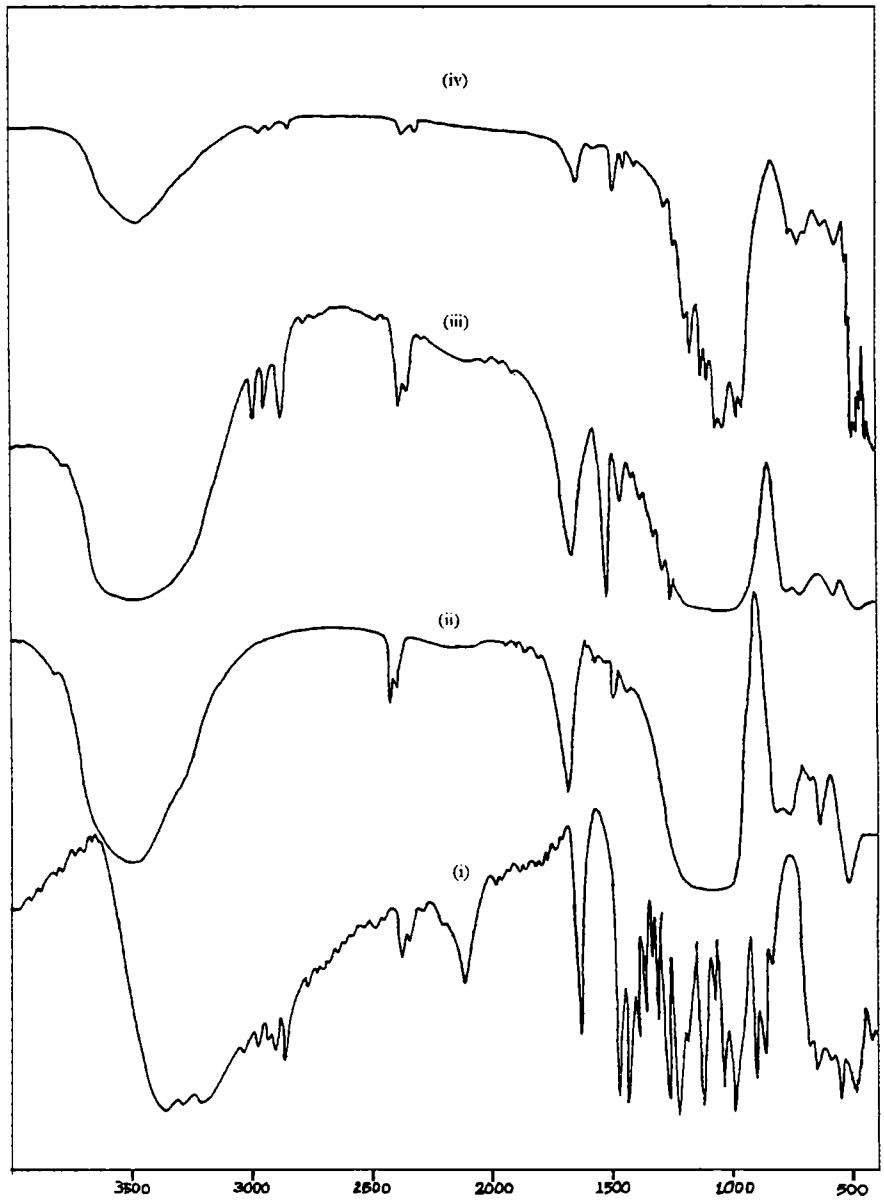

Figure 5B.4 Infrared spectra
i) MDTC and ii) CoYMDTC iii) NiYMDTC, iv) CuYMDTC

5B.4.8. EPR spectrum

Figure 5B.5 shows the EPR spectrum of CuYMDTC at liquid nitrogen temperature. The calculated EPR parameters are given in Table 5B.6. The EPR spectrum at room temperature is broad, and that at liquid nitrogen temperature shows hyperfine splittings. The g_{II} value of 2.31 suggests a square planar structure.

Table 5B.6 EPR parameters

g_{II}	2.31
A_{II}	211.5 x 10^{-4} cm^{-1}
g_{II}/A_{II}	109.2cm
$g_{\perp}$	2.02
$A_{\perp}$	8.41 x 10^{-4} cm^{-1}
α^2	0.9445
μ_{eff}	1.84 BM
P	0.1509

The ratio g_{II}/A_{II} is 109.2 cm for CuYMTDC, suggesting a square planar environment around Cu (II) ion. The value of α^2 is 0.9495, suggesting ionic environment for the Cu^{2+} ions in the zeolite cavity. The magnetic moment calculated using EPR parameters is 1.84 BM, which is in agreement with the value obtained by Gouy method. All these suggest a square planar structure for the zeolite encapsulated copper morpholinecarbodithioate complex.

Figure 5B.5 EPR spectrum of CuYMDTC complex

5B.4.9. TG analysis

TG curves are shown in Figure 5B.6 and the TG data are tabulated in Table 5B.7.

Table 5B.7 Thermal decomposition data

CoYMDTC		NiYMDTC		CuYMDTC	
Temp range (°C)	% Mass loss	Temp range (°C)	% Mass loss	Temp range (°C)	% Mass loss
31 – 100	5.80	30 – 101	5.67	30 – 100	5.61
100 – 400	12.52	101 – 400	12.36	100 – 460	12.51
400 – 799	0.36	400 – 798	0.34	460 – 798	0.44

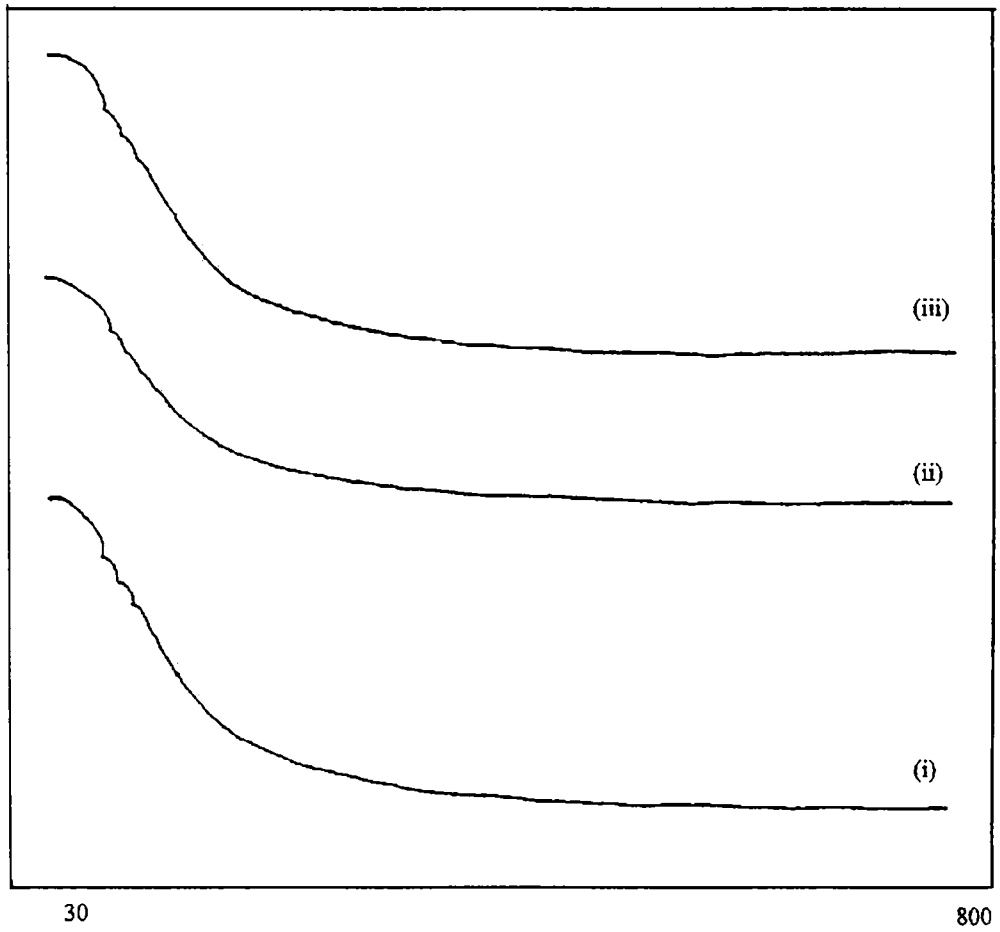

Figure 5B.6 TG curves of MDTC complexes
(i) CoYMDTC, (ii) NiYMDTC, and (iii) CuYMDTC

All the complexes lose free water in the temperature range 30 – 101 °C . The mass loss in the temperature range 101 – 400 °C corresponds to the loss of coordinated water and the partial decomposition of the ligand. The mass loss corresponding to this stage is ~ 12 %. The very small mass loss of ~ 0.34 % - 0.44 % in the temperature range 400 – 798 °C in each case can be due to the partial decomposition of the complex as well as that of the zeolite.

References

1. D.F. Lewis, S.J. Lippard, and J.A. Zubieta, *Inorg. Chem.* 11 (1972) 823.
2. G.N. Schrauzer, *Transition Met. Chem.* 4 (1968) 299.
3. L.H. Pignolet and S. H. Wheeler, *Inorg. Chem.* 19 (1980) 935.
4. J.R. Hendrickson, J.M. Hope, and R.L. Martin, *J. Chem. Soc. Dalton. Trans.* (1976) 2032.
5. K.W. Given, B.M. Mattson, M.F. McGuiggan, G.L. Miessler, and L.H. Pignolet, *J. Am. Chem. Soc.* 99 (1977) 4855.
6. G.L. Miessler and L.H. Pignolet, *Inorg. Chem.* 18 (1979) 210.
7. N.M. Coleman, J.R. Shelton and J.L. Koering, *Ind. Engng. Chem. Prod. Res. Develop.* 13 (1974) 154.
8. D. Coucouvanis, *Prog. Inorg. Chem.* 11 (1970) 233.
9. D. Coucouvanis, *Prog. Inorg. Chem.* 26 (1979) 301.
10. R. Eisenberg, *Prog. Inorg. Chem.* 12 (1970) 295.
11. J. Willemse, J.A. Cras, J.J. Steggerda, and C.P. Keijzers, *Struct. Bonding* (Berlin) 28 (1976) 83.
12. K. Tsuchiya, M. Yoshizumi, H. Houchi, and R.P. Mason, *J. Biol. Chem.* 275, 3 (2000) 1551.
13. A. Godelitsas, D. Charistos, J. Dwyer, C. Tsipis, A. Filippidis, A. Hatzidimitriou, and E. Pavlidou, *Microporous and Mesoporous Materials* 33 (1999) 77.
14. N.N. Greenwood and A. Earnshaw, *Chemistry of Elements* (1^{st} edn.), Pergamon Press, Oxford, 1984. Rpt.1989.
15. F.A. Cotton and G. Wilkinson, *Advanced Inorganic Chemistry* (5^{th} edn .), John Wiley and Sons, New York, 1988.
16. P. Gallezot, Y.B. Taarit, and B. Imolik, *J. Catal.* 26 (1972) 205.
17. H.D. Simpson and H. Steinfink, *J. Am. Chem. Soc.* 91 (1969) 6229.
18. A.B.P. Lever, *Inorganic Electronic Spectroscopy,* Elsevier, Amsterdam, 1968.
19. K.K.M. Yusuff and E.J. Mathew, Synth. *React. Inorg. Met. -Org. Chem.* 19,1 (1989) 15.
20 L.M. Engelhardt, P.C. Healy, R.M. Shephard, B.W. Skelton, and A.H. White, *Inorg. Chem.* 27 (1988) 2371.
21. K.A. Jensen and L. Henriksen, *Acta. Chem. Scand.* 22 (1968) 1107.
22. K.S. Arulsamy, R.F.N. Ashok and U.C. Agarwala, *Ind. J. Chem.* 23A (1984) 127.
23. N.T. Madhu and P.K. Radhakrishnan, *Synth. React. Inorg. Met.-Org. Chem.* 31, 2 (2001) 315.
24. U. Sakaguchi and A.W. Addison, *J. Chem. Soc., Dalton Trans.* (1979) 600.

Chapter 6

Zeolite encapsulated palladium complexes

Abstract

Palladium compounds have been used as catalysts in a number of oxidation reactions because of their activity even at very low concentrations. The possibility of using zeolite Y encapsulated palladium complexes as oxidation catalysts was explored in the present study. Zeolite encapsulated palladium compounds of DMG, MDTC and SALSC were synthesized using the flexible ligand method. These compounds were characterized using chemical analysis, XRD, SEM, surface area and pore volume analysis, DRS, FTIR, and TG measurements.

6.1. Introduction

Palladium has gained importance as an active component in catalytic reactions in recent years. The most common use of palladium-based catalysts has been in hydrogenation reactions. In recent times they are increasingly being used in C-C coupling reactions of aromatic and vinylic systems [1-3]. Some compounds of palladium in low oxidation states can also act as good oxidation catalysts. The method for the oxidation of ethylene to acetaldehyde catalyzed by palladium(II) compounds, commonly referred to as the Wacker process, was reported by Smidt and co workers [4-7]. The commercial success of the Wacker process provided an enormous stimulus for further studies of palladium complexes as homogeneous catalysts [8]. But Wacker process has some major disadvantages. The low pH of the solution, high chloride concentration, and the formation of chlorinated byproducts caused serious technical and environmental problems.

Homogeneous palladium catalysts are prone to a number of deactivation reactions. One way out was to heterogenize the soluble catalyst. A number of supports were used by Viswanathan for the study of palladium [9]. It has been reported that the nature of the support used for palladium catalyst has a role to play in modifying the selectivity towards useful products [10]. Supported palladium is an efficient automotive catalyst and has been studied using a wide variety of methods [11,12]. Supported palladium catalyst is found to be resistant to the action of poison, especially with nitrogen donor poisons [13].

Palladium, like other precious metals and their compounds, is used in many industrial processes in spite of its cost. These compounds are preferred because of their high activity even at low concentration level, and their high specificity. The possibility of using zeolite Y encapsulated palladium complexes as oxidation catalysts was explored in the present study.

Complexes with nitrogen, oxygen, and sulphur donor ligands capable of forming stable four, five, or six membered ring compounds with metal are well known. Ligands can not only stabilize a metal complex catalyst but also fundamentally change its selectivity and activity. Dithiocarbamates, dimethylglyoximes, and semicarbazones can form complexes of palladium with four, five, or six membered rings. Dithiocarbamates yield two 4-membered ring compounds and dimethylglyoxime produces two 5-membered ring compounds whereas salicylaldehyde semicarbazone produces one 6-membered and one 5-membered rings.

In the present investigation, palladium complexes of DMG, SALSC and MDTC were encapsulated in zeolite for spectral and catalytic studies. The oxidative property shown by Pd(II) complexes was found to be retained on encapsulation. Though the encapsulation of these complexes involves only physical entrapment, selectivity, activity and recyclability were found to increase several times. The results of our studies on these complexes are presented in this chapter. The structures of SALSC and MDTC are presented in Figure 3B.1 (Chapter 3) and in Figure 5.1 (Chapter 5) respectively. The structure of dimethylglyoxime is shown below.

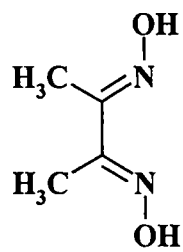

Figure 6.1 Structure of dimethylglyoxime (DMG)

6.2. Experimental

Details regarding the synthesis and purification of the ligands salicylaldehydesemicarbazone (SALSC), dimethylglyoxime (DMG), and morpholinecarbodithioate (MDTC) are given in Chapter 2. Palladium exchanged zeolite was prepared according to the procedure given in Chapter 2.

6.2.1. Synthesis of zeolite encapsulated palladium complexes

Palladium exchanged zeolite (3.0g) was treated with dimethylglyoxime so that the ligand to metal ratio was greater than 2. The mixture was heated in a sealed ampule at 120 °C for 18 hours. Impure PdYDMG was soxhlet extracted using methanol. A similar method was followed for the preparation of PdYSALSC (ligand to metal ratio slightly higher than 1) with the temperature at 200 °C for 6 hours. The impure compound was purified by soxhlet extraction using methanol and chloroform.

PdYMDTC was prepared by adding PdY (3.0g) to a solution of MDTC in water (ligand to metal ratio slightly higher than 2). It was refluxed for 5 hours. After washing with water, surface species were removed using soxhlet extraction with methanol. All the complexes were back exchanged with NaCl and washed to remove chloride ions. They were dried at 110 °C for 2 hours and stored in vacuum over anhydrous calcium chloride.

6.3. Characterization techniques

Details regarding the analytical methods and characterization techniques are given in Chapter 2.

6.4. Results and Discussion

6.4.1. Chemical analysis

The results of chemical analysis are given in Table 6.1. The Si/Al ratio of ~ 2.4 for the complexes is in the range expected for zeolite Y. The metal content is low. All the metal ions present seem to be complexed. The good catalytic activity can be the result of low metal ion concentration with high dispersion.

Table 6.1 Analytical data

Sample	% Si	% Al	% Na	%C	% Pd
PdYDMG	18.50	7.65	5.72	0.09	0.10
PdYSALSC	18.49	7.70	5.80	0.08	0.09
PdYMDTC	18.54	7.80	5.65	0.03	0.03

6.4.2. X-ray diffraction patterns

The XRD patterns of NaY, PdYDMG, PdYSALSC, and PdYMDTC are given in Figure 6.2 .The XRD patterns of the palladium compounds show no peaks corresponding to any palladium species. The main peaks are associated with the crystallinity of the zeolite support. X-ray diffraction patterns indicate the good crystallinity of these complexes. The XRD patterns of all these complexes were similar to those of NaY, showing that the zeolite framework has remained unaffected during the synthesis of the complexes.

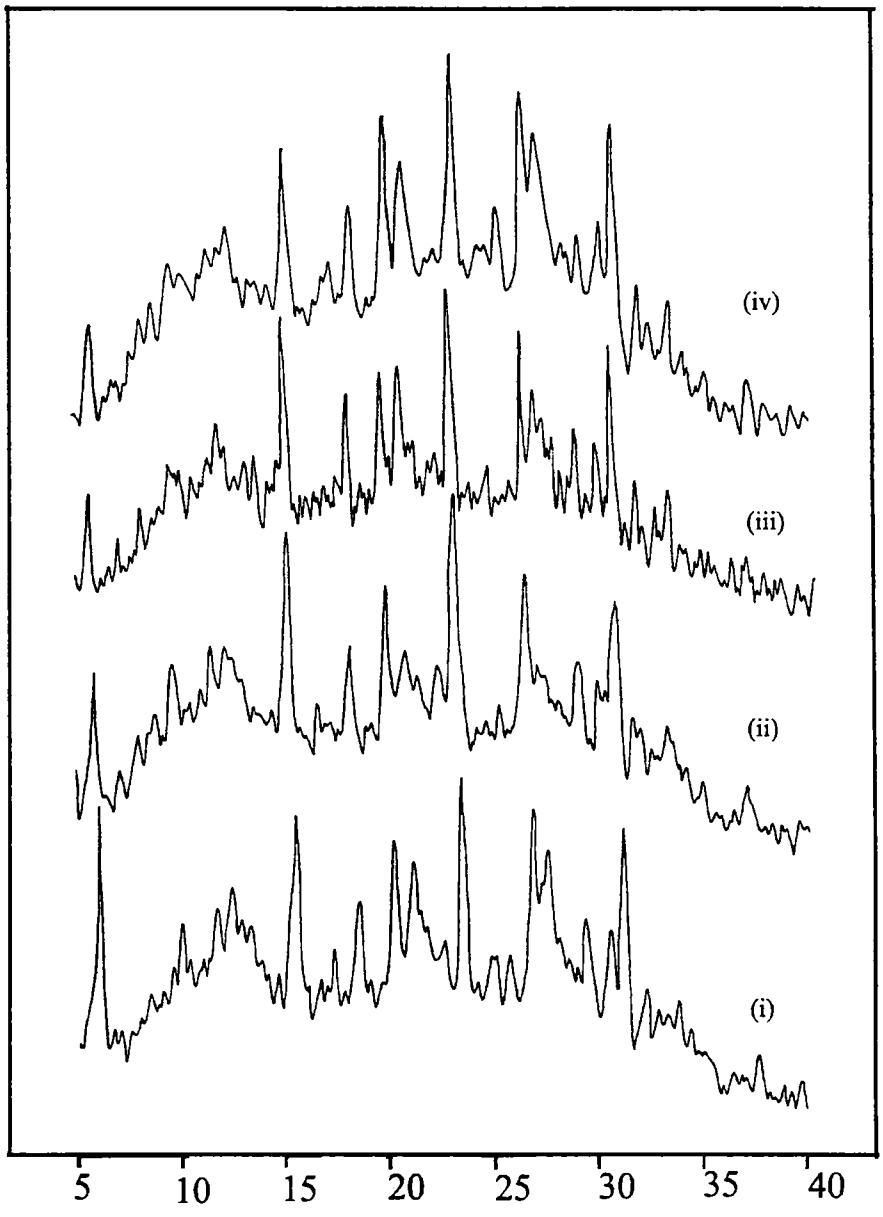

Figure 6.2 XRD patterns of (i) NaY, (ii) PdYDMG, (iii) PdYSALSC and (iv) PdYMDTC

6.4.3. Scanning electron microscopy

(i)

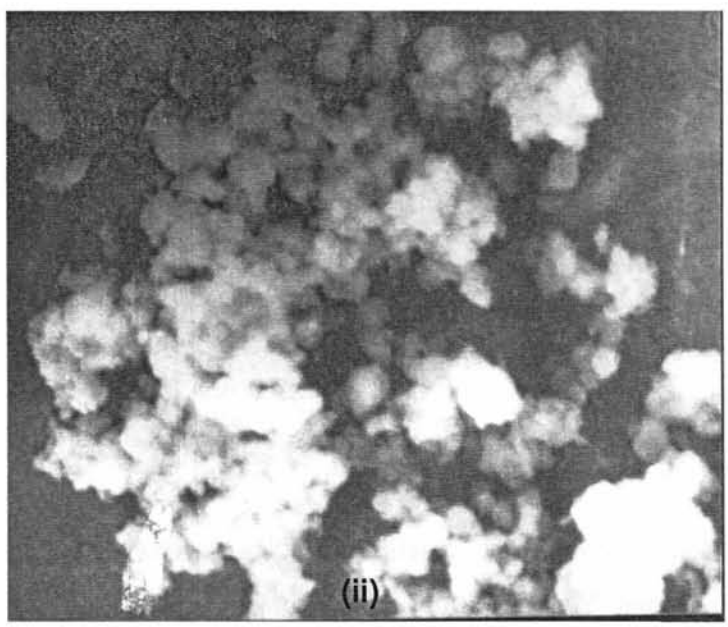

Figure 6.3 SEM

i) Before soxhlet extraction
ii) After soxhlet extraction

The scanning electron micrographs of the palladium dimethylgloxime complex taken before and after soxhlet extraction indicate the removal of surface adsorbed species. This is clear from the figure.

6.4.4. Surface area and pore volume

The BET surface area and pore volume data are given in Table 6.2. The encapsulation of PdYDMG, PdYSALSC, and PdYMDTC complexes inside the zeolite cavity is indicated by the lowering of surface area and pore volume compared to the metal exchanged zeolite.

Table 6.2 Surface area and pore volume data

Sample	Surface area (m^2/g)			Pore volume (ml/g)		
	PdY	PdYL	% loss	PdY	PdYL	% loss
PdYDMG	500	220	56.0	0.2898	0.1300	55.0
PdYMDTC	500	180	64.0	0.2898	0.1021	64.7
PdYSALSC	500	228	54.4	0.2898	0.1352	53.7

6.4.5. Magnetic moment

Magnetic moment values calculated from room temperature magnetic susceptibility methods suggest that all the zeolite Y encapsulated palladium complexes are diamagnetic. This suggests square planar geometry for the palladium complexes.

6.4.6. Diffuse reflectance spectra

The diffuse reflectance spectral data are given in Table 6.3 and the spectra are presented in Figure 6.4. Similar transitions are seen in all the zeoliteY encapsulated complexes arising form the $^1A_{1g}$ level. The band at 21370cm^{-1}seen in all the complexes is due to $^1A_{2g} \leftarrow {}^1A_{1g}$ transition. The band seen at 26600cm^{-1} in the case of PdYDMG and that at 27000cm^{-1} in the case of PdYMDTC and PdYSALSC are due to $^1E_g \leftarrow {}^1A_{1g}$ transition. The band at 33000cm^{-1} in all the complexes is the result of $^1B_{1g} \leftarrow {}^1A_{1g}$. These are characteristic of square planar geometry, and indicate square planar geometry for palladium complexes [14]. Room temperature magnetic measurement further supports this inference.

Table 6.3 Electronic spectral data

Sample	Abs. max. (cm^{-1})	Assignment
PdYDMG	21370	$^1A_{2g} \leftarrow {}^1A_{1g}$
	26600	$^1E_g \leftarrow {}^1A_{1g}$
	33000	$^1B_{1g} \leftarrow {}^1A_{1g}$
PdYSALSC	21370	$^1A_{2g} \leftarrow {}^1A_{1g}$
	27000	$^1E_g \leftarrow {}^1A_{1g}$
	33000	$^1B_{1g} \leftarrow {}^1A_{1g}$
PdYMDTC	21370	$^1A_{2g} \leftarrow {}^1A_{1g}$
	27000	$^1E_g \leftarrow {}^1A_{1g}$
	33000	$^1B_{1g} \leftarrow {}^1A_{1g}$

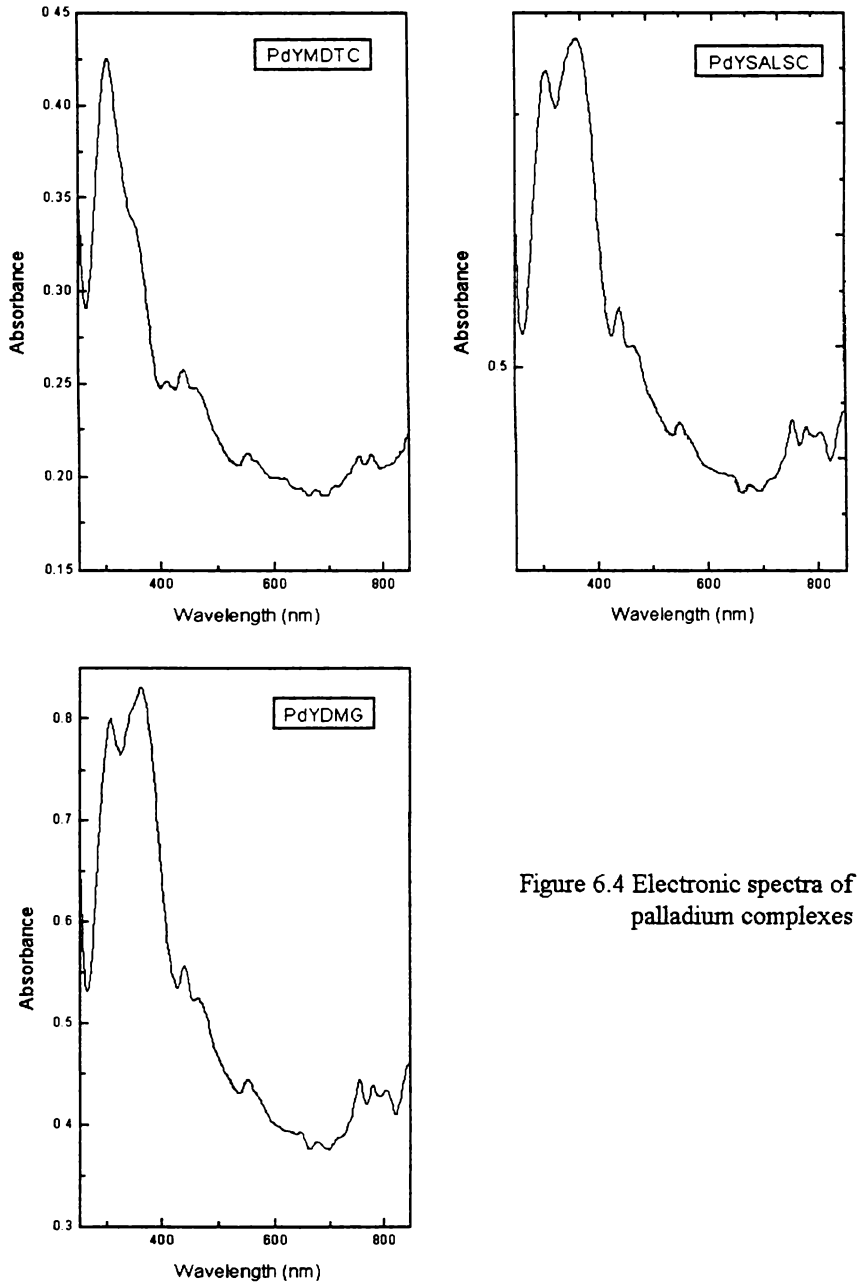

Figure 6.4 Electronic spectra of palladium complexes

6.4.7. FTIR spectra

A comparative study of the spectra of the ligands and the complexes was made. The IR spectra of DMG and PdYDMG are shown in Figure 6.5, those of SALSC and PdYSALSC in Figure 6.6, and of MDTC and PdYMDTC in Figure 6.7. The spectral data are shown in Table 6.4. The IR spectra of DMG and its complexes have been studied extensively by Shpiro et al. [15]. In the spectrum of ligand DMG, two absorptions each have been reported for C=N and N-O vibrations. These two bands can be due to unequal C=N and N-O linkages. In the case of free DMG ligand, the bands which occur at 1440cm^{-1} and 1594cm^{-1}are due to C=N stretching vibration and those at 980cm^{-1} and 1143cm^{-1}are due to N-O stretching frequencies. In the spectrum of the complex, the band at 1530cm^{-1} can be due to the C=N stretching vibration. The shifting of the band at 1594cm^{-1} to lower frequency suggests coordination through nitrogen. The peak due to N-O stretching vibration is not seen in the spectrum of the complex as it is masked by the broad band of zeolite.

In the spectrum of the ligand salicylaldehyde semicarbazone, the absorption at 3460cm^{-1} arises as a result of νO-H and νNH_2 vibrations [16]. The ligand band at 1620cm^{-1}due to νC=O in the ligand is shifted to 1600 cm^{-1} in the complex. The νC=N stretch at 1485 cm^{-1} is shifted to lower frequency indicating that coordination has occurred also through nitrogen. The νC-O of the phenolic group is masked by absorption of the zeolite. The absorption bands of νNH and δNH_2, which are expected to remain unaltered in the spectrum of the complexes, are masked by the absorption of water.

In the dithiocarbamate, the bonding to the central metal is through the sulphur atoms of the ligand. The $\nu N{=}CS_2$ absorption of morpholinecarbodithioate is seen at 1461cm^{-1}. In the spectrum of the complex, this band is observed as a very weak band at 1493cm^{-1}. This positive shift indicates the interaction of chelated sulphur atoms with the metal ion [17].

Table 6.4 Infrared spectral data

DMG cm^{-1}	PdYDMG cm^{-1}	SALSC cm^{-1}	PdYSALSC cm^{-1}	MDTC cm^{-1}	PdYMDTC cm^{-1}
466		458		482	476
		561		540	580
705	618	678	617	637	618
753	722	750	773	868	
				892	
902		894		980	
980		980		1023	1004
	1038	1030	1032		1036
				1063	
1143		1110		1112	1097
1365		1150		1215	
1440		1201		1261	
1594	1530	1273		1300	
	1637	1353		1346	
1941		1384	1380	1385	
2369	2369	1485	1415	1418	
3214		1620	1600	1461	1492
			1640		
		2367	2368	1625	1640
3687	3465	2829	2832	2112	
		3416	3460	2335	2335
				2361	2361
				2756	
				2852	
				3196	
				3279	
				3364	3480

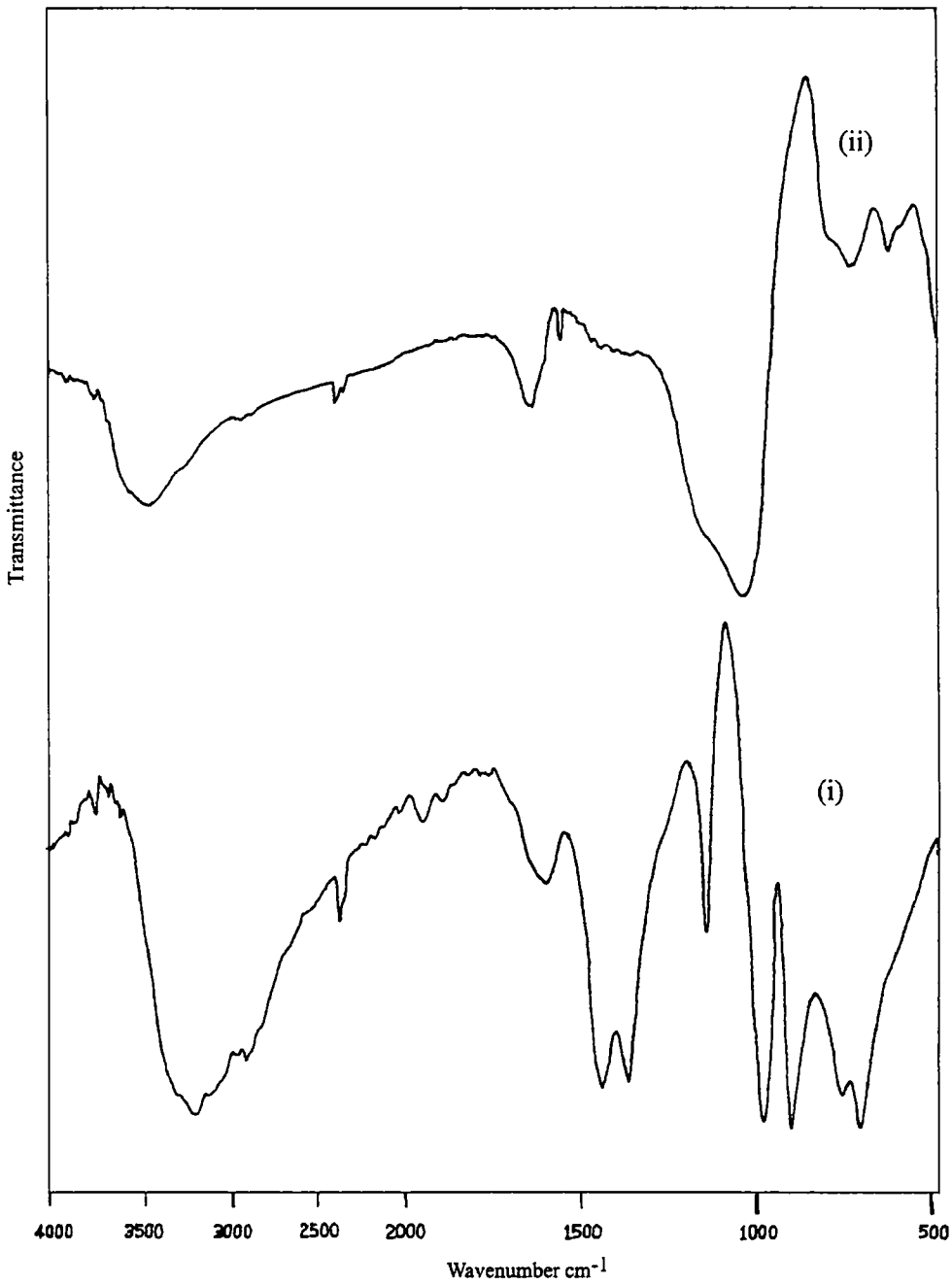

Figure 6.5 IR of ligand DMG and DMG complex

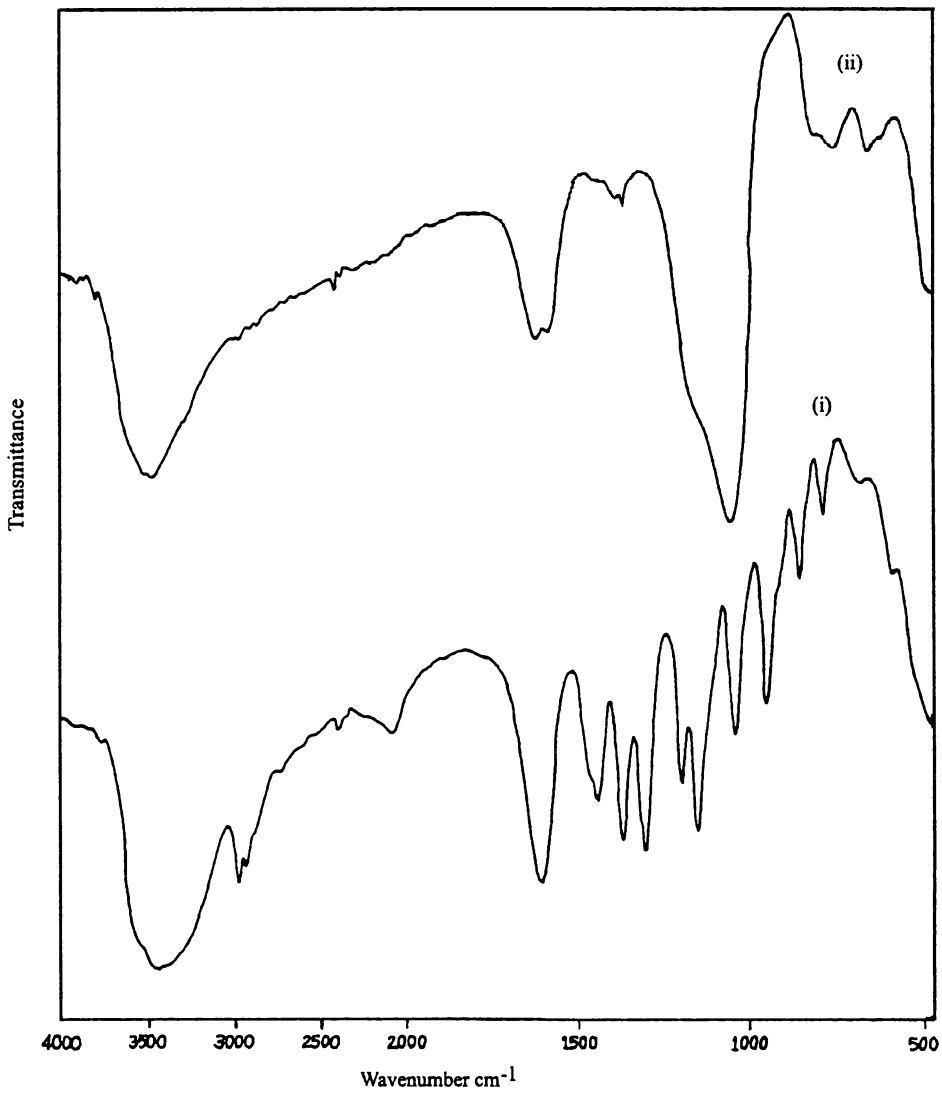

Figure 6.6 IR of ligand SALSC and SALSC complex

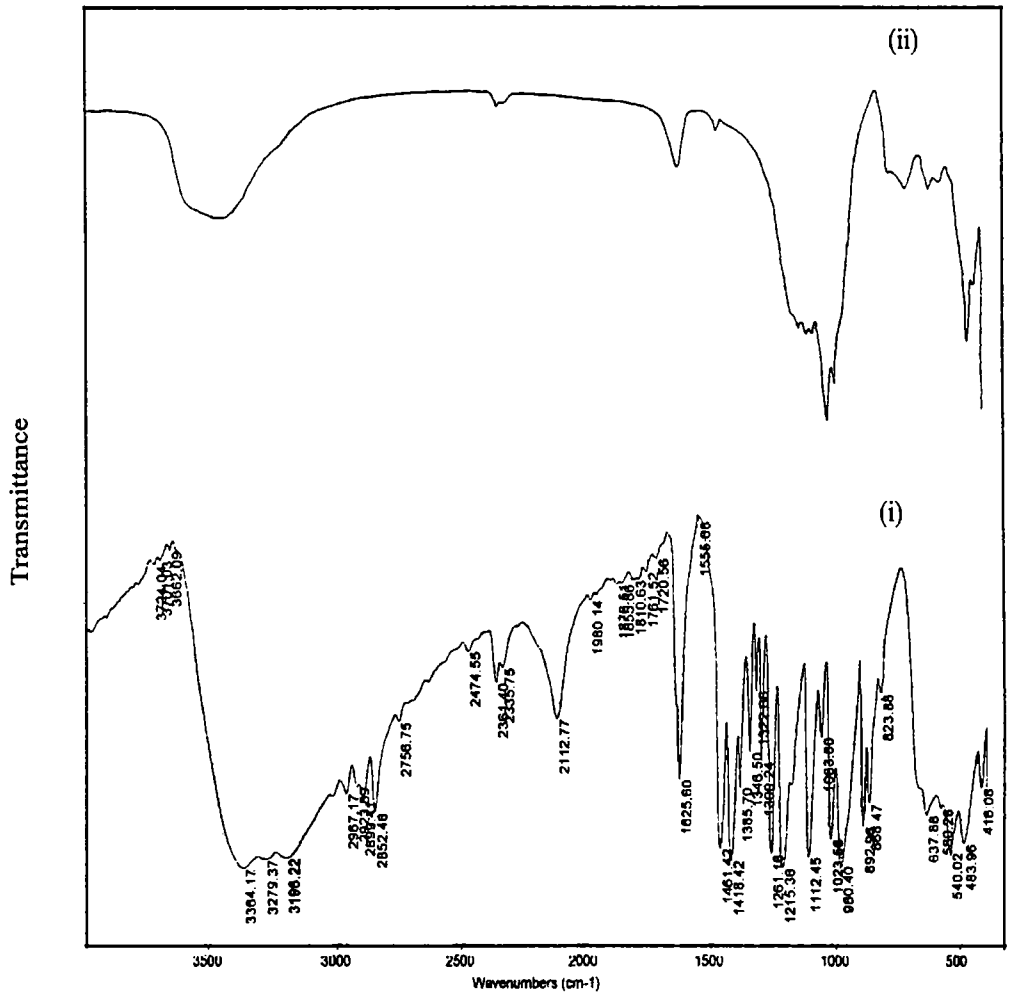

Figure 6.7 IR spectra
i) MDTC and ii) PdYMDTC complex

6.4.8. TG analysis

The TG curves of PdYDMG were recorded in an atmosphere of nitrogen from room temperature to 800 °C at a heating rate of 10 °/min. Figure 6.7 shows the TG curve of PdYDMG. Thermo analytical data for the complexes are presented in Table 6.5.

Table 6.5 Thermal decomposition data

PdYDMG	
Temp Range (°C)	% Mass loss
40 -120	8.0
120 - 400	6.3
400 – 780	4.4

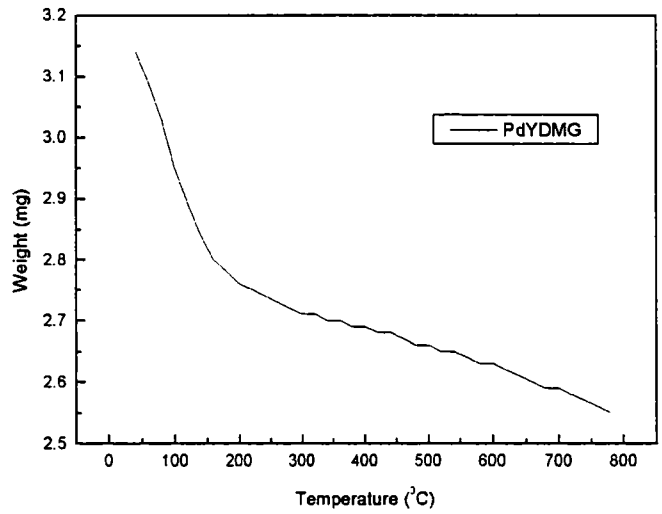

Figure 6.8 TG curve of PdYDMG

The percentage mass loss of PdYDMG at different temperature ranges is given in the table. The loss of free and coordinated water occurs up to 125 °C. The decomposition of the ligand and the partial decomposition of zeolite occur as a continuous process. We get only a qualitative idea from this curve.

References

1. J. Tsuji, *Palladium Reagents and Catalysts*, Wiley, New York, 1996.
2. I.P. Beletskaya and A.V. Cheprakov, *Chem. Rev.* 100 (2000) 3009.
3. Jairton Dupont, Roberto F. de Souza, and Paulo A.Z. Suarez, *Chem. Rev.* 102 (2002) 3667.
4. J. Smidt, *Chem. Int.* (London) (1962) 54.
5. H. Arai, T. Yamashiro, T. Kubo, and H. Tominago *Bull, Jpn. Pet. Inst.* 18 (1976) 39.
6. T .Kubota, F. Kumada, H. Tominago, and T. Kanugi, *Int. Chem. Eng.* 13 (1973) 539.
7. J. Smidt, W. Hafner, R. Jira, J. Sedlmeier, and A. Sabel, *Angew. Chem. Int. Ed.* 1 (1962) 80.
8. P. M. Maitlis, *The Organic Chemistry of Palladium, Vols. 1 and 2*, Academic Press, New York, 1971.
9. N. Mahata, K.V. Raghavan, and V. Viswanathan, *Bulletin of the Catalysis Society of India* 9, 1-2 (1999) 75.
10. S. Chandra Shekar, A. Venugopal, K.S. Rama Rao, P.S. Sai Prasad, R. Srinivas, and P. Kanta Rao, in *Recent Advances in Basic and Applied Aspects of Industrial Catalysis* (*Studies in Surface Science and Catalysis 113*), T.S.R. Prasad Rao and G. Murali Dhar (Eds.), Elsevier Science, 1998, 391.
11. A.V. Kucherov and M. Shelef, *Catal. Lett.* 75, 1-2 (2001) 19.
12. A. Fritz and V. Pitchon, *Appl. Catal.* B13 (1997) 1.
13 C.C. Costa Augusto, J. Luiz, Zotin, and Arnaldo da Costa Faro Jr., *Catal. Lett.* 75, 1-2 (2001) 37.
14. A.B.P. Lever, *Inorganic Electronic Spectroscopy*, Elsevier, Amsterdam, 1968.
15. E.S. Shpiro, G.V. Antoshin, O.P. Tkachenko, S.V. Gudkov, B.V. Romanovsky, and Kh.M. Minachev, *Stud. Surf. Sci. Catal.* 18 (1984) 31.
16. K. Nakamoto, *Infrared Spectra of Inorganic and Coordination Compounds*, John Wiley, New York, 1970.
17. L.M. Engelhardt, P.C. Healy, R.M. Shephard, B.W. Skelton, and A.H. White, *Inorg. Chem.* 27 (1988) 2371.

Chapter 7

Catalytic activity of zeolite encapsulated complexes in the decomposition of hydrogen peroxide

Abstract

Hydrogen peroxide participates in a variety of chemical reactions. The activity of zeolite Y supported transition metal complexes in the decomposition of hydrogen peroxide has been studied in detail with a view to screening the catalytic activity of the complexes in oxidation reactions. The reaction was studied by measuring the volume of oxygen evolved using a gas burette. The neat complex and ion exchanged zeolite were also screened for the catalytic activity. Among the various catalysts investigated, PdYSALSC was found to be the most active catalyst, with CuYMDTC coming next. The catalytic activity was studied by varying parameters like the volume of H_2O_2, amount of catalyst, and solvent polarity. The effects of the addition of pyridine and the use of recycled catalysts were also studied.

7.1. Introduction

Zeolite encapsulated complexes are known to exhibit similar/ better catalytic behaviour compared to homogeneous complex catalysts. The study of catalysis by encapsulated complexes started with the heterogenization of the complexes of known catalytic activity in solution. In the encapsulated state it is possible to obtain catalytically active centres that are unusual for complexes in solution. The chief advantage of encapsulated complexes is the ease in separation from the reaction mixture, which reduces cost of recovery. Hydrogen peroxide is industrially and chemically important because of its use in a variety of processes [1-3]. The decomposition of hydrogen peroxide represented by the reaction

$$2\,H_2O_2 \rightarrow 2\,H_2O + O_2$$

is considered a standard reaction to determine the catalytic activity of metal complexes [4]. The above reaction can be catalyzed by several transition metal ions and transition metal complexes, provided the coordination sphere is accessible to the H_2O_2 or HOO^- ion [5-6]. The efficiency of such systems depends to a large extent on the structural and electronic properties of encapsulated complexes. The zeolite support plays an important role in the dispersion of metal complex and in increasing the stability of the catalyst in addition to influencing catalytic properties. Considering the significance of oxidation reactions using hydrogen peroxide as oxidant for the synthesis of fine chemicals, pharmaceuticals, speciality products and so on, it was thought important to study the decomposition of hydrogen peroxide using the different encapsulated complexes.

7.2. Experimental

7.2.1. Materials

Zeolite encapsulated complexes of SPO, SPP, SALSC, SB, DTC and DMG were used for catalytic studies. The encapsulated complexes were prepared according to the procedures reported in Chapters 3, 4, 5, and 6. Neat complexes of

most catalytically active encapsulated complexes were also prepared according to reported procedures for comparison of the catalytic activity. The various reagents used are mentioned in Chapter 2.

7.2.2. Procedure for the decomposition of hydrogen peroxide

All the catalysts were activated by heating to 120 °C for two hours. A plastic float containing the sample catalyst was placed over hydrogen peroxide taken in a reaction flask of 50ml capacity containing a magnetic paddle for stirring. The quantities of different reagents used are specified in each table. A gas burette was used for collecting the oxygen evolved. The gas burette was filled with 20 % NaCl solution acidified with dilute hydrochloric acid and coloured using methyl red. The solution levels in both arms of the gas burette were equalised at zero before sealing the reaction flask. The magnetic stirrer was switched on, starting a stopwatch simultaneously. The catalyst was dispersed in hydrogen peroxide solution by magnetic stirring. As the reaction proceeded, oxygen was liberated and it got collected in the right arm of the gas burette. The volume of oxygen liberated was noted after equalizing the solution levels in both arms at intervals of 5 minutes. The experiment was continued for 30 minutes/until 10ml of gas was collected in the burette. The reaction was carried out under different conditions. The conditions specific to each test are given along the results. The catalyst was washed with acetone and heated at 120 °C for 2 hours and reused.

7.3. Results

7.3.1. Screening studies

A comparison of the catalytic activities of SALSC, DTC, SB, SPO, SPP and DMG encapsulated complexes in the decomposition of 30 %(w/v) H_2O_2 at

Table 7.1 A comparison of the catalytic activity of various solid catalysts in the decomposition of 30% (w/v) H_2O_2 at room temperature

	Volume of oxygen evolved (ml)					
	SALSC	MDTC	SB	SPO	SPP	DMG
FeY	-	0.1	-	0.1	0.1	-
CoY	0.2	0.3	-	0.6	0.2	-
NiY	0.15	0.2	-	0.15	0.1	-
CuY	0.9	4.1	1.2	0.6	0.3	-
PdY	9	0.9	-	-	-	0.1

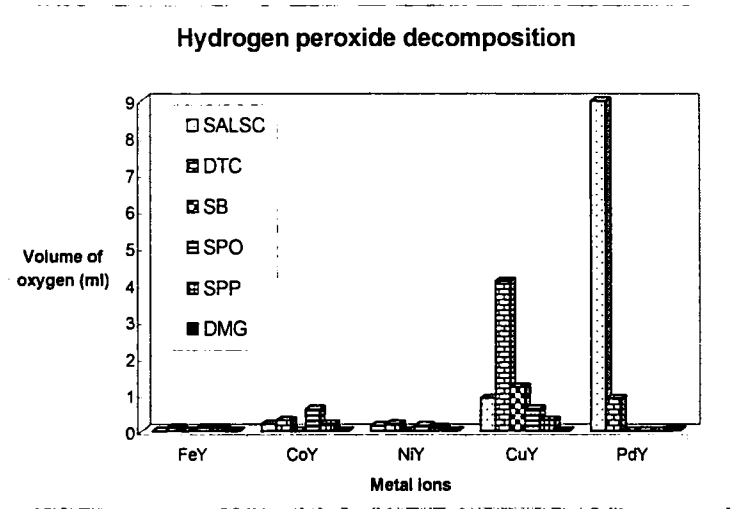

Figure 7.1 Volume of oxygen liberated using different catalysts

Reaction condition

Weight of catalyst : 10 mg
Temperature : 30 °C
Duration : 30 min

Vol. of 30% H_2O_2 : 10 ml
Vol. of H_2O : 10 ml

Table 7.2 A comparison of the catalytic activities of PdYSALSC, CuYMDTC, and CuYSB for H_2O_2 decomposition

Time (min)	Volume of O_2 liberated (ml)		
	PdYSALSC	CuYMDTC	CuYSB
0	0.1	0.1	0.1
5	1	0.5	0.15
10	2.5	1.1	0.25
15	4.45	1.7	0.5
20	6.55	2.5	0.65
25	9.0	3.2	0.95
30	—	4.1	1.2

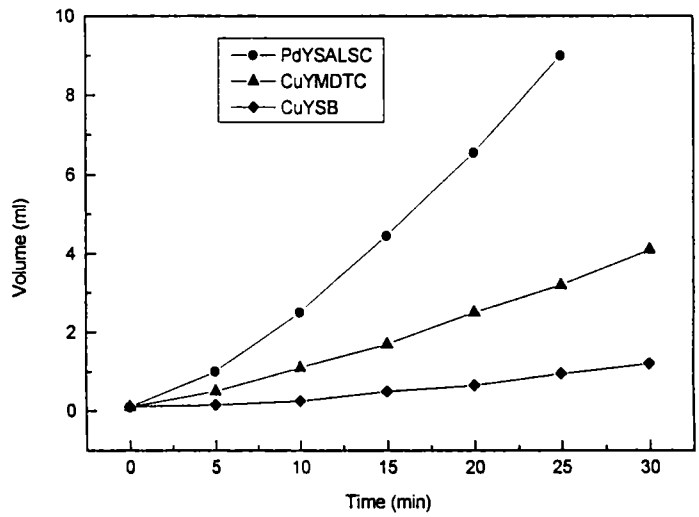

Figure 7.2 Volume of oxygen evolved versus time

Reaction condition

Weight of catalyst : 10 mg
Temperature : 30 °C
Duration : 30 min

Vol. of 30% H_2O_2 : 10 ml
Vol. of H_2O : 10 ml

room temperature is given in Table 7.1. A bar chart diagram drawn with the volume of oxygen liberated against the different complexes is shown in Figure 7.1. The reaction was continued for 30 minutes or until 10 ml of oxygen was evolved. Figure 7.2 shows the volume of oxygen against time for the three complexes PdYSALSC, CuYMDTC and CuYSB; and Table 7.2 gives a comparison of the catalytic activities of PdYSALSC, CuYMDTC and CuYSB for hydrogen peroxide decomposition. The decomposition data show that PdYSALSC is the most active catalyst. CuYMDTC is found to be moderately active, while CuYSB is weakly active. There is only minor difference in the activities of CuYSALSC, PdYMDTC and CuYSPO. The catalytic activity of PdYMDTC is significantly less than that of PdYSALSC even though the metal ions are the same. The activity of CuYMDTC is much higher compared to that of CuYSB. This shows that catalysis greatly depends on the type of chelating ligand employed [7].

7.3.2. Blank run

The decomposition reaction was studied under conditions identical with those of screening experiments, but without adding the catalysts. There was no measurable decomposition of hydrogen peroxide for up to 30 minutes. The decomposition reaction was further studied using various metal exchanged zeolites under conditions identical to those of the above-mentioned blank. The volume of oxygen liberated with each metal exchanged zeolite is shown in Table 7.3. Figure 7.3 is a plot of volume of oxygen liberated for the different metal exchanged zeolites. Of all the metal exchanged zeolites, PdY showed maximum activity. But this was low compared with the volume of oxygen liberated using PdYSALSC. The catalytic activity of PdYSALSC was approximately five times greater than the activity of PdY. The volume of oxygen liberated with other metal exchanged zeolites was negligibly low.

Table. 7.3 Comparison of the catalytic activity of various ion exchanged zeolites in the decomposition of 30 % H_2O_2 at room temperature

Metal exchanged zeolite	Volume of oxygen (ml)
FeY	0.1
CoY	0.2
NiY	0.1
CuY	0.3
PdY	2.5

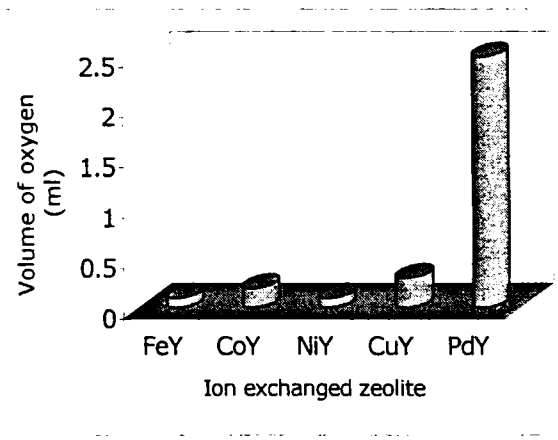

Figure 7.3 Ion exchanged zeolite versus volume of oxygen

Reaction condition

Weight of catalyst : 10 mg
Temperature : 30 °C
Duration : 30 min

Vol. of 30% H_2O_2 : 10 ml
Vol. of H_2O : 10 ml

The decomposition of hydrogen peroxide was also studied under identical conditions using neat $Cu(MDTC)_2$, Pd(SALSC)Cl and $Cu(SB)_2Cl_2$. Neat $Cu(SB)_2Cl_2$ showed no activity. Oxygen evolution occurred with neat $Cu(MDTC)_2$ and neat Pd(SALSC)Cl. But the activity observed with neat $Cu(MDTC)_2$ and neat Pd(SALSC)Cl was very small compared to that shown by encapsulated complexes.

7.3.3. Factors influencing the decomposition of hydrogen peroxide

In order to understand the catalytic nature of PdYSALSC, CuYMDTC and CuYSB on the decomposition of hydrogen peroxide, the various factors which influence the decomposition of H_2O_2 were studied. The factors studied were:

- volume of H_2O_2
- amount of catalyst
- solvent polarity of the reacting solute
- addition of pyridine
- addition of alkali
- using recycled catalysts

7.3.3.1. Influence of the volume of hydrogen peroxide

The effect of H_2O_2/H_2O volume ratio on the decomposition of H_2O_2 with PdYSALSC, CuYMDTC, and CuYSB was studied. The results are given in Table 7.4. The total volume of the mixture of H_2O_2 and water was kept constant. The reaction conditions were identical to those in the earlier cases. The effect was studied by varying the amount of hydrogen peroxide. It was found that the volume of oxygen evolved also increased with the increase in the volume of H_2O_2. The same effect was observed in all the three cases.

Table 7.4 Effect of H_2O_2/H_2O volume ratios on the decomposition of H_2O_2 with PdYSALSC, CuYMDTC, and CuYSB as catalysts

H_2O_2/H_2O (ml)	Volume of oxygen (ml)		
	PdYSALSC	CuYMDTC	CuYSB
5:15	7.2	—	—
10:10	9	3.2	0.95
15:5	9	4.15	2.1
20:0	—	6	2.75

Reaction condition

Weight of catalyst: 10 mg
Temperature : 30 °C
Duration : 25 min

7.3.3.2. Influence of the amount of catalyst

The effect of varying the amount of catalyst was studied in the case of PdYSALSC, CuYMDTC, and CuYSB. The mass of the catalyst was varied from 5 mg to 15 mg. The proportion of the mixture of H_2O_2 and H_2O is kept constant at 10 ml: 10 ml. The reaction was carried out under identical conditions as that of the screening test. The oxygen evolution increased with increase in the amount of the catalyst in the case of PdYSALSC and CuYMDTC. The results are given in Table 7.5, and Figure7.4 shows the volume of oxygen evolved with amount of catalyst.

Table 7.5 Effect of variation in the amount of catalyst on the decomposition of H_2O_2

Weight of Catalyst (mg)	Volume of oxygen (ml)		
	PdYSALSC	CuYMDTC	CuYSB
5	3.2	1.8	0.4
10	6.7	2.5	0.7
15	10.0	4.0	0.7

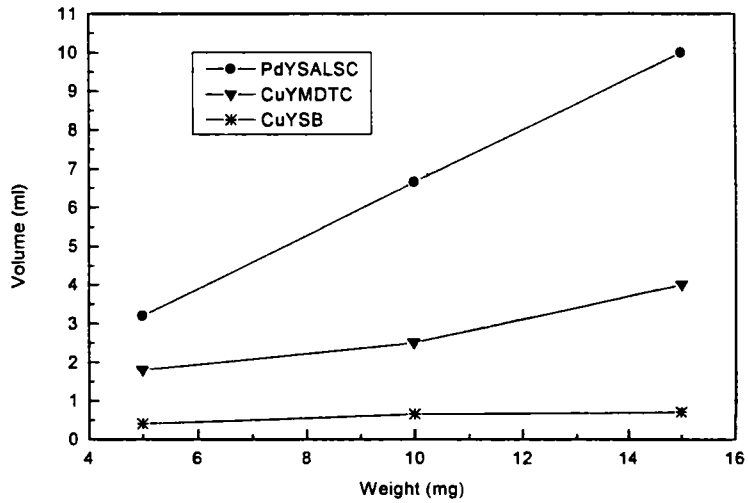

Figure 7.4 Amount of catalyst versus volume of oxygen

Reaction condition

Temperature : 30 °C
Duration : 20 min
Volume of 30% H_2O_2 : 10ml
Volume of H_2O : 10 ml

7.3.3.3. Influence of solvent polarity of the reaction solution

The effect of the solvent polarity of the reaction solution was studied. The reaction was studied by adding methanol to the reaction mixture (by changing the volume of water and methanol in such a manner as to keep the total volume constant). The dielectric constant of the medium was calculated assuming a linear relationship between the individual dielectric constants and the composition of the solvent. Thus if ε is the resultant dielectric constant, ε_1 and ε_2 the dielectric constants of water and methanol, and V_1 and V_2 their volumes employed respectively, ε may be given as

$$\varepsilon = \frac{\varepsilon_1 V_1 + \varepsilon_2 V_2}{V}$$

where V is the total volume of the reaction mixture.

The values of ε_1 and ε_2 are 78.54 and 32.63 respectively. The results obtained in the case of PdYSALSC is given in Table7.6, with CuYMDTC in Table 7.7 and CuYSB in Table 7.8. Decomposition of hydrogen peroxide was found to be slowed by the addition of methanol in all the three cases.

Table 7.6 Effect of solvent polarity on the reaction solution with PdYSALSC

H_2O: CH_3OH (ml)	Volume of oxygen (ml)
10: 0	9
9: 1	6.9
8: 2	5.5

Reaction condition

Weight of Catalyst: 10 mg
Temperature : 30 °C
Volume of H_2O_2 : 10 ml
Time : 25 min

Table 7.7 Effect of the solvent polarity on the reaction solution with CuYMDTC

H_2O: CH_3OH (ml)	Volume of oxygen (ml)
10: 0	4.1
9: 1	0.5
8: 2	0.3

Reaction condition

Weight of catalyst : 10 mg
Temperature : 30 °C
Volume of H_2O_2 : 10 ml
Time : 30 min

Table 7.8 Effect of the solvent polarity on the reaction solution with CuYSB

H_2O: CH_3OH (ml)	Volume of oxygen (ml)
10: 0	1.2
9: 1	1.2
8: 2	0.9

Reaction condition

Weight of catalyst: 10 mg
Temperature : 30 °C
Volume of H_2O_2 : 10 ml
Time : 30 min

7.3.4. Addition of pyridine

The effect of adding traces (two drops) of pyridine to the reaction mixture was studied in the case of PdYSALSC and CuYMDTC. The experiment was conducted in two ways.

i) By adding pyridine to the catalyst before adding hydrogen peroxide to it. No decomposition of hydrogen peroxide was observed.

ii) By adding the catalyst to the mixture of hydrogen peroxide and water and then adding pyridine. Instead of deactivating the effect there was an increase in the decomposition rate.

The results are presented in Tables 7.9 and 7.10.

Table 7.9 Effect of adding traces of pyridine on using PdYSALSC catalyst

Time (min)	Volume of oxygen (ml)
0	0.1
5.0	3.0
10	9.7

Reaction condition

Temperature : 30 °C
Volume of H_2O_2 : 10 ml
Volume of H_2O : 10 ml
Amount of pyridine: 2 drops

Table 7.10 Effect of adding traces of pyridine on using CuYMDTC catalyst

Time (min)	Volume of oxygen (ml)
0	0
5	1.7
10	3.45
15	5.05
20	6.7
25	7.3

Reaction condition
Temperature : 30 °C
Volume of H_2O_2 : 10 ml
Volume of H_2O : 10 ml
Amount of pyridine: 2 drops

7.3.5. Recycled catalysts

The catalysts once used were washed with acetone, and dried in oven at 120 °C for two hours. The recycled catalyst was characterized using XRD, IR, and electronic spectroscopy.

The XRD patterns of the recycled catalysts were similar to those of fresh catalysts. This showed that the crystalline structure was retained even after the regeneration process. The IR of the recycled sample resembled that of the fresh sample. From this it was inferred that the complex remains unaffected in the cages of zeolite Y. The electronic spectra of the used sample were similar to those of the fresh sample, showing that there is no change in the structure even after recycling.

Table 7.11 Effect of using recycled catalyst on the decomposition on H_2O_2

Time (min)	Volume of oxygen evolved (ml)		
	CuYSB	CuYMDTC	PdYSALSC
0	0.1	0.1	0.1
5	0.1	0.3	0.3
10	0.3	0.7	1.0
15	0.5	1.2	1.7
20	0.7	1.8	2.6
25	0.9	2.4	3.5
30	1.2	3.1	4.8

Reaction condition

Temperature : 30 °C
Volume of H_2O_2 : 10 ml
Volume of H_2O :10 ml
Weight of catalyst:10 mg

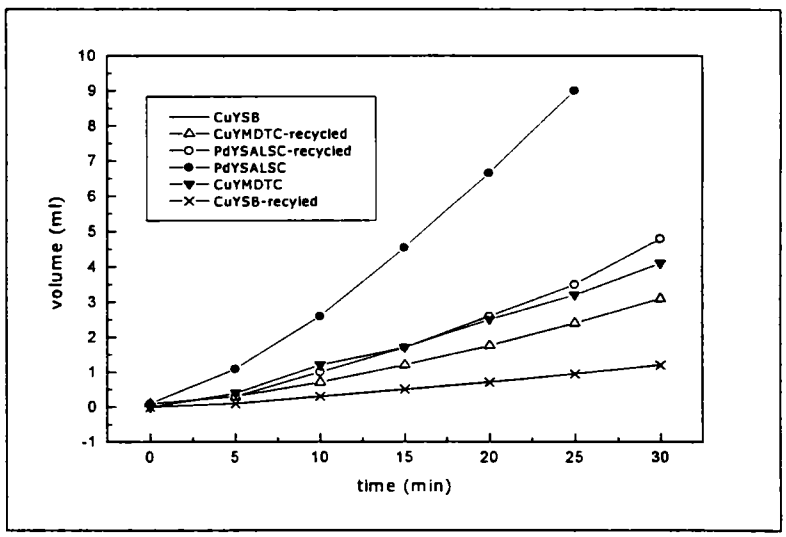

Figure 7.5 Comparison of activity on using recycled catalyst and unused catalyst in the decomposition of H_2O_2

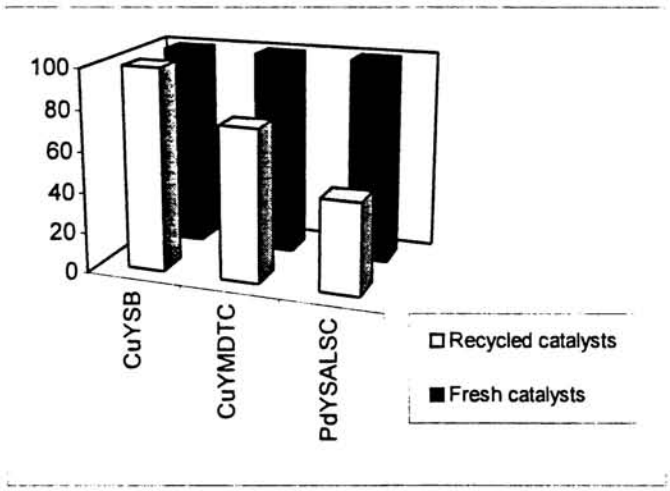

Figure 7.6 Comparison of the retained activity and loss in activity of the three catalysts

The electronic spectra of the used sample were similar to that of the fresh sample, showing that there is no change in the structure even after recycling. The reaction mixture after the first cycle was filtered to remove the catalyst. The resulting solution was analyzed for metal content using atomic absorption spectroscopy. The absence of metal ions in the reaction medium indicated that there was no leaching out of the metal ions from the pores of the zeolite. This again proved that the complexes were intact within the cages. The reaction was carried out under identical conditions using recycled PdYSALSC, CuYMDTC, and CuYSB. The results obtained are tabulated in Table 7.11 and presented graphically in Figure 7.5 and Figure 7.6. In the case of CuYSB the activity of the recycled catalyst was the same as that of the unused catalyst, as shown in Figure 7.6. Recycled CuYMDTC showed ~ 75% activity as compared to the fresh sample. The most deactivated was the highly catalytic PdYSALSC.

7.4. Discussion

The decomposition of hydrogen peroxide was studied both using catalysts and without using catalysts. Of the catalyzed reactions, those with encapsulated complexes showed much higher activity compared to those with neat complexes and ion exchanged zeolites. PdYSALSC was found to have a five times greater activity than PdY at the same pH and other conditions. The activity of other ion exchanged zeolites was negligible compared to that of encapsulated complexes. The activity shown by neat complexes was also negligible compared to that of encapsulated complexes. Though the encapsulated complex shows the general characteristics of homogeneous catalysts, it also has the merits of heterogeneous systems.

Many possible mechanisms have been proposed for the decomposition of hydrogen peroxide. All these mechanisms involve the oxidation or reduction of the substrate, i.e., the decomposition is facilitated by a redox cycle between the oxidation states of the metal. One mechanism which can be applied in the case of zeolite encapsulated complexes can be as follows:

$$2H_2O_2 \rightarrow 2HOO^- + 2H^+ \qquad \text{Eq. VII.1}$$

$$2(LM)^{n+} + 2HOO^- \rightarrow 2(LM)^{(n-1)+} + 2HOO\cdot \qquad \text{Eq. VII.2}$$

$$2HOO \rightarrow O_2 + H_2O_2 \qquad \text{Eq. VII.3}$$

$$2(LM)^{(n-1)+} + H_2O_2 \rightarrow 2(LM)^{n+} + 2OH^- \qquad \text{Eq. VII.4}$$

Combining Eq.VII.2 and Eq. VII.4 and cancelling the catalyst term will give

$$2HOO^- + H_2O_2 \rightarrow 2HOO\cdot + 2OH^- \qquad \text{Eq. VII.5}$$

The redox potential of the active metal plays a vital role in the decomposition of hydrogen peroxide because the catalytic activity of the metal ion depends on its redox potential. The complex will have a modified potential, which will increase the catalytic activity.

In another mechanism proposed, the decomposition reaction occurs in the coordination sphere of the metal ion. This involves the formation of an

intermediate peroxo species. The following pathway may be suggested for this mechanism:

$(LM)^{n+} + H_2O_2 \rightarrow (LMH_2O_2)^{n+}$ Eq. VII.6

$(LMH_2O_2)^{n+} \rightarrow LM(HOO)^{(n-1)+} + H^+$ Eq. VII.7

$LM(HOO)^{(n-1)+} + H_2O_2 \rightarrow LM(HOO)(H_2O_2)^{(n-1)+}$ Eq. VII.8

$LM(HOO)(H_2O_2)^{(n-1)+} \rightarrow (LM)^{n+} + O_2 + H_2O + OH^-$ Eq. VII.9

The peroxo intermediate can also be formed by the action of HOO^- generated from the free H_2O_2 molecules in solution.

$H_2O_2 \rightarrow H^+ + HOO^-$ Eq. VII.10

$(LM)^{n+} + HOO^- \rightarrow LM(HOO)^{(n-1)+}$ Eq. VII.11

According to Sharma and Schubert, the peroxide entity in the transition state in Eq. VII.7 can become highly reactive [8]. The accessibility of the coordination sphere for H_2O_2 or HOO^- and the availability of at least two free vacant coordination sites at the metal ion are the main requirements for the decomposition to proceed via this mechanism.

Helmut Sigel has found that the decomposition rate is high with copper polyammine chelates with vacant coordination sites whereas it is low when the copper complexes are fully coordinated [9]. According to Sharma et al., complexes having less than two free sites on the metal ion are inactive [8]. This observation can be related to the bidentate nature of peroxide anion or to the fact that the remaining free positions on the intermediate will facilitate its reactions with the second peroxide anion.

Decomposition data show that the encapsulated Pd(II) and Cu(II) complexes are very active in the decomposition of hydrogen peroxide. These two complexes have square planar structure. This provides vacant coordination sites and facilitates the formation of peroxo intermediates which are highly reactive species leading to the rapid decomposition of hydrogen peroxide. The mechanism involving peroxo intermediate seems to be applicable in the case of encapsulated Pd and Cu complexes, as these complexes showed a colour change on coming in

contact with hydrogen peroxide. This colour change is indicative of the formation of intermediate peroxo species. Similar colour change has been found in the case of Cu(II) complexes by earlier workers [10].

A steady increase in pH occurs during the decomposition of hydrogen peroxide, confirming the liberation of OH^- ions as suggested by the above mechanism. Such an increase in pH has been reported by earlier experimenters [11].

The catalytic activities were found to be modified to a considerable extent by ligands [12]. The effect of the ligands on the catalytic activity of the complexes has been pointed out by Sharma and Schubert [8]. They have pointed out that the reduction of Cu(II) coordinated to two nitrogen atoms is much faster than that of aquo cupric ion. Wang suggests that the enhancement in catalytic activity is due to the strain around the metal ion catalyst provoked by the ligand molecules [13]. Sharma and Schubert have pointed out that there is a trend towards higher catalytic activity on increasing the ring size of the chelate [8]. This is in agreement with the observation in the present study that SALSC complexes with six membered and five membered rings exhibit maximum activity, and MDTC with two 4-membered rings chelates with medium activity and SB without chelation has the lowest activity. The higher activity of the 6-membered ring chelate can be related to the greater ease with which it can remain coordinated to the metal ion during its reversible oxidation – reduction [8].

The catalytic activity of the encapsulated Pd(II) and Cu(II) complexes were much higher compared to that of the corresponding neat complexes. According to one earlier report there is no significant difference in the kinetics of reactions using supported catalyst and non-supported catalyst except in the enhancement of rate [14]. This very much agrees with what we have found in our study. The encapsulated systems were found to be much more active compared to neat complexes. Enhanced activity with supported catalyst has been reported by Wilson

[15]. The enhanced activity of the supported system can be due to the formation of a modified catalyst precursor involved in the rate-determining step [14], or due to the greater stability of the encapsulated complex compared to the neat complex.

The decomposition reaction was studied by varying the volume of hydrogen peroxide. The volume of oxygen evolved increased with the volume of hydrogen peroxide. The rate of decomposition increased with the amount of the catalyst in the case of PdYSALSC and CuYMDTC. Such an observation was made by earlier workers [7,16]. This effect was negligible in the case of CuYSB.

The addition of methanol was found to slow down the decomposition reaction. This was observed with all the three catalysts. Since methanol is of lower polarity than water, the decrease in reaction rate observed here must be because of the decease in polarity.

The rate of a reaction is given by the equation

$$\ln k = \ln k_o - \frac{Z_A Z_B e^2}{\varepsilon d_{AB} kT}$$

where:

k	– rate constant
$\mathbf{k_o}$	– rate constant in a solvent of infinite dielectric constant
Z_Ae, Z_Be	– charges of the reactive species in the transition state respectively
ε	– dielectric constant of the solvent
d_{AB}	– diameter of the activated complex
k	– Boltzmann's constant
T	– absolute temperature

From the equation it is clear that the reactive species participating in the formation of the transition state are either both positively charged or both negatively charged for ln**k** to decrease. Pure complex is positively charged, and H_2O_2 and O_2 are neutral species. As there is a possibility of H_2O_2 getting ionised

to $H^+ + HOO^-$, it might be the HOO^- species that would be reacting with the complex catalyst. The solvent effect studies indicate that the complex also might be acting as a negative species, which can be formed inside the zeolite cavity due to interaction with oxide ions of the lattice. Since the spectral indication is square planar, the matrix can be distantly coordinated to the metal ion.

The addition of pyridine to the catalyst gave different results. The experiment with the direct addition of pyridine to the catalyst before adding hydrogen peroxide produced no decomposition of hydrogen peroxide. This can be because the pyridine complex formed is less reactive than the original complex. The experiment with the addition of catalysts to the mixture of hydrogen peroxide and water followed by the addition of pyridine showed very high rate of decomposition. This can be because pyridine acts as a base and decomposes hydrogen peroxide as per the equation

$$H_2O_2 \rightarrow H^+ + HOO^-$$

HOO^- ion is a better reactant than H_2O_2 . The acceleration observed in the present reaction can be due to the increased concentration of the HO_2^- ion. It has also been reported that alkalinity has a strong influence on the activity of heavy metal catalyzing species in the decomposition of hydrogen peroxide [17].

Recycled PdYSALSC and CuYMDTC showed less activity compared to fresh catalyst. CuYSB showed no deactivation at all.

References

1. S. Tamagaki, M. Sasaki, and W. Tagaki, *Bull. Chem. Soc. Jpn.* 62 (1989) 153.
2. J.H. Buxendak, *Adv. Catal.* 4 (1952) 39.
3. H.M. Cota, T. Katan, M. Chin, and F.J. Schoenweis, *Nature*, 203 (1964) 1281.
4. R. Sreekala and K.K. Mohammed Yusuff, *Ind. J. Chem.*, 34A (1995) 994.
5. H. Sigel, *Angew. Chem.* 81 (1969) 161.
6. H. Sigel, *Angew. Chem., Int. Ed. Engl.* 8 (1969) 167.
7. Isao Mochida, Akio Kato, and Tetsuro Suiyama, *Bull. Chem. Soc. Jpn.* 45 (1972) 2230.
8. V.S. Sharma and J. Schubert, *Inorg. Chem.* 10, 2 (1971) 251.
9. Helmut Sigel, Kurt Wyss, Beda E. Fischer, and Bernhard Prijs, *Inorg. Chem.* 18, 5 (1979) 1354.
10. R.V. Prasad and N.V. Thakkar, *Ind. J. Chem.* 33A (1994) 861.
11. Beena Pandit and Uma Chadusama, in *Recent Advances in Basic and Applied Aspects of Industrial Catalysis* (*Studies in Surface Science and Catalysis 113*), T.S.R. Prasada Rao and G. Murali Dhar (Eds.), Elsevier Science, 1998, 865.
12. Isao Mochida and Kenjiro Takeshita, *J. Phys. Chem.* 78,16 (1974) 1654.
13. J.H. Wang, *Account Chem. Res.* 3 (1970) 90.
14. Jubaraj B. Baruah and Lipika Nath, *Ind. J. Chem.* 36A (1997) 795.
15. R.G. Wilkins, *The Study of the Kinetics and Mechanisn of Reactions of Transition Metal complexes*, Allyn and Bacon, Boston, 1974.
16. Susanta K. Sengupta and Preeti Lahiri, *Ind. J. Technol.* 30 (1992) 172.
17. O. Spalek, J. Balez, and I. Ponseka, *J. Chem. Soc. Faraday Trans.* 1, 78 (1982) 2349.

Chapter 8

Hydroxylation of phenol to hydroquinone using zeolite encapsulated complexes

Abstract

Hydroxylation of phenol is a reaction that has great commercial importance. Phenol hydroxylation was carried out at room temperature using H_2O_2 as oxidant. Encapsulated Cu(II) complexes of morpholine–*N*–carbodithioate and salicylaldehydesemicarbazone were found to be very effective for the selective oxidation of phenol. The reaction products were analyzed using gas chromatograph. Due to size and shape selective effects, hydroquinone was obtained as the only product. Influence of various parameters like reaction time, amount of catalyst, oxidant/substrate ratio, solvent, and temperature were studied. Poison resistance and recyclability were also checked. The complexes get deactivated by the addition of poison, and exhibit some loss in activity on recycling.

8.1. Introduction

Organic synthesis today emphasizes on achieving selectivity of products. Weisz and coworkers were among the first to report shape selective catalysis using zeolite [1-3]. According to Weisz, the unique role and purpose of a catalyst is to provide selectivity to direct chemical transformation along a specific, desired path. Since these pioneering studies, shape selective catalysis has made great strides, and has led to the development of many new industrial processes.

The catalytic activity shown by the encapsulated complexes can be correlated to the well-defined structure of the active site inside the zeolite pore. Now attempts are being made by researchers to develop new zeolite compounds that mimic biological enzymes. These so called "zeozymes" are constructed by trapping various metal complexes inside the crystalline framework of zeolites [4]. The unique feature of these zeozymes is that the catalyst remains in the solid phase during the entire reaction and can be easily filtered off at the end of the reaction. This aspect is significant, as it would reduce processing cost during large-scale application.

In the present study, zeolite encapsulated complexes of SPO, SPP, SALSC, SB, DTC and DMG have been used for the oxidation of phenol with hydrogen peroxide with the main aim of obtaining the *p*-isomer as the only product. The results of these studies are presented in this chapter.

8. 2. Experimental

8.2.1. Materials

The details of the materials used for the catalytic study are given in Chapter 2. Zeolite encapsulated complexes of SPO, SPP, SALSC, SB, DTC and DMG were used for catalytic studies. Their neat analogues were also prepared and used

in catalytic studies to enable a comparison between neat and encapsulated complexes.

8.2.2. Procedure for the hydroxylation of phenol

The hydroxylation of phenol was carried out in a 50 ml round bottomed flask fitted with a reflux condenser. Phenol, catalyst, and water were introduced into the reaction vessel and the reaction was initiated by adding hydrogen peroxide. The mixture was stirred for a definite period of time using a magnetic stirrer and a magnetic paddle at the set temperature. The reaction conditions are given in the tables for each experiment. The catalyst was removed by filtration and the analysis of the reaction product for hydroquinone was done using a gas chromatograph. An SE-30 column was used for separating various components in the reaction mixture. The components can be differentiated from the peaks that appear on the recorder. The concentration of the component in the mixture was determined from the peak area for that component.

The reaction was carried out under different conditions for testing the influence of various parameters like time, amount of catalyst, oxidant/substrate ratio, solvent and temperature. The recyclability of the catalyst and the poison resistance were also studied.

8.3. Results

8.3.1. Screening studies

The data of the catalytic activity of SALSC, DTC, SPP, SPO, DMG and SB encapsulated complexes in the hydroxylation of phenol using dilute hydrogen peroxide as oxidant at room temperature is given in Table 8.1. A graph showing percentage conversion of phenol to hydroquinone for the different

Table 8. 1 Conversion of phenol to hydroquinone

	% Conversion					
	SALSC	MDTC	SPP	SPO	DMG	SB
FeY	–	0.2	0	0	–	–
CoY	3	4	1	1	–	–
NiY	1	2	1	0.5	–	–
CuY	97	99	2	0	–	0.5
PdY	1	2	–	–	0.5	–

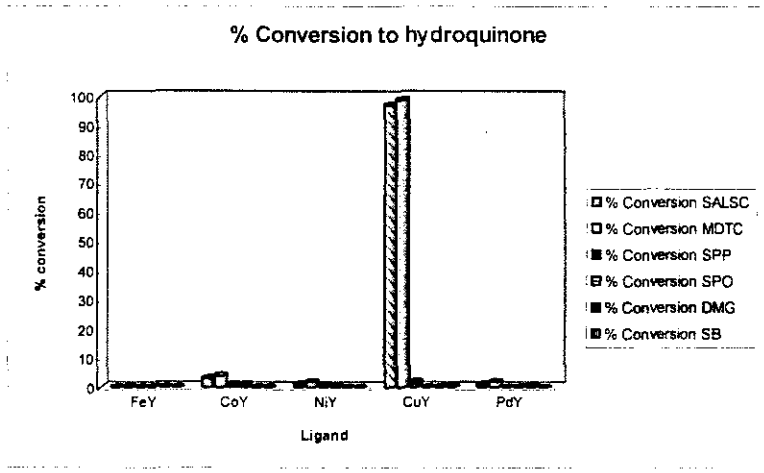

Figure 8.1 Conversion of phenol to hydroquinone

Reaction condition

Volume of phenol	: 1 ml
Duration	:4 h
Temperature	:30 °C
Weight of catalyst	:40 mg
Volume of H_2O_2	:5 ml
Volume of solvent (H_2O)	:5 ml

complexes is shown in Figure 8.1. From the table it is clear that the maximum conversion to hydroquinone was obtained in the case of CuYMDTC, with CuYSALSC coming next. Water was used as a solvent in all the reactions.

8.3.2. Blank run

The hydroxylation of phenol was carried out using CuY under conditions identical to those of the screening experiments. It was found that the only product formed was catechol, and no hydroquinone was formed. Experiments were also carried out using neat complexes of MDTC and SALSC [{$Cu(MDTC)_2$} and CuClSALSC]. Tarry products were obtained which could not be identified. The reaction was repeated under identical conditions without adding catalyst. No catechol or hydroquinone was found to be formed in this case.

8.3.3. Factors influencing the hydroxylation of phenol to form hydroquinone

CuYSALSC and CuYMDTC were found to be very effective for the hydroxylation of phenol to hydroquinone. So further studies were made using CuYSALSC and CuYMDTC and varying the following parameters to understand the factors influencing the hydroxylation of phenol:

i) reaction time
ii) amount of catalyst
iii) H_2O_2 - phenol ratio
iv) solvents
v) reaction temperature.

8.3.3.1. Influence of reaction time

The reaction was carried out for different durations varying from one hour to six hours, using CuYMDTC and CuYSALSC, and the resulting products were analyzed.

Table 8.2 Effect of reaction time on conversion of phenol to hydroquinone

Duration	CuYSALSC		CuYMDTC	
(h)	% Conversion	% Hydroquinone	% Conversion	% Hydroquinone
1	1	0	10	5
2	64	30	99	98
3	85	77	99	98
4	95	92	99	99
5	99	99	99	tar formed

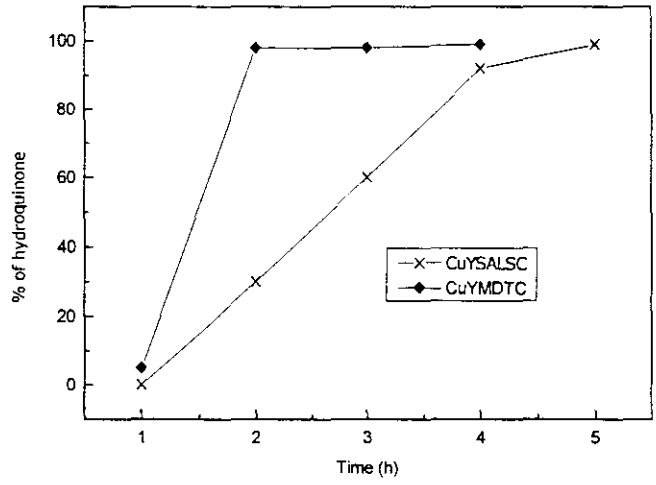

Figure 8. 2 Effect of reaction time on conversion of phenol to hydroquinone

Reaction condition

Volume of phenol :1 ml
Volume of H_2O_2 :5 ml
Volume of solvent (H_2O) :5 ml
Weight of catalysts :50 mg
Temperature :30 °C

The percentage conversion to hydroquinone is given in Table 7. 2, and the graph showing the percentage of hydroquinone formed with time is presented in Figure 7.2. The percentage conversion of phenol to hydroquinone increased with time. After one hour there was a sharp increase in the percentage conversion of phenol.

In the case of CuYMDTC, 99 % conversion with 100 % selectivity was obtained within two hours. The reaction was continued for five hours and the products were analyzed at the end of each hour. Tarry products were obtained at the end of 5 hours. The darkening of the solution with time indicates tar formation. CuYSALSC took 5 hours for 99 % conversion with 100 % selectivity. Tarry products were formed after 5 hours. The optimum time for the reaction using CuYMDTC was taken as 2 hours, and for the reaction using CuYSALSC it was taken as 5 hours. After an optimum time of reaction, only tarry products are formed.

8.3.3.2. Influence of the amount of catalyst

The progress of the reaction was studied by varying the amount of catalyst from 20 mg to 50mg. The results are presented in Table 8.3, and Figure 8. 3 give the percentage conversion of phenol to hydroquinone against varying amounts of catalyst. It can be seen that the percentage conversion to hydroquinone increases with increase in the amount of the catalyst. In the case of CuYMDTC, the maximum conversion was obtained with 30 mg of catalyst while in the case of CuYSALSC maximum conversion with 100 % selectivity was reached with 40 mg of catalyst. Further increase in the weight of the catalyst had no effect on the oxidation of phenol to hydroquinone.

Table 8.3 Effect of the amount of the catalyst on the conversion of phenol to hydroquinone

Weight of catalyst (mg)	CuYSALSC		CuYMDTC	
	% Conversion	% Hydroquinone	% Conversion	% Hydroquinone
20	4	0	50	55
30	33	31	99	99
40	99	99	99	99
50	99	99	99	99

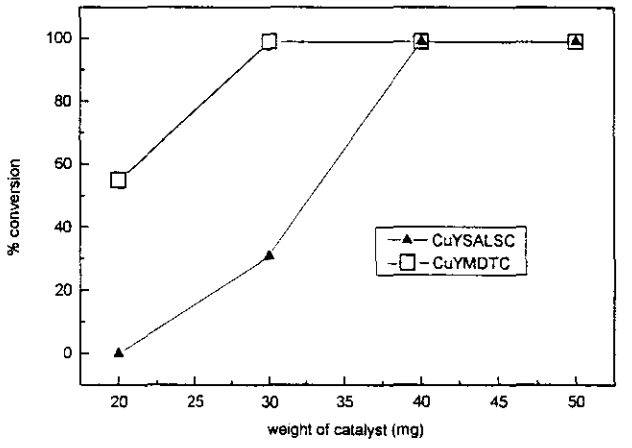

Figure 8.3 Effect of the amount of the catalyst on the conversion of phenol to hydroquinone

Reaction condition

Volume of phenol :1 ml
Volume of H_2O_2 :5 ml
Volume of solvent (H_2O) :5 ml
Temperature :30 °C
Duration
CuYSALSC : 5 h
CuYMDTC : 2 h

8.3.3.3. Influence of H_2O_2 : phenol (oxidant/substrate) ratio

The reactions were carried out under identical conditions but by varying the volume of hydrogen peroxide. The results showing the dependence of percentage conversion to hydroquinone on the volume of H_2O_2 are given in Table 8.4. The reaction conditions are also given in the table. From the table it is seen that percentage conversion increases with increase in the volume of H_2O_2 {keeping the volume of phenol constant (1ml.)} to a certain point, and thereafter an increase in the volume of H_2O_2 leads to the production of tarry products.

Table 8.4 Effect of the amount of hydrogen peroxide on the conversion of phenol to hydroquinone

Volume of H_2O_2 (ml)	CuYSALSC		CuYMDTC	
	% Conversion	% Hydroquinone	% Conversion	% Hydroquinone
4	90	90	91	90
5	99	99	99	99
6	99	Tarry products	99	Tarry products

Reaction condition

Volume of phenol :1 ml
Volume of solvent (H_2O) :5 ml
Temperature :30 °C
Weight of catalyst :50 mg
Duration
CuYSALSC: 5 h
CuYMDTC : 2 h

8.3.3.4. Influence of solvents

The reaction was studied in different solvents like water, acetone, methanol and benzene under similar reaction conditions. The effect of solvents on the activity and selectivity of the catalysts is indicated in the Table 8.5.

Table 8.5 Effect of various solvents on the conversion of phenol to hydroquinone

Solvents	CuYSALSC		CuYMDTC	
	% Conversion	% Hydroquinone	% Conversion	% Hydroquinone
Methanol	99	0	99	0
Benzene	99	0	99	0
Acetone	99	0	99	0
Water	99	99	99	99

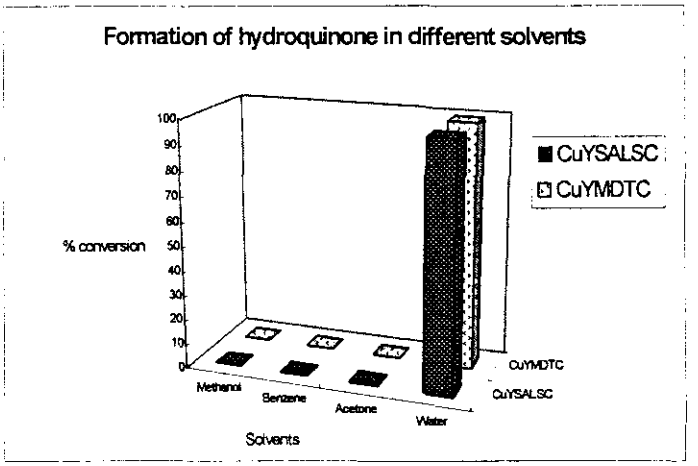

Figure 8.4 Effect of solvents on the conversion of phenol to hydroquinone

Reaction condition

Volume of phenol :1 ml
Volume of H_2O_2 :5 ml
Volume of solvent (H_2O) :5 ml

Temperature :30 °C
Weight of catalyst :50 mg
Duration
CuYSALSC : 5 h
CuYMDTC : 2 h

Water was found to be the best solvent for phenol hydroxylation with 99 % conversion and 100 % selectivity towards hydroquinone. Tarry products were formed in methanol and acetone. There was no reaction at all when benzene was used as solvent.

8.3.3.5. Influence of reaction temperature

To study the influence of temperature on the conversion of phenol to hydroquinone, the reaction was studied at three different temperatures, 30 °C, 50 °C, and 70 °C. The maximum conversion to hydroquinone was obtained at room temperature (30°C). The yield of products in many reactions depends on temperature. The results of the study are given in Table 8.6. With CuSALSC and CuYMDTC, the percentage conversion to hydroquinone decreased to 0 % as temperature was raised to 50 °C. At 70 °C, tarry products were formed with both CuYSALSC and CuYMDTC.

Table 8.6 Effect of reaction temperature on the conversion of phenol to hydroquinone

Temperature (°C)	CuYSALSC		CuYMDTC	
	% Conversion	% Hydroquinone	% Conversion	% Hydroquinone
30	99	99	99	99
50	99	0	99	0
70	99	0	99	0

Reaction condition

Volume of phenol	:1 ml	Duration:	
Volume of H_2O_2	:5 ml	CuYSALSC	:5 h
Volume of solvent (H_2O)	:5 ml	CuYMDTC	: 2 h
Weight of catalyst	:50 mg		

8.3.4. Addition of poison

The poison resistance of the catalysts was studied by adding some foreign compound to the catalyst reactant system. The effect of poison on CuYSALSC and CuYMDTC was studied by examining the activity of the catalyst in presence of traces of pyridine. The percentage loss in activity would indicate the extent of deactivation on poisoning. This was carried out in two ways:

i) by directly adding pyridine to the catalyst, and

ii) by adding pyridine after adding phenol to the catalyst.

The catalysts were completely deactivated in the first case. In the second case the two catalysts CuYSALSC and CuYMDTC were found to be resistant to the action of poison.

8.3.5. Recycled catalyst

The reaction was carried out using used catalysts. The catalyst was filtered, washed with acetone, and activated in the oven for two hours. This was to remove any impurities attached to the active sites of the catalyst. X - Ray diffraction studies of both the used catalysts (CuYMDTC and CuYSALSC) showed no loss in crystallinity. The FTIR spectra of the used and unused catalysts were similar. Catalytic runs were carried out under similar conditions using the recycled catalyst. The results obtained for CuYSALSC and CuYMDTC are shown in Figure 8.5, and the percentage conversions are given in Table 8.7. CuYSALSC showed ~ 60 % activity compared to the activity with fresh sample while CuYMDTC showed ~ 50%.

Table 8.7 Effect of recycled catalyst on the conversion of phenol to hydroquinone

Recycled catalyst	% Conversion	% Hydroquinone	% Loss in activity
CuYSALSC	60	60	40
CuYMDTC	55	51	49

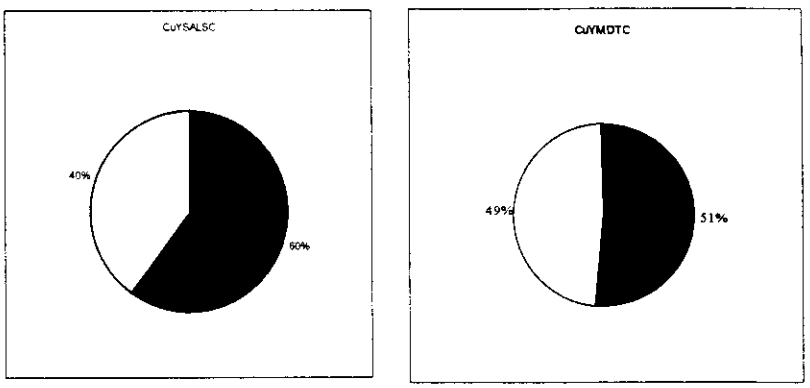

Figure 8.5 Comparison of the activity and loss in activity of recycled catalyst

Reaction condition

Volume of phenol :1 ml
Volume of H_2O_2 :5 ml
Volume of solvent (H_2O) :5 ml
Weight of catalyst :50 mg
Duration:
CuYSALSC :5 h
CuYMDTC : 2 h

8.4. Discussion

A comparison of the catalytic activity and selectivity of the zeolite encapsulated SALSC, MDTC, SPO, SPP, DMG and SB complexes reveals that CuYSALSC and CuYMDTC are the most efficient catalysts for the hydroxylation of phenol to hydroquinone. There are reports that redox zeolites act as active catalysts for hydrogen peroxide mediated oxidation reactions such as the hydroxylation of phenol to the corresponding hydroxylated aromatics [3]. This could be the result of various factors like surface area, pore volume, redox properties of metal complexes, and the electric field gradient inside the zeolite.

Phenol hydroxylation reaction can take place at the external surface as well as in the internal pores. The reaction in the internal pores leads mainly to the formation of hydroquinone whereas reaction on the external surface leads to the production of catechol as well as tarry products. The formation of hydroquinone as the only product suggests that the reaction occurs entirely inside the pores of the zeolite. This might be due to the ligand field effect, which improves the selectivity, and stability of the catalyst. Here the preferential formation of hydroquinone (para isomer) is the result of product shape selectivity. Constraints imposed on the diffusion of the products from the pores to the outside bring about enhanced para selectivity. This is indicated in Figure 8.6.

From the percentage conversion taken as a function of the reaction time for the two catalyst systems CuYSALSC and CuYMDTC, it is found that there is an optimum time for maximum hydroquinone conversion. The appearance of an induction period and the increase in the percentage conversion with time suggest the involvement of a free radical mechanism. On carrying out the reaction for a longer time, unwanted products were formed. The darkening of the solution with time indicates tar formation.

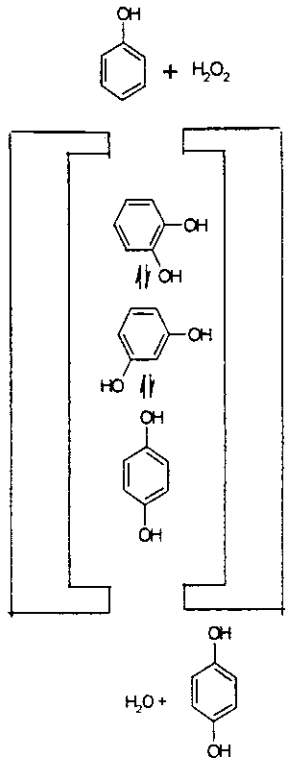

Figure 8.6 Influence of shape selectivity

The minimum amount of catalyst required for a particular reaction was also optimized. There was no effect on increasing the weight of the catalyst above a certain level.

The study of the effect of reaction temperature on hydroquinone conversion shows that the maximum yield is obtained at room temperature. As temperature increased to 50 °C, percentage conversion decreased. The reduction in the percentage conversion to hydroquinone can be due to two reasons:

i) the formation of other products resulting from the slow diffusivity at higher production ratio from the pore leading to further reaction;

ii) the decomposition of hydrogen peroxide at higher temperatures.

At 70 °C, tarry products are formed with both CuYSALSC and CuYMDTC. This can be due to the exothermic nature of the reaction or due to over oxidation or due to side reactions.

The study of the effect of solvents on the activity shows that water is the best solvent for hydroquinone conversion. This is because phenol and hydrogen peroxide can reach the active sites more easily with water than with organic solvents. It has been reported that the activity for this reaction in water is much higher than in any other solvent [5]. No hydroquinone conversion was observed with methanol and acetone. This can be due to the radical scavenging property of methanol and acetone, which removes the reactive phenol radicals. In benzene there is no conversion at all, which might be due to the insolubility of hydrogen peroxide in benzene.

The hydrogen peroxide - phenol ratio is important in deciding the activity. The maximum conversion to hydroquinone was obtained when the hydrogen peroxide - phenol volume ratio was 5. Increase in the volume of H_2O_2 beyond that results in the production of tarry products. The formation of tarry products might be due to over oxidation of phenol at high hydrogen peroxide concentration.

Both the catalysts were completely deactivated on adding pyridine. The formation of catalytically inactive complex with pyridine with no vacant coordination site might be the reason for the deactivation, which is indicated by the colour change of the complex. However, CuYSALSC and CuYMDTC showed no loss in activity on adding pyridine to the mixture of phenol and the catalysts. This again suggests the possibility of the existence of phenoxide ions, which get attached to the catalysts.

CuYSALSC and CuYMDTC can be reused after the used samples are washed and heated (to activate the catalysts by removing the by-products covering some active centres) [6]. The phenol conversion is in the range 50 - 60 % compared to that for the first run. This again confirms that the complex inside the zeolite pore is stable. The reaction of metal complexes with peroxides is important in organic synthesis since peroxides are useful forms of "active

oxygen" reagents for oxidative transformation [7]. Many possible mechanisms have been suggested for phenol hydroxylation. As zeolite encapsulated complexes are heterogenised homogeneous catalysts, the hydroxylation of phenol can be assumed to follow a heterogeneous – homogeneous reaction mechanism [8-9].

The high susceptibility of the aromatic ring of phenols towards oxidation can be due to the generation of the phenoxy radical via proton removal. The generation of phenoxy radical may occur on the catalyst surface. There have been reports of proton transfer from phenol to a potential active site prior to hydroxylation during enzyme catalysis of phenol using phenol hydroxylase.

The mechanism involving homolytic hydroxyl radical pathway and heterolytic pathway involving $H_3O_2^+$ ion is presented in Scheme I and Scheme II [10]. The first step in both the schemes involves the reaction between phenol and the complex, in which an electron is transferred to the metal ion. This results in the formation of phenoxy radical on the catalyst surface. At the same time the catalytic surface can trigger the homolytic cleavage of hydrogen peroxide, or form the very reactive species $H_3O_2^+$, the acidic sites of zeolite providing the acidity requirements for the formation of this species. The formation of catechol and hydroquinone is believed to be the result of the attack of HO· on the benzene ring or by the attack of $H_3O_2^+$.

As per the inferences from our study, the mechanism occurring in this case can be the one following Scheme II, utilizing $H_3O_2^+$. Since the catalyst support is zeolite there is strong possibility for the formation of $H_3O_2^+$. The acidity requirements for the formation of $H_3O_2^+$ may be supplied by the acid sites.

$$H_2O_2 + H^+ \leftrightharpoons H_3O_2^+$$

This is further supported by the fact that hydroquinone conversion is maximum at a very high concentration of hydrogen peroxide. The presence of acid sites of zeolite and the high concentration of hydrogen peroxide shift the above

equilibrium to the right. This explains the high conversion observed with high H_2O_2/phenol ratio.

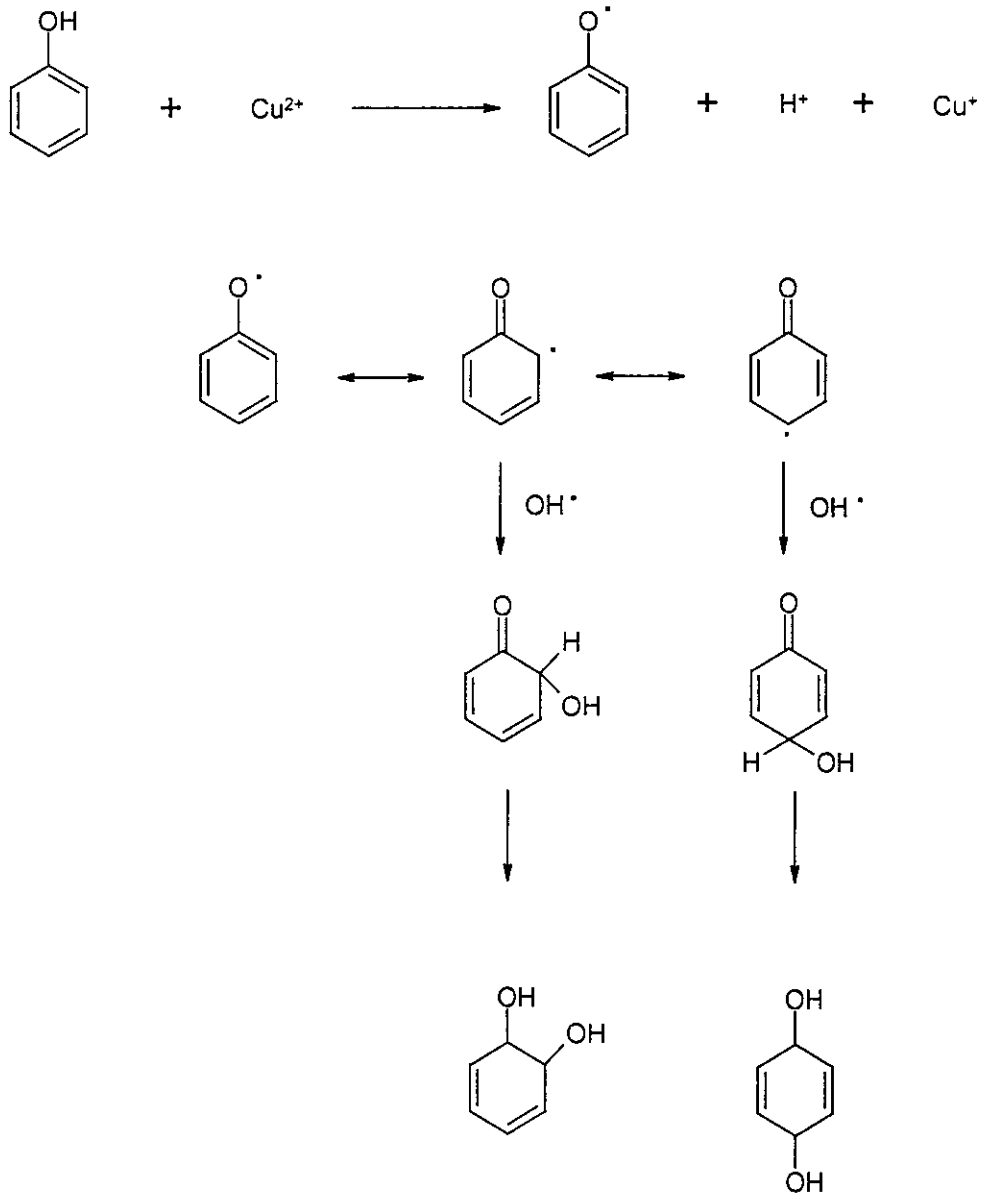

Scheme I Mechanism of phenol hydroxylation

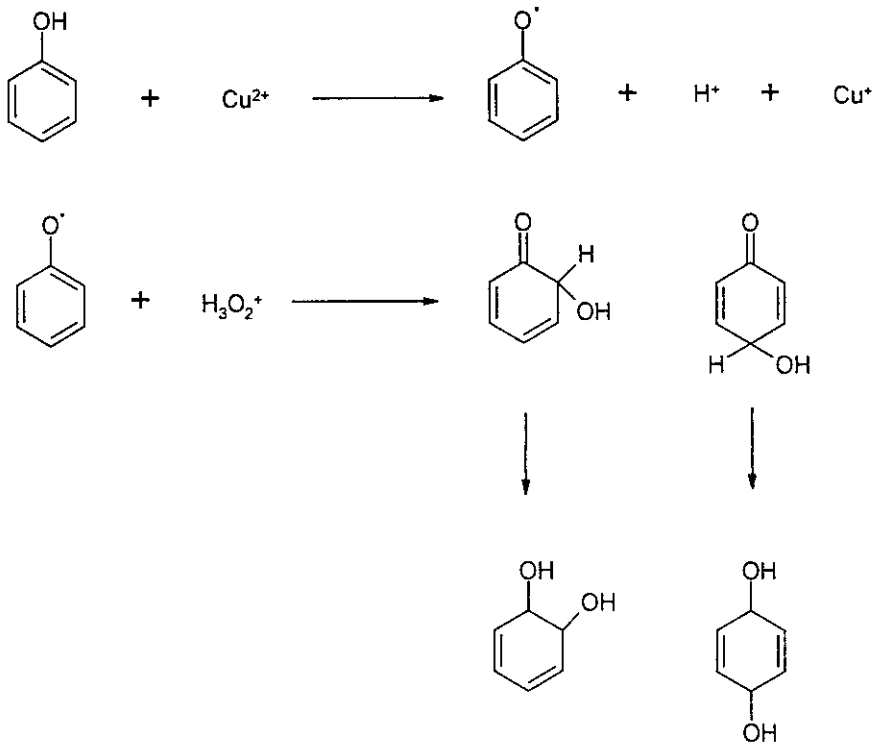

Scheme II Mechanism of phenol hydroxylation

References

1. P.B. Weisz and V.J. Frilette, *J. Phys. Chem.* 64 (1960) 382.
2. P.B. Weisz, V.J. Frilette , R.W. Maatman, and E.B. Mower, *J. Catal.* 1 (1962) 307.
3. Chandra R Jacob, Saji P. Varkey, and Paul Ratnasamy, *Appl. Catal. A.* 168 (1998) 353.
4. R.F. Parton, D.E. De Vos, and P.A. Jacobs in *Proceedings of the NATO Advanced Study Institute on Zeolite Microporous Solids: Synthesis, Structure and Reactivity*, E.G. Derouane, F. Lemos, C. Naccache, and F.R. Ribeiro (Eds.), Kluwer, Dodrecht, 555, 578, 1992.
5. Dirk E. De Vos, Mieke Dama, Bert F. Sels, and P.A. Jacobs, *Chem. Rev.* 102 (2002) 3615.
6. Wei Zhao, Yunfei Luo, Peng Deng, and Quanzhi Li, *Catal. Lett.* 73, 2-4 (2001) 199.
7. Roger A. Sheldon and Jay K. Kochi, *Metal – Catalyzed Oxidations of Organic Compounds*, Academic Press, New York, 1981.
8. C. Meyer, G. Clement, and J.C. Balaceanu, *Proc. 3rd Int. Congr. on Catalysis*, 1 (1965) 184.
9. A. Sadana and J.R. Katzer, *J. Catal.* 35 (1974) 140.
10. G. Bellussi and C. Perego in *Handbook of Heterogeneous Catalysis*, Vol. 5, G. Ertl, H. Knözinger, and J. Weitkamp (Eds.), Wiley-VCH, New York, 2329, 1997.

Chapter 9

Catalytic activity of zeolite encapsulated complexes in the partial oxidation of benzyl alcohol to benzaldehyde

Abstract

Molecular sieves containing transition metal complexes exhibit very good properties as catalysts for a variety of oxidation reactions with peroxide as oxidant. The partial oxidation of benzyl alcohol using zeolite encapsulated complexes was carried out in the presence of hydrogen peroxide as oxidant at room temperature. Benzaldehyde was the only detectable product. The influence of various parameters such as temperature, amount of catalyst, and oxidant to substrate ratio was studied. Significant variation was observed on changing the solvent. The effect of catalyst poison was studied by adding pyridine. Higher activity was observed in the case of PdYDMG and CuYSPP. The efficiency of the catalysts on recycling was also studied.

9.1. Introduction

The oxidation of primary and secondary alcohols to aldehydes, ketones and carboxylic acids is a pivotal reaction in organic syntheses [1-2]. Traditionally such reactions have been performed with inorganic oxidants containing chromium(VI) reagents. The emphasis in recent times is on developing recyclable catalysts to bring about oxidation reactions using clean oxidants such as oxygen and hydrogen peroxide, under mild conditions compared to classical oxidations. Metal complexes have attracted attention as dioxygen activating catalysts. Per-oxo complexes act as oxidants in different reactions [3]. Per-oxo compound are generated by adding hydrogen peroxide to metal complexes But these homogeneous systems have several drawbacks, as they show a tendency for self degradation, and there is difficulty in reusing them. One means of overcoming these problems was to encapsulate them in zeolite pores, as zeolite encapsulated systems have the advantages of both homogeneous and heterogeneous catalysts.

Zeolite encapsulated per-oxo compounds provide an attractive route for the preparation of synthetic intermediates and other oxygen-containing organic substrates. Partial oxidation of benzyl alcohol is of great importance in the preparation of fine chemicals. In this chapter the results of our studies on the oxidation of benzyl alcohol to benzaldehyde in the presence of PdYDMG and CuYSPP complexes as catalysts are presented.

9.2. Experimental

9.2.1. Materials

Zeolite Y encapsulated complexes of SPO, SPP, SALSC, SB, DMG, and MDTC were prepared and characterized. Details of all the materials used for the activity studies are explained in Chapter 2. Neat complexes of the catalytically active ligands were also synthesized.

9.2.2. Procedure for the partial oxidation of benzyl alcohol to benzaldehyde

Benzyl alcohol, hydrogen peroxide, the activated catalyst, and the solvent were taken in a reaction flask of 50ml capacity. The reaction mixture was stirred for a definite period of time using a magnetic paddle. The conditions specific to each test are indicated along with the results in the table for each reaction.

After the reaction the solution was filtered to remove the catalyst. Then the aqueous and organic layers were separated. The organic layer was washed with water and analysed using thin layer chromatography (TLC) to detect the formation of benzaldehyde. It was finally analysed using gas chromatography to quantify the amount of substrate and product. The reaction was repeated, varying parameters like time, amount of catalyst, oxidant/substrate ratio, solvent, and temperature. The poison resistance and the activity on reusing the catalyst were examined here also.

9.3. Results

9.3.1. Screening studies

The partial oxidation of benzyl alcohol to benzaldehyde was studied using SPO, SPP, MDTC, DMG, SB and SALSC complexes in the liquid phase. The activities corresponding to these zeolite-encapsulated complexes are given in Table 9.1, and the percentage conversion to benzaldehyde for the different complexes is shown in Figure 9.1. Of all the complexes, PdYDMG and CuYSPP showed more than 95% conversion with 100% selectivity, while PdYSALSC showed only 49% conversion. Conversion is represented as turnover number (TON) calculated as moles of benzyl alcohol converted per mole of metal ion present in the catalyst.

Table 9.1 Activity for benzyl alcohol oxidation

	Percentage of benzaldehyde					
	DMG	SPP	SPO	SALSC	MDTC	SB
FeY	—	0.1	0.1	—	0.1	—
CoY	—	4.0	0.5	0.5	6.0	—
NiY	—	0.1	0.1	0.1	0.1	—
CuY	—	98	6.2	3.5	25	4.0
PdY	99	—	—	49	2.1	—

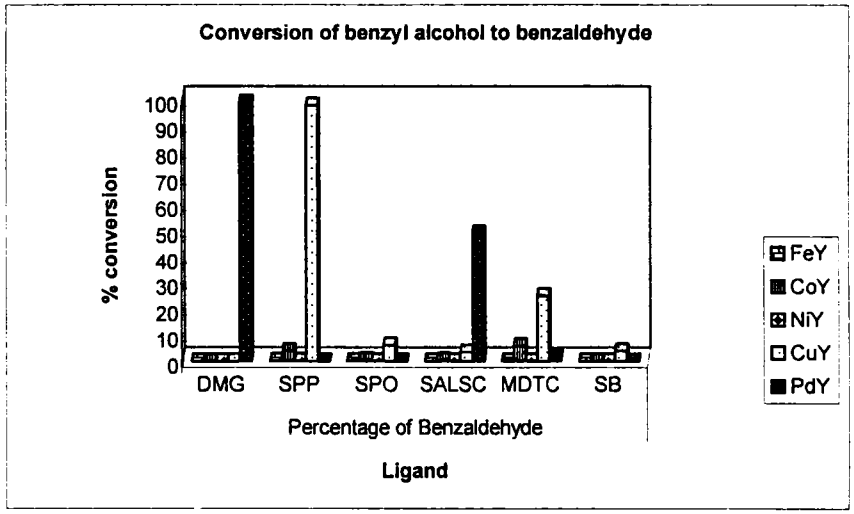

Figure 9.1 % Conversion of benzyl alcohol to benzaldehyde

Reaction condition

Oxidant to substrate mole ratio: 1.5
Temperature : 30 °C
Catalyst weight : 60 mg
Solvent : water
Duration : 4 hours

9.3.2. Blank run

The oxidation of benzyl alcohol to benzaldehyde was carried out under conditions identical to those of the screening experiments but without adding the catalyst. Benzaldehyde was not formed. This makes it clear that hydrogen peroxide by itself is unable to oxidize the benzyl alcohol in the absence of the catalyst. The reactions were carried out using NaY, CuY and PdY. Formation of benzaldehyde was not observed in these cases either. Experiments using neat complexes of DMG and SPP were also carried out. The absence of benzaldehyde in all these cases indicated that the conversion was possible only in presence of the catalysts.

9.3.3. Factors influencing the partial oxidation of benzyl alcohol to benzaldehyde

The oxidation of benzyl alcohol to benzaldehyde was studied under varied conditions, and the results observed were tabulated. It is seen that PdYDMG and CuYSPP give good conversion for benzyl alcohol oxidation. Further studies were done using PdYDMG and CuYSPP by varying the following parameters:

i) reaction time
ii) amount of catalyst
iii) oxidant to substrate ratio
iv) solvents
v) reaction temperature.

9.3.3.1. Effect of reaction time

The effect of reaction time was studied by carrying out the reaction for different time intervals ranging from 1 hour to 5 hours using PdYDMG and CuYSPP. The percentage conversion increased with increase in time. At the end of four hours 99% conversion was obtained with both the catalysts, with 100 %

selectivity to benzaldehyde. An induction time of 2 hours was observed in these cases.

Table 9.2 Effect of reaction time on conversion of benzyl alcohol

Time	PdYDMG		CuYSPP	
(h)	% Conversion	% Benzaldehyde	% Conversion	% Benzaldehyde
1	0	0	0	0
2	0	0	0	0
3	40	36	34	33
4	99	99	99	99
5	99	99	99	99

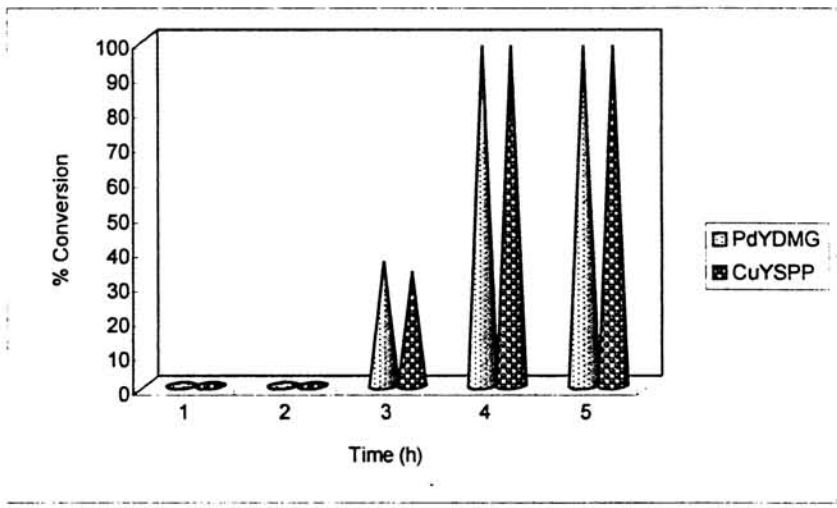

Figure 9.2 Reaction time versus % conversion

Reaction condition

Oxidant/substrate mole ratio : 1.5
Weight of catalyst : 60 mg
Solvent : water
Temperature : 30 °C

There was no change in the amount or product on carrying out the reaction for 5 hours. The effect of contact time on conversion and selectivity is represented in Table 9.2 and this is shown graphically in Figure 9.2.

9.3.3.2. Effect of the amount of catalyst

The reactions were carried out with PdYDMG and CuYSPP under identical conditions by varying the amount of catalyst from 20mg to 60mg. It was found that activity increased with increase in the amount of the catalyst. The results are tabulated in Table 9.3 and are presented graphically in Figure 9.3. The maximum conversion was obtained with 60mg of catalyst. So for all the reactions the amount of the catalyst was fixed as 60mg.

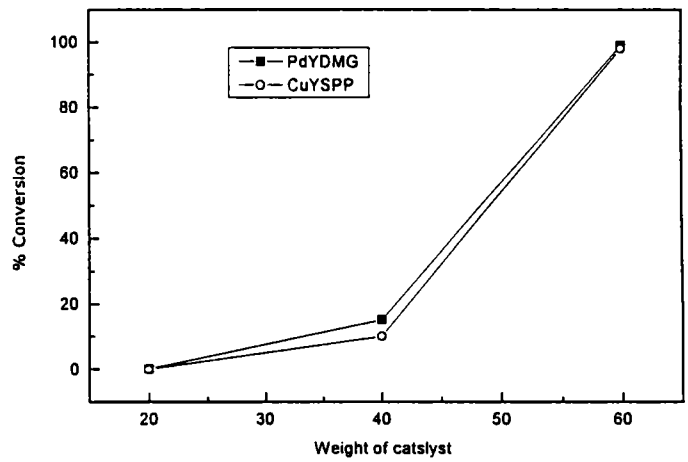

Figure 9.3 Effect of the amount of catalyst on benzyl alcohol oxidation

Reaction condition

Oxidant/substrate mole ratio : 1.5
Solvent : water
Temperature : 30 °C
Duration : 4 hrs

Table 9.3 Effect of the amount of catalyst on benzyl alcohol oxidation

Amount of catalyst	PdYDMG		CuYSPP	
	% Conversion	% Benzaldehyde	% Conversion	% Benzaldehyde
20	1	0.1	1	0
40	10	15	5	10
60	99	99	99	99

9.3.3.3. Effect of oxidant: substrate ratio

The effect of oxidant: substrate ratio on benzaldehyde oxidation was studied in the case of PdYDMG and CuYSPP. The extent of oxidation depends on the concentration of oxidant in the reaction mixture. The reaction was repeated under identical conditions but by varying the oxidant: substrate ratio. The percentage conversion to benzaldehyde increased as oxidant/substrate mole ratio increased. The maximum conversion was obtained at oxidant/substrate mole ratio 1.5. There was no further change in conversion as the ratio was increased. So further studies were carried out fixing the oxidant/substrate mole ratio at 1.5. The results are presented in Table 9.4.

Reaction condition

Temperature : 30 °C
Duration : 4 hrs
Weight of catalyst : 60 mg
Solvent : water

Table 9.4 Effect of varying the oxidant/substrate ratio on the conversion of phenol to hydroquinone

Solvent	PdYDMG		CuYSPP	
	% Conversion	% Benzaldehyde	% Conversion	% Benzaldehyde
1	2	0	0	0
1.5	99	99	99	99
2.5	99	99	99	99

9.3.3.4. Effect of solvents

The study of the oxidation of benzyl alcohol was carried out in two solvents, benzene and water. The effect of solvents was studied for two catalysts, PdYDMG and CuYSPP. The results are presented in Table 9.5 and represented pictorially in Figure 9.4. Using water as solvent, 99% conversion was observed with 100% selectivity to benzaldehyde. In benzene, 100% conversion of benzyl alcohol occurred but no benzaldehyde was formed.

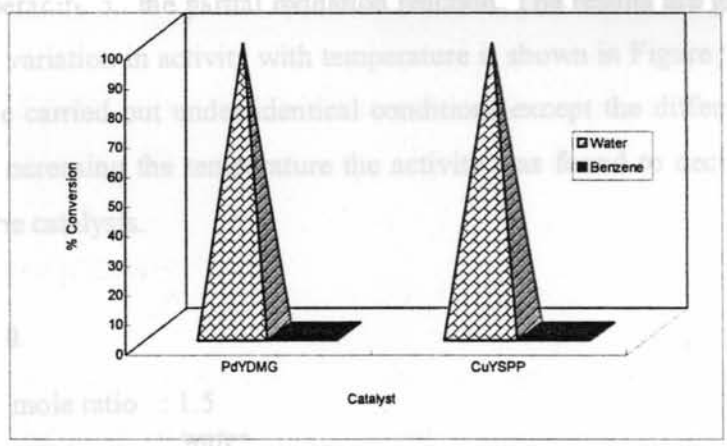

Figure 9.4 Effect of solvents on the conversion of benzyl alcohol to benzaldehyde

Table 9.5 Effect of solvent on benzyl alcohol oxidation

Solvent	PdYDMG		CuYSPP	
	% Conversion	% Benzaldehyde	% Conversion	% Benzaldehyde
Water	99	98	99	98
Benzene	99	0	99	0

Reaction condition

Oxidant/substrate mole ratio : 1.5
Temperature : 30 °C
Duration : 4 hrs
Weight of catalyst : 60 mg

9.3.3.5. Effect of reaction temperature

The oxidation of benzyl alcohol was carried out at three different temperatures 30°, 50°and 70 °C, using PdYDMG and CuYSPP to find the influence of temperature on the partial oxidation reaction. The results are given in Table 9.6 and the variation in activity with temperature is shown in Figure 9.5. All the reactions were carried out under identical conditions except the difference in temperature. On increasing the temperature the activity was found to decrease in the case of both the catalysts.

Reaction condition

Oxidant/substrate mole ratio : 1.5
Solvent : water
Weight of catalyst : 60 mg
Duration : 4 hrs

Table 9.6 Effect of reaction temperature on benzyl alcohol oxidation

Reaction temperature	PdYDMG		CuYSPP	
	% Conversion	% Benzaldehyde	% Conversion	% Benzaldehyde
30°C	99	98	99	98
50°C	2	1.2	2	1.5
70°C	1	0.6	1	0.1

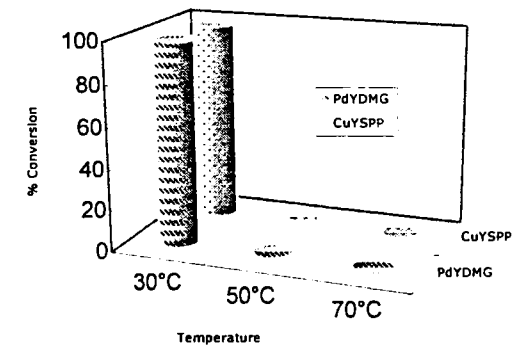

Figure 9.5 Effect of reaction temperature on benzyl alcohol oxidation

9.3.4. Addition of poison

The poison resistance of PdYDMG and CuYSPP was evaluated by using pyridine. Pyridine was added to the catalysts for poisoning them. Then the reaction was carried out using the poisoned catalysts under identical conditions. Both the catalysts were seen to be deactivated.

9.3.5. Recycled catalyst

Use of recycled catalyst is very important from the point of view of economical considerations. The used catalyst was filtered off from the reaction mixture and washed with acetone and dried in the oven at 120 °C for 2 hours. XRD patterns were found to remain similar after the first run, indicating the retention of the zeolite structure. IR spectra indicated that the complex was intact in the cages. Pd(II) and Cu(II) ions were not detected in the reaction phase of the mixture. Therefore the Pd and Cu complexes have not leached from the zeolite pore during the reaction. PdYDMG showed 67% activity after recycling while in the case of CuYSPP, there was no loss in activity on recycling. A comparison of the activities of fresh and recycled catalysts is given in Figure 9.6 and the corresponding conversions and percentage loss in activity are given in Table 9.7.

Table 9.7 Effect of recycled catalyst on benzyl alcohol oxidation

Catalyst used	% Conversion		% Loss in activity
	Before recycling	After recycling	
PdYDMG	98	67	33
CuYSPP	98	98	0

Reaction condition

Oxidant/ substrate mole ratio : 1.5
Temperature : 30 °C
Duration : 4 hrs
Solvent : water
Weight of catalyst : 60 mg

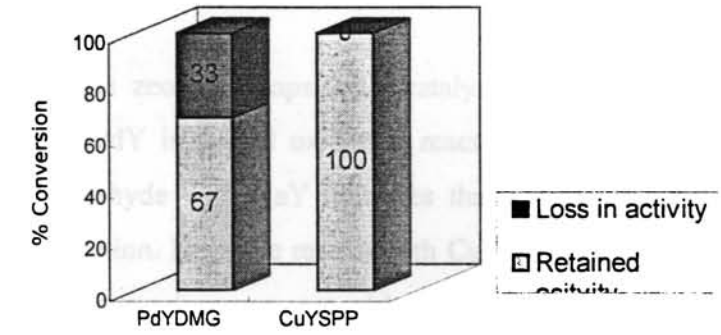

Figure 9.6 Activity on using recycled catalysts

9.4. Discussion

Zeolite encapsulated complexes of SPO, SPP, MDTC, SB, DMG and SALSC were used in the oxidation of benzyl alcohol. A comparison of the activity indicates that PdYDMG and CuYSPP are the most effective catalysts for the partial oxidation of benzyl alcohol, and there was 100% selectivity to benzaldehyde. In terms of turn over number, the conversion for PdYDMG was 2540 and that for CuYSPP was 1682. PdYSALSC and CuYMDTC showed moderate activity compared to PdYDMG and CuYSPP. Benzoic acid or any other oxidation products were not detected in the reaction mixture on analysis using gas chromatography. This shows that zeolite encapsulated complexes are very effective catalysts for the partial oxidation of benzyl alcohol, and that PdYDMG and CuYSPP are eco-friendly catalysts in that they leave no waste products. Similar behaviour of encapsulated complexes in the partial oxidation of benzyl alcohol has been reported by Zsigmond [4]. The aqueous and the organic phases were separated and the aqueous phase was tested for the presence of any metal ions using atomic absorption spectroscopy after the screening studies. The absence of metal ions in the solution phase indicated that no leaching of complexes had

occurred during the reaction. This shows that the complexes are intact inside the zeolite pores. This explains the high stability of the complex inside the zeolite pore.

The activities of the zeolite encapsulated catalysts were compared with those of NaY, CuY, and PdY in partial oxidation reaction. The absence of the oxidation product benzaldehyde with NaY indicates that the zeolite support in itself does not ensure oxidation. Negative results with CuY and PdY indicate that Cu^{2+} and Pd^{2+} ions by themselves are not able to influence benzyl alcohol oxidation. Neat complexes of Pd(II) and Cu(II) did not yield benzaldehyde as the product on the oxidation of benzyl alcohol. This could be due to multi molecular deactivation. On the other hand, zeolite encapsulated complexes showed high activity. This can be explained by the site isolation theory. The complexes are held within the zeolite pores by physical force. Confinement of the transition metal complexes inside the cavities can activate the catalyst because of the strong electrostatic interaction between the catalyst and the support. They are free to move inside the pore but are prevented from coming out due to the restrictive size of the pore openings. This prevents deactivation by multi molecular association. It has been reported that a metal complex in the zeolite cage behaves like neat complexes in solution [4].

The effect of varying the amount of the catalysts was studied. The conversion increased with an increase in the amount of the catalyst upto a certain limit at which maximum conversion was obtained, and further addition of catalyst had no effect. The increase in conversion can be due to the increase in the number of active sites.

In the case of both the catalysts, there was an induction period of 2 hours after which the conversion to benzaldehyde slowly increased. The time required for the completion of the reaction was 4 hours. There are reports that the oxidation

of benzyl alcohol is a slow process [5]. No further reaction products were observed on continuing the reaction beyond 4 hours.

The choice of solvent was found to have a big influence on activity. Very high activity was observed when the solvent used was water. Benzaldehyde formation was not detected on using benzene as solvent. This can be due to the low solubility of hydrogen peroxide in benzene.

The effect of temperature was studied, conducting the reaction at three different temperatures, 30°C, 50 °C, and 70 °C. Conversion was maximum at room temperature, and room temperature was taken as the optimum temperature for benzyl alcohol oxidation. According to earlier reports, the reaction is to take place at higher temperatures [6]. In the present case, the conversion to benzaldehyde decreased as the temperature was raised. This could be due to the decomposition of hydrogen peroxide at higher temperatures. There is an induction period of 2 hours for this reaction. The decomposition of hydrogen peroxide must have occurred within that time at higher temperatures.

The maximum conversion was obtained when the oxidant/substrate mole ratio was 1.5. There have been reports of experiments in which the reaction was carried out with the oxidant/substrate mole ratio at 2.5 [6]. On adding poison to the catalyst it was completely deactivated by the action of poison. One of the most attractive features of zeolite encapsulated complexes is their ability to be recycled. CuYSPP maintained the same activity after recycling, while PdYDMG showed 63% activity as compared to the fresh catalyst. This shows their tendency to withstand the conditions of regeneration processes. The use of recycled catalyst reduces the possibility of environmental pollution and enables the continuity of the process.

According to the mechanism proposed by Puzari et al., some excess hydrogen peroxide is needed because the reaction involves the decomposition of

hydrogen peroxide. As per this mechanism, the catalytic oxidation of benzyl alcohol by hydrogen peroxide involves two simultaneous processes: decomposition of hydrogen peroxide itself resulting in the liberation of oxygen, and the liberated oxygen reacting with benzyl alcohol [7]. In our observation, the oxidation of benzyl alcohol takes place along a single route. Besides, the oxidant/substrate mole ratio used in our method is lower than that reported earlier [6]. The mechanism proposed here involves the interaction of the encapsulated complex with hydrogen peroxide to form a catalyst precursor. The precursor is formed by the coordination of an oxygen atom to the vacant metal site in the complex. The catalyst precursor interacts with benzyl alcohol oxidizing it to benzaldehyde. Similar mechanisms have been reported earlier [8-10].

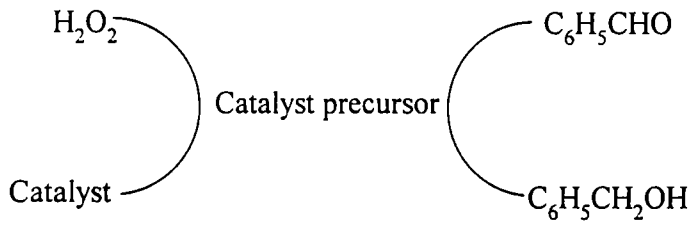

Scheme I Oxidation of benzyl alcohol to benzaldehyde

PdYDMG and CuYSPP, which were found effective in the oxidation of benzyl alcohol, have square planar geometry. So there is enough space around the metal for the coordination of one or more ligand. The precursor is formed by the coordination of an oxygen atom to the vacant metal site in the complex.

The use of encapsulated systems has certain advantages over the use of homogeneous systems. It is very easy to separate the encapsulated catalyst from the reaction medium by simple filtration. Even the used catalyst showed high activity while the free complex had no activity. Further, there is no need to use an extra axial ligand as in the case of the homogeneous catalyst [4]. The other advantages were the possibility of recycling and amenability to continuous processing.

References

1. M. Hudlicky, *Oxidations in Organic Chemistry*, American Chemical Society, Washington DC, 1990.
2. R.A. Sheldon, I.W.C.E. Arends, Gerd-Jan T. Brink, and A. Duksman, *Acc. Chem. Res.* 35 (2002) 774.
3. Won K. Seok, *Bull. Korean Chem. Soc.* 20, 4 (1999) 395.
4. Á. Zsigmond, F. Notheisz, Z. Fráter, and J. E. Bäckvall, in *Heterogeneous Catalysis and Fine Chemicals IV*, H.U. Blaser, A. Baiker, and R. Prins (Eds.) Elsevier Science B.V. (1997) 453.
5. L. Palombi, L. Arista, A. Lattanzi, F. Bonadies, and A. Scettri, *Tetrahedron Lett.* 37, 43 (1996) 7849.
6. K.O. Xavier, J. Chacko, and K.K. Mohammed Yusuff, *J. Mol. Catal.* 178, (2002) 275.
7. A. Puzari, L. Nath, and Jubaraj B. Baruah, *Ind. J. Chem.* 37 A (1998) 723.
8. R. A. Sheldon and J.K. Kochi, *Metal Catalyzed Oxidation of Organic Compounds*, Academic Press, New York, 1981.
9. Y. Kamiya and M. Kashima, *Bull. Chem. Soc. Jpn.* 46 (1974) 905.
10. A. Onopchencko and J.G.D. Schultz, *J. Org. Chem.* 37 (1972) 2564.

Summary and conclusion

With increasing awareness about the dangers of environmental degradation, research in chemistry is getting increasingly geared to the development of "green chemistry," by designing environmentally friendly products and processes that bring down the generation and use of hazardous substances. The priority in many chemical processes now is to develop new solid catalysts with selective and effective transformation possibilities for oxidation reactions with high yield.

Catalysis by metal complexes encapsulated in the cavities of zeolites and other molecular sieves has many features of homogeneous, heterogeneous, and enzymatic catalysis. Serious attempts have been made to gain product selectivity in catalysis by means of enzyme mimicking. Immobilization of the active center in the zeolite pores is the essence of synthetic biomimetic chemistry, and is responsible for the shape selective properties of such catalysts. The notable superiority of this kind of catalytic system is in single–site reactions, high selectivity, and tenability (which are the advantages of homogeneous catalysts) together with ease of separation of products from reactants, durability, stability, and easy handling (advantages of heterogeneous catalysts). The catalytic activity shown by the encapsulated complexes can be correlated to the structure of the active site inside the zeolite pore.

Chapter 1 of the thesis presents a general introduction about the zeolite encapsulated metal complexes and the catalytic activity of metal complex catalysts in certain oxidation reactions, particularly in the decomposition of hydrogen peroxide, hydroxylation of phenol, and the partial oxidation of benzyl alcohol. Information regarding the methods used for the synthesis of zeolite encapsulated complexes, the role of zeolites as micro reactors and as enzyme mimics, and the interaction between the guest and the host is also included in this chapter. The

chapter ends with a discussion of the significance of the work undertaken and its scope, followed by relevant references.

Chapter 2 presents the details regarding materials and methods used for the synthesis and characterization of the complexes. The techniques employed for the characterization of the complexes include CHN analysis, AAS, XRD, SEM, BET surface area and pore volume, magnetic measurements, DRS, FTIR, EPR, and TG. The methods and techniques used for carrying out catalytic activity studies and estimating the percentage conversion are also included in this chapter.

Chapter 3 is divided into two sections: Section A and Section B. Section A describes the synthesis and characterization of zeolite Y encapsulated Fe(III), Co(II), Ni(II), and Cu(II) complexes of the Schiff bases *N,N'*-bis(3-pyridylidene)-1,2-phenylenediamine (SPO) and *N,N'*-bis(3-pyridylidene)-1,4-phenylenediamine (SPP). Section B deals with Co(II), Ni(II), and Cu(II) complexes of salicylaldehyde semicarbazone (SALSC).

Ion exchanged zeolites MY (M= Fe, Co, Ni, Cu, and Pd) were prepared and characterized. All the encapsulated complexes were synthesized using the flexible ligand method and purified by soxhlet extraction. SEM taken before and after encapsulation indicates the absence of surface adsorbed species. XRD patterns indicate that there is no loss in crystallinity for the zeolite structure even after encapsulation. The Si/Al ratio of the encapsulated complex is the same as that of the ion exchanged zeolite showing the retention of zeolite structure after encapsulation. The lower surface area and pore volume of the encapsulated complex compared to the ion-exchanged zeolite suggest encapsulation of the metal complex inside the zeolite pore.

The coordination sites of ligands to the metals were arrived at from the IR spectra. The strong bands at 1581cm^{-1} and 1610 cm^{-1} in the spectra of the ligand SPO and SPP are shifted to the lower energy region in the spectra of complexes,

indicating coordination of azo-methine nitrogen. The ligand absorption of SALSC at 1620cm^{-1} due to υC=O is shifted to a lower region (1550-1545cm^{-1}) in the complexes. On the basis of magnetic moment, electronic spectra, and EPR of Cu(II) complexes, an octahedral geometry was tentatively assigned for the encapsulated complexes of FeYSPO, CoYSPO, NiYSPO, FeYSPP, CoYSPP, NiYSPP, CoYSALSC, and NiYSALSC; and square planar geometry was assigned for CuYSPO, CuYSPP, and CuYSALSC from EPR spectra. The α^2 values between 0.87 and 0.91 for the copper complexes of SPO, SPP, and SALSC suggest an ionic environment for Cu(II) ions. Neat SPO complexes of Co(II) and Ni(II) have been reported to be square planar. The change in geometry in the case of Ni(II) complexes can be attributed to the interaction of the oxide ions of the zeolite framework. Only a qualitative idea regarding the decomposition patterns of zeolite encapsulated complexes was obtained from the TG curves. The mass loss around 100-125 °C is due to loss of free water and coordinated water. The major mass loss from 125-500 °C can be due to the decomposition of the complexes. However distinct stages of decomposition were not observed in any of the TG curves.

Chapter 4 presents a comparative study of neat and encapsulated 2-styrylbenzimidazole complexes of Cu(II). The analytical data confirm the composition of the neat complex to be $Cu(SB)_2Cl_2$. The Si/Al ratio and the XRD patterns of the encapsulated complex suggest that there is no collapse of the zeolite framework on encapsulation. The formation of the complex in the zeolite cage is further confirmed by surface area analysis, pore volume analysis, and the absence of surface species was noted from SEM.

The IR spectral data indicate that the coordination of the ligand is through the νC=N of styrylbenzimidazole. Magnetic moment, diffuse reflectance spectra and EPR spectra of the two complexes suggest square planar structure for the neat and encapsulated complexes. The TG/DTG of the neat complex gives clear idea regarding the decomposition pattern of the complex whereas the TG of the encapsulated complex gives only qualitative idea regarding the decomposition.

There are two stages of decomposition for the neat complex. The mass loss in the first stage might be due to expulsion of one styrylbenzimidazole and the mass loss in the second stage of decomposition corresponds to the removal of one styrylbenzimidazole and two chlorine atoms. The TG curve of the encapsulated complex shows that most of the intrazeolite free water molecules are released in the temperature range 30-100 °C. The mass loss in the temperature range 100-534 °C can be due to the removal of ligands and coordinated water if any.

Chapter 5 is divided into two sections: Section A and Section B. Section A deals with the synthesis and characterization of zeolite encapsulated complexes of Fe(III) dithicarbamates of MDTC, EPDTC and IPDTC, and Section B deals with the studies on Co(III), Ni(II), and Cu(II) morpholinedithiocarbamtes. The Si/Al ratio and the XRD patterns indicate the retention of zeolite framework. Decrease in surface area and pore volume confirms encapsulation of complexes and SEM indicates the absence of surface species. The positive shift of $\nu N{=}CS_2$ seen in the IR spectra is an indication of the interaction of the chelated sulphur atoms with the metal. This indicates that coordination has occurred through sulphur atoms.

Magnetic moment studies indicate octahedral structure for the encapsulated Fe(III) complexes, suggesting that there is no change in structure on encapsulation. The cobalt complex was found to be diamagnetic,suggesting a low spin octahedral structure for the complex. The neat Ni(II) dithiocarbamate complexes which were reported to have square planar appears to have octahedral structure when inside the zeolite cages. The Cu(II) complex which is square planar showed no change in geometry on encapsulation. The structure of copper complex is further supported by diffuse reflectance spectroscopy and the EPR spectrum. The ratio g_{II}/A_{II} is 109.2 cm for CuYMTDC suggesting a square planar environment around Cu (II) ion. The value of α^2 is 0.9495, suggesting ionic environment for the Cu^{2+} ions in the zeolite cavity. TG curves are continuous and so the stages of decomposition are not distinct.

Chapter 6 reports the study of the zeolite encapsulated palladium complexes of DMG, SALSC and MDTC. Chemical analysis reveals that the complexes are present as monomeric species in the zeolite lattice. The lowering of the surface area and pore volume values confirm the presence of the complex inside the zeolite pore, and the XRD patterns indicate the retention of zeolite crystallinity. The shift of the C=N stretching vibration to lower energy region of ligand DMG; the positive shift of $\nu N{=}CS_2$ of morpholinecarbodithioate; and the shift of $\nu C{=}O$ stretch of salicylaldehyde semicarbazone to 1600 cm^{-1} are observed in the IR spectra of PdYDMG, PdYMDTC, and PdYSALSC respectively, which support the coordination of the ligand to the metal in the complexes. All the palladium-encapsulated complexes were found to be diamagnetic. Electronic spectra also support square planar geometry for the complexes.

Chapter 7 deals with the studies on the decomposition of hydrogen peroxide in the presence of complexes of SPO, SPP, SALSC, SB, MDTC, and DMG. The catalytic activity of PdYSALSC, CuYMDTC and CuYSB was studied in detail. PdYSALSC was found to be the most active catalyst in the decomposition; CuYMDTC showed moderate activity, while CuYSB showed much lower activity. The difference in activity can be correlated to the structural features (geometry) of the complex. All the active complexes have square planar geometry. Complexes having two free sites on the metal ion facilitates the reaction of the intermediate $LM(HOO)^{(n-1)+}$ with a second peroxide ion. The highly reactive species formed enhances the decomposition process. The activity of the encapsulated complex was much higher compared to that of the ion exchanged zeolites indicating the influence of the ligand. In the present study, activity with regard to the ligand was found to vary as follows:

SALSC > MDTC > SB.

Therefore it appears that the chelate formation and the ring size of the chelate have a role in the activity.

The rate of decomposition reveals that the encapsulated complexes are more active than the neat complexes. The decomposition of hydrogen peroxide with each of the three catalysts was found to increase with increase in the weight of the catalyst. A change in the solvent polarity of the reaction medium slowed down the decomposition reaction indicating the involvement of the HOO^- species in catalysis. The direct addition of pyridine to the catalyst deactivated the decomposition processes while the addition of pyridine to the mixture of hydrogen peroxide and catalyst increased the rate of the reaction. This again confirms that hydrogen peroxide decomposes according to the equation

$$H_2O_2 \rightarrow H^+ + HOO^-$$

HOO^- being the species involved in catalysis. The activity of the Cu complexes was retained / slightly lost on recycling while the activity of the encapsulated Pd complex was considerably reduced.

Chapter 8 of the thesis presents our studies on the hydroxylation of phenol using the encapsulated complexes. The hydroxylation of phenol to hydroquinone was carried out at room temperature with 30 % hydrogen peroxide as oxidant. From the screening studies, CuYSALSC and CuYMDTC were found to be the most active catalysts. GC analysis of the product of the reaction revealed that these catalysts exhibit high para selectivity in the product stream. Selectivity to hydroquinone was greater than 95 % with both the catalysts. Apart from high selectivity, high hydroquinone yield was also observed in both the cases. This method is simple and economical and minimizes the formation of undesired products. The reaction was screened using metal exchanged zeolite (CuY) and neat complexes. On screening with CuY, catechol was found to be the only product. In the case of neat complexes, tarry products were obtained, which might be due to the presence of too many active centers. Thus encapsulation increases the activity and para selectivity in these cases. Another feature of the reaction is that the catalyst remains in the solid phase during the entire reaction and can be easily filtered off at the end of the reaction. Activity increased with increase in the amount of the catalyst up to a certain level. Further increase in the amount of the

catalyst had no effect at all. It was observed that there is an optimum time for each catalyst for the completion of the reaction. The optimum time for CuYSALSC was 5 hours and that for CuYMDTC was 2 hours. Unwanted products were obtained when the reaction was allowed to proceed beyond this time. This might be due to over oxidation or due to the decomposition of hydrogen peroxide. The induction period observed in the cases of the two catalysts suggests a free radical mechanism for these two catalysts.

The catalytic activity showed a strong dependence on the hydrogen peroxide - phenol volume ratio. Tarry products were obtained on increasing the volume of hydrogen peroxide. This can be due to the over oxidation of phenol at high hydrogen peroxide concentration. The maximum yield of hydroquinone was obtained when the H_2O_2 – phenol volume ratio was 5. This suggests that the possible mechanism can be via the formation of $H_3O_2^+$.

The yield of hydroquinone decreased as temperature increased from 30 °C to 70 °C. The reduction in the percentage conversion to hydroquinone on increasing the temperature to 50 °C may be due to the formation of some other products resulting from the slow diffusivity at higher production ratio from the pore, leading to further reaction or due to the decomposition of hydrogen peroxide at higher temperatures. Tarry products are formed at 70 °C with both CuYSALSC and CuYMDTC, and this can be the result of the exothermic nature of the reaction or due to over oxidation, or some other side reaction.

Water appears to be the best solvent for the reaction compared to methanol, acetone and benzene. The radical scavenging methanol and acetone may remove the reactive phenol radicals and affect the catalytic reaction. In benzene there is no conversion at all. This can be because hydrogen peroxide is insoluble in benzene. The catalyst showed good resistance to deactivation on adding poison (pyridine). On recycling they showed 50-60% activity compared to unused catalysts. This again confirms the stability of the catalysts inside the zeolite pore.

Chapter 9 deals with our studies on the partial oxidation of benzyl alcohol to benzaldehyde. The oxidation was carried out using hydrogen peroxide as oxidant in presence of PdYDMG and CuYSPP as catalysts. The product (benzaldehyde) was detected using TLC and confirmed using GC.

The catalytic activity of the complexes was tested for oxidation under various conditions. The operating conditions like the amount of the catalyst, reaction time, oxidant to substrate ratio, reaction temperature, and solvents have been optimized. No further oxidation products were obtained on continuing the reaction for four hours beyond the optimum time. Maximum conversion was obtained at room temperature and the percentage conversion decreased with increase in temperature. Activity was found to be dependent on the solvent used.

The poison resistance of the catalysts was checked by adding pyridine. Both the catalysts were deactivated by poison. The activity of the recycled catalysts was also studied. CuYSPP showed no change in activity on first recycling while the activity of PdYDMG was reduced to almost 67 % of the fresh catalyst.

Both PdYDMG and CuYSPP have square planar geometry indicating the influence of structure in catalytic activity. It appears that the precursor formed by the coordination of an oxygen atom to the vacant metal site in the complex might be responsible for the oxidation of benzyl alcohol to benzaldehyde. Further more, in these reactions, there was 100% selectivity towards benzaldehyde. In effect these catalysts satisfy the basic need of green chemistry, making chemical synthesis more environmentally friendly.